DESIGN, SIMULATION AND THERMO-ECONOMIC ASSESSMENT OF A TRANSCRITICAL CARBON DIOXIDE SOLAR POWER PLANT FOR MEDIUM-SCALE ELECTRICITY AND HEAT GENERATION

A Thesis

by

ADRIAN ALVAREZ SANCHEZ

Submitted to the Office of Graduate and Professional Studies of
Texas A&M University
in partial fulfillment of the requirements for the degree of

MASTER OF SCIENCE

Chair of Committee,	Michael B. Pate
Committee Members,	Alan B. Palazzolo
	Maria King
Head of Department,	Andreas A. Polycarpou

May 2020

Major Subject: Mechanical Engineering

ABSTRACT

This project comprises the engineering design and assessment of the novel above critical-point Carbon Dioxide cycle technology integrated with a solar Parabolic Trough Collector (PTC) plant. To accomplish this, preliminary studies were first performed on initial simple calculations of the thermodynamics of the different CO_2 cycles and solar energy technology. Knowledge was also acquired through an ongoing literature review.

A design model was then developed in EES, to assist in the design of the different systems of the power plant including the solar field, power block and components such as turbomachines and heat exchangers. Another model was developed in EES to simulate for average and median days for each month in the year by inputting a meteorological TMY3 data set and obtaining performance results. Pre-processing of data inputs and post-processing of outputs was done with MATLAB, as well as the understanding of the meteorological design conditions of the location chosen for the analysis, which is College Station, TX. Next, the results were confirmed with more advanced simulation software, namely SAM, provided by NREL.

A one 1-MW facility with a simple transcritical CO_2 cycle, which also provided cogeneration heat for a small industry (case A), was proposed as a baseline plant. Other alternatives studied were: a 10-MW facility for University Campus Utilities (case B), a 1-MW plant with a Recompression CO_2 cycle (case C), and finally a 1-MW plant with a supercritical CO_2 cycle (case D).

Results obtained for the baseline plant show an LCOE of $0.2915/kWh while lowest LCOE obtained was the one for alternative B: $0.2613/kWh. Although it was concluded that this technology not in position to make a market penetration, a sensitivity analysis was performed revealing important clues as to how the energy cost could be reduced so as to make it more viable in the future.

DEDICATION

I want to dedicate this work to my Father, God and to my mother the Most Holy Virgin Mary. I am thankful for this period of my life, as a Master's student that I have been able to enjoy to the fullest at Universidad Politécnica de Madrid and Texas A&M University. I also want to dedicate this work to my uncle, Carlos. He is the one that truly inspired me to become an engineer, a good man and a man of God. He left this world before this work was finished, but I am sure he will be able to appreciate it from a better place. I am thankful for his life, for being almost like a father for me, and for his still ongoing help and inspiration.

ACKNOWLEDGEMENTS

I would like to thank my committee chair, Dr. Pate, and my committee members, Dr. Palazzolo and Dr. King for their guidance and support throughout the course of this research. I want to appreciate as well the support from the Mechanical Engineering Department Faculty at Texas A&M University, and for the education I have received here.

I also want to thank Dr. Ignacio Lopez Paniagua and Dr. Javier Rodriguez Martin from Universidad Politecnica de Madrid for their guidance and support. I am thankful for the very solid education I received in this college in Spain.

Special thanks to the Rafael del Pino Foundation, the sponsoring organization of my studies at Texas A&M University. The economical support provided by the Foundation has covered all my needs during my studies abroad and has therefore made it possible for me to focus on my research and education, not having to worry about financial shortage.

I want to thank the community at St Mary's Catholic Center for the enormous abundance of joy and peace I have received from them and their ministry. I am very happy to say I belong to the aggie-catholic community.

Thanks also go to my friends and colleagues: Ryan, Jeremy, Carlie, Brian, the Prayer Benchers, the Mission Trip teams, Carlos, Uche, Kaushtub, Axel, I-Lun, Jesús, Jacobo, Sofía and many more! Thanks to the aggies for making my time at Texas A&M University a great experience.

Special thanks to Martin Ssembatya for giving me the idea of making my thesis about this topic, and for the help and support I got from him at the beginning of this project.

Thanks to my family, my mother, Maria Antonia, my grandmother, Aurora for their unconditional support and to my sister, Irene for her encouragement. Thanks to my cousins for always helping me to have a good time. Thank you to my extended family for their support as well. Thank you to the Alvarez-Fernandez family. Thank you to the Sanchez family.

Thank you to my father, Jose Antonio, to my grandfather, Antonio, and to my uncle, Carlos, for being with me and supporting me from Heaven.

Thank you, Jesus, for your unconditional Love and Grace, for being my best friend, for giving joy to my life and meaning to my struggles; for being my Father, my Courage and my Peace. Thank you, Mary, for being my Mother.

CONTRIBUTORS AND FUNDING SOURCES

Contributors

This work was supervised by a thesis committee consisting of Professor Michael Pate and Professor Alan Palazzolo of the Department of Mechanical Engineering, and Professor Maria King of the Department of Biological and Agricultural Engineering.

This work was also supervised by Dr. Ignacio Lopez Paniagua and Dr. Javier Rodriguez Martin of the department of Energy Engineering at the Superior Technical School of Industrial Engineers of the Technical University of Madrid (Universidad Politécnica de Madrid).

The Preliminary Studies were conducted in part by Martin Ssembatya, PhD student of the Department of Mechanical Engineering.

All other work conducted for the thesis was completed by the student independently.

Funding Sources

Graduate study was supported by a fellowship from Rafael del Pino Foundation in Madrid, Spain.

TABLE OF CONTENTS

Page

LIST OF FIGURES

Page

LIST OF TABLES

Page

1. INTRODUCTION

Energy generation and efficiency is one of the most challenging problems given to engineers at the current age. Renewable energy sources have not yet proved to be an appropriate substitute for conventional and fossil energy sources. Further research and development on the current renewable energy technologies is needed to address the energy problem, along with the improvement of conventional energy technologies, which might still be present for a relatively long time.

Solar energy is one of the technologies under development. Although it has already some commercial penetration it is still under development and still catching up.

A new technology that promises energy savings for electrical generation is under development and it is based on a thermodynamic power cycle that uses CO_2 at very high pressures as the power the cycle working fluid. Ongoing research reveals promising results for this technology as a potential substitute for conventional power generation plants.

In addition, if solar energy is used as the heat source for this power cycle, then sustainability and clean energy can be promoted over fossil fuel use.

1.1. Problem Identification: Context of Need for Sustainability in Energy

The current outlook of energy generation shows that it is heavily dependent on fossil fuel sources such as oil, gas and coal. These energy sources generate greenhouse gas emissions and their reservoirs are not infinite, which means they cannot be used indefinitely. As shown in Figure 1-1, fossil energy sources account for 74% of the

energy mix in the US. As to the End-Use sector, also shown in Figure 1-1, transportation is the largest one followed very closely by industry and the electrical system energy losses.

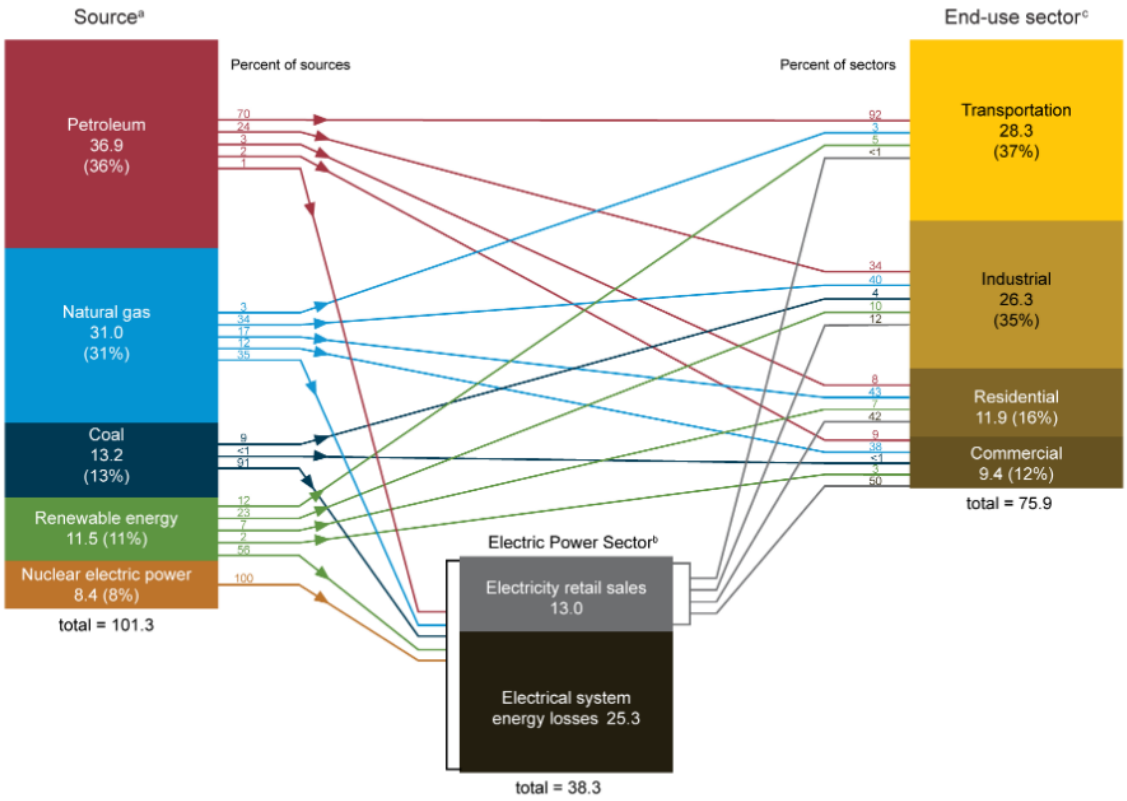

Figure 1-1: US Energy Consumption by Source and Sector, 2018 (Quadrillion Btu), reprinted from [1]

Fore any number of reasons, there is a need for sustainable, clean energy, with the property of being renewable and at the same time minimizing waste and emissions. At the same time, much of the primary energy consumption goes into energy losses, which means there is a need for more efficient energy generation and distribution technologies, as well as for the improvement of the existing ones not only in generation and distribution, but also in terms of increasing the efficiency of the end-use sector.

1.2. Solar Energy

The state of the art of solar energy production consists of two main trends. Photovoltaic solar energy is a technology that is maturing at a high speed. in the last few years, solar PV prices have dramatically dropped to $1 to $2/W in medium to large scale generation and industrial applications [2], making it difficult for other non-concentrating solar systems to be competitive against PV. The second trend of solar energy research is solar concentrated thermal power. Only some clear advantages of concentrating solar power would justify the investment with a few examples being:

- **Higher efficiencies**: concentrating solar plants can obtain an annual efficiency (solar to electric) of about 15% [3], while commercial solar PV systems typically obtain a rated efficiency of 10 to 17% [4].
- **Higher capacity factors**: Concentrating solar plants also have a higher capacity factor (28 to 33%, 1-2% higher than PV), and could still improve due to advances in thermal energy storage [5]. In contrast, electrical energy is not easily stored.
- **Combined heat and power generation (CHP)**: solar PV cells generate electricity (typically in direct current), but its energy losses are low-quality thermal energy (low temperature). For additional thermal needs, thermal solar power (even non-concentrating), can provide high temperature, which is usually the best choice as some case studies reveal [6], [7].

Interest in solar energy research advancement is often revealed by research support provided by the US government. Specifically, in March 2019, an amount of $26

million was announced for solar photovoltaic research and development, and even higher amount of $33 million for concentrated solar power (from now on, referred to as CSP) [10]. At the same time, in Spain, the second country in the world for solar power generation, the government has also developed a national plan: PNIEC 2021-2030; with the objectives of increasing energy efficiency and increasing the percentage of renewable energy in the Spanish energy mix. Spain is the country with the most solar-thermal installed power with 2300 MW, while the national plan sets the goal even higher, achieving 7300 MW of installed solar-thermal power by the year 2030 [8].

1.3. Supercritical and Transcritical CO_2 Cycle Technologies

Carbon dioxide started to be considered as a potential substitute for steam in Rankine generation plants only recently. It was in the year 2004 when a dissertation was published that contained a study on a nuclear generation plant running on supercritical CO2 instead of steam. The results showed that the s-CO2 recompression cycle is more efficient, simpler and more compact than an optimized steam cycle [1]. The transcritical cycle is similar to the supercritical cycle but incorporates a condenser, which produces a potentially higher efficiency if the temperature can be lowered enough.

Countless studies have been accomplished since this original 2004 study, with most of these studies focusing on the s-CO2 Brayton cycle, offering thermodynamic optimizations for different case constraints, exergy analyses and economic evaluations, with some studies of its applications for solar power, which is the subject of this thesis. In addition to the Brayton cycles, the Rankine cycle has also been investigated as evidenced by publications in the open literature. Two of the most recent papers that align

with this thesis are [2] and [3]. In both of these studies, a complete literature search is presented in the introduction sections, providing insight into the main advances in this topic.

1.4. Proposed Solution

This project focuses on improving the efficiency and sustainability of energy production for the industrial and commercial sectors by studying the cost-effectiveness and applicability of solar energy technologies along with high-pressure CO_2 thermodynamic cycles for medium-scale electrical and thermal needs.

In this thesis, solar thermal power is the main topic. Non-concentrating thermal solar systems offer a low efficiency and an unclear economical advantage (if any advantage, in terms of the cost of the panels and additional items). Because the output temperatures are low, it can be concluded that CSP, with its higher temperature, is the best technology to assess in terms of suitability for combined power and heat generation, and the most advanced of the common CSP technologies are the parabolic trough collectors working with a steam Rankine cycle as the configuration of the power block for electrical generation.

The innovation included in this thesis consists of proposing a new model of energy generation by incorporating a Carbon Dioxide cycle in the power block and studying its cost-effectiveness. The cycle proposed herein is the transcritical CO_2 cycle, because less research has been done compared to the supercritical one, and of special importance it may provide for a higher efficiency when solar energy is used as the heat source.

2. PROJECT OUTLINE

2.1. Design Approach

The evaluation of the technology proposed herein was made by defining boundary conditions consistent with the needs of the Texas A&M college campus or a small industry like a brewery.

Additionally, this evaluation was made considering different alternatives and end-users by using modeling and simulation of the system under different conditions and designs. Even though this study is not using dedicated experiments, it is in fact based on knowledge and information coming from existing experimental data.

This project consists of a combination of two design approaches commonly used in engineering and industry:

- **Top-down**: This approach requires extensive preliminary studies and literature review before defining the objectives and scope of a project. Once this is completed, the project is performed following a defined scheme and methodology.
- **Bottom-up**: This approach starts by developing all the different pieces that make up the concept of the project and then putting them together. Although the goals are defined, the project scope is not defined before starting it, unlike the top-down approach, and it therefore makes the project outcome uncertain because it relies more in experimentalism.

This project is not just a work of engineering but also research. The main challenges therefore come because of the many unknowns associated with new

technologies, of which knowledge is still being created. As a result, as much as the boundaries of the project are delimited with a top-down approach, a bottom-down methodology is inevitably present in the development of the project.

2.2. Statement of Plant Boundary Conditions and Needs

Before entering in any dimensioning or design of a CO_2 system, it is necessary to state the needs this system is to satisfy. As discussed before, this system would work as a power and heat generation unit in an industrial plant or a commercial building.

2.2.1. A Small Industry: The Spoetzl Brewery

The scale of power needs for these purposes has a range from about 1 MW to many hundreds of MW, depending on the industry, the plant size and the energy intensity. In a first approach the focus is to design a plant to produce 1 MW of electrical energy for a small-to-medium size industrial facility.

As to the thermal needs, it is not only important to know the amount of heat, but also the temperature at which this heat must be made available. Table 2-1 provides a summary of the temperatures required in different industrial processes and sectors. Assuming the waste heat from the solar plant has a maximum available temperature of 110^{o}C, it could supply heat for processes with thermal needs of about 60-100^{o}C, depending on the specific need, the amount of heat required and the temperature drop required in the process, etc. As observed in Table 2-1, most of the processes in the food and beverage industry could potentially work with the solar plant. Many processes in other industries also have the potential to work with the studied solar system, and

ultimately, every facility has a need for building heating or chilling depending on the season.

Table 2-1: Industrial process heat typical temperature requirements [9]

Industrial Sector	Process	T [C]
Food	Drying	30-90
	Washing	60-90
	Pasteurising	60-80
	Boiling	95-105
	Sterilising	110-120
	Heat Treatment	40-60
Beverages	Washing	60-80
	Sterilising	60-90
	Pasteurising	60-70
Paper Industry	Cooking and Drying	60-80
	Boiler feed water	60-90
	Bleaching	130-150
Metal Surface Treatment	Treatment, electroplating, etc.	30-80
Bricks and Blocks	Curing	60-140
Textile Industry	Bleaching	60-100
	Dyeing	70-90
	Drying, De-greasing	100-130
	Washing	40-80
	Fixing	160-180
	Pressing	80-100
Chemical Industry	Soaps	200-260
	Synthetic rubber	150-200
	Processing heat	120-180
	Pre-heating water	60-90
Plastic Industry	Preparation	120-140
	Distillation	140-150
	Separation	200-220
	Extension	140-160
	Drying	180-200
	Blending	120-140
	Flour By-products Sterilising	60-90
All Industrial Sectors	Pre-heating of boiler feed water	30-100
	Industrial solar cooling	55-180
	Heating of factory buildings	30-80

With this knowledge, a specific plant was picked as an example where to project the solar system, specifically, Shiner Beer Factory (Spoetzl Brewery), which is located in Texas, is a facility where the implementation of this solar system would be suitable, and some calculations were made to estimate this suitability.

The Spoetzl Brewery was estimated to have a potential area for solar collection (rooftop and plain) of *500x500 = 250,000 ft^2 = 24,414 m^2*, as shown in Figure 2-1. In addition, Shiner produces an average of 1642.8 barrels of beer per day (600,000 per year), and its planning to double this quantity [10]. In breweries it is estimated that the electricity consumed is 12 to 22 kWh/bbl; and the thermal energy required is 1.3 to 1.5 Therms/bbl or 10^5 Btu/bbl [11]. Then, assuming 17 kWh per bbl (barrel), the electrical demand of the brewery is 1.163 MWe, while the thermal energy demand is 2.807 MWth. These values make a heat-to-power ratio of 2.41. Therefore, to match the Shiner facility, the percentages of the heat and electricity generated from solar energy should be:

$$\frac{1}{1+2.41} = 29.3\%\ electrical$$

$$\frac{2.41}{1+2.41} = 70.7\%\ thermal$$

These values represent the electrical efficiency and the thermal fraction of the plant that best matches the Shiner facility. As observed, they are close to the values obtained from the thermodynamic analysis performed in the Preliminary Studies section: 25% electrical efficiency and 75% thermal fraction for the base case. Therefore, the solar system can be reasonably dimensioned to supply 1 MW of electricity and 3 MW of thermal energy, adding up to a 4-MW heat input.

Figure 2-1: Area estimation of the Spoetzl Brewery, reprinted from [12]

In addition, the area required to collect this heat must also be estimated sufficient. Given that the plant would produce 1 MW, it was found in the literature that the typical surface area requirement per MW for existing PTC plants ranges from 6070 m^2/MW (Holaniku at Keahole) to 40,000 m^2/MW (plants in Spain) [3]. It is therefore estimated that the potential available area at the Shiner factory is sufficient to build a 1 MW solar power plant.

To summarize the outcome of this section, the solar system discussed in this thesis will be designed to supply a demand of 1 MW electrical energy and roughly 3 MW of thermal energy available at 100^{o}C so as to meet the needs of the Spoetzl Brewery, which is a facility taken as the most suitable type to match the solar system.

2.2.2. A College Campus: The Texas A&M University Utility Plant

Another application proposed for study in this thesis is the incorporation of a renewable energy plant, namely, a solar thermal energy plant with a CO_2 cycle, to the already-existing cogeneration plant at Texas A&M University.

As shown in Figure 2-2, the cogeneration plant has a Heat Recovery Steam Generator (HRSG), that produces superheated steam at 600 psi and 750°F (400°C), which is then expanded in a steam turbine. When it is hot on campus, the electricity demand is increased by air conditioning needs, which demand more chilled water.

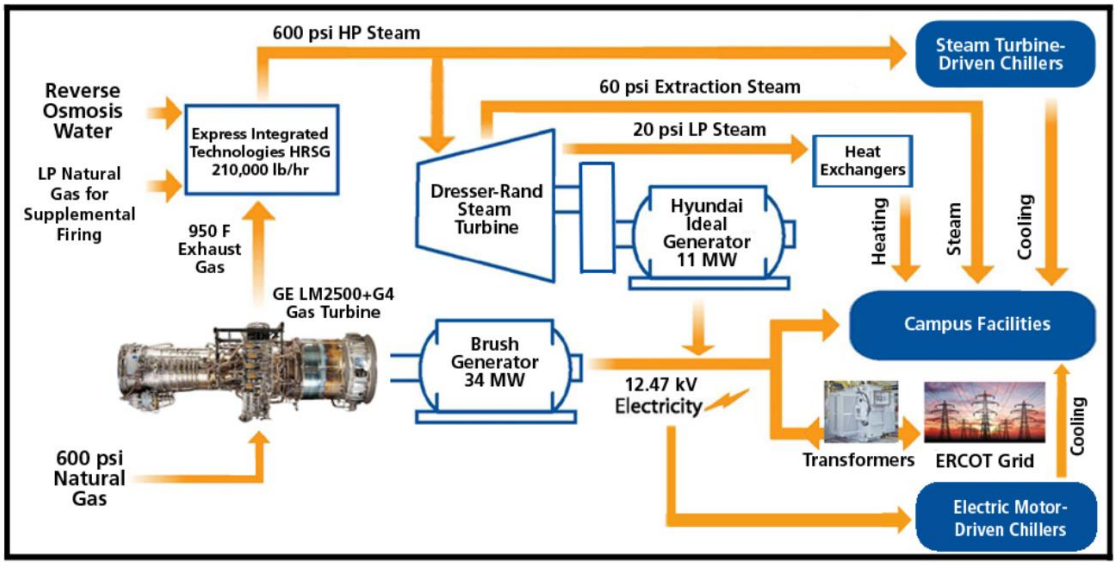

Figure 2-2: CHP system for campus power generation, heating and cooling at Texas A&M University, reprinted from [13]

The increase in electrical demand that takes place on campus when it is sunny could be covered by a solar system. In addition, since less steam is required to drive the chillers, some of the exhaust energy coming from the gas turbine could be used to boost

the efficiency of the CO_2 cycle, heating it up to 400°C with solar energy, and then heating it further with the exhaust of the turbine.

The size of this system is 10 MW, in comparison with the 11 MW steam turbine generator already present on campus, which provides an opportunity to study the applicability of the CO_2 system at a larger scale.

There are a number of barriers to implementation of this system, like the availability of an open space for a solar field on campus and the coupling of the system with the existent CHP plant to boost the efficiency. Therefore, the study of this case requires some idealizations.

To provide some indication of area magnitudes, The Golf Club at Texas A&M has an extension of more than 400,000 m^2 (a square with a side of 0.4 miles), meaning, if the solar plant was to be implemented, it might require almost half of this area, assuming the land area requirement is proportional to the MW produced by solar energy (1 MW requires roughly 20,000 m^2, therefore, 10 MW would require 200,000 m^2).

2.3. Proposed System Rankine Baseline Layout

Figure 2-3 shows the Rankine cycle plant schematic with all the main components and outputs. The solar field will receive the main energy input, with the option of having additional heat supply with a natural gas boiler, and heat will be transferred to the CO_2, which is the working fluid in the power block.

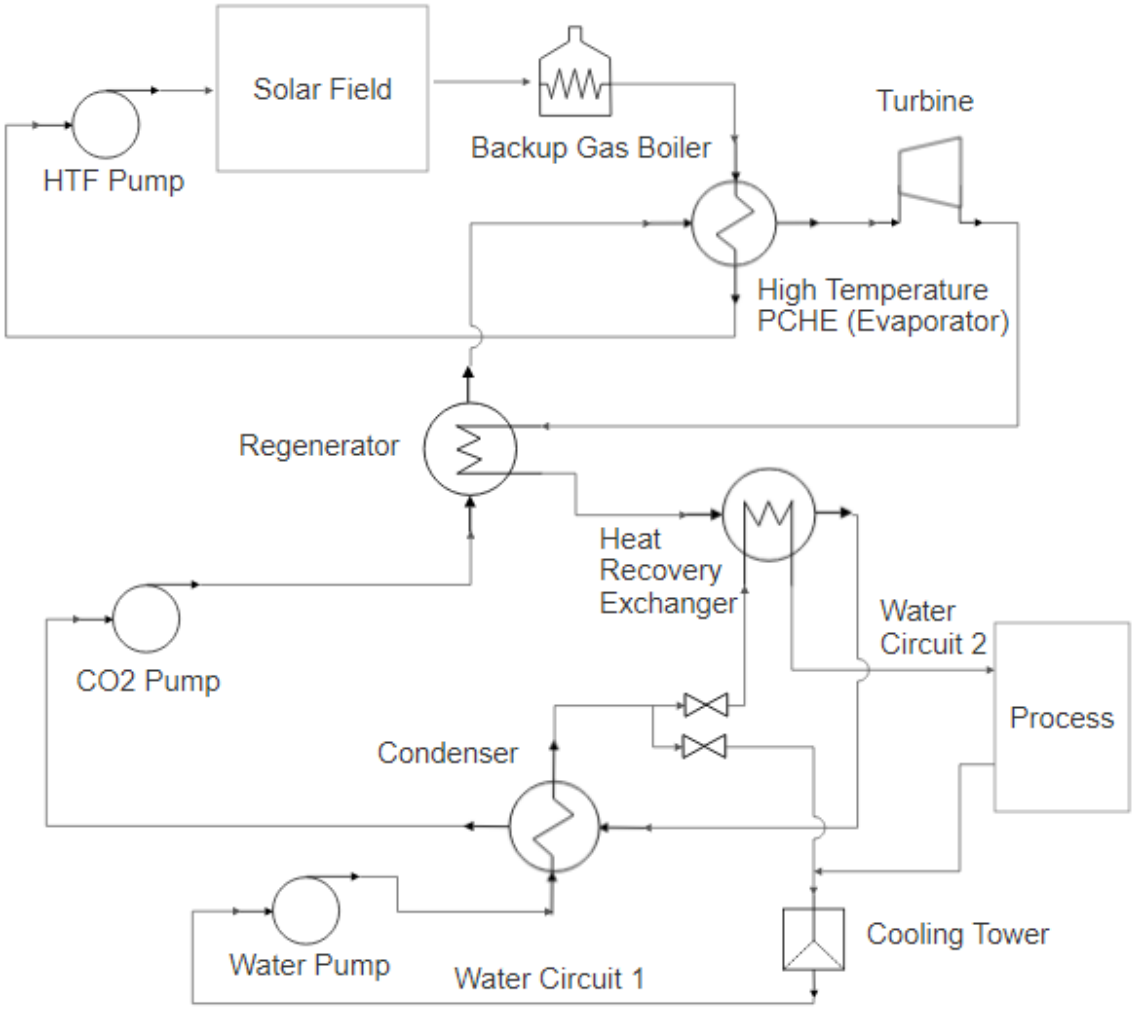

Figure 2-3: Solar plant schematic

2.4. Proposed Alternatives to the Baseline Layout

The study herein was completed for the baseline plant, which is a transcritical Rankine cycle, and iterated for the following alternative layouts:

- **Alternative C. Recompression Cycle**: Preliminary studies showed that an increase of efficiency was available with the recompression cycle.

- **Alternative D. Fully Supercritical Brayton Cycle**: There is an interest in finding out if the condenser provides an actual improvement to the cycle and in what situations it is cost-effective.

2.5. Work Plan

The project consists of three phases: Preliminary Studies, Plant Design and Modeling and Assessment.

- **Preliminary Studies**: This phase includes the basic previous studies on which this proposal is based as well as further investigations on thermal energy storage, cooling and solar energy technology
- **Plant Design and Modeling**: This phase includes the design of the solar field, the power block and its component dimensioning and main features. These components were modeled in order to be simulated with input average weather data. Additionally, this phase was completed for all three alternatives simultaneously and it involved the creation of two major simulation codes:
    i. The Design Simulation Code assists in the design of the plant with simplified modeling that yields approximate performance simulations to assess the impact of different design decisions
    ii. The Analysis Simulation Code assists the Design Simulation Code with a less-simplified modeling that yields performance simulations of the plant for average days of each month in a typical meteorological year.

- **Assessment**: An economic cost model was developed and parameters such as LCOE were estimated for all the proposed alternatives. Conclusions were extracted from this analysis. A sensitivity analysis was also conducted for the baseline cycle, consisting on finding the parameters have the highest impact on the assessment results.

These three phases were accomplished for the two scenarios (A and B, 1 MW and 10 MW, respectively) and three alternatives (Baseline, C, D), but with the focus on the base cases, namely, 1 MW and Baseline cycle. Once the study was accomplished for the base cases, the results would be extrapolated when possible ore else the analysis was repeated when further investigation is of interest.

2.6. Budget and Timeline

The project will have mainly the expenses of engineering labor hours and software licensing. Student licenses are required for Excel, EES and MATLAB, while SAM is a free-use software.

The engineering labor hours allocated to this project consist of a full-time academic semester, which amount to 560 hours. At a rate of $20/hour, typical labor cost for a junior engineer, the project budget will roughly be of $12,000. Since this project has an academic purpose, the actual cost will just be that of the software licenses.

Figure 2-4 contains the Gantt chart of the project with the major tasks and its duration period. All the tasks were accomplished in a total of four semesters, from the Fall of 2018 to the Spring of 2020.

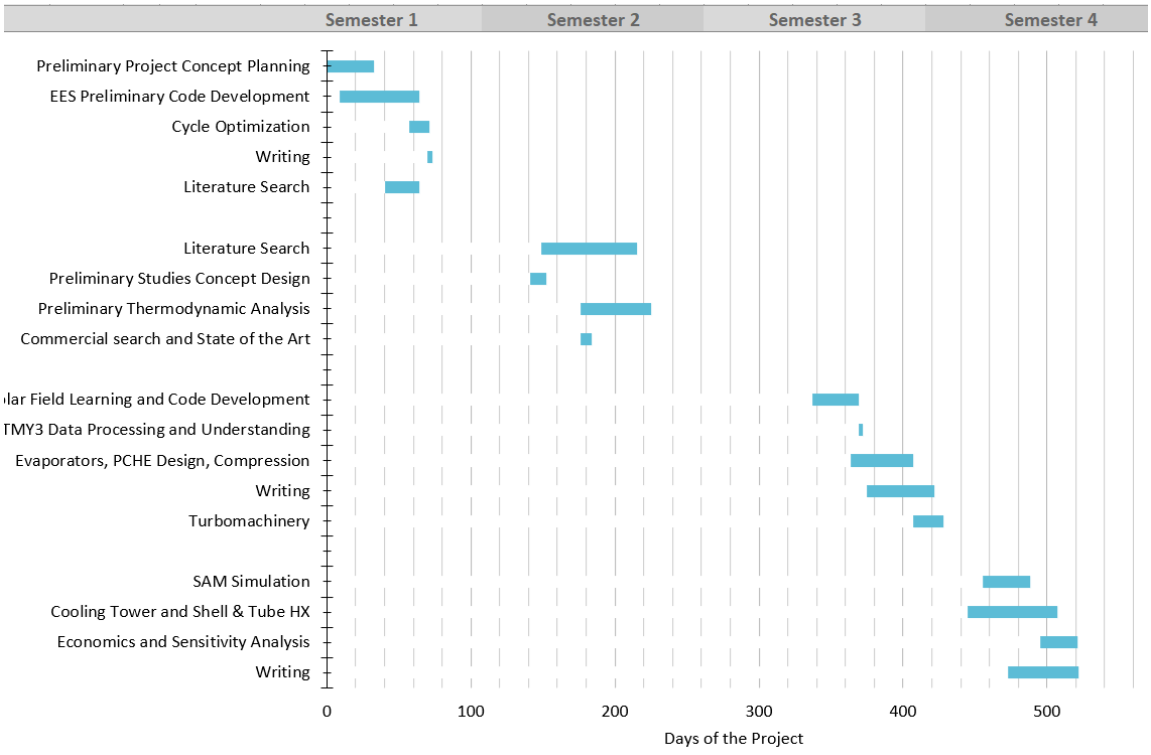

Figure 2-4: Gantt Chart of the project

3. METHODOLOGY

The methodology followed in this project follows a typical pattern that consists first of a learning stage, then design, and then simulation. The steps are described below.

1. **Literature review and learning phase**. By surveying the State-of-the-art and acquiring general knowledge about the topic, enough capability was gained to perform an analysis on the technology. For example, dealing with solar collectors and solar field design, a study of the literature revealed the equations that could be used to model the behavior and main variables of a solar field and collectors. The same learning process was replicated for turbomachinery characterization, heat exchangers, and even the simulation software.
2. **Design and Modeling phase**. For this phase, commercial software was used such as MATLAB, Excel, EES or SAM. For example, solar radiation was modeled with MATLAB by developing a code to process weather data and calculating average radiation values considering the different projection angles. Excel was usually a previous step to EES, which allows by taking certain design assumptions, to obtain parameters dealing with performance of the solar field, power block, etc. Finally, the highest level was achieved with SAM, which is a program developed by NREL that was capable of performing complex calculations and simulations thus allowing the user to input certain parameters in the model. Although SAM is the most user-friendly software, it also constrains the user to the already-developed model. For new technology models, the lower-level software programs provided a more in-depth perspective and allow a better analysis.

3. **Simulation and evaluation of results**. In this final stage, the results were obtained, and observations were made.
4. **Sensitivity and qualification of assumptions**. The simulation would provide at first rough results due to strong assumptions taken for simplifying the model. As progress was made, some assumptions would no longer be valid and in order to obtain more realistic results, models would have to grow in complexity, also incorporating new parameters that make the model more robust and complete.

All in all, the method used for this project consisted of developing models and simulations, starting with simplified versions and then making them more complex. Figure 3-1 shows the methodology flow chart of the project with the main inputs and outputs from each stage. As explained, the iteration of this methodology will lead to more reliable models and better design of the plant as well as more accuracy in the prediction of plant performance and results.

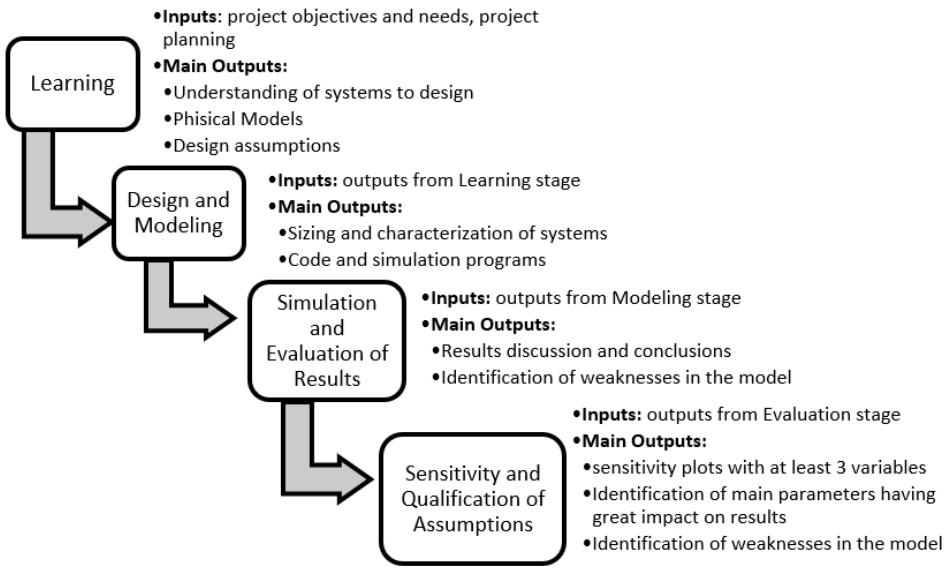

Figure 3-1: Methodology flow chart with inputs and outputs of each stage.

4. PRELIMINARY STUDIES

4.1. Literature Review and State of the Art

An extensive literature review was carried out as a means of learning about different approaches and achievements related to this topic. A recent and thorough overview of the current state of the art of concentrating solar power (CSP) can be found in reference [14], which focuses on the current state of different CSP technologies in terms of efficiencies and other parameters. Parabolic trough collectors (PTC) are shown to be the most penetrating CSP technology. Information on current trends of thermal energy storage (TES) can be found in reference [15], which reveals that TES improves the dispatchability or independence of weather conditions of a CSP plant, and that the most prominent technology is currently the two-tank sensible molten salt storage system.

Also, in the literature, there are a number of student theses that have similar objectives to the present one. A thesis by William Seidel with the title *Model Development and Annual Simulation of the Supercritical Carbon Dioxide Brayton Cycle for Concentrating Solar Power Applications* [16] provided a solid example for the development of the present thesis. This past thesis performed mainly modeling work and unlike the present thesis, it assesses the supercritical CO_2 Brayton cycle. Also, different Brayton cycle configurations were using simplified EES (*Engineering Equation Solver*) models, and finally the simple Brayton with regeneration was selected for further study. As A result, a more detailed model was developed with a deeper insight in the heat exchangers' design and different cooling techniques (water/air/hybrid cooling). This

model was implemented in the TRNSYS software through linear regression for modeling of molten salts storage and simulation of annual performance. The result was an annual net efficiency of 41.6% for high temperatures and pressures of 900 K and 25 MPa, respectively, which were achieved by means of additional fossil fuel burning.

A thesis by Abdullah AlZahrani with the title *Development and Analysis of a Solar-Based Integrated System with a CO2 Rankine Power Cycle* [17] served also as an useful example of previous work. This study was based on the supercritical CO_2 Rankine cycle integrated with a PTC field, a two-tank thermal energy storage and an absorption refrigeration system with the function of recovering the low grade heat from solar collection (low grade meaning with a temperature not high enough to fuel the cycle) to produce an additional chilling effect that lowers the temperature of heat rejection and therefore increases the cycle efficiency. In the aforementioned work, the focus is on the system's performance through energy and exergy analyses, with the result being that the cycle reaches an energy efficiency of 31.6%, with the overall heat-to electric efficiency being 11.73%.

Another interesting study was performed by Angela M. Patnode, who wrote a thesis under the title *Simulation and Performance Evaluation of Parabolic Trough Solar Power Plants* [18]. A whole PTC plant with a steam Rankine power cycle was modeled, and it was found that while the solar field efficiency decreases with increasing the field outlet temperature, the power cycle efficiency increases. As a result, the net change in overall efficiency with outlet temperature change is small, revealing that there is an

optimal operating outlet temperature in the solar field, which was estimated at around 350ºC according to this model.

The dissertation by Vaclav Dostal, *A supercritical Carbon Dioxide Cycle for Next Generation Nuclear Reactors* [19] is an exhaustive work that lays the foundations for research on CO_2 power cycles. A system design and optimization was performed that concluded that the recompression cycle is the one that outperforms in simplicity, compactness, cost and thermal efficiency. The high temperature and pressure for the working fluid in the study was 550ºC and 20 MPa respectively, showing that this design is suitable for nuclear reactors. An economic analysis was also performed to estimate the cost of the power plant with the cycle thermal efficiency being as high as 45% and the cost reduction of the power plant 18%. Turbomachinery design and heat exchangers design are also included in this work.

Numerous articles and conference proceedings have been made available through the International Supercritical CO_2 Power Cycles Symposiums [20]. These are conferences that gather all the different research contributions to the investigation on this technology. A remarkable work is *A Practical Look at Assumptions and Constraints for Steady State Modeling of sCO2 Brayton Power Cycles*, by Nathan Weiland and David Thimsen [21]. This work sums up the appropriate design conditions for these kind of cycles.

Other important references from the sCO_2 symposium were [22], [23], [24] and [25] from Southwest Research Institute (Dr. Jeff Moore), from HEATRIC (Renaud LePierres), from NETL (Mr. Nathan Weiland) and from SuperCritical Technologies

(Mr. Steven Wright). These references cover analysis of the cycle components as well as design and performance.

4.2. Solar Technology Selection

Different approaches have been made to implement the CO_2 Rankine cycle with some of them using non-concentrating solar collectors, while others used concentrating solar power. In this thesis the first question to be answered was: what are the advantages of each technology and which one is the most suitable for the study that is being carried out herein?

4.2.1. Solar Evacuated Tube Plant at a Rooftop in Texas A&M University

An initial study was carried out with non-concentrating ETC (evacuated tube collectors) as the solar collecting equipment. A fictional plant was designed for installation on a rooftop of a commercial building in College Station, TX, and simulated with a simplified model following several references: [26], [27], [28]. The working fluid was also the heat collecting fluid. The plant was composed of a total of 280 collectors of the type of U-pipe VDF-30 SunMaxx-30U, with their aperture area being 28.8 ft^2 (2.677 m2), representing a total collecting area of 750 m^2. The assumptions made in this study are as follows:

- Heat sink temperature. The heat sink was assumed to be a stream of water available throughout the entire year at temperatures below 22^oC based on the possible use of cooling towers achieving the lower wet bulb temperature if needed. This temperature was a lower limit for the temperature to which the CO_2 can be cooled and therefore,

the CO_2 condensing temperature was set at 25ºC, assuming a 3-degree temperature was sufficient.

- Heat collecting pressure. For all commercial ETC, the highest value encountered in the literature was 1 MPa, which if used would limit the efficiency. As a result, there was a need to assume that the collectors used in this study are more advanced than existing commercial ones since the cycle requires a higher pressure to be feasible. The research conducted [26] shows that it is possible to increase the pressure to values from 7 to 10 MPa, and therefore, a design maximum pressure of 10 MPa was assumed.
- Maximum temperature and heat collecting efficiency. The modeling of the heat transfer inside the ETC, although feasible, was beyond the scope of this project. Therefore, the cycle was designed for the maximum reachable temperature, required to maximize the power output from the turbine. Also, it was assumed the heat input would be given by the typical efficiency of the collector. It was found that the experimentally measured values of the maximum temperature are around 170ºC [26]; however, a maximum operating temperature of 250ºC for the collector materials at high pressure was also reported [26]. Also, the solar collecting efficiency lies between 65 and 70% [26]. The values of maximum temperature and heat collecting efficiency were therefore set at 175ºC and 68% respectively.
- Pressure losses were assumed to be zero in an initial approach.
- For the pump and turbine components, there was a shortage of information for commercial items were found. Research is currently ongoing for CO_2 turbines, and

those states that result in high efficiencies [29]. Similarly, pump efficiencies are being evaluated and they are typically quite high [30]. The theoretical values of the isentropic efficiencies for both pumps and turbines were therefore set at 90%.

- The inlet to the pump was assumed to be saturated liquid following the constraint of not going below the condensation temperature while cooling.

The plant was simulated under typical meteorological conditions throughout the year. For this purpose, a mean day for each month's meteorological data was used as input to the model, coded in the EES software. An exergy analysis was also performed and cycle improvements were studied by incorporating pre-compression i.e., cooling at lower pressures and then compressing before condensation, and regeneration i.e., preheating the fluid by using the waste heat in the turbine outlet. The following conclusions were reached:

- The output power was 35kW for nominal (standard) conditions and the baseline cycle which corresponds to an annual average of 150kWh per day (equal to constant 6.25 kW during 24 hours). This power is be enough to light the building on whose rooftop the plant is placed. With the discussed improvements, the efficiency of the plant can be increased in the range of 8-14%.
- The surface area is roughly 10,000 ft^2 or 1000 m^2 (collecting surface plus additional surface) which makes a power per unit surface of 35W/m^2. As a result, the collecting surface is roughly 750 m^2.
- Other interesting findings were that increasing the maximum temperature does not make a difference when it is above a certain value and improvements in the cycle,

such as ideal regeneration, can make a significant difference by possibly doubling the output power.

- Thermodynamic cycle values were fixed based on certain assumptions, which are allowable in a design phase. However, the real performance of the plant may be affected by other conditions that are not being considered such as the following:
  i. Mass flow may not be independent of pump pressure. In order to keep as close as possible to design values mass flow must be allowed to vary in a range from 0.1 to 1.6 kg/s. Commercial rotordynamic pumps have been found that may adapt to these requirements (thomasnet.com/products/carbon-dioxide-pumps-64320500-1). Once the mass flow is determined, the actual plant could be simulated and optimized for maximum efficiency and power output. However, this is beyond the scope of the preliminary studies.
  ii. Cycle maximum temperature: This value depends on the available mass flow and the heat transfer through the collectors. The collection efficiency was set as a constant, and efficiency optimization throughout the year should be affected by the qualification of this assumption.
  iii. Temperature of cooling water was unknown. An upper limit of 22^{o}C was assumed, but it is likely that in the winter the minimum temperature of the cycle can be lowered obtaining a higher efficiency.
- The actual cost of the plant is likely not competitive since it seems to be more expensive than other technologies in the market. To achieve high efficiencies, higher

pressures must be reached. The components of the plant, such as turbine and solar collectors, although yielding great performance levels are yet not marketable.

- Comparison with photovoltaics: commercial photovoltaic solar cells tend to have a minimum price of 1700$/kW in Texas [31] with a commercial efficiency from 8 up to 20%. Because the cost of a photovoltaic plant of the same nominal output power (35kW) is $60,000, one would expect the Rankine system to be competitive if it had a comparable cost.

4.2.2. Economic Analysis for Non-concentrating Solar Power

Given the output from the previous section, the main concern was to make the solar plant competitive against current market trends such as photovoltaics. For commercial and industrial applications, the price of solar photovoltaic energy is estimated at 1.8 $/W [2]. This is the price per rated power of the solar cell. The rated power of a solar cell is measured under certain conditions such as 1000 W/m^2 of solar irradiation, AM1.5 (air mass) and a 25^{o}C junction temperature [32].

Under similar solar irradiation, the studied rooftop ETC plant was simulated, for more unfavorable assumptions, such as decreasing the turbine isentropic efficiency to 80%. However, regeneration was incorporated, rising the plant efficiency by 12% under nominal conditions. The solar collecting area would be 750 m^2, as discussed in the previous section, and with 1000 W/m^2 the impinging heat would be 750 kW. With a solar collecting efficiency of 70% and a cycle thermal efficiency of 12%, the output or "rated" power of the ETC plant would be:

$$0.7 \cdot 0.12 \cdot 750 = 63kW$$

The same rated power in photovoltaics would cost $113,400. If the studied plant has 280 collectors, as described in the previous section, each collector should cost a maximum of $405 for the plant to be cheaper or comparable in price to a photovoltaic one. After looking up typical commercial prices for ETC it was concluded that such low price would be unreachable for the studied plant herein. Even if those prices were matched by existing component costs, which is possible through wholesalers, the additional equipment and installation costs would certainly make it difficult to compete in the market. In addition, it is doubtful that a low price ETC, with its lower performance, would yield a temperature high enough to achieve a cycle efficiency that would allow for an investment payoff.

The above argument is also applicable to flat plate solar collectors. Although they are cheaper, the outlet temperature is not high enough to compete in terms of efficiency, with this fact being proved in a later section during a thermodynamic cycle analysis. An additional investment complication is that the solar collectors would have to be designed to work with CO_2, which is not an established marketable technology.

In addition, it was found in the open literature that solar thermal prices can be 20% of the cost of PV [33]; however, this article was written in 2008, when the price of PV was about 5 times higher [2]. Currently, solar PV cells provide better performance in electrical energy generation than what solar thermal non-concentrating systems can achieve for the same cost. Case studies of solar thermal systems in industry reveal that to achieve reasonable efficiencies temperatures are insufficient in non-concentrating

systems [34]. However, high temperatures are still possible with ETC if reflector plates are incorporated, which evidently increases the cost.

A case study reveals that a solar thermal system that delivers 10 therms per day (293 kWh) would have a capital investment of some $60,000 [35]. If this system was to fuel a CO_2 power plant, the average input power to that plant would be 12.2 kW; and the net output power from that plant would be 1.465 kW; assuming the constant heat-to-power efficiency. This case study is located in Oakland, CA, where the annual average global solar irradiation is 4.5kWh/m^2-day, or 187.5 W/m^2 [36]. Extrapolating to rating conditions of 1000 W/m^2, this plant would have an output electrical *rated* power of 7.8 kW as shown below.

$$1.465kWe \cdot \frac{1000 \text{ rating}}{187.5 \text{ annual average}} = 7.8kWe$$

A PV plant with the same output power would cost $14,064 (at $1.8/W). This example clearly shows that a solar-thermal non-concentrating generation plant is not economically competitive, although substantial aid from the government to start and suggest the technology might make it viable. This technology does not produce an advantage against solar PV except for the collection of energy in the form of heat, which might be desirable for some cases. In California, where the solar resource is not scarce, conditions are favorable for the solar thermal plant to collect more energy for the same cost.

One last case study, also in California i.e. San Marcos, satisfied a gross annual heat demand of 3900 therms, or 10.68 therms/day [37]. The investment out-of-pocket for the project was $43,600, which per thermal kilowatt means $3,340/kWth, or $3.3/Wth.

This thermal kilowatt is produced for 5.4 kWh/m^2-day, or an average of 225 kW/m^2. Extrapolating to the same rating conditions as for PV, a price per rated thermal watt of $0.74/Wth would be obtained. Again, this proves it not competitive in the solar energy market of power generation, knowing that for every thermal watt, roughly 0.12 electrical watts would be produced.

As a result of this study, it was concluded that the implementation of the transcritical CO_2 cycle needs a solar thermal technology that provides a more clear advantage, such as concentrating solar power. Efficiencies achieved with CSP might then be higher than those of PV due to higher outlet temperature. Moreover, the waste heat from the electricity generation process may still have a temperature high enough to be useful in a cogeneration system. In addition, concentration is also favorable because it supplies more energy with less of an area requirement.

4.3. Thermodynamic Analysis

After the first approach for the thermodynamic cycle studied in the rooftop plant at Texas A&M University, a more in-depth analysis of this cycle under different constraints still had to be performed. In this section, different improvements to the cycle were considered as well as the influence of different conditions for the cycle operation, such as the maximum temperature of the cycle. For instance, the value of the maximum temperature could be low (flat plate solar collectors), medium (evacuated tube solar collectors) or high (parabolic trough solar collectors).

Heat input for the cycle would vary between 200 and 1000 kW. With this value depending on the hours of storage and the hours of generation. At this point of the study

it does not matter if the plant operates for 6 hours receiving 500 kW or for 12 hours receiving 250 kW from the storage. However, the heat input does provide useful information for pipe sizing, since the more heat input, the more mass flow rate of CO_2 would be needed to achieve the same high temperature, which is a cycle design constraint.

4.3.1. Simple Rankine with Regeneration for Medium Temperature and Pipe Sizing

The assumptions taken were the following:

- Maximum temperature: 175ºC. Assuming energy is stored at around 200ºC, CO_2 would collect heat from storage.
- Maximum pressure 10 MPa.
- Condensation temperature: 25ºC. Assuming water is available to drop heat to at a maximum temperature of some 20ºC.
- Heat input: 500 kW.
- Pump and turbine efficiencies: 80%. Reasonable value.
- Pressure losses assumed zero.
- Regeneration efficiency assumed 100%.
- Heat losses and pressure drops in pipes assumed zero.

Cycle performance was summarized in the efficiency results, with the first law efficiency being 11.24%. The second law efficiency (ratio of the efficiency of the cycle with respect to a Carnot cycle efficiency operating between the same extreme temperatures) was 33.59%. Figure 4-1 shows the temperature-entropy diagram for this cycle, with points 5 and 6 in the diagram being the reference points for regeneration.

Heat is absorbed in the high-pressure stream from 4 up to 6, and this heat comes from the low pressure stream from 2 to 5. The temperature at 6 should not be higher than at 2, and temperature at 5 should not be lower than at 4. The most constraining requirement is the latter one.

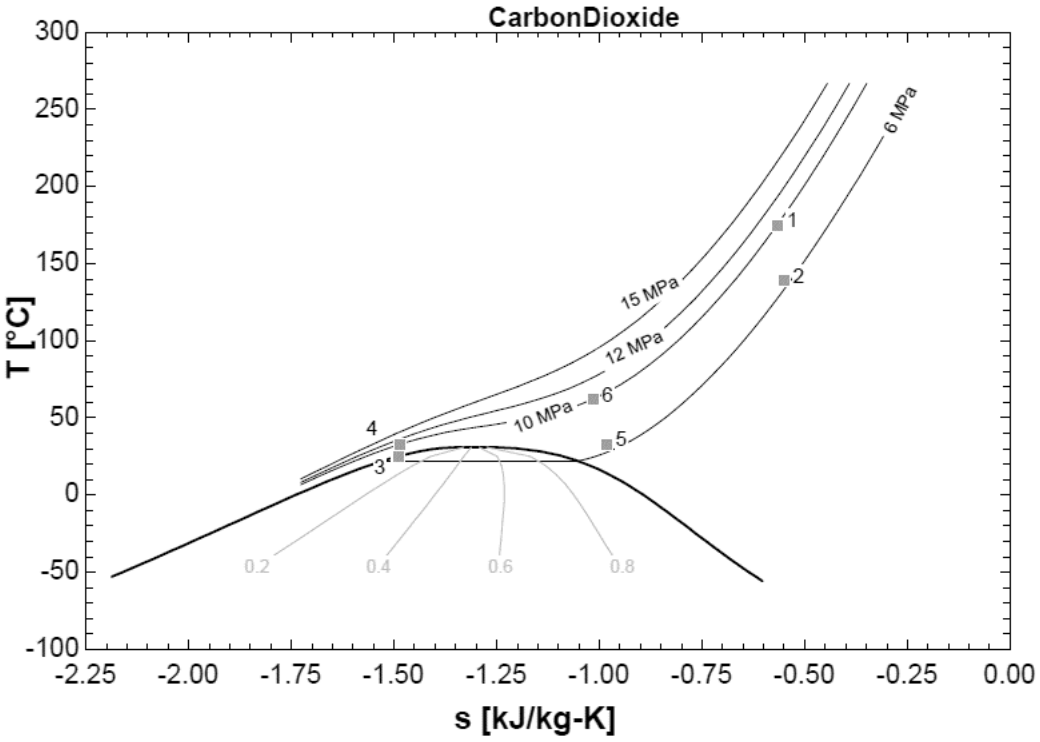

Figure 4-1: Simple Rankine with regeneration T-s diagram

One concern about the CO_2 cycle was the high pressure required in the heat collection process. If pipes need to be large in order to transport the CO_2 flow rate, the high pressure makes large pipes more expensive compared to small pipes. A first approach study was performed to determine whether pipe sizing could make high pressures feasible.

The CO_2 mass flow rate is 2.923 kg/s in this Rankine cycle configuration. In pipe sizing, typical fluid velocities in pipes must be followed to avoid problems such as

vibrations or pipe wear. Air, hydrogen and natural gas in pipes usually have a fluid velocity of 20 to 30 m/s [38], while liquids typically have a velocity of 1.2 to 1.8 m/s. The assumption was made that these velocities are comparable to the design velocities for CO_2 at high pressure. Densities were calculated for points 1 and 4 in the cycle, which are the two extremes at high pressure. With a 1 ½ inch carbon steel pipe, schedule 80, CO_2 fluid velocity at point 1 in the cycle is 19.35 m/s. Although it is low, it is on the order of typical gas velocities. As to the liquid fluid velocity, at point 4 in the cycle, it is 3 m/s, which is on the order of liquid velocities too. Reynolds numbers for both points are turbulent as they should be in a typical pipe flow.

The maximum allowed pressure allowed at 200ºC for this pipe is 3977 psi, or 27.42 MPa [39]. This is an allowable limit that is way above the actual pressure used in the cycle. Although certain inaccurate assumptions were taken to perform this estimation, the viability of the high pressure is well assured with carbon steel pipes.

4.3.2. Simple Rankine with Low Temperature

This simulation analyzes the performance of the CO_2 cycle operating with flat plate solar collectors storing energy at some 90ºC. The assumptions taken were the following:

- Maximum temperature: 75ºC. Assuming we are able to store energy at around 90ºC.
- Condensation temperature: 25ºC. Assuming we have water to drop heat to at a maximum temperature of some 20ºC.

  Maximum Carnot efficiency with those temperatures is 14%.
- Maximum pressure: in a range from 10 to 21 MPa.

- Heat input: 800 kW. Bigger to keep the mass flow rate not too far from the previous one. However, note that if pipes are smaller, pressure is allowable to be higer.
- Pump and turbine efficiencies: 80%. Reasonable value.
- Pressure losses assumed zero.
- No regeneration.
- Pipe inside diameter 1.939” for a 2 in pipe schedule 80.
- Heat losses and pressure drops in pipes assumed zero.

Results for this cycle are not favorable. However, the main outcome of this simulation is the finding that there is an optimum maximum pressure for a set of maximum and minimum temperatures in the cycle. If the pressure were too high, the pump specific work would surpass turbine work, and if it were too low, the turbine specific work will not be very high. For this system, the optimal pressure is about 12 MPa. Figure 4-2 shows the temperature-entropy diagram for the optimized cycle. The efficiency achieved is 4.9%, which is very low and not competitive against other technologies.

Figure 4-3 shows the contour plot achieved for the parametric variation of both the maximum temperature and the maximum pressure of the cycle. As it can be observed, a maximum energy efficiency of 6% can be achieved if the maximum temperature of the cycle is below 100^{o}C. After this, the optimal pressure was also obtained through parametric table simulation in EES for the previous case (maximum temperature of 175^{o}C), resulting in a value of 17 MPa. The cycle efficiency for this

pressure would 14.8%, which shows a significant improvement with respect to the 11.2% with 20 MPa.

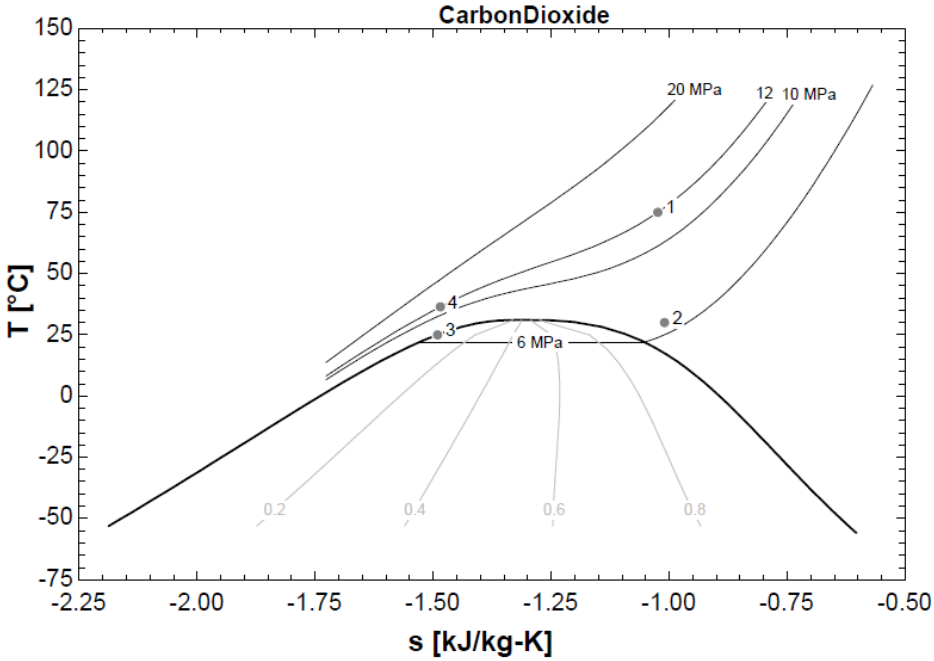

Figure 4-2: T-s diagram, simple Rankine, low temperature

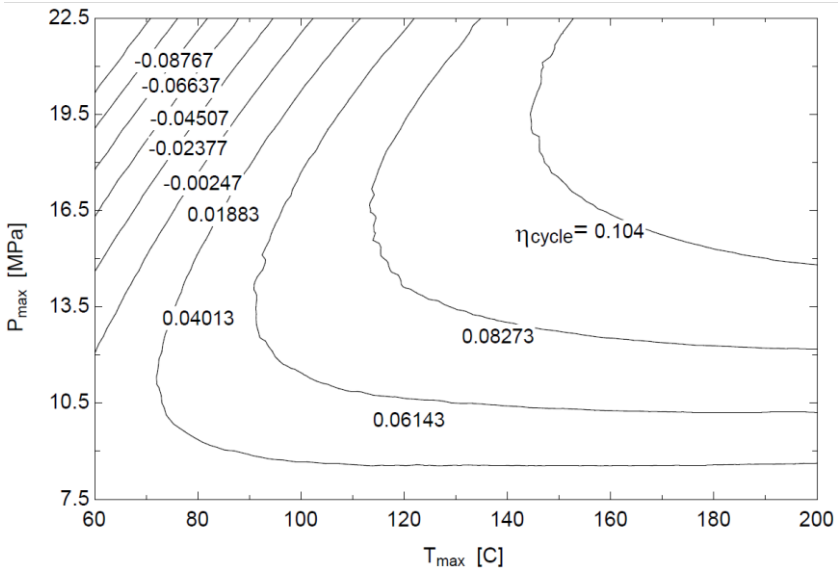

Figure 4-3: Efficiency contour plot for different values of maximum pressure and maximum temperature

4.3.3. Reheating Rankine with Low Temperature

An option to try to "save" the previous cycle was to incorporate the reheating technique, which consists of expanding the working fluid to an intermediate pressure and then heating it again up to the maximum temperature to expand it afterwards in a second turbine. This introduces a new parameter to consider, namely the intermediate pressure. With the same assumptions as in the previous case (maximum temperature of 75°C, etc.) a contour plot was developed to find the highest efficiency for a set of high and intermediate pressures. Figure 4-4 shows this plot. It was found that a peak efficiency is in the region of 12 MPa maximum pressure and 10.5 MPa intermediate pressure. With an efficiency of 5.95% being achieved at these conditions. Figure 4-5 shows the T-s diagram for this cycle, with points 7 and 8 being the new points for the reheating process.

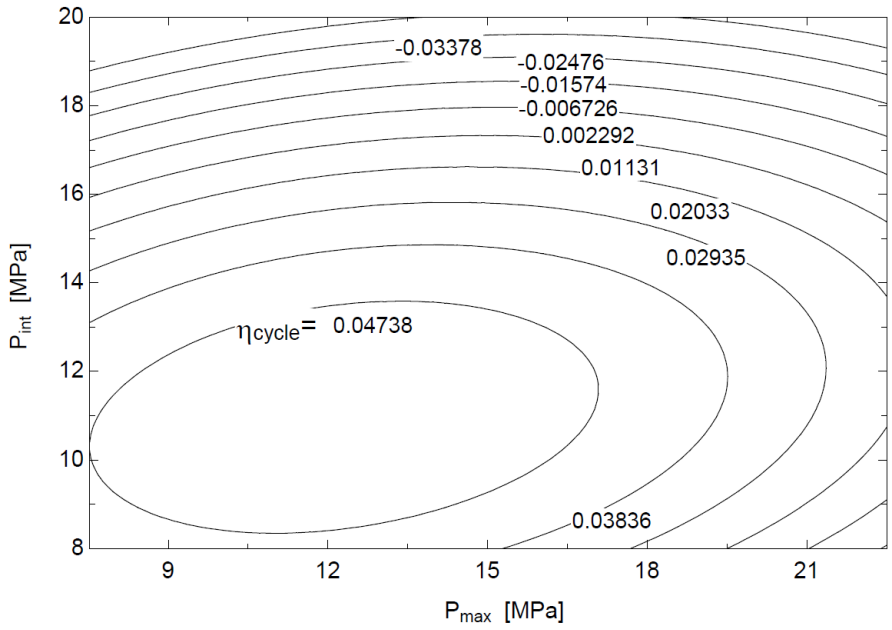

Figure 4-4: Efficiency contour plot for maximum and intermediate pressures

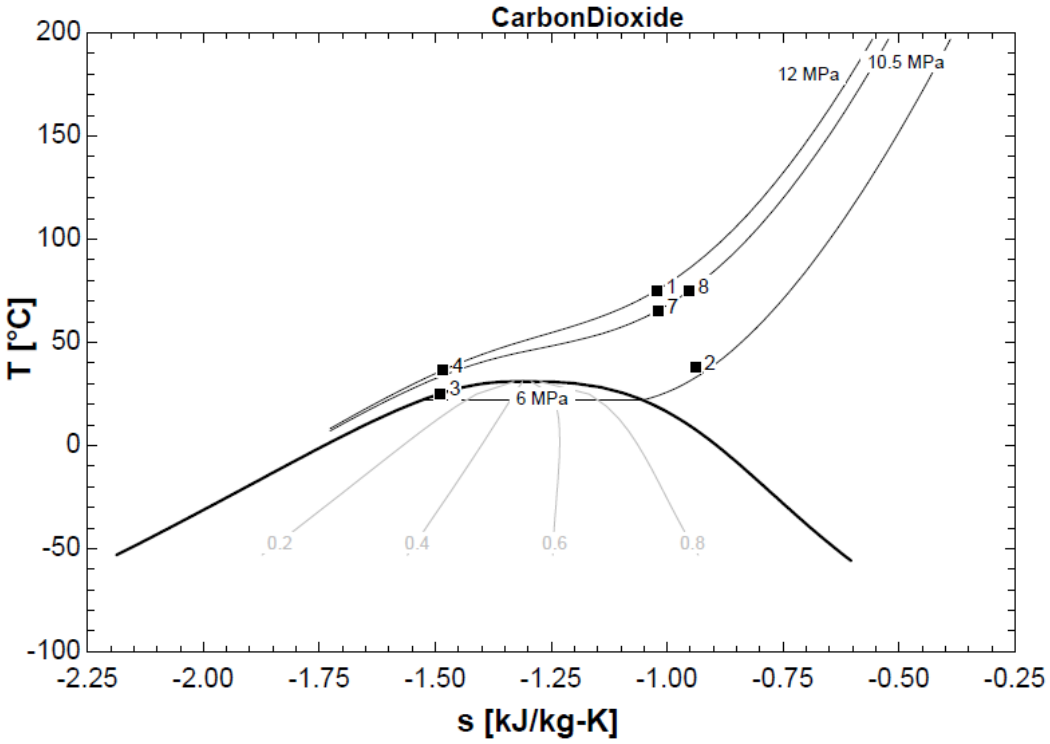

Figure 4-5: T-s diagram, low temperature, reheating

Although efficiency has improved approximately 1 percentage point, it is still very low and not competitive. This shows that the improvement is not likely worth the investment.

4.3.4. Simple Rankine with Regeneration for High Temperature

For this model, the assumptions are more realistic in terms of heat exchanger effectiveness and pressure drops:

- Maximum temperature: 325ºC. Assuming energy can be stored at around 350ºC through parabolic trough collectors (PTC).
- Condensation temperature: 25ºC. Assuming water is available to transfer heat to at a max temperature of some 20ºC.

  Maximum Carnot efficiency with these temperatures is 50%.

- Maximum pressure: in a range from 16 to 40 MPa, which could be larger depending on the pipe size.
- Heat input: 1000 kW. Higher than previous models, but the kJ/kg collected by the CO_2 in the cycle is also higher as represented by the area below the upper constant pressure line from 6 to 1 in the T-s diagram.
- Isentropic efficiencies: pump 80%, turbine 90%.
- Pressure losses assumed on the order of 1 atm (it should be much less). The condenser pressure drop is even less than in the evaporator, namely 1% according to a reference of commercial HVAC coils. [40].
- Regenerator heat exchanger effectiveness is 80%, the enthalpy change from points 2 to 5 is 80% of the ideal enthalpy change (when $T_5 = T_4$).
- Losses to the environment from heat exchangers and pipes are assumed negligible.
- Pipe inside diameter 1.939” for a 2 in pipe schedule 80.

Figure 4-6 shows the T-s diagram for the cycle. The dashed lines illustrate the entropy generation in the expansion and compression processes. As shown in Figure 4-7, the optimal pressure for this cycle was found to be about 33 MPa, with an efficiency of 23.93% and a second law efficiency of 47.19%. Both first law and second law efficiencies are relatively high.

If the turbine isentropic efficiency is increased to 90%, which is a value consistent with the literature [19], the plant efficiency is increased to 27.57%. Of course, for this new turbine efficiency there is a new optimal pressure at 35 MPa, which results

in an efficiency value of 27.6%, close to the previous one. In this case, even a maximum pressure of 27 MPa has efficiency above 27%.

There is also an interest to find out if the low temperature heat rejection can be applied to a cogeneration system. In the case of 90% turbine isentropic efficiency the turbine outlet temperature is always above 150°C for maximum pressures higher than 27 MPa. After regeneration, T_5 is always above 70°C. As a result, hot water could be produced for low temperature applications.

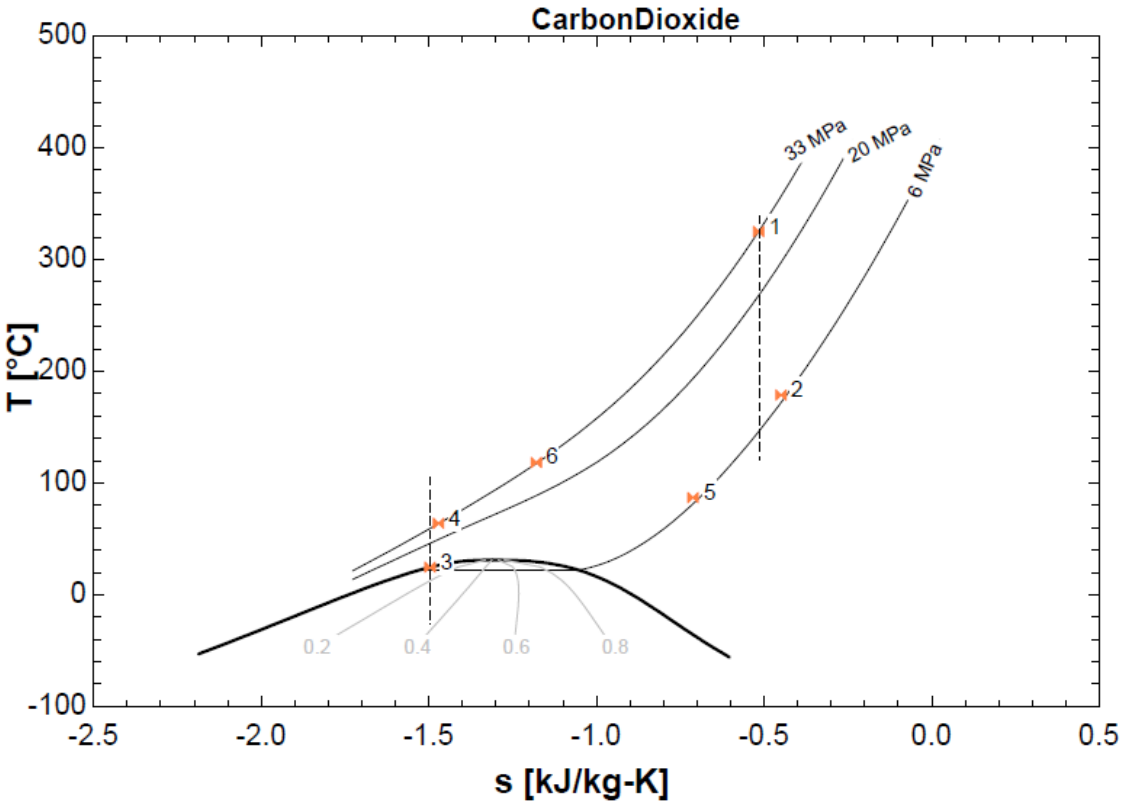

Figure 4-6: T-s diagram, high temperature, regeneration

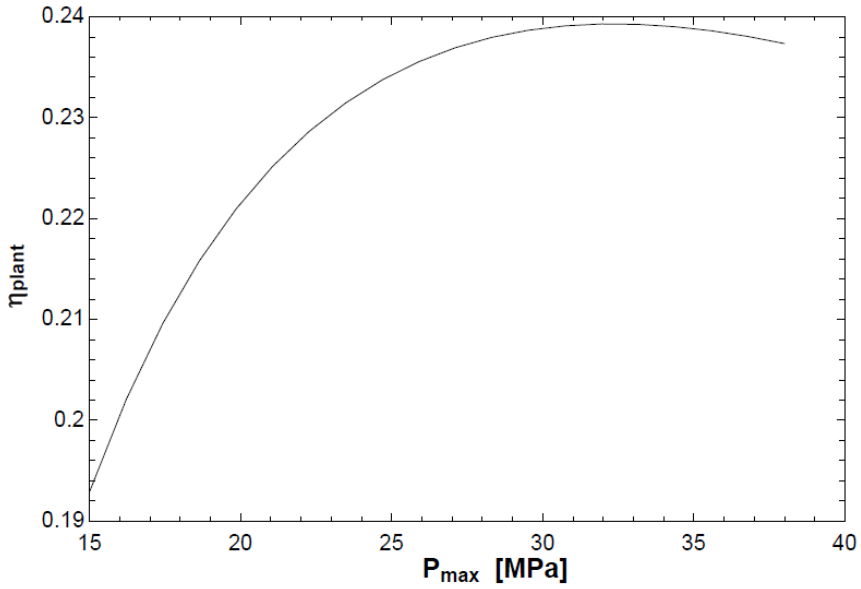

Figure 4-7: Variation of efficiency with maximum pressure for the T_{maz}=325ºC cycle with regeneration

The regeneration process can also be interrupted at some intermediate temperature between the two temperature points discussed (150 and 70ºC) for the low-pressure stream in the event of needing process heat at a higher temperature. For example, stopping regeneration at 110ºC (T_5 = 110ºC) would result in a cycle efficiency of 25%. This action has the advantage in that the cycle efficiency is still high, and a higher temperature is achieved in case it is needed for the process heat. Figure 4-8 shows the T-s diagram for these cycle conditions with the implementation of the discussed changes.

Comparisons with studies in the literature were made too, in order to validate these results. With 500ºC turbine inlet temperature and 95% regeneration effectiveness, Munoz finds the efficiency of a supercritical CO_2 Brayton cycle to be 33% [41], while in this study, with 325ºC and 80% regeneration effectiveness, the cycle efficiency is 30%.

These results align with this research and in addition it is logical that for a higher maximum temperature, a higher efficiency is achieved. In addition, the Brayton cycle typically operates with a higher minimum temperature above critical point, which, in contrast, decreases efficiency. All in all, results are reasonable.

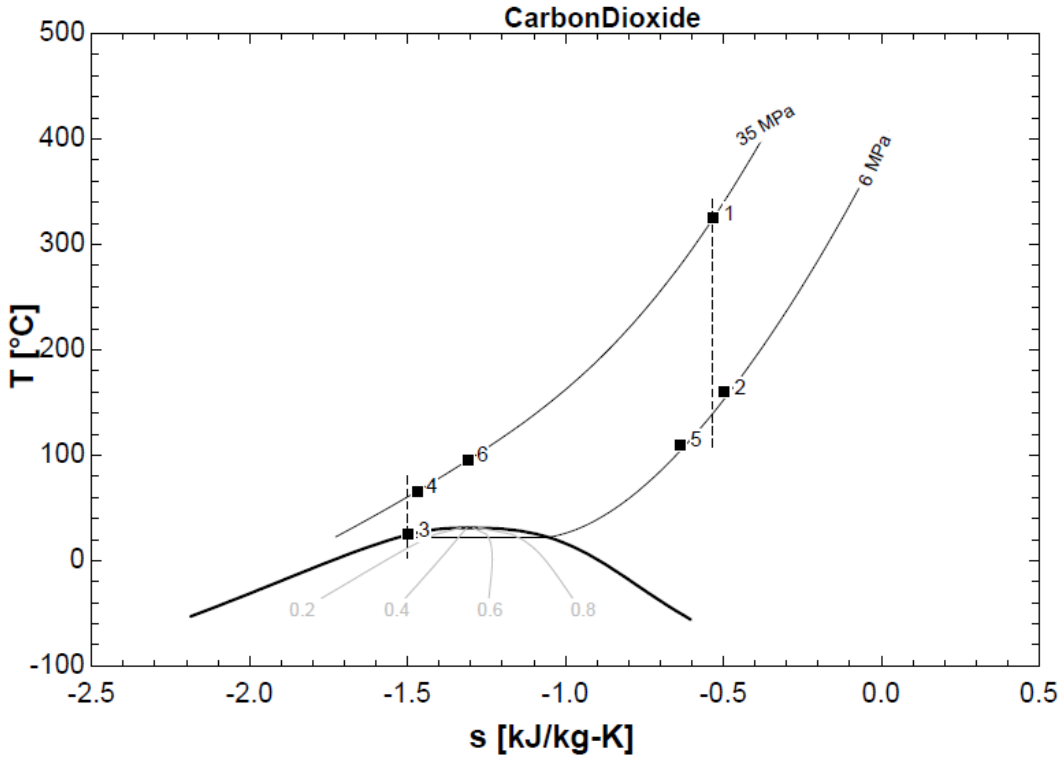

Figure 4-8: T-s, high temperature, maximum pressure optimized for turbine isentropic efficiency of 90%, regeneration interrupted at 110ºC

In the case of a steam power plant, cycle efficiencies found in literature amount to 38% for a 50 MW power plant [42]. Patnode [18] found the maximum global efficiency for their PTC plant working with a steam cycle to be 22%. From this, one can conclude that unless CO_2 provides an advantage in terms of cogeneration at industrial scale or reduction of capital cost, it is doubtful that CO_2 systems would be preferable to steam, in terms of electric efficiencies. However, the CO_2 Rankine can still be further

optimized, and as explained in the Introduction Chapter, CO_2 systems are much more compact and likely cheaper than steam systems.

4.3.5. Reheating Rankine with High Temperature and Regeneration

The assumptions for this system were fundamentally the same as the ones discussed in the previous section. Turbine efficiency was set at 90% following the literature information [19]. Reheating at an intermediate pressure was incorporated in that its advantages are not only an increase in efficiency but also an increase in temperature available for process heat at the outlet of the regeneration process. Another advantage of reheating is having less mass flow rate for the same input heat at high temperatures, meaning that as the fluid is reheated, the kJ/kg increase results in less mass flow rate needed to collect the same kW from the high temperature source.

Figure 4-9 is a result of pressure optimization. Compressing first to 30 MPa and then reheating at 17 MPa gives a high efficiency to the cycle, namely 29.04%. Reheating increases the efficiency roughly one and a half percentage points from the 27.4% value achieved at 30 MPa with no reheating. The mass flow rate for the simple optimized Rankine Cycle with a 90% isentropic turbine efficiency was of 3.0 kg/s, and the temperature after regeneration is $T_5 = 82.8^oC$. Several plots were generated to provide insight into the effect of reheating in the cycle. The first one (Figure 4-10) is also the one used to find the optimal combination of maximum and reheating pressures. For all these following plots, the value for the cycle without reheating can be found where $P_{max} = P_{reh}$, or in other words, in the line that crosses the plot diagonally. Also, it can be observed

that the values above this line have no physical meaning since the reheating pressure is designed to be below the maximum pressure.

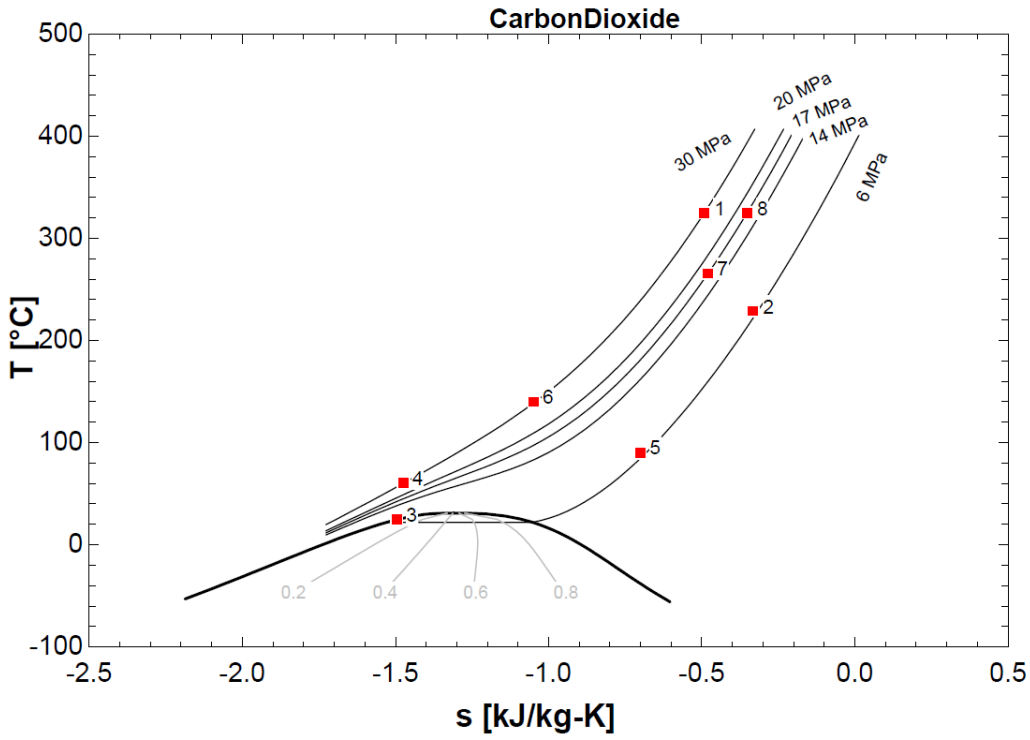

Figure 4-9: T_s diagram, high temperature, reheating, regeneration

Figure 4-10 is the efficiency contour plot for a range of maximum and reheat pressures. The improvement in efficiency increases for higher maximum pressures. For instance, at 30 MPa of maximum pressure, if the reheating pressure is also 30 (no reheating), the efficiency is about 27%, while if reheating pressure is decreased to 17 MPa, efficiency is increased to 29%. However, if the reheating pressure, P_{reh} is decreased too much, the efficiency will start decreasing again more sharply. Figure 4-11 shows a mass flow rate contour plot for a range of maximum and reheat pressures. If the objective is to look for a smaller pipe to withhold the pressure, which is better from a design standpoint, a lower mass flow rate would be beneficial. Therefore, reheating is

also good for piping design, as observed in the contour plot, where the mass flow rate decreases when we decrease the reheating pressure.

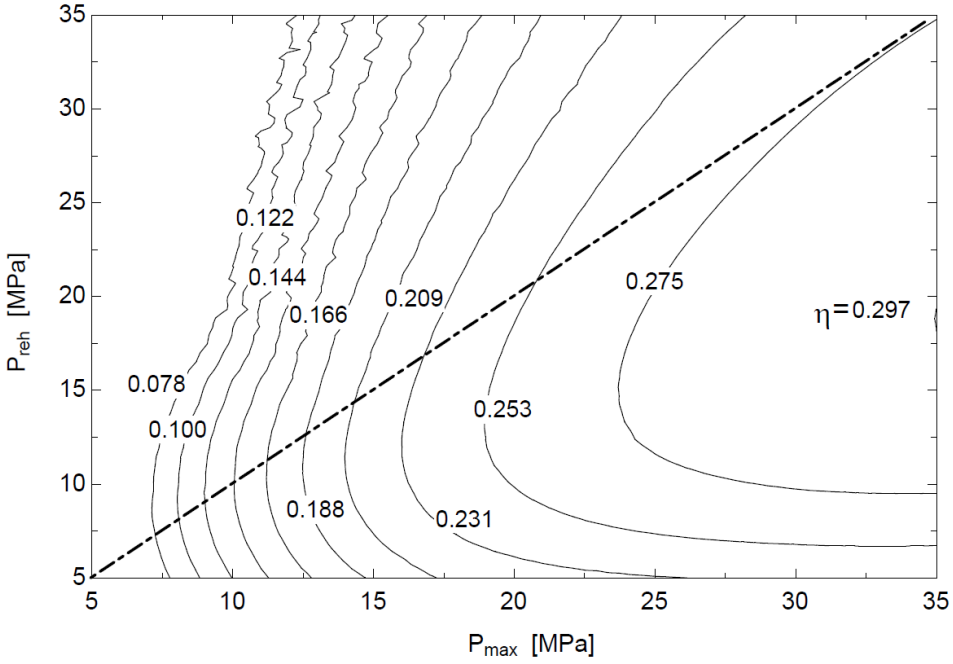

Figure 4-10: Efficiency contour plot for maximum and reheating pressures

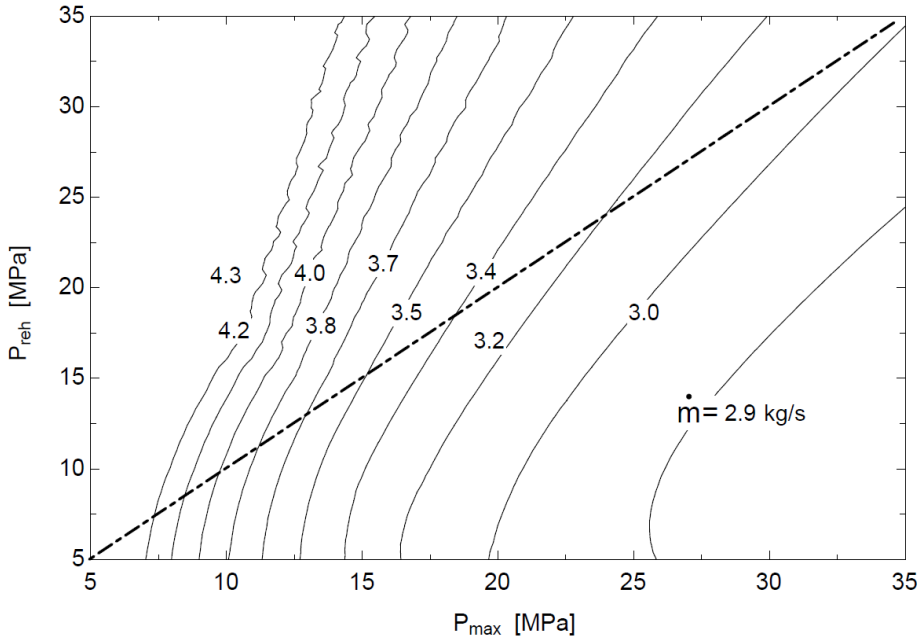

Figure 4-11: Mass flow rate contour plot for maximum and reheating pressures

Figure 4-12 and Figure 4-13 show the cycle potential for cogeneration. The higher the temperatures, then the more useful is the heat rejected. The fluid temperature after the turbine outlet depends only on the reheating pressure in that the temperature increases for a decreasing P_{reh}. As to the temperature after regeneration, T_5, it also increases with reheating, but its increase is not too steep.

Another measure of the cogeneration potential is the amount of heat rejected. It is logical that if cycle efficiency increases, then the heat transferred to the low temperature might be less, recalling the equation of the cycle efficiency:

$$\eta = 1 - \frac{\dot{Q}_L}{\dot{Q}_H}$$

As Figure 4-14 and Figure 4-15 show, the heat in regeneration increases to some extent with reheating, but the heat available after regeneration decreases. This behavior follows a trend that is the same as that of the cycle efficiency, which is logical, since the heat input in kW, $\dot{Q}_H$, has been set to a fixed value.

The possibility of interrupting regeneration was also studied for the reheating cycle. For example, T_5 could be set at 130°C, and the cycle efficiency would still amount to 25.5%. It is observed that reheating is beneficial because a higher temperature is available for the same efficiency, which also helps to get a smaller mass flow rate since the lower regeneration makes the heat collected (kJ/kg) higher for the same heat input (kW). Compared to the cycle without reheating, this one requires 2.55 kg/s versus 2.77 kg/s for the simple Rankine.

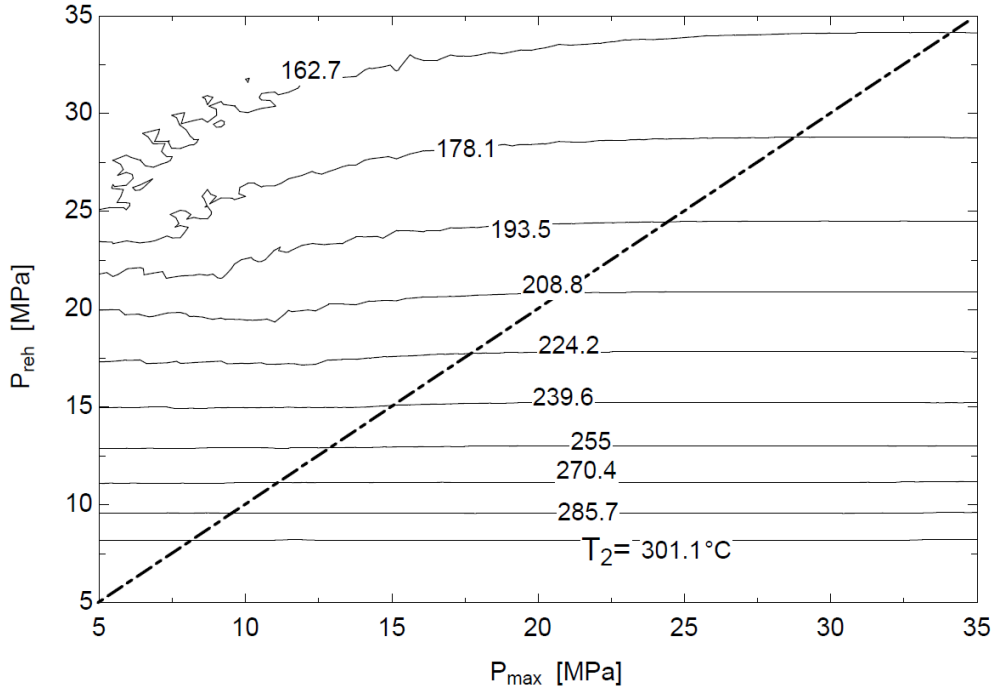

Figure 4-12: Contour plot for the temperature at the turbine outlet, T_2

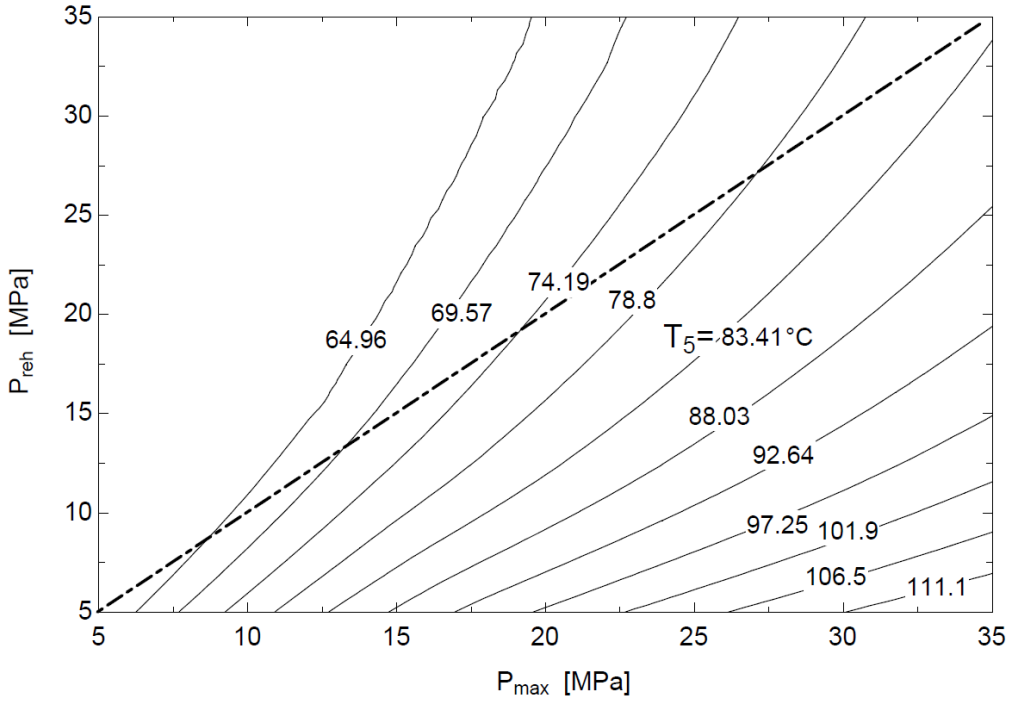

Figure 4-13: Contour plot for the temperature after regeneration, T_5

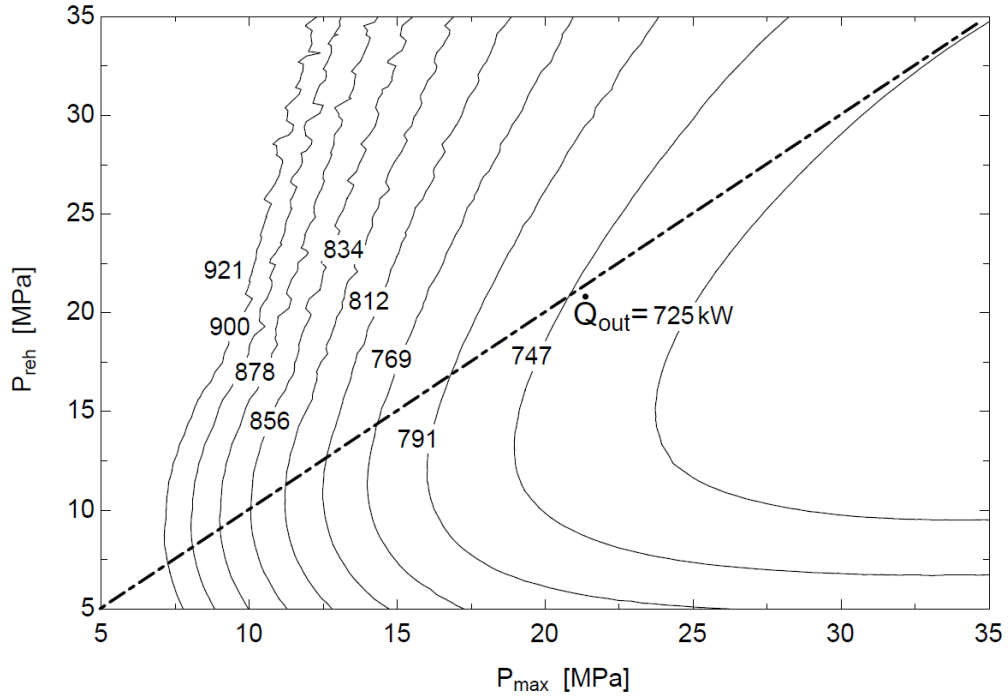

Figure 4-14: Contour plot for regeneration heat

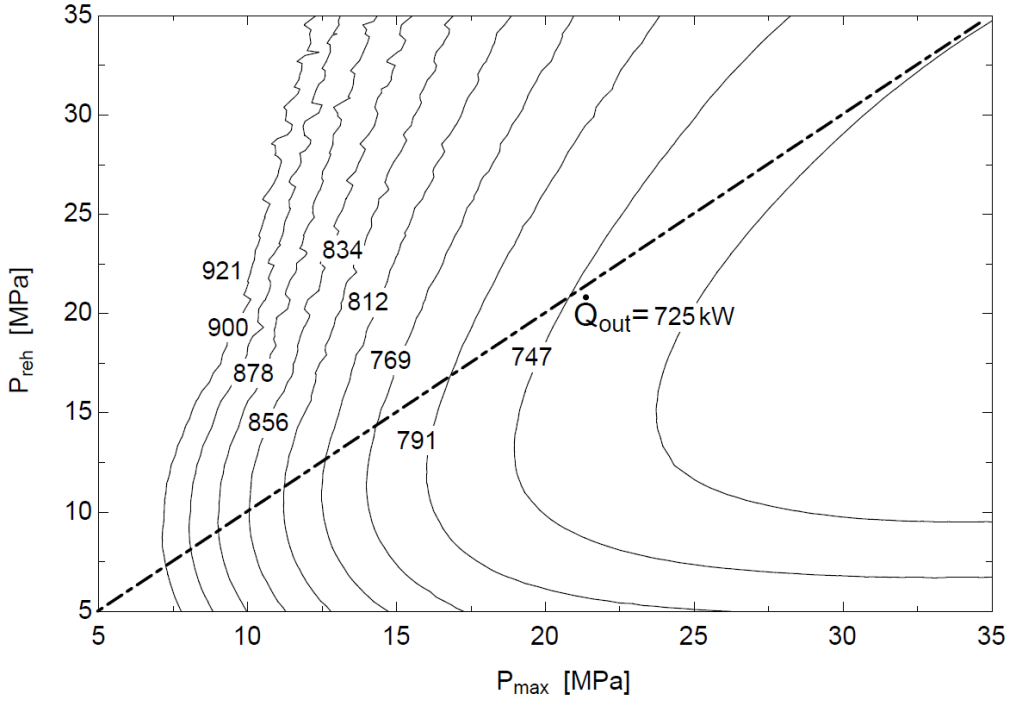

Figure 4-15: Contour plot for heat rejected to low temperature

In case the high pressure is still a limitation, and a maximum pressure of 20 MPa is selected, then a maximum efficiency of 26% for a reheating pressure of 14 MPa results. For the same maximum pressure, the cycle without reheating has an efficiency of 25.3%, which an insignificant difference, so that reheating might not be worth the investment.

4.3.6. Recompression Rankine with Regeneration and High Temperature

Recompression has been found to be a technique that provides a significant improvement in the Brayton supercritical Carbon Dioxide (s-CO_2) cycle [19]. The reason behind this is the exergy conservation in the regenerator. In the simple cycle, heat is transferred from low pressure and high temperature CO_2 to a high pressure close-to-critical-point s-CO_2. Near the critical point and up to 150^{o}C, CO_2 has a high specific heat, and as a result small temperature increases are achieved in the cold stream of the regenerator for a significant temperature decrease in the hot stream [43]. Since temperature is lost in the regeneration process, exergy is destroyed; meaning, the energy recovered loses some of its ability to produce work due to its lower temperature. However, the way to avoid the exergy destruction is to recompress part of the flow at low pressure, right after the regeneration process, so that only part of the fluid is cooled further. As a result, the heat capacity of the cold stream of the regenerator is lower because is mass flow rate is smaller and, therefore, its temperature increase will be larger. For this cycle model, the assumptions taken were the following:

- Maximum temperature: 325^{o}C. Assuming we are able to store energy at around 350^{o}C through parabolic trough collectors (PTC).

- Condensation temperature: 25ºC. Assuming we have water to transfer heat to at a max temperature of some 20ºC.

  Maximum Carnot efficiency with these temperatures is 50%.
- Maximum pressure: in a range from 15 to 30 MPa. However, it could be larger depending on the pipe size.
- Heat input: 1000 kW.
- Isentropic efficiencies of pump 80%, turbine 90%, and compressor 85%.
- Pressure losses assumed on the order of 1% of the absolute pressure in the pipes. For the intermediate points partial pressure loss was assumed as a fraction of the total.
- Regenerator heat exchanger effectiveness is 80% with an enthalpy change from points 2 to 5 which is 80% of the ideal enthalpy change (when $T_5 = T_4$).
- Heat losses to environment from heat exchangers and pipes are assumed negligible.

As shown in Figure 4-16, the recompression cycle incorporates points 9 and 10. Point 9 is the end of regeneration for the hot stream at low pressure, and it is also the recompression point, where the flow is split into two streams, one to be recompressed and the other to the condenser. Point 10 is the outlet of the compressor (whose inlet is point 9). Also, point 10 receives the higher pressure cold stream from the regenerator. The flow split is calculated to achieve that point 10 is merging both the streams of recompression and regeneration at low temperature. The regeneration effectiveness is used to calculate point 9 for a given point 4. Once the amount of heat transferred in the regenerator is known, point 10 and the flow split are calculated.

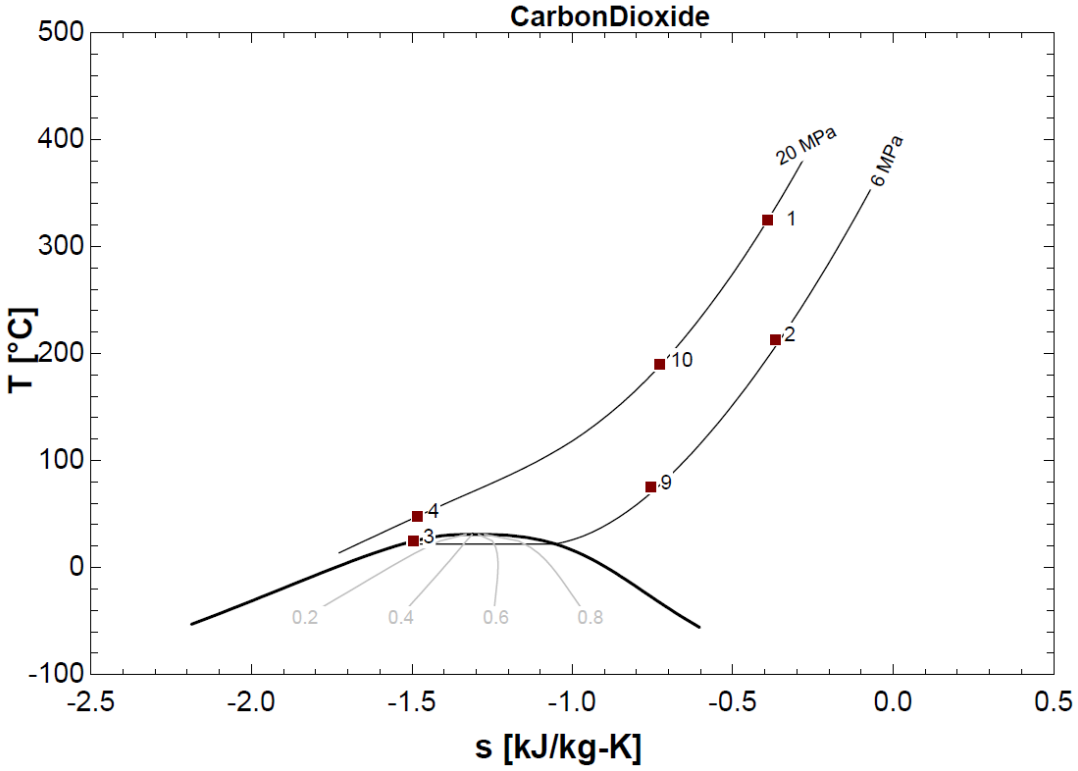

Figure 4-16: Recompression Rankine CO_2 cycle

The optimal maximum pressure for this cycle is 25.5 MPa, which results in an efficiency of 29.8%, which is a significant increase from the previous cases. For 20 MPa of maximum pressure, the efficiency is still above 28%. Recompression of the cycle provides a slightly better efficiency than reheating, but only at a considerably lower pressure, as shown in Figure 4-17. As to the mass flow rate, it is greatly increased up to 7 kg/s, as shown in Figure 4-18 at a 25 MPa maximum pressure, which complicates the pipe design with the need for larger pipes holding high pressure. As to the temperature after regeneration, in this case, T_9, it stays in the range from 70 to 80^{o}C, as observed in Figure 4-19. Another interesting parameter is the flow split, which is the fraction of mass

flow rate that is not condensed but recompressed. It is observed in Figure 4-20 that the maximum efficiencies are achieved when the flow split is close to 0.5.

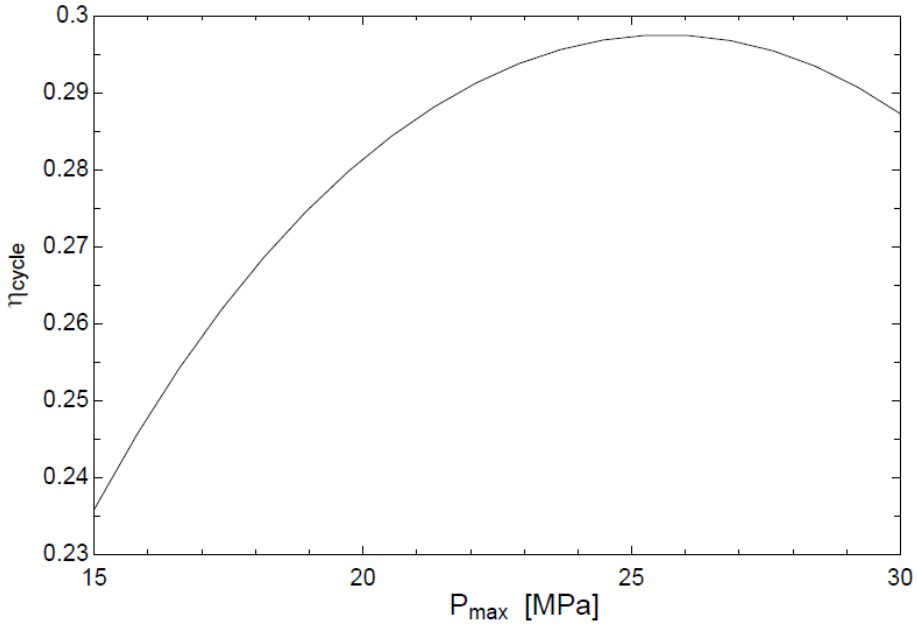

Figure 4-17: Variation of cycle efficiency with maximum pressure

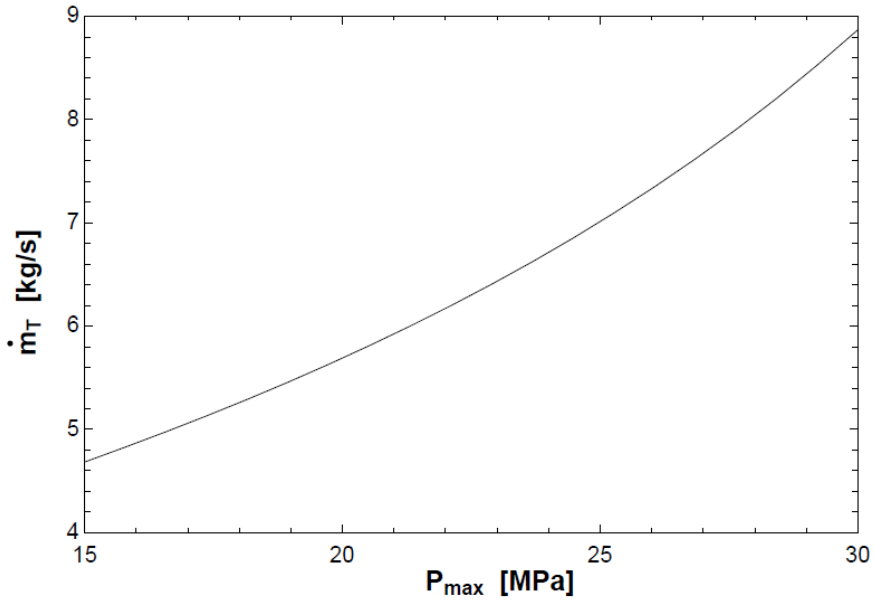

Figure 4-18: Variation of mass flow rate with maximum pressure

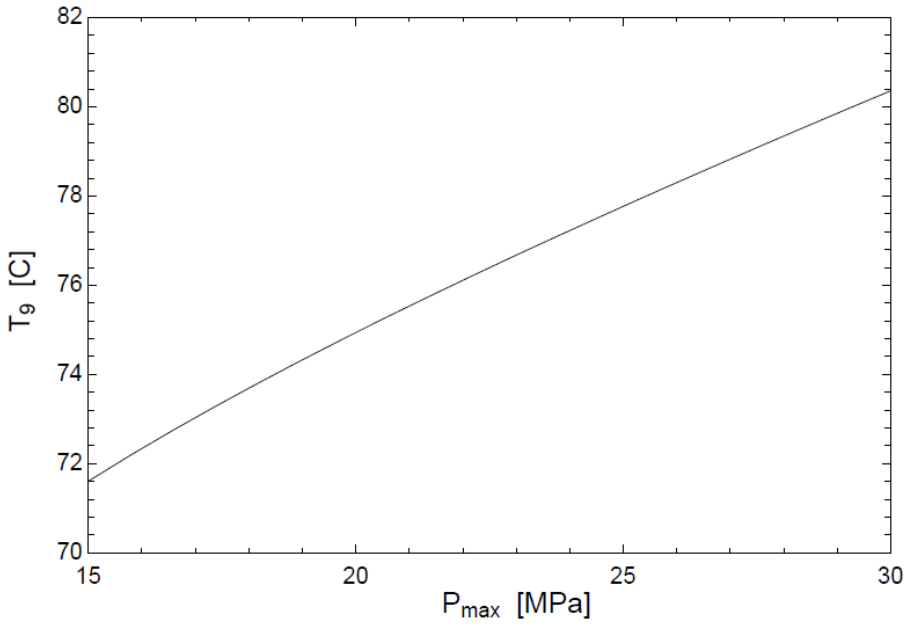

Figure 4-19: Variation of temperature after regeneration with maximum pressure

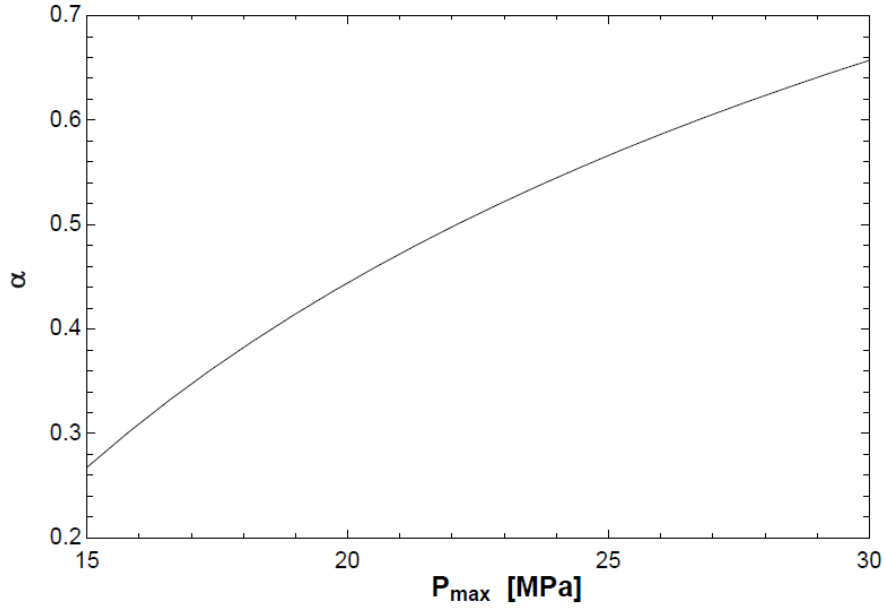

Figure 4-20: Variation of flow split with maximum pressure

In the recompression cycle, the technique of interrupting regeneration is totally unfavorable. If T_9 is kept at 110°C and the cycle is optimized again for this condition,

the maximum efficiency would be 22.25% for a maximum pressure of 19.5 MPa, which is a significant decrease in efficiency as compared to the simple Rankine, whose efficiency decreases 2 or 3 percentage points.

Another idea that was explored herein is the placement of an intermediate turbine after regeneration. The fluid would be preheated in the regenerator at a higher pressure, therefore, the cycle more closely resembles the Carnot Cycle. However, the increase in efficiency was not significant, with the result being 30.59% optimized efficiency for maximum and intermediate pressures of 29 and 25 MPa.

Finally, following system modifications investigated in the literature [19], an additional regenerator was implemented for high temperatures. It would appear from the literature that the regeneration process is more efficient when the cold stream is above 150^{o}C as a result of the specific heat of CO_2 being higher; therefore, a flow split is no longer needed in this range of temperatures to achieve a more exergy efficient regenerator. The dashed lines in Figure 4-21, which includes Points 5 and 6, represent that the hot stream in each of the regenerators is never cooled below the inlet temperature of the cold stream. Similarly, the outlet of the cold stream is never hotter than the inlet of the hot stream. The recompression process is represented with the line from point 9 to point 10.

This technique improves the cycle efficiency with values reaching 30.04% for a lower optimal maximum pressure of 18.16 MPa, as illustrated in Figure 4-22.

The Brayton cycle is similar to all these previous cycles, being the only difference that the minimum temperature would be above the critical point temperature.

The increase of the minimum temperature decreases the cycle efficiency, which is why the Brayton cycle is less efficient than the Rankine cycle for the assumptions considered.

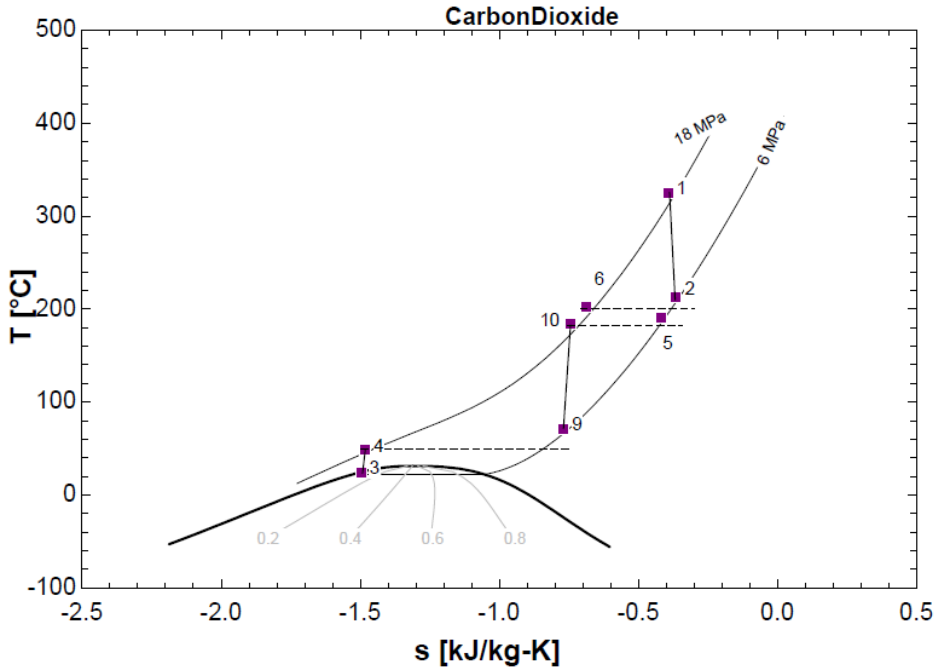

Figure 4-21: Double regenerator recompression Rankine with high temperature

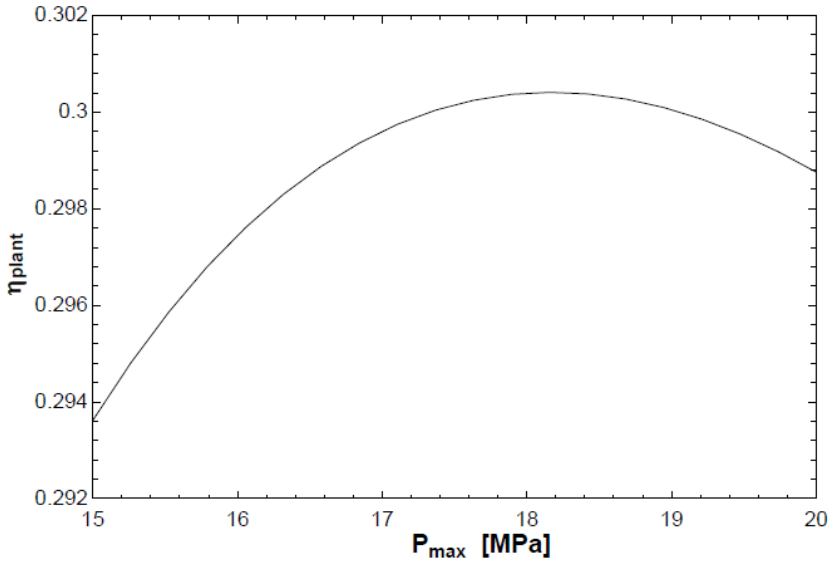

Figure 4-22: Variation of efficiency with maximum pressure for the double regenerator cycle

4.3.7. Thermodynamic Analysis Summary and Conclusions

In the following tables the main parameters and variables analyzed in this section are shown in a more compact way to assist with reaching accurate conclusions. Table 2-1 contains the parameters or assumptions taken in the different cycle models analyzed in this section, while Table 2-2 contains the main results for each of these cycles including:

- **Cycle efficiency**
- **Carnot efficiency**: calculated according to maximum and minimum cycle temperatures
- **Second law efficiency**: ratio of the cycle efficiency with respect to Carnot
- **Mass per MJ heat input** (or mass flow rate per heat rate input), it allows to compare all the cycles' mass flow rate scaling their heat input to 1MW. This is why this variable is measured in kg/s/MW or kg/MJ.
- **Cogeneration temperatures**: information about what temperatures are available for heat recovery and industrial process heat.
- **BWR**: back-work ratio, it is a ratio between the expansion work (sum of all turbines) and the compression work (sum of all pumps and compressors).

These cycles were also compared to literature as shown in the lower part of the table, where information from different references were also analyzed and compared: [41], [44], [43], [45], [42].

In the tables, there are three highlighted cycles. They were selected for their outstanding combination of performance measures. Between these three cycles, one was chosen to be the baseline cycle for future studies.

Table 4-1: Summary of cycle parameters analyzed

Cycle description	Cycle parameters								
	Maximum temperature [C]	Maximum pressure [MPa]	Second pressure [MPa]	Condensation temperature [C]	Heat input [kW]	Turbine efficiency	Regeneration effectiveness	Reheating	Recompression
Simple, medium temperature	175	10	n/a	25	500	0.8	1	NO	NO
Simple, medium temperature, optimized	175	17	n/a	25	500	0.8	1	NO	NO
Simple, low temperature	75	20	n/a	25	500	0.8	n/a	NO	NO
Simple, low temperature, optimized	75	12	n/a	25	500	0.8	n/a	NO	NO
Simple, low temperature, optimized	90	13.5	n/a	25	500	0.8	n/a	NO	NO
Reheating, low temperature, optimized	75	12	11	25	500	0.8	n/a	YES	NO
Simple, high temperature	325	17	n/a	25	800	0.9	0.8	NO	NO
Simple, high temperature, optimized	325	35	n/a	25	800	0.9	0.8	NO	NO
Simple, high temperature, regeneration interrupted	325	35	n/a	25	1000	0.9	0.8	NO	NO
Reheating, high temperature	325	30	17	25	1000	0.9	0.8	YES	NO
Reheating, high temperature, lower pressure	325	20	14	25	1000	0.9	0.8	YES	NO
Reheating, high temperature, regeneration interrupted	325	30	17	25	1000	0.9	0.8	YES	NO
Reheating, high temperature, regeneration interrupted	325	30	17	25	1000	0.9	0.8	YES	NO
Recompression, high temperature	325	20	n/a	25	1000	0.9	0.8	NO	YES
Recompression, high temperature, optimized	325	25.5	n/a	25	1000	0.9	0.8	NO	YES
Recompression, high temperature, regeneration interrupted	325	19.5	n/a	25	1000	0.9	0.8	NO	YES
Recompression, high temperature, double regeneration	325	18.5	n/a	25	1000	0.9	0.8	NO	YES
Recompression, high temperature, double regeneration interrupted	325	18.5	n/a	25	1000	0.9	0.8	NO	YES
Reference									
[30] Brayton s-CO2, high temperature	500	10	n/a	45	n/a	0.9	0.95	NO	NO
[33] Brayton s-CO2, high temperature and pressure	500	25	n/a	30	3.79E+06	0.93	0.9	NO	YES
[32] Rankine, high temperature	600	20	n/a	20	n/a	0.9	0.95	NO	NO
[34] Rankine with absorption chiller	390	15	7.5	3	2777.8	0.9	0.98	YES	NO
[31] Rankine STEAM optimized for PTC	370	9	n/a	41.51	1.32E+05	0.875	0.98	n/a	n/a

Table 4-2: Summary of Cycle Results

Cycle description	Cycle results										
	Cycle/plant efficiency	Carnot efficiency	Second law efficiency	Plant power [kW]	Maximum mass flow rate (kg/s)	Mass per MJ heat input [kg/MJ]	Maximum cogeneration temperature [C]	Second cogeneration temperature [C]	Pump specific work [kJ/kg]	Turbine specific work [kJ/kg]	BWR
Simple, medium temperature	11.2%	33.5%	33.6%	56.2	2.923	5.846	139.1	32.72	6.11	25.34	4.15
Simple, medium temperature, optimized	15.7%	33.5%	46.8%	78.4	2.397	4.794	94.92	44.39	17.49	48.35	2.76
Simple, low temperature	0.0%	14.4%	0.0%	0	7.56	15.12	25	n/a	22.21	20.29	0.91
Simple, low temperature, optimized	5.0%	14.4%	34.7%	24.91	3.31	6.62	29.99	n/a	9.53	16.96	1.78
Simple, low temperature, optimized	6.3%	17.9%	35.0%	31.33	2.988	5.976	34.62	n/a	11.88	22.37	1.88
Reheating, low temperature, optimized	5.5%	14.4%	38.6%	27.72	2.996	5.992	35.02	n/a	9.43	18.512	1.96
Simple, high temperature	23.5%	50.2%	46.7%	187.6	2.731	3.41375	228.9	72.95	17.74	86.44	4.87
Simple, high temperature, optimized	27.6%	50.2%	55.0%	220.8	2.441	3.05125	160.1	82.82	45.13	135.6	3.00
Simple, high temperature, regeneration interrupted	25.0%	50.2%	49.9%	250.4	2.768	2.768	160.1	110	45.13	135.6	3.00
Reheating, high temperature	29.0%	50.2%	57.9%	290.4	2.883	2.883	228.9	89.8	37.73	138.46	3.67
Reheating, high temperature, lower pressure	25.9%	50.2%	51.6%	258.9	3.16	3.16	247.9	80.7	22.47	104.4	4.65
Reheating, high temperature, regeneration interrupted	24.1%	50.2%	48.1%	241.2	2.395	2.395	228.9	150	37.73	138.46	3.67
Reheating, high temperature, regeneration interrupted	25.5%	50.2%	50.8%	255.1	2.533	2.533	228.9	130	38.73	138.46	3.58
Recompression, high temperature	28.1%	50.2%	56.1%	281.4	5.69	5.69	213.1	74.94	22.47	98.61	4.39
Recompression, high temperature, optimized	29.8%	50.2%	59.3%	297.6	7.168	7.168	189.7	78.04	30.94	115.5	3.73
Recompression, high temperature, regeneration interrupted	22.3%	50.2%	44.4%	222.5	12.09	12.09	189.7	110	30.94	115.5	3.73
Recompression, high temperature, double regeneration	30.0%	50.2%	59.9%	300.4	6.453	6.453	222.5	179.6/66.88	19.58	91.46	4.67
Recompression, high temperature, double regeneration interrupted	22.3%	50.2%	44.4%	222.8	7.74	7.74	222.5	221,9/110	19.58	91.46	4.67
Reference											
[30] Brayton s-CO2, high temperature	33.3%	58.9%	56.6%	n/a	n/a	n/a	n/a	n/a	n/a	n/a	n/a
[33] Brayton s-CO2, high temperature and pressure	43.3%	60.8%	71.2%	2E+06	15988	4.22	360	187	n/a	n/a	n/a
[32] Rankine, high temperature	40.3%	66.4%	60.7%	n/a	n/a	n/a	449	368/129	19.4	169.9	8.76
[34] Rankine with absorption chiller	36.0%	58.4%	61.7%	1000	9.402	3.38	298.8	22.52	n/a	n/a	n/a
[31] Rankine STEAM optimized for PTC	38.0%	51.1%	74.4%	50000	63.42	0.48	n/a	n/a	14.04	n/a	n/a

Comparing cycles to references it differences in efficiencies and other results were found, as expected. A remarkable finding is that for any given MW of heat input to the plant, steam works with a much lower mass flow rate than CO_2. However, as to installed pipe sizing, which is based on fluid velocity limitations, the effect of mass flow difference is compensated through the higher densities of CO_2 gas. For example, at 9 MPa and 350ºC, CO_2 density is twice the density of water vapor. Moreover, since CO_2 works with higher pressures, its density is even higher.

The cycle chosen as baseline was the simple Rankine Cycle with high temperature and interrupted regeneration. The reasons behind selecting the Rankine cycle were:

- Its simplicity, which allows for easy assess the influences of different parameters. Since it has the lowest number of devices (turbine, pump), it is a good reference to compare more complex cycles incorporating additional devices.
- Its low mass flow rate, allowing compactness; the higher densities associated with higher pressures also contribute to compactness
- Its stable efficiency as evidence that it does not decrease significantly when lowering its maximum pressure
- Relatively high temperatures are available for cogeneration, without losing much efficiency (from 27% to 25%).

The main disadvantage of this cycle is its high pressure of 35 MPa, meaning care is required when choosing or designing the working devices.

5. DESIGN AND MODELING

5.1. Overview

The purpose of this section is to present the design methodology for the solar power plant and the implementation of the system model including its components, which will allow simulation with typical meteorological data. For the thermodynamic analysis, the power block was thermodynamically designed, so as to provide the specifications of fluid properties and sizing.

In this chapter, the focus will be on the design of the baseline cycle, for 1-MW electrical power production applicable to a small industry during 8 hours every day. Assuming a 25% efficiency, the power block was therefore designed for an input heat of 4 MW, as a result, the solar field was sized for a heat output of 4 MW, considering a design point based on appropriate solar radiation and meteorological conditions.

This chapter has four major sections. Two of them consist of the development of two major codes in EES for simulation, which were presented in the first chapter of this thesis. These sections were made in parallel, not in series over time, meaning, results of some section were used to complete some other.

- **Typical Meteorological Year Analysis Code**. This code was written in MATLAB, and it is a previous step to any design or modeling attempts because it allows one to understand the meteorological conditions of solar radiation and environment temperatures for which the solar plant must be

designed. The equations implemented in this code are presented in the first section of this chapter.

- **Design Simulation Code**: Written in EES, it assists in the design of the plant with simplified modeling that yields approximate performance simulations to assess the impact of different design decisions. The equations implemented in this code are presented in the second section of this chapter.
- **Analysis Simulation Code**: It assists the Design Simulation Code with a less-simplified modeling that yields performance simulations of the plant for average days of each month in a typical meteorological year. The equations implemented in this code are presented in the third section of this chapter.
- **Special complement Codes**: In addition to these global design programs, a more detailed design was performed for some special components, which were of interest due to their particularities, such as the heat exchangers and turbomachines. This work can be found in the fourth section of this chapter.

The geographical location for which this study is conducted is College Station, TX, however, the methodologies and procedures introduced are applicable to any location. Even though the Spoetzl Brewery is not located in this town, the meteorological conditions are similar to those of the Texas A&M college campus, which is located in this town.

5.2. Solar Radiation and Meteorological Data Modeling

In a design phase, it is necessary to find a design point for the system. In other words, although a great amount of data is available through the TMY3 (typical

meteorological year) data sources, it is necessary to process this data to find maximums, minimums and averages that will facilitate the design of the solar plant. In addition to this, it is necessary to know the trends and how the meteorological data is to be inputted in the solar plant model. Raw data always needs processing, and in the case of solar radiation, the component of radiation (direct, diffuse, etc.) that will be inputted needs to be distinguished.

A MATLAB code was developed to process the data that would be inputted to the solar radiation model. For the development of this code, it was necessary to have knowledge of the different solar radiation components and angles.

5.2.1. MATLAB code equations

The main code achievement is that it is able to store the monthly weather values classifying the data by month, day and hour. This was done through a cell array composed of multidimensional matrices. The code can perform this task for any TMY3 data. Although the focus here is in College Station, TX, the same results can be obtained for any location.

The solar time is different from the standard time, which means that the hour when a value was measured and recorded in the TMY3 data is not necessarily the same hour in terms of solar angles. Therefore, solar time had to be computed from standard time using solar angle information and equations as follows, where t_{solar} and t_{std} are the solar time and the standard time in hours, L_{std} and L_{loc} are the standard and local longitudes in degrees and E is the so called equation of time, which introduces the effect of the elliptical orbit of the Earth around the Sun [46].

$$t_{solar} = t_{std} - 0.5 + \frac{L_{std} - L_{loc}}{15^{\circ} / hour} + E(n)/60 \tag{5.1}$$

$$E = 229.18 \times (0.000075 + 0.001868\cos(B) - \\ -0.032077\sin(B) - 0.014615\cos(2B) - 0.04089\sin(2B)) \tag{5.2}$$

$$B = B(n) = 2\pi \frac{(n\text{-}1)}{365} \tag{5.3}$$

To convert to solar time, half an hour needs to be subtracted from the standard time because in the TMY3 files, the recorded time is the one at the end of the hour in which the data was measured. Therefore, the average time where the measurement occurred is a half hour before the recorded time. The equation of time is a function of the number of the day in the year, *n*, and its magnitude is given in minutes, which is the reason why it needs to be divided by 60 to convert minutes to hours.

The TMY3 data does not give the wet bulb temperature, but it does provide the dry bulb temperature and relative humidity. Using a correlation [47], the wet-bulb temperature can be obtained, where the temperatures are in Celsius and the relative humidity is expressed as a percentage. The correlation is confirmed at sea level; therefore, when incorporating this equation, the assumption was made that the influence of elevation is negligible.

$$T_{WB} = T_{DB} \times \arctan(0.151977(rh + 8.313659)^{(1/2)}) + \arctan(T_{DB} + rh) \\ - \arctan(rh - 1.676331) + 0.00391838(rh)^{(3/2)} \arctan(0.023101 rh) - 4.686035 \tag{5.4}$$

5.2.2. Results of TMY3 data processing

For each of the studied meteorological variables, yearly and monthly averages were taken for each hour with the purpose of helping design the solar plant. The yearly

average data served to estimate the overall behavior of the weather during a day and the limits in which the studied variables were enclosed.

Figure 5-1 shows the yearly average, median and scatter data for DNI (Direct Normal Insolation) in College Station, TX. The median day of the year was calculated based on the total DNI received and projected on a tracking surface. For the months the DNI received (not projected) was used, which means, summing the DNI of each hour for each day and getting the day that contained the median.

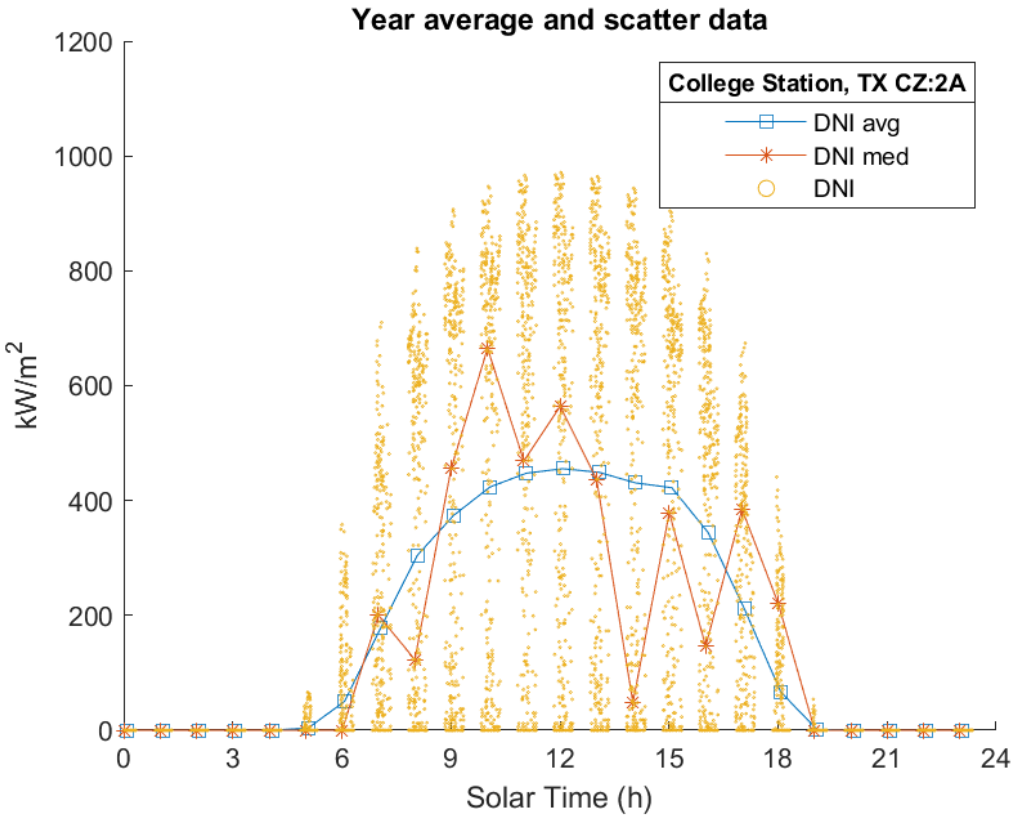

Figure 5-1: Direct Normal Insolation yearly average and scatter data for College Station, TX

It can be appreciated in Figure 5-1 that the values are concentrated either on top or at the bottom of the figure, meaning that while many days are clear (DNI around 800

kW/m^2), many other days are cloudy (zero DNI). Another observation is that during a day, while the average DNI remains fairly constant, the median DNI reveals that there is intermittent cloudiness, for solar plant operation it is better to have a constant heat input over a long period of time, rather than having a peak too far from the average, which would increase part-load operating periods.

Figure 5-2 illustrates the same data processing for a different location: Phoenix, AZ. It can be observed that DNI for this location is fairly consistent during the day, while sharply increasing/decreasing at sunrise/sunset.

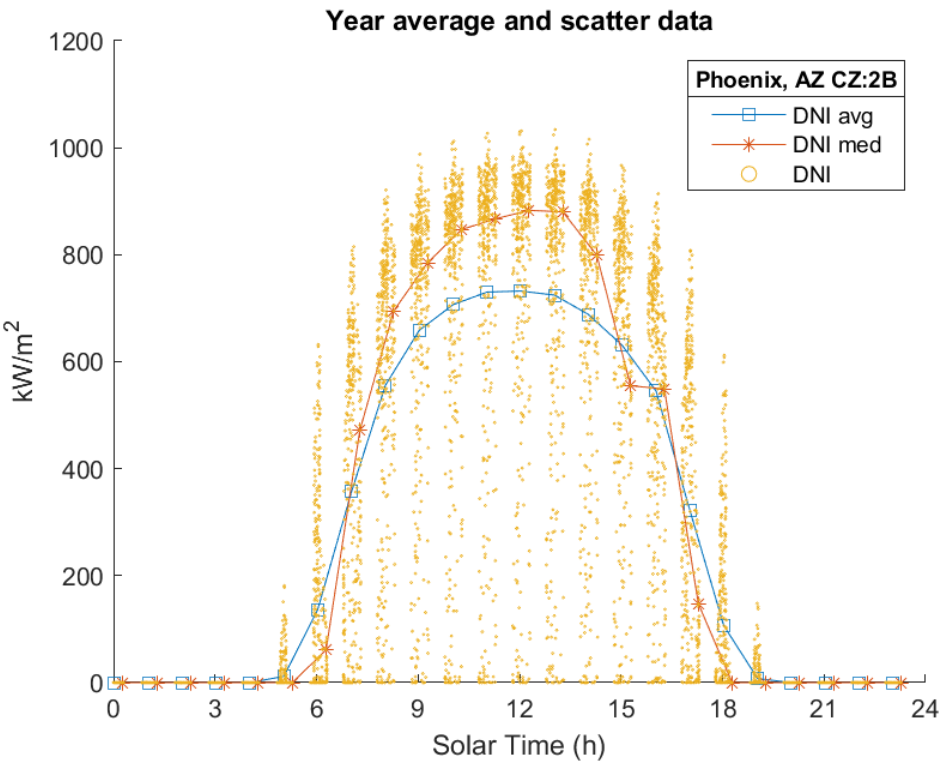

Figure 5-2: Direct Normal Insolation yearly average and scatter data for Phoenix, AZ

The monthly average and median days were also obtained and are shown in Figure 5-3. The scatter data reveals that the average values are not common in that

radiation levels are typically either high or low, meaning the weather is either very sunny or very cloudy. Another observation is that radiation peaks are approximately the same regardless of the season: around 800 W/m^2; however, the day length varies with the season, meaning the total energy available, kW-h/m^2 varies. The constant peak is also good for design purposes, since it makes the design point more independent from the season.

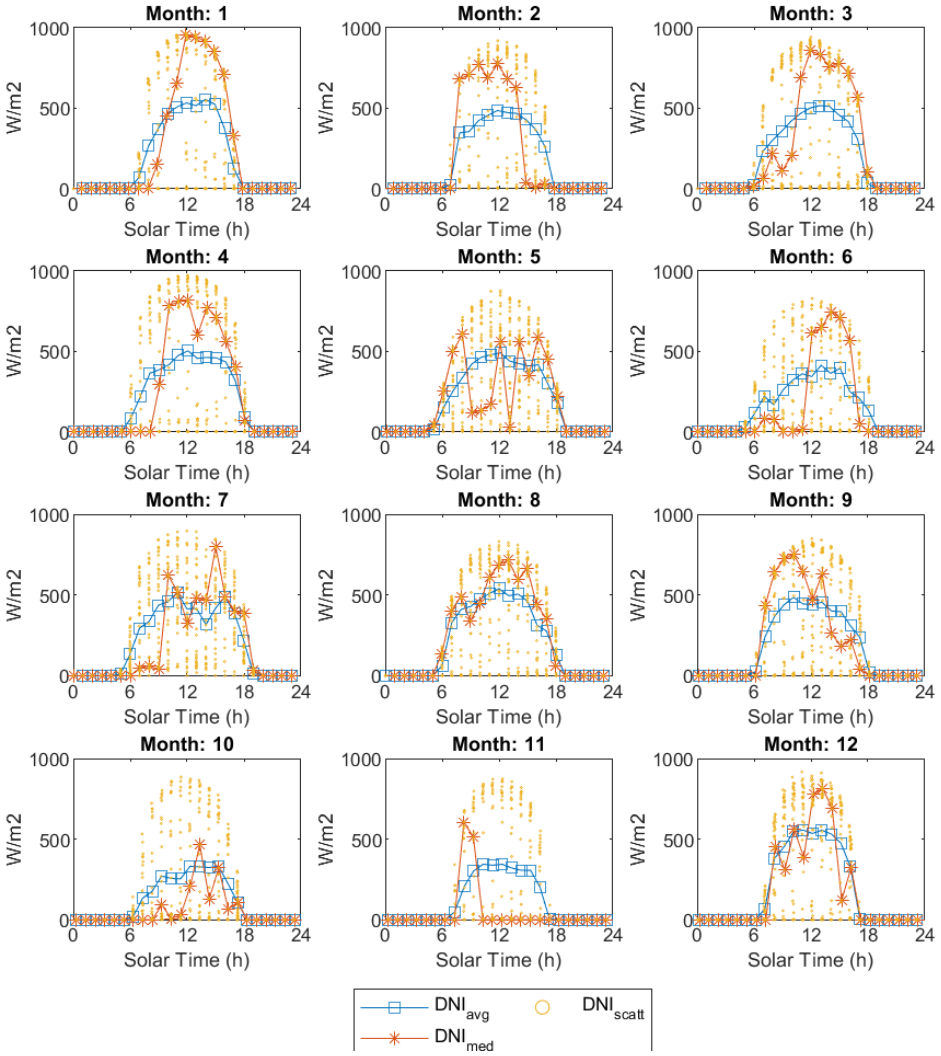

Figure 5-3: DNI monthly average and scatter data for College Station, TX.

Figure 5-4 reveals the frequency of radiation levels in hours per year. This plot is useful to generate another plot that is shown in Figure 5-5, which contains the integral below the curve in Figure 5-4 between 50% and 125% of each radiation level, therefore obtaining the energy yield of each radiation level working as the design radiation level. Figure 5-5 was generated to assist in choosing the design radiation, assuming that the plant will be able to operate between 0.5 and 1.25 times the design radiation. If solar-to-electric efficiency is assumed to be the same at partial loads as at full load, the ideal energy generated by the plant can be obtained per square meter.

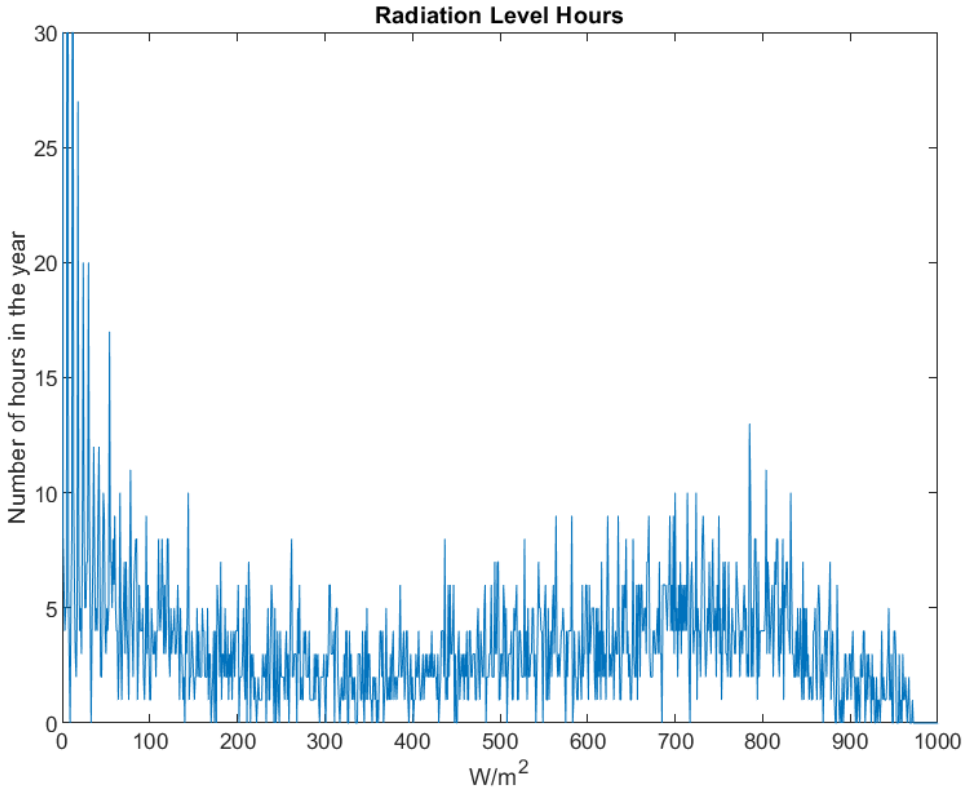

Figure 5-4: Radiation level hours count

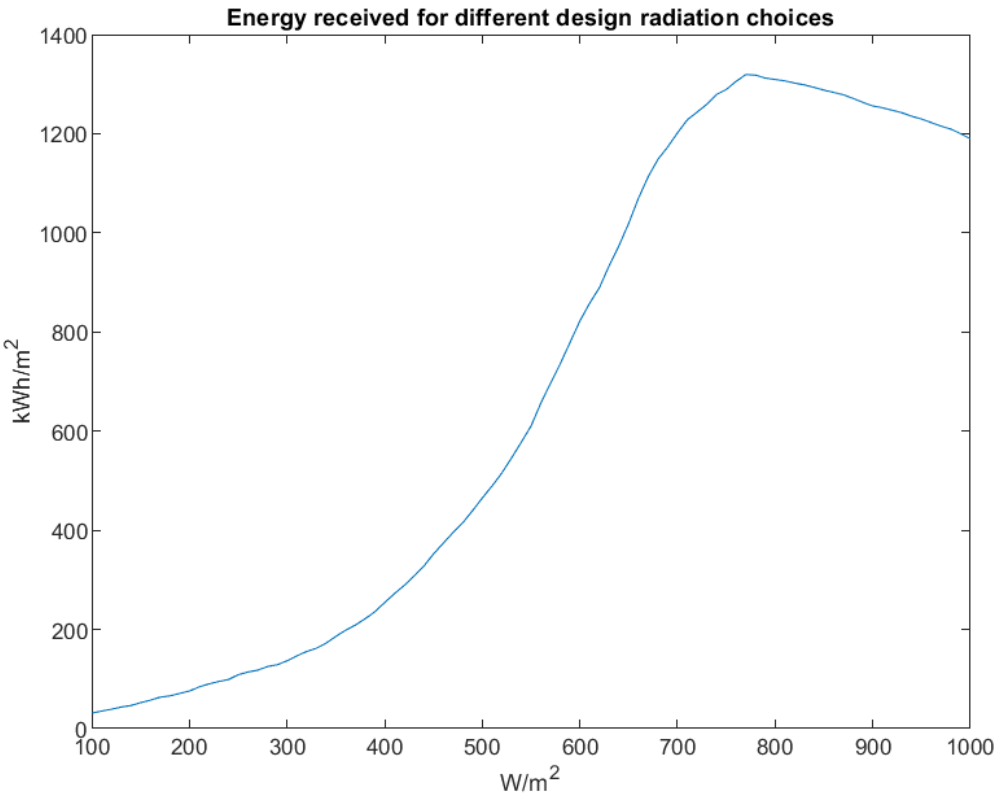

Figure 5-5: Solar energy received per unit collector surface throughout the year while choosing different levels of radiation as the design point.

Other weather variables were also studied such like ambient dry-bulb and wet-bulb temperatures, relative humidity, barometric pressure and wind speed. Figure 5-6 shows the results. Ambient temperatures help to determine the temperature that constrains the thermodynamic cycle heat sink. If a cooling tower is used to provide additional (evaporative) cooling then the wet-bulb temperature and the relative humidity are the determining factors. Figure 5-7 shows average and scatter temperature days for each month. The wind speed was later used in the solar field model for heat loss calculations.

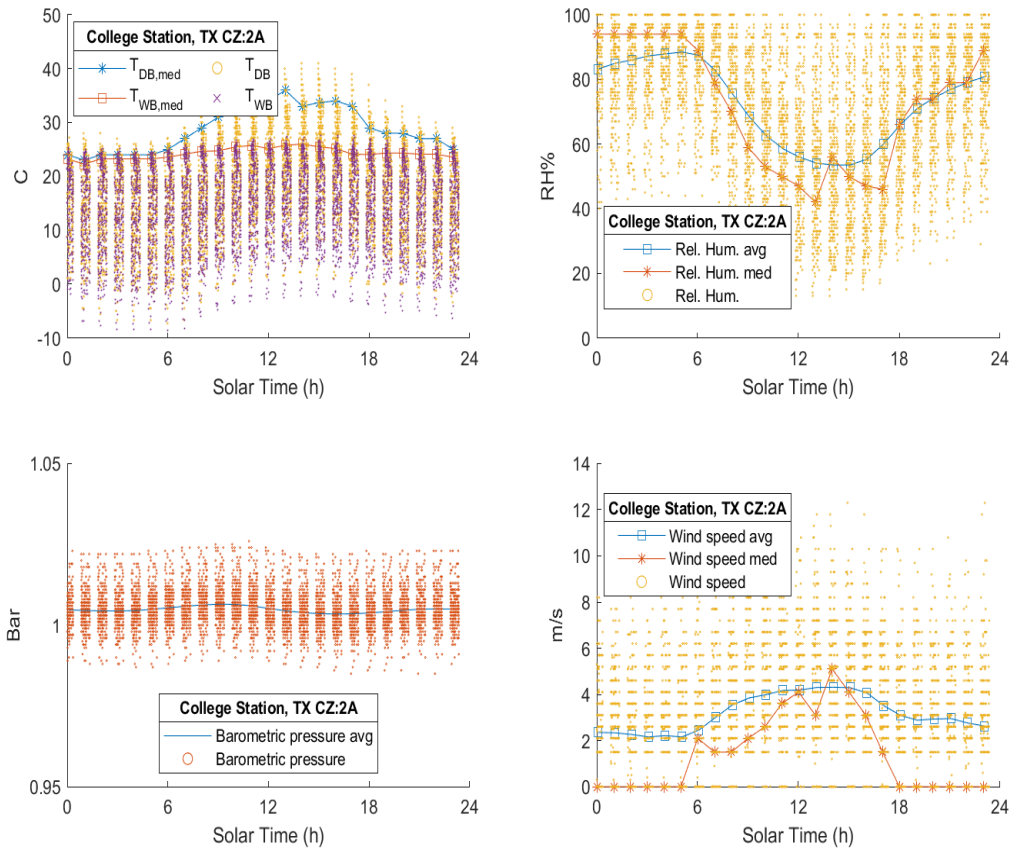

Figure 5-6: Weather variables averages, medians and boundaries

It can be seen that in the winter, while not in the summer there is significant dispersion in the temperature data. This variability is not good for design purposes since it makes the system operate outside its design point unless adaptability is implemented through variable heat sink temperatures in the plant.

It should be stated that when the plot legend mentions medians, it is referring to the values of these variables occurring on the median day, which was obtained for solar radiation received, rather than the actual (statistical) median values of the variables.

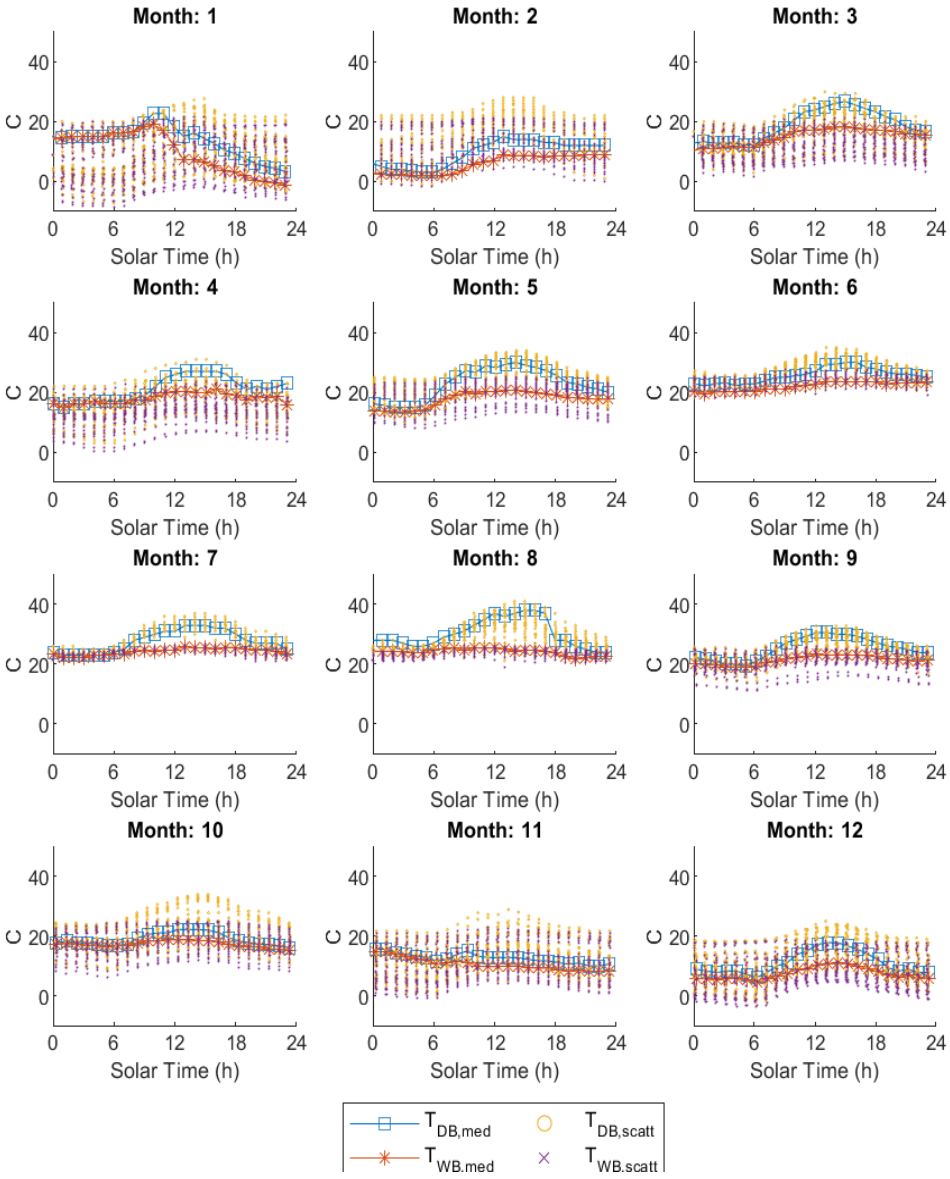

Figure 5-7: Monthly median and scatter temperature data at College Station, TX

5.3. Global Solar Plant Design and Modeling

The purpose of this stage of the project was to provide a basic dimensional, thermal and thermodynamic design of the solar plant.

Figure 5-8 shows the basic plant schematic with all the main components and outputs. The solar field will receive the main energy input, with the option of having additional heat supplied from a gas furnace. The heat will be transferred to the CO_2, which is the working fluid in the power block. Due to its high pressure, all the high temperature heat exchangers for the CO_2 must be Printed Circuit Heat Exchangers (PCHE), [19], [48]. After the turbine expansion, the CO_2 will go through heat recovery processes until reaching the condenser, which operates with cooling water pumped through a cooling tower. Notice that the water flow is split in two circuits, both end up going to the cooling tower but one goes first through the heat recovery exchanger and then provides heat for a process. These two circuits will be discussed more in detail in the sections to come.

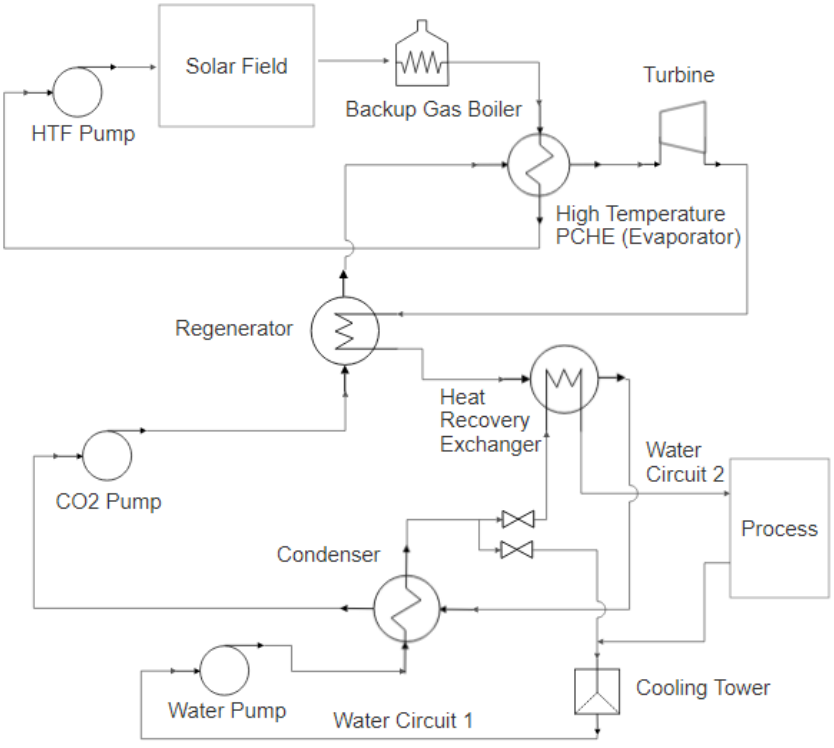

Figure 5-8: Solar plant schematic

The design point is determined by conditions that are external to the cycle, namely the meteorological data. The choice of design conditions is explained below.

- **Day of the year**: 231. Any day between the spring equinox and the fall equinox could work. Day 231 is the day with yearly median radiation received.
- **Solar time**: 12pm. Solar noon is the design point for this plant.
- **DNI**: 780 W/m^2. This is the radiation that yields the most solar energy operating between 0.5 and 1.25 times its value in College Station, TX, as illustrated in Figure 5-5.
- **Ambient temperature**; $T_0 = 23.3^oC$. With the aid of MATLAB, this was calculated as the year-median temperature in College Station, in the 8 middle hours of the day. The year-average DB temperature between 8 am and 4 pm is 22.78^oC, while the year-average temperature at noon is 23.75^oC.
- **Wet-bulb temperature and relative humidity**: $T_{WB} = 18.5^oC$, RH=60%. These two variables are coupled at a fixed dry bulb temperature. The year-average wet-bulb temperature in the interval of plant operations (from 8am to 4pm) is 17.75^oC, while the median is 18.5^oC, which means that there are the same number of hours in this interval with a temperature above as below 18.5^oC. The wet bulb temperature is rarely above 26^oC, but it does oscillate over the year. As to the relative humidity, its median value within the operation time interval happens to be the one associated with the median wet-bulb temperature at the median dry-bulb temperature.

- **Atmospheric pressure**: 1.02325 bar. This is the conventional value for atmospheric pressure.
- **Wind speed**: The median-day wind speed at noon is 4.5 m/s, and this is the design value chosen.

5.3.1. Solar Field Design and Modeling

For the solar field design, the following specifications need to be satisfied in order to couple the solar field with the preliminarily design power block.

- Heat output of the solar field must be roughly 4 MW
- Temperature output of the solar field must be high enough to produce a high temperature in the CO_2 (power block working fluid) of 325^{o}C
- Hours of operation: it is desired that the solar plant is operative during most of the day, namely, 8 hours, which is also the typical length of a work shift. Energy storage will not be implemented in the first design.

In this section, the general knowledge required for the design of a PTC solar field is presented, followed by the steps of designing the solar field and implementing its governing equations in EES.

5.3.1.1. Basic Concepts of the Solar Field Design

PTCs (Parabolic Trough Collectors) are normally N-S axis-oriented and track the sun E-W. A SCA (Solar Collector Assembly) is an assembly of PTCs on a metallic support structure. SCAs are composed of parabolic mirrors, receiver/absorber tubes (where the Heat Transfer Fluid - HTF flows), a hydraulic drive unit and pylon supports. SCAs are assembled in series to form loops. Loops are connected in parallel with a

header pipe. There are different ways of connecting loops, the most common for large scale electricity generation is the central feed configuration with I or H layout [49].

The typical HTF (Heat Transfer Fluid) used is a thermal oil. Many thermal oils are available, but for this design, it is assumed that the solar field operates with Therminol VP-1.

The PTC absorber is usually made of a glass tube containing a vacuum and a receiver tube to reduce radiative and convective losses.

Pressure drop in the solar field is one of the highest parasitic losses [49]. In solar PTC plants, a VFD (Variable Frequency Drive) pump motor is used to pump the HTF to provide additional efficiency and compensate for the energy loss.

An expansion tank is also present in the solar field. This tank is 25% full at cold and 75% full at normal operating conditions. Its non-liquid space is filled with nitrogen to provide a nonreactive atmosphere, and it is positively pressurized to prevent leaks to the inside.

5.3.1.2. Solar Field Sizing and Thermal Design. Evaporator Design.

Once a single PTC has been characterized, the solar field can be designed with the known average performance of the PTC, based on solving for the following variables:

- Number of collectors in the field
- Field area requirement
- Number of loops and number of collectors per loop
- Pumping power required to pump the HTF through the solar field circuit

The two main design specifications for the solar field are the heat output of the solar field must be 4000 kW or 4 MW, and the design radiation will be 0.78 kW/m^2. This design radiation was chosen following Figure 5-5. These are

Looking at the performance of the PTCs (Figure 5-26 and Figure 5-29), the design efficiency of a PTC (product of optical and thermal efficiencies) was chosen at 0.6. With this value, the number of PTCs required is obtained.

$$N_{PTC} = \frac{\dot{Q}_{col,T}}{DNI \cdot A_a \cdot \eta_{opt} \cdot \eta_{th}} = \frac{4000}{0.7 \cdot 39 \cdot 0.6} = 243 \text{ PTCs} \tag{5.5}$$

Using a spacing between collector rows of 10 m (which is enough to prevent row-shadowing between 8 a.m. and 4 p.m. solar times), and knowing that the collector length is 7.8 m, it is concluded that each collector takes up a space of 10 m by 7.8m, for an area of 78 m^2. Therefore, multiplying by the number of PTCs a total area requirement of 20,470 m^2 is obtained, of which the aperture area accounts for 46%. These design results are summarized in Table 5-1.

Table 5-1: Solar field design parameters

DNI_{Design}	0.78 kW/m^2
$\dot{Q}_{col}$	4000 kW
Collector design point efficiency	60%
Aperture Area of each PTC	39 m^2
Heat collection of one PTC at design conditions	18 kW
Number of collectors (PTCs)	221
Total aperture area	8619 m^2
Row spacing	10 m
Total field area	17238 m^2
Aperture-to-total ratio	50%

In order to make a thermal design of the solar field, the CO_2 evaporator needs to be sized. From the preliminary-study power-block design, the CO_2 enters the evaporator at a temperature of 97.22ºC and reaches a temperature as high as 370ºC. The average heat capacity of the CO_2 can be calculated as shown in Eq. (5.6).

$$C_{CO2,avg} = \frac{h_1 - h_6}{T_1 - T_6} = \frac{(\Delta h)_{CO2,evap}}{(\Delta T)_{CO2,evap}} = (\dot{m}c_p)_{CO2,avg} = C_{CO2} = 17.5 \text{ kW/K} \quad (5.6)$$

There are three evaporator parameters that must be selected in order to implement the best design. These parameters are as follows.

- **Heat capacity ratio**. It is the ratio of the minimum to the maximum heat capacity of the fluids in the evaporator.

$$C_r = \frac{C_{\min}}{C_{\max}} \quad (5.7)$$

- **Number of loops in the solar field**. This parameter is the ratio between the total mass flow rate of HTF and the flow through each loop. Since each loop has the same number of PTC in series, the flow through each loop is the flow through each PTC. It is also used in the calculation of the number of PTC for each loop as follows.

$$N_{loops} = \frac{N_{PTC}}{N_{PTC,loop}} = \frac{\dot{m}_{HTF,T}}{\dot{m}_{HTF,loop}} \text{ ; for simplicity: } \dot{m}_{HTF,loop} = \dot{m}_{HTF} \quad (5.8)$$

- **Evaporator effectiveness**. Effectiveness is the ratio of the actual to the maximum possible heat transferred in the evaporator. A value of 90% was assumed based on the knowledge provided by PCHE manufacturers and previous studies, [19] [50] [51] [52] [23]. According to [21], the cost of the heat exchanger dramatically increases for values of effectiveness higher than 93%. The maximum possible heat transferred

is always calculated assuming that one of the fluids achieves the overall maximum and minimum temperatures in the heat exchanger. For example, this would mean that the hot inlet temperature decreases to the cold inlet or else the cold inlet temperature increases to the hot inlet. The best candidate to achieve this maximum temperature difference is the one with the lowest heat capacity, $C_{\min}$.

$$\varepsilon = \frac{\dot{Q}}{\dot{Q}_{\max}} = \frac{\dot{Q}}{C_{\min}(T_{\max} - T_{\min})} \tag{5.9}$$

The average specific heat and properties of the HTF are calculated at the HTF average heat transfer temperature, which is known after choosing the three described parameters. In the following equations, the HTF properties such as specific heat, $c_{p,HTF}$, density, ρ_{HTF} and viscosity, μ_{HTF} , refer to the average properties calculated at this temperature. With the help of these averaged variables, the solar field can be designed and coupled with the evaporator in a much simpler way.

The decision must be made ad to which of the two fluids, namely CO2 or HTF, is going to be the one with the minimum heat capacity. Both cases were considered.

5.3.1.2.1. CO_2 as the Fluid with Minimum Heat Capacity

The equations for the evaporator design are presented below. Equation (5.10) yields the maximum temperature of the HTF, T_M, which is also the temperature at which it must leave the solar field.

$$T_{max,evap} = T_{HTF,\max} = T_M = T_{\min,evap} + \frac{\dot{Q}}{\varepsilon C_{CO2}} = T_{CO2,\min} + \frac{\dot{Q}}{\varepsilon C_{CO2}} \tag{5.10}$$

$$C_{HTF} = \frac{C_{CO2}}{C_r} \tag{5.11}$$

$$T_{HTF,min} = T_M - \frac{\dot{Q}}{C_{HTF}} = T_M - \Delta T_{HTF} \tag{5.12}$$

$$\dot{m}_{HTF} = \dot{m}_{loop} = \frac{C_{HTF}}{c_{p,HTF} N_{loops}} = \frac{\dot{m}_{HTF,T}}{N_{loops}} \tag{5.13}$$

$$\dot{V}_{HTF} = \frac{\dot{m}_{HTF}}{\rho_{HTF}} = \frac{\dot{V}_{HTF,T}}{N_{loops}} \tag{5.14}$$

It should be noted that the fluid properties (specific heat, density, heat capacity) are average properties. In the case of the HTF, properties were calculated at a mean temperature, while for the CO_2, properties were obtained from the known enthalpy and temperature bounds, as explained above.

According to a reference, the velocity through the PTCs is recommended to be between 2 and 4 m/s, [49]. The fluid velocity can now be calculated.

$$v_{HTF} = \frac{\dot{V}_{HTF}}{\frac{\pi}{4} D_{ci}^{\ 2}} \tag{5.15}$$

The pressure drop and pumping power required in the solar field can be estimated by solving the following equations, [53].

$$\mathrm{Re} = \frac{4\dot{m}_{HTF}}{\pi D_{ci} \mu_{HTF}} \tag{5.16}$$

$$f = (0.79 \ln(\mathrm{Re}) - 1.64)^{-2} \tag{5.17}$$

$$\Delta P_{PTC} = f \frac{L_{PTC}}{D_{ci}} \frac{1}{2} \rho_{HTF} v_{HTF}^{\ 2} \tag{5.18}$$

$$\dot{W}_{pump,\,field} = \dot{V}_{HTF,T} N_{PTC,loop} \Delta P_{PTC} \tag{5.19}$$

The above solution assumes that there are no other pressure losses than those occurring at the collector tubes, and all the loops (connected in parallel) have the same pressure drop, which is the individual pressure loss at each PTC multiplied by the number of PTCs in the loop.

5.3.1.2.2. Therminol (HTF) as the Fluid with Minimum Heat Capacity

The thermal analysis procedure is similar to the previous case of CO_2 with minimum heat capacity, but the equations are different, assuming that the effectiveness equation is for the HTF, (5.21) as follows.

$$C_{HTF} = C_r C_{CO2} \tag{5.20}$$

$$T_M = T_{\min,evap} + \frac{\dot{Q}}{\varepsilon C_{HTF}} = T_{CO2,\min} + \frac{\dot{Q}}{\varepsilon C_{HTF}} \tag{5.21}$$

$$T_{HTF,min} = T_M - \frac{\dot{Q}}{C_{HTF}} = T_M - \Delta T_{HTF} \tag{5.22}$$

The rest of the equations are the same as in the case of CO_2 with minimum heat capacity, Eq. (5.13) to (5.19).

5.3.1.2.3. Solar Field Design Results

Two evaporator and solar field designs are discussed here. The constraints of the design are implemented in the equations in a way that choosing three input parameters will yield a plausible design. However, there is one additional constraint: the fluid velocity through the collector pipes must be between 2 and 4 m/s [49]. The designs were therefore adjusted through trial and error.

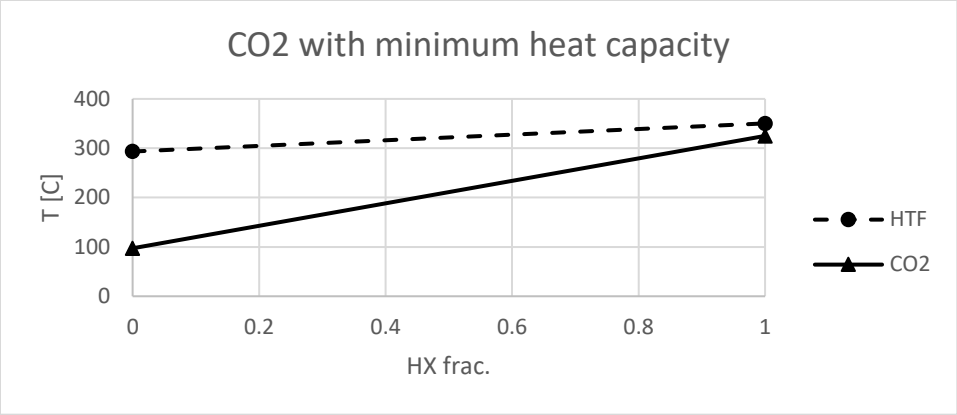

Figure 5-9: Design 1 – Heat capacity of HTF is higher than that of CO_2

Design 1 is summarized in Table 5-2. The high temperature difference between the HTF and the CO_2 (as shown in Figure 5-9), makes the UA value of the evaporator low. However, to accomplish this, the heat capacity of the HTF must be much higher than that of the CO_2, which increases the flow of HTF In order to achieve an adequate fluid velocity, the number of loops of PTCs must be set at 4 in that more loops would make the HTF velocity too small. A higher evaporator effectiveness would require less UA value, but it would increase the maximum temperature of the HTF.

Table 5-2: Design 1 summary – CO_2 with minimum heat capacity

Choice parameters	
Number of loops	4
Heat capacity ratio (min/max)	0.25
Evaporator effectiveness	90%
Resulting parameters	
HTF maximum temperature	350^{o}C
HTF minimum temperature	287^{o}C
HTF velocity through collector pipes	2.73 m/s
Total HTF volume flow	0.0373 m^3/s (591.2 gpm)
NTU (evaporator)	2.73
UA (evaporator)	48 kW/K
Pressure drop in each loop	240.3 kPa (34.85 psi)
Pumping power through all loops	8.97 kW

Design 2 is summarized in Table 5-3. It should be noted that the heat capacity ratio now expresses CO_2 over HTF because the HTF now has the lowest heat capacity.

Table 5-3: Design 2 summary – HTF with minimum heat capacity

Choice parameters	
Number of loops	1
Heat capacity ratio (min/max)	0.85
Evaporator effectiveness	90%
Resulting parameters	
HTF maximum temperature	395ºC
HTF minimum temperature	127ºC
HTF velocity through collector pipes	2.3 m/s
Total HTF volume flow	0.00789 m^3/s (125 gpm)
NTU (evaporator)	5.7
UA (evaporator)	85 kW/K
Pressure drop in each loop	731.5 kPa (106.1 psi)
Pumping power through all loops	5.77 kW

The disadvantages of this design are:

- More expensive evaporator (almost double UA-value)
- Non-conventional temperature range and mass flow rate, which makes the design more expensive.
- The use of only one loop in series diminishes the flexibility of having parallel loops. Specifically, parallel loops respond better to transient conditions as well as in regulating the HTF temperature and they also allow the plant to work when one of the loops is under maintenance or repair.

This design has different advantages with respect to the previous one:

- It has less HTF volumetric flow, which reduces the capital cost of HTF

- Less pumping power required
- Exergetically more efficient, better heat recovery than steam because temperature is increased unlike with steam evaporation.
- The HTF minimum temperature is lower, which is better for starting the plant, and is still above the freezing protection temperature limit for the HTF.

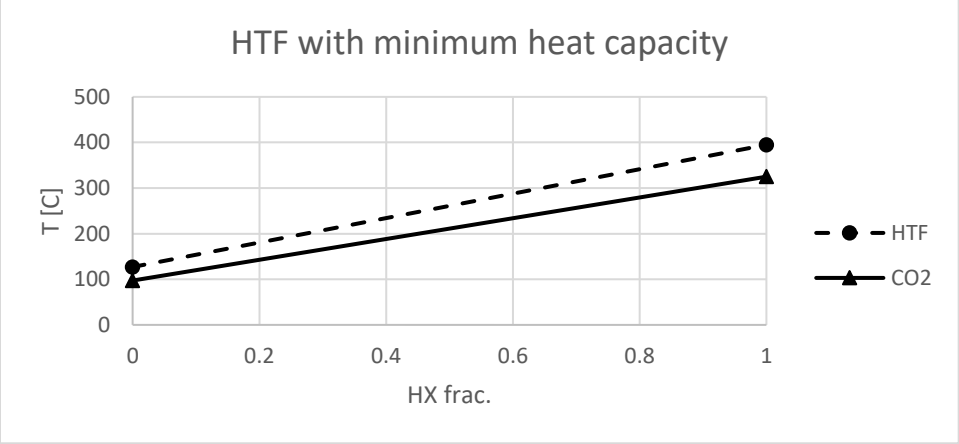

Figure 5-10: Design 1 – Heat capacity of CO_2 is higher than that of HTF

Another alternative for the design of the solar field would be to choose collectors with smaller pipes. This approach would allow for less flow through each collector, increasing the temperature change in the HTF while still having a number of parallel loops. The constraint for Design 2 is that if the number of parallel loops is increased, then the fluid velocity will no longer fall within the specified limits. However, a lower velocity would decrease the pumping power.

5.3.1.3. Code Implementation

The solar field design was implemented in EES (Engineering Equation Solver) by using the input and output variables contained in Table 5-4. Some of the input variables are design choices while others come from calculations previously performed

such as those associated with the thermodynamic cycle. The end result of the procedure is that one can obtain the CO_2 with minimum heat capacity solution.

The design heat collected from the solar field is calculated by assuming values of efficiencies of 97% for the evaporator and 91% to account for parasitic losses. The cycle efficiency comes from the calculation of the cycle variables at design conditions. The subscript 'D' means 'design', and it refers to the value of the variable at the design point. Assumptions are explained here:

- **Evaporator efficiency**: 3% of the evaporator heat is assumed to be lost to the ambient; therefore, the value of efficiency is 97%.
- **Parasitic losses**: For design purposes, the parasitic losses were estimated as 9% of the design cycle input heat, which is calculated with Eq. (5.23) as follows.

$$\dot{Q}_{col,D} = \frac{\dot{W}_D}{\eta_{cycle,D} \cdot \eta_{ev,D} \cdot \eta_{parasitics,D}} \tag{5.23}$$

Table 5-4: Solar field design procedure inputs and outputs

Inputs	**Outputs**
Design Radiation, DNI_D	Design number of collectors, $N_{col,D}$
Design heat collected from solar field, $\dot{Q}_{col,D}$	Field total area, A_{field}
Solar collector design efficiency, $\eta_{PTC,D} = 0.6$	Collectors' number per loop, $N_{col,loop}$
Collector dimensions: L_{PTC}, A_a, D_{ri}	Field temperatures, $T_{M,D}$, $T_{min,HTF}$
Row-spacing of collectors in the field, $L_{spacing}$	HTF mass flow rate (loop), $\dot{m}_{HTF}$
Heat capacity ratio in the evaporator, C_r	HTF volume flow rate (total), $\dot{V}_{HTF,DT}$
Number of loops choice, N_{loops}	HTF velocity in the loop
Evaporator effectiveness, $\varepsilon_{ev,D}$	Evaporator UA-value, $UA_{ev,D}$
CO_2 temperatures in the evaporator: $T_{6,D}$, $T_{1,D}$	Power required to pump the HTF in ideal conditions, $\dot{W}_{HTF,ideal}$
CO_2 mass flow rate in the evaporator, $\dot{m}_D$	
CO_2 enthalpy difference, $q_{col,D}$	
HTF pressure, P_{HTF}	

5.3.2. Power Block Design and Modeling

A majority of the power block design was accomplished in the preliminary studies. The T-s diagram of the base-case cycle integrated with the solar field is shown in Figure 5-11. The processes in the cycle are explained in Table 5-5. The T-h diagram in Figure 5-12 illustrates heat and power exchange by showing the enthalpy differences in the working fluid.

Table 5-5: Explanation of Cycle diagram components and processes

Diagram points	Process
1-2	Turbine adiabatic expansion
2-5	Regeneration hot side
5-3	Cooling
3-4	Adiabatic compression
4-6	Regeneration cold side
6-1	Heating (“Evaporator”).

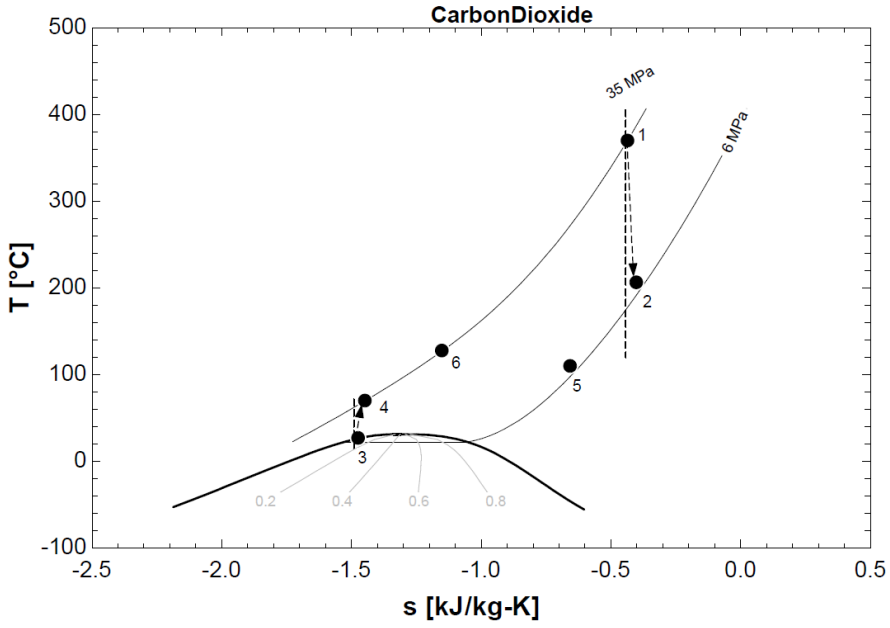

Figure 5-11: Power block thermodynamic base-case cycle T-s diagram

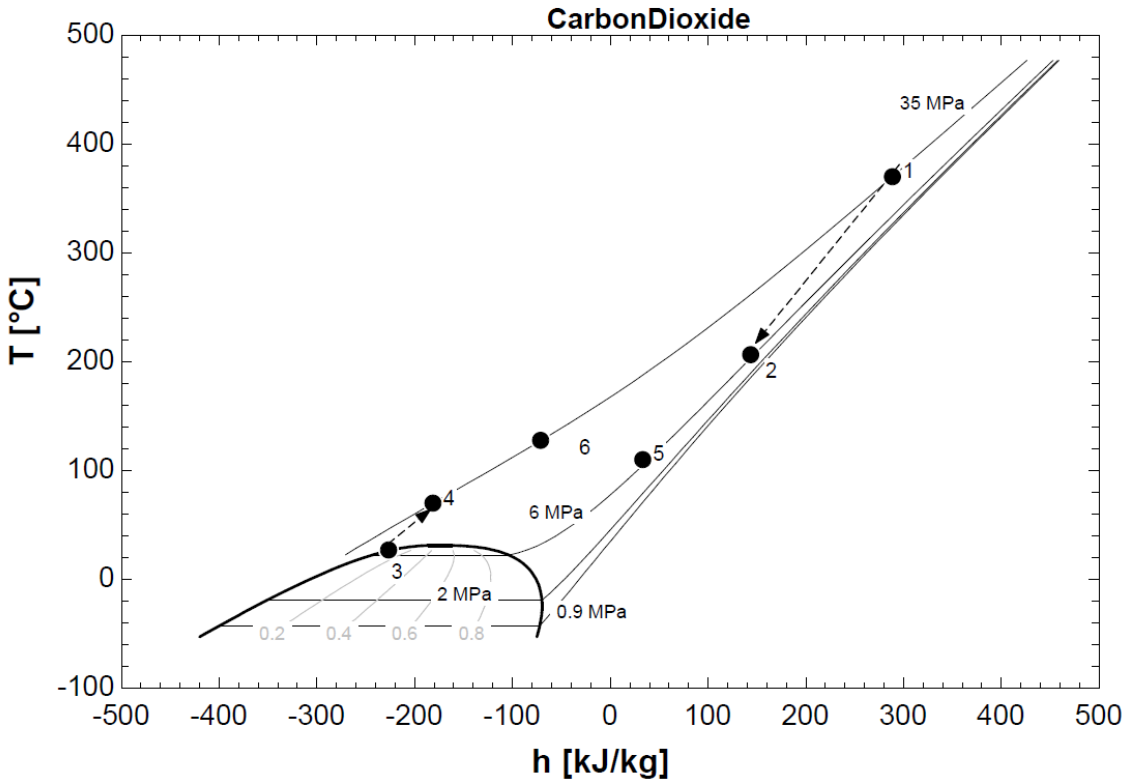

Figure 5-12: Power block thermodynamic base-case cycle T-h diagram

For this stage of the design and simulation, some of the design constraints are specified such as:

- Net electric power of the solar plant: about 1MW
- Heat input of 4 MW. This requirement comes from the assumption that the plant efficiency must be around 25%.

Some assumptions were taken based on literature and other calculations made in this project:

- The maximum cycle temperature of 370^{o}C was estimated for a maximum HTF temperature of 396^{o}C and an evaporator effectiveness of 90% ([50], [50]).

- The maximum pressure of 35 MPa comes from the optimization of the cycle in a preliminary study for a maximum temperature of 325ºC and a minimum temperature (condensation) of 25ºC. Although these two extreme temperatures have now changed for the actual design, the value of the maximum pressure was kept because there is not a lower pressure that would improve the efficiency of the cycle with the new design conditions. Plus, reference, [21], states that 35 MPa is the maximum turbine inlet pressure allowable considering the effect on wall thicknesses that in turn requires more expensive materials.
- The turbomachines isentropic efficiencies are assumed to be 85% for the turbine and 80% for the compressor [24], [54]. Although the conditions for turbomachinery design are different in reference papers, the efficiencies required for the study performed herein should be similar. Plus, these are the values recommended by [21] given that for less than 30 MW they are radial turbomachines.
- Condensation temperature and minimum cycle temperature. After many iterations, this value was finally set at 9ºC above the wet-bulb temperature, as explained below.

5.3.2.1. Regeneration

An approximate sizing was made for the recuperator. Assuming it is a PCHE counterflow heat exchanger type, the LMTD method is used to estimate the UA-value at 60.75 kW/K.

$$UA_{reg} = \frac{\dot{Q}_{reg}}{LMTD_{reg}} \tag{5.24}$$

$$LMTD_{reg} = \frac{(T_{H,in} - T_{C,out}) - (T_{H,out} - T_{C,in})}{\ln\left(\frac{T_{H,in} - T_{C,out}}{T_{H,out} - T_{C,in}}\right)} \quad (5.25)$$

The LMTD method is valid because the considered pressure is far enough from the critical point [51].

5.3.2.2. Condensation Temperature and Cycle Cooling Discussion

There was a concern regarding the minimum temperature of the cycle. Looking at the weather data, there are days in which the wet bulb temperature is equal or above 25ºC. In those days, cooling the CO_2 down to 25ºC is impossible even with a cooling tower. Other cooling alternatives studied were the following.

- **Ground cooling**: the temperature of the ground at 10 m of depth remains fairly constant at around 25ºC throughout the year and it is therefore a potential heat sink at constant temperature. Some associated problems might be that the ground might heat up rapidly if not enough ground area is used to cool down the cycle.
- **Night cooling**: Radiation to the night sky provides cooling to temperatures that are below the wet bulb temperature. In a sense, the idea here is to "store cold" during the night to later use it for cooling during the day. In other words, the heat would be stored during the day in water between 18 and 22ºC and in the night this water would be circulated through a surface exposed to the sky so that the heat can be rejected. A simple calculation was made for this by using equations (5.26) to (5.29) below. The area required to evacuate the heat during the night would be 14,198 m^2 as calculated with reasonable assumptions.

$$A_{req} = \dot{Q}_{rad} / (q_{rad} - q_{conv}) = 14198 \text{ m}^2 \quad (5.26)$$

$$\dot{Q}_{rad} = \dot{Q}_{cond} \frac{t_{op,day}}{t_{cool,night}} = 2500kW \frac{8h}{8h} \quad (5.27)$$

$$q_{rad} = \sigma\varepsilon(T_s^4 - T_{sky}^4) \quad ; \quad \text{where: } T_s = T_{water,avg} = 20^oC \text{ , } T_{sky} = -40^oC \text{ , } \varepsilon = 0.9 \quad (5.28)$$

$$q_{conv} = h_{air}(T_{air} - T_s) \quad ; \text{ where: } h_{air} = 5 \text{ W/m}^2\text{K and } T_{air} = 30^oC \quad (5.29)$$

However, the option of storing a day of cooling in the form of water temperature from 18 to 22°C was assessed and deemed more feasible compared to the two previous options of night cooling and ground cooling. A whole 8 hours of continuous 2.5 MW of heat rejected in the condenser would only require a water volume of 4310 m^3, which equals to a cube of 16 meters or 50 feet, which is of the size of a small building. This technology could be used in the situation where heat cannot be rejected at a sufficient rate to the ground or to the environment through a cooling tower during the daytime operation hours. Additionally, the cooling tower could be left on in the night.

Another concern regarding the cold part of the cycle is whether there are problems associated with operating close to the critical point. The design of the heat exchanger and pump is affected when operating close to the critical point due to the rapid change of density and other properties of the fluid, including specific heat capacity.

5.3.2.3. Heat Recovery and Heat Rejection Heat Exchangers and Cooling Tower

The cycle was designed to produce cogeneration heat through a heat recovery unit that collects heat in the 60°C to 90°C temperature range for process heat. A minimum CO_2 temperature was established at 62°C because below this temperature the heat transferred to the cooling water can no longer be considered useful to cogeneration.

The cycle cooling-cogeneration system consists of two heat exchangers and a cooling tower. The first heat exchanger after the cooling tower is also called Water Circuit 1 (WC1), and it receives the heat from the condensing CO_2. The water flow is then divided so that a fraction goes to the Water Circuit 2 (WC2) and the rest goes back to the cooling tower. In WC2, the water receives heat from the non-condensing part of the CO_2 cooling, and then it is heated up to 80^{o}C. From there, the water goes to the industrial process (additional heat might be produced by a burner), and gives up the cogeneration heat, which returns to 60^{o}C. Next, this water stream is directed to the cooling water and therefore mixed with the stream coming from WC1.

Before explaining the different circuits in more detail, different alternatives for the cycle that were considered in the design process are highlighted here:

- Single stage absorption Chiller: The possibility of having an absorption chiller to receive the cogeneration heat and thus cooling down even further the CO_2 was discarded because of the unsuitability of the temperatures and the heat fractions. A COP of 0.7 is not enough to cool down all the condensing CO_2.
- Double stage absorption chiller: This option would require higher temperatures, thus eliminating the cycle regeneration, which lowers the cycle efficiency almost 4 percentage points, with the COP still not enough to produce all the cooling needed. This option was therefore discarded as well.
- Cooling the cycle with a vapor-compression chiller, instead of a cooling tower. With a COP of 7, the vapor compression would require electrical energy that would reduce the cycle efficiency from 27% down to 22%, making it unsatisfactory.

The reason why so many different options were considered is that the cooling tower might not always produce the needed temperatures in the water to condense the CO_2 far enough from the critical point (31°C). Indeed, in the summer, the wet-bulb temperature can be as high as 26°C, which means being below the supercritical point is impossible assuming the condensation temperature must be some 9°C above the wet-bulb temperature. Above the critical temperature, the design of the cycle components will be completely different, as a result, unless some external cooling is used, the plant will not be able to operate after the wet-bulb temperature reaches a certain value.

5.3.2.3.1. Cooling Tower

Using a design wet-bulb temperature of 18.5°C. Relevant information about commercial cooling towers was gathered, and performance curves of commercial cooling towers are presented below.

- Cooling towers can cool water to within 2 to 3 K of the ambient wet-bulb temperature [55]. The difference between the cooled water leaving temperature and the entering air wet-bulb temperature is called the temperature approach, and the difference between entering and leaving cooled water temperatures is the called temperature range.
- The reference ratio for water flow rate and refrigeration power is 54 mL/s per kW or 3gpm per ton [55] for a range of 10°F or 5°C.
- The auxiliary power required to operate a cooling tower is 16 kWe/MWth for mechanical draft towers, and 10 kWe/MWth for natural draft towers [21].

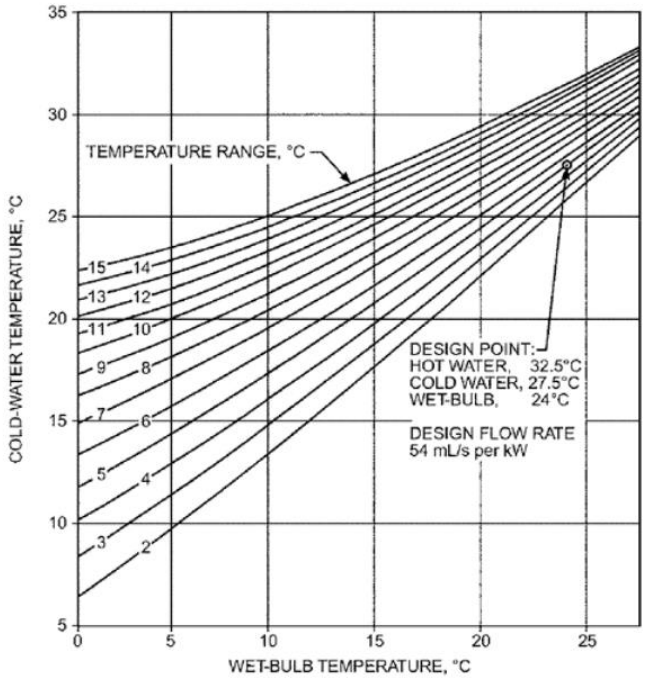

Figure 5-13: Cooling tower performance curves for design flow rate, reprinted from [55]

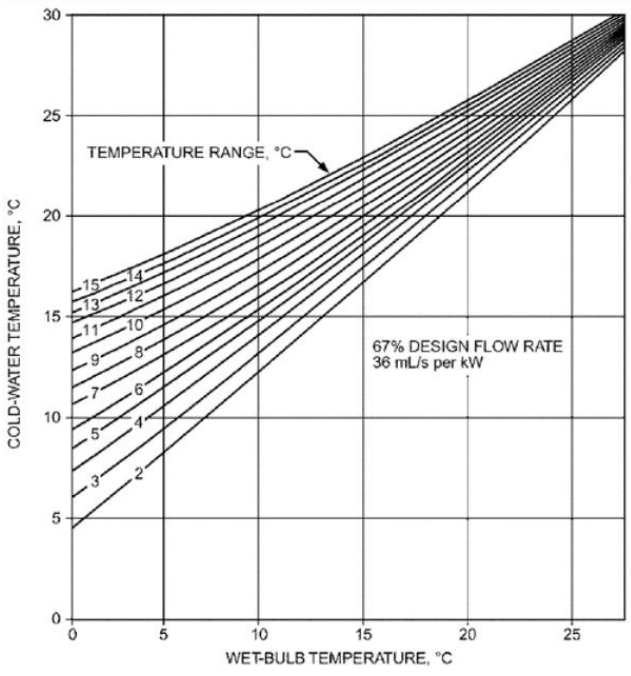

Figure 5-14: Cooling tower performance curves for 2/3 design flow rate, reprinted from [55]

It can be observed from the performance curves data that the temperature approach decreases when the mass flow rate is decreased, as well as when the temperature range is decreased. This behavior makes sense because it means that at lower demand of cooling, lower temperatures can be reached.

A potential design point for the cooling tower is 3ºC approach with 5ºC range, which the design point that the reference [55] has identified on Figure 5-13. However, for this design it is preferable to have a smaller temperature approach and range so that condensation can be attained at a low temperature.

The heat that must be rejected to ambient rejected in the form of water cooled down in the cooling tower at design conditions amounts to 2560 kWth or 728 ton, which is approximately the same regardless of the condensation temperature or pressure: for T_{cond} = 30ºC, it is 672 ton. For a bigger flow rate of water, if the heat is the same, the temperature range should be less: more flow rate means less temperature difference in the water for equal energy transfer rate.

An iterative calculation was accomplished to find out a suitable design point. The temperature difference of the water in the condenser was first selected. Then, this selection would result in a certain cooling water range after calculating the mixed temperature of the water going directly from the condenser to the cooling tower (WC1) and the water coming from the cogeneration process at 60ºC (WC2). Knowing the temperature range and the wet-bulb temperature, the temperature approach was calculated using the performance curves, namely Figure 5-13 and Figure 5-14. A procedure for this iterative calculation process is shown below.

$$T_{w1,in}\ \text{(guess)} \rightarrow T_{w1,out} = T_{w1,in} + \Delta T_{w1,cond}\ (\Delta T_{w1,cond}\ \text{choice}) \rightarrow$$

$$\xrightarrow{\text{EES calculation}} \begin{cases} T_{tower,in} = x_{w1}T_{w1,out} + x_{w2}T_{w2,out} \\ \Delta T_{range} = T_{tower,in} - T_{w1,in} \\ \dot{m}_w = \dot{Q}/(c_{p,w}\Delta T_{range}) \end{cases} \xrightarrow[Curves]{Performance}$$

$$\rightarrow T_{w1,in} = T_{WB} + \Delta T_{approach} \rightarrow \text{ Iterate with new } T_{w1,in}$$

The result reached with this calculation has a temperature range of 3°C with a flow rate of water of 3300 gpm or 212.3 kg/s. In this design point, the other variables are summarized below:

Table 5-6: Cooling tower design resulting values

Variable	Value	Variable	Value
T_{WB}	18.5°C	$\Delta T_{w,cond}$	1.5 °C
$T_{tower,in}$	23.1°C	$T_{w1,in}$	20.25°C
$T_{tower,out}$	20.25°C	$T_{w1,out}$	21.75°C
ΔT_{range}	2.84°C	$T_{w2,in}$	21.75°C
$\Delta T_{approach}$	1.75°C	$T_{w2,out}$	80°C

In the design, the temperature approach was forced to be as low as possible based on the performance plots. Therefore, at a temperature range of approximately 3°C, and a wet-bulb temperature of 18.5°C, a temperature approach of 2°C is reasonable.

5.3.2.3.1.1. Commercial Cooling Tower Selection Example

In order to attain an approach even lower, the design point of the cooling tower will be placed at 67% of its capacity. This means that the performance curve used will be that of Figure 5-14, allowing for smaller temperature approaches and knowing that the actual capacity of the tower is not 700 but 1000 tons (the design point is at 2/3 of the tower's full load).

An example of a suitable cooling tower for this application is that found in [56]. Its capacity is 1000 tons (a unit is shown in Figure 5-15) and it allows for a water flow rate higher than 4000 gpm, which is desirable for off-design operation.

Figure 5-15: 1000-Ton Commercial Cooling Tower, reprinted from [56]

5.3.2.3.1.2. Off-Design conditions

At off-design conditions, the wet-bulb temperature could rise, and so, the pressure in the condenser should rise as well to allow for the CO_2 to condense. This could easily be controlled with a pressure controlling device similar to those used in refrigeration condensers.

According to the cooling tower performance curves, approaches are smaller at higher wet-bulb temperatures, which is beneficial to performance. Plus, in order not to go above 30^{o}C condensation of CO_2 (recommended limit to stay far from the critical point, [21]), the temperature difference between the CO_2 and the water should be reduced; therefore, the UA-value in the condenser should increase. According to Eq. (5.30), [42], [18], this increase is possible by increasing the flow of water, which is beneficial for lowering the temperature approach, for the same cooling tower duty.

$$\frac{UA}{UA_{ref}} = \left(\frac{\dot{m}}{\dot{m}_{ref}} \right)^{0.8} \tag{5.30}$$

Meteorological analysis reveals that between 8am and 4pm solar times, in a typical year in College Station, there are 806 hours of wet-bulb temperatures above 24°C and 454 hours above 25°C, which is a significant number. Since it has been shown that the plant operating at condensation temperatures higher than 30°C might have to shut down or have a cold-water storage to respond to these high temperatures.

The off-design behavior of the cooling system, although covered qualitatively here and not quantitatively, reveals that the plant might still be able to condense the CO_2 below 30°C for wet-bulb temperatures as high as 26°C. However, in a conservative approach, the hours of operation used in the economic analysis of the plant might have to be reduced by 800 or 500.

5.3.2.3.2. Shell and Tube Cooling Heat Exchangers

The design of the condenser is based on a shell-and-tube heat exchanger. Condensation of CO_2 occurs on the shell side because phase change from vapor to liquid significantly increases the pressure drop the tube side due to changes in fluid velocity, which should be avoided. Given that the CO_2 is non-corrosive, a fixed tubesheet type is appropriate so that cleaning is easier on the tube side, where the water flows.

A simple calculation was made to ensure that the high pressure in the shell would not compromise safety. The maximum diameter of a shell is 3 m; this is a manufacturer's limit. The shell material could be aluminum or carbon steel because CO_2 is non-corrosive. The allowable stress in the material is therefore assumed to be 200

MPa. Knowing that the critical stress in a cylinder is circumferential (rather than longitudinal), the minimum shell thickness is calculated for the most unfavorable case.

$$\sigma_{\max} = \frac{pD}{2t} \Rightarrow t_{\min} = \frac{pD}{2\sigma} = \frac{6MPa \cdot 3m}{2 \cdot 200MPa} = 4.5cm = 1.77in \tag{5.31}$$

This thickness is not particularly high, therefore the high pressure should not be a problem in the actual design of the condenser.

5.3.2.3.2.1. Water Circuit 1 – Shell and Tube Heat Exchanger

The UA-value of the condenser is calculated with the following equations [53] using the effectiveness-NTU method.

$$NTU = -\ln(1-\varepsilon) \tag{5.32}$$

$$UA_{cond} = NTU \cdot C_{\min} = NTU \cdot \dot{m}_{w1} c_{pw} \tag{5.33}$$

At design conditions, the calculated UA-value is 282 kW/K. This value will be used later to estimate costs. This required UA would be much more costly if this was a PCHE.

The design condensation temperature was chosen to be 4^{o}C above the highest water temperature. Therefore, the condensation temperature at the design point is 7.5^{o}C above the wet-bulb temperature. A capture of the T-s diagram in Figure 5-16 is used to show the different temperatures in the condenser.

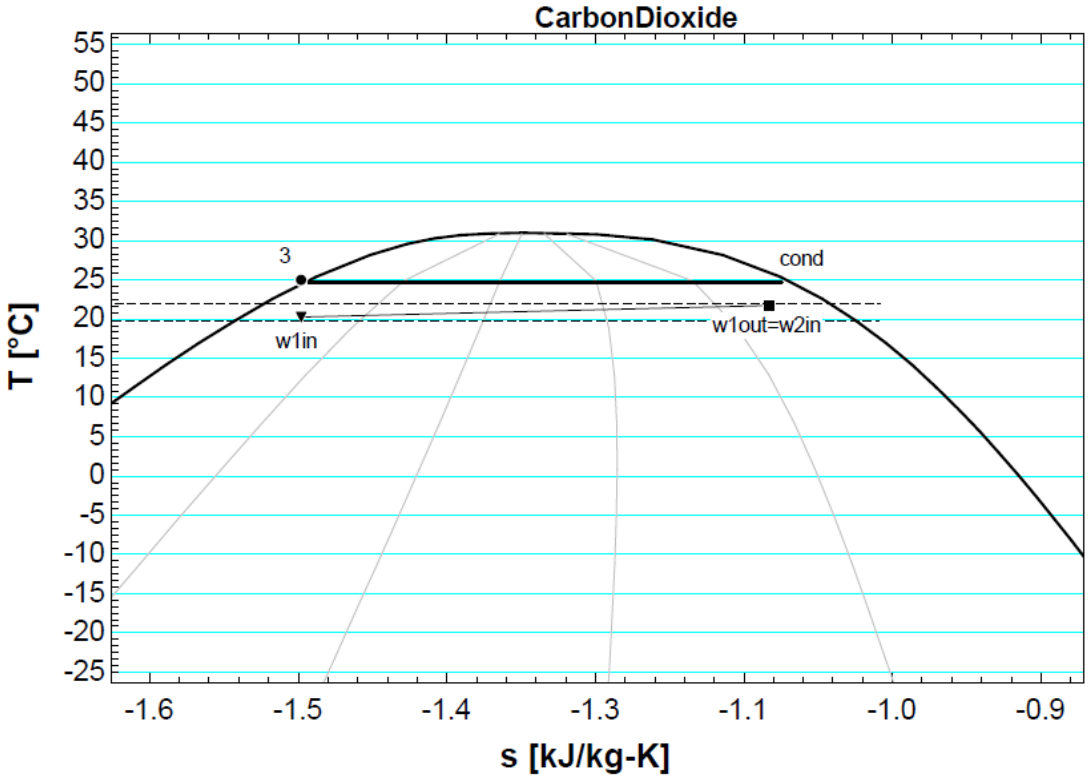

Figure 5-16: T-s diagram showing heat exchanging process in the condenser

5.3.2.3.2.2. Water Circuit 2 – Shell and Tube Heat Exchanger

The LMTD method was used for this heat exchanger design. In this case, the CO_2 will be on the tube side because its state is consistently gas, and it has a high pressure. An online calculator, [57], was used to estimate the necessary parameters for shell and tube heat exchangers in the LMTD method. The equations are attached here as well as a T-s diagram for further information.

$$\mathrm{UA}_{\mathrm{heatRecovery}} = \frac{\dot{\mathrm{Q}}_{hR}}{\mathrm{LMTD}_{hR} \cdot \mathrm{F}} \quad ; \text{F: correction factor (obtained online)}$$
$$\dot{\mathrm{Q}}_{hR} = \dot{m}_{w2} \cdot c_{pw} \cdot (T_{w2out} - T_{w2in}) \; ; \; T_{w2out} = 80^{o}\mathrm{C} \; ; \; T_{w2in} = T_{w1out} \tag{5.34}$$

$$\dot{Q}_{cog} = \dot{m}_{w2} \cdot c_{pw} \cdot (T_{w2out} - T_{w2cog})$$
$$T_{w2cog} = 60^{o}\text{C (returning water from cogeneration)} \quad (5.35)$$

The correction factor, F, depends on the temperatures and the heat exchanger type. This heat exchanger was conceived as a U-tube with simple shell, which facilitates the cleaning of the shell surface that is exposed to the most corrosive fluid: water.

Since the temperature difference between the two fluids is small, the number of shells must be increased to achieve a real F correction factor. In the first design, 4 shells with two tube passes each yielded an F-factor of 0.75, which is reasonable and does not make the UA-value much higher. A lower number of shells would result in too low of a F-factor or even a non-existing conclusion and thus an impossible design. A higher number of shells should be considered in the detailed design to increase the F-factor, obtaining a lower UA-value at design conditions. However, there must be a limit where the area reduction in the heat exchanger is no longer beneficial due to increased costs of manufacturing a greater number of shells.

As shown in Figure 5-17, the minimum temperature used for cogeneration is 60^{o}C. A heat recovery efficiency or effectiveness can be calculated as the ratio between the heat received by the water and the heat transferred from the CO_2. If this efficiency is higher than one, it means that there has been a pinch-point violation, meaning that at some point of the heat exchanging process the temperature of the water has surpassed that of the CO_2. This is technically unfeasible because heat cannot be transferred from lower to higher temperature. Therefore, the mass flow rate of water must be reduced.

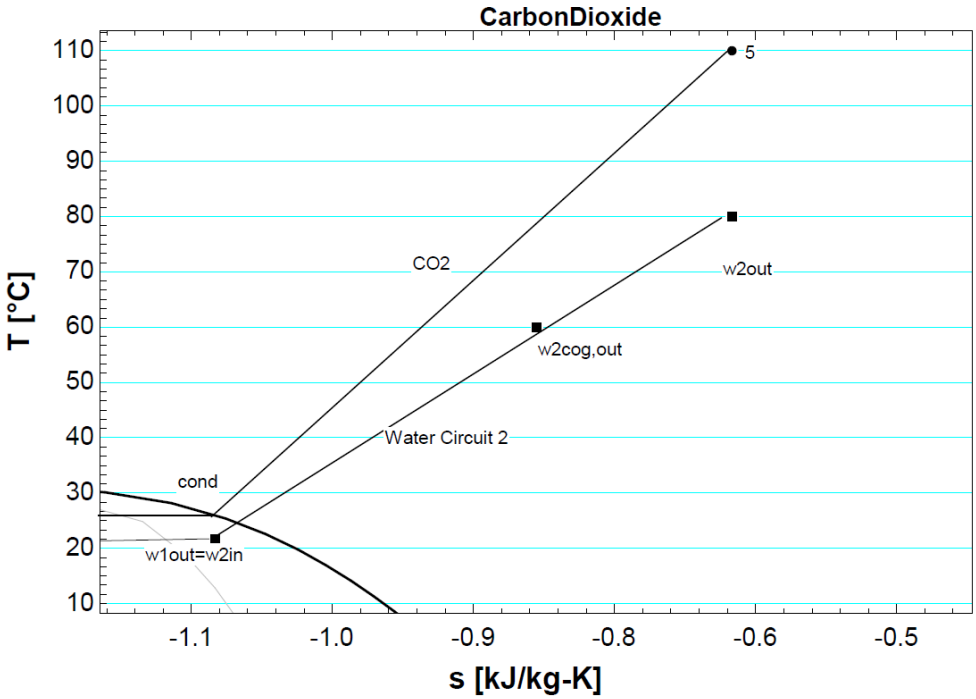

Figure 5-17: T-s diagram showing heat exchanging process in the heat recovery exchanger

As a result, the heat contained in the water from 80°C down to 60°C is smaller than the heat contained in the CO_2 from 110°C down to 60°C. Still we need the 110°C in the CO_2 to drive the heat transfer and make the exchanger cost lower.

$$\eta_{heat\,\mathrm{Recovery}} = \frac{\dot{Q}_{cog,w}}{\dot{Q}_{cog,CO2}} = \frac{\dot{m}_{w2} \cdot c_{pw} \cdot (T_{w2out} - T_{w2cog})}{\dot{m}_{CO2} \cdot (h_{cog,1} - h_{cog,2})} \tag{5.36}$$

5.3.2.4. Compression Device Discussion

The question mark regarding the condenser and pump was resolved after attending a conference by Dr. Jeff Moore, a researcher from the Southwest Research Institute. Dr. Jeff Moore is an expert in turbomachinery and agreed that condensing the fluid is possible and that it is easier to compress it when it is a liquid. Above the critical

point on the left of the dome the fluid is something between a liquid and a gas, and it is possible to fit a device that can be called a pump there even when closer to the critical point. The main consideration is not to have two-phase flow and to ensure a positive NPSH for the pump. The compressing device, as stated, would still be a pump of some kind, even with the density change. Research is being conducted on turbomachinery for CO_2, and it is characterized by being compact and also expensive to manufacture due to the high temperatures and pressures required for design. Testing is already being conducted, which means these machines have already been built and operated, and the business case estimates a favorable cost of energy.

The aim of this project is also to propose different alternatives as to the design of the cycle. This optimization will be discussed in the last chapter of this document, namely, with the goal of determining if a condenser and a pump are more cost-effective than a compressor. In other words, if for this application, the transcritical cycle is actually better than the supercritical one.

If a compressor was implemented, it would require much more compressing power with less cooling as compared to a pump. Taking the compression ratio of the base-case cycle: 4.7 (from a pressure about 6 to 35 MPa), an analysis was performed to find out how much more compression work is required in other points of the T-s diagram, assuming the same compression ratio. Figure 5-18 reveals that if the compression is started at 50^{o}C, the compression work could be doubled as compared to the original case below 30^{o}C. As temperature increases, the fluid behaves more like a gas, becoming more difficult and expensive to compress. Figure 5-19 and Figure 5-20

show the density behavior, with the density of point 3 (before compression in the base-case cycle) being higher as the pressure increases and entropy decreases. As to the outlet-to-inlet density ratio, a liquid behavior is observed as well in the zones with less entropy than the critical point.

It can be concluded from an analysis of this set of plots that indeed the fluid is easier to compress and behaves more like a liquid on the left side of the dome at lower temperatures. Therefore, knowing that near the critical point, compression is feasible, the design aim was to cool down the CO_2 as much as possible (by lowering the condenser temperature), and in those cases where it was not possible to condense (because wet bulb temperature is high), the pump will be assumed to operate above the critical point, since properties are not too far from those of a liquid.

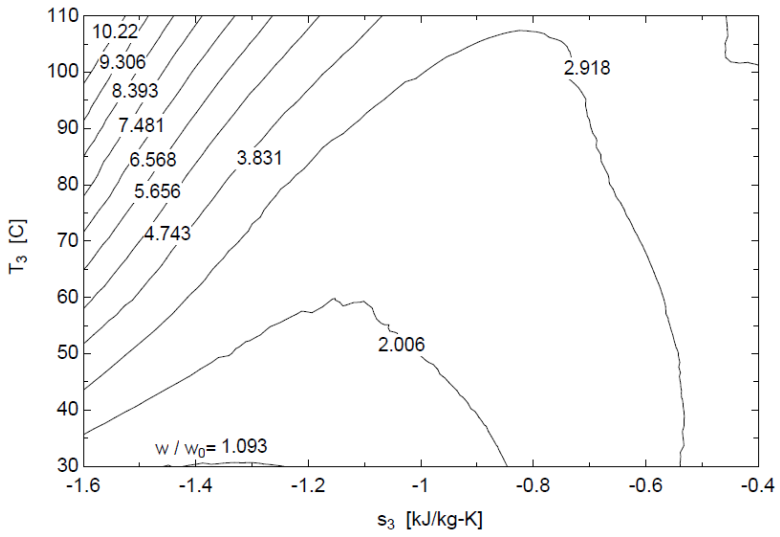

Figure 5-18: Ratio of compression work with respect to base-case cycle required compression work for a compression ratio of 4.7

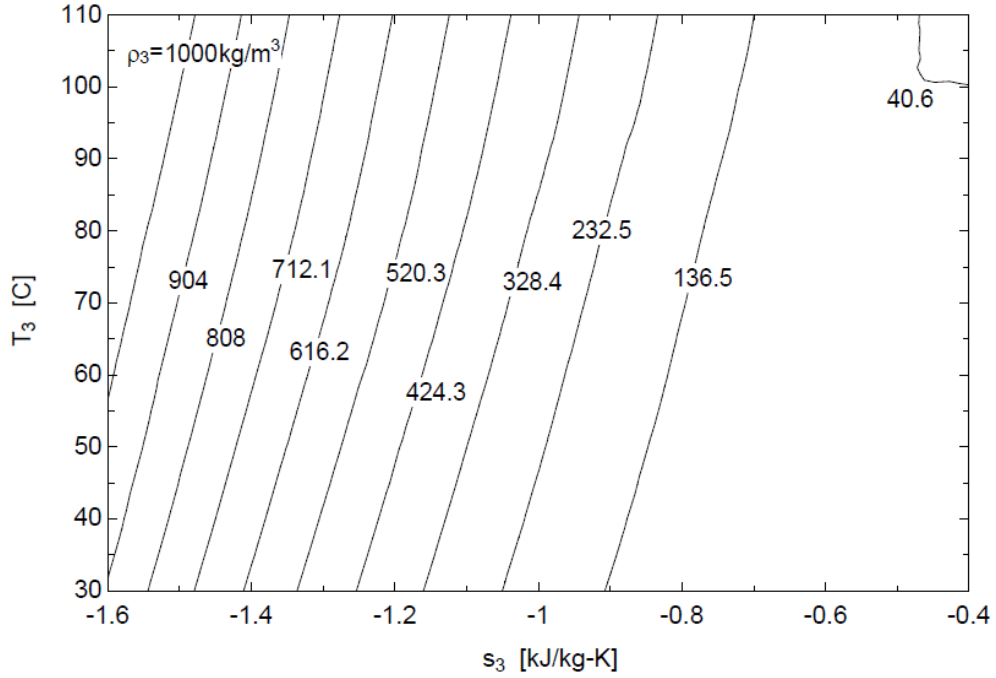

Figure 5-19: Density of point 3 (of the base-case cycle) with respect to temperature and entropy

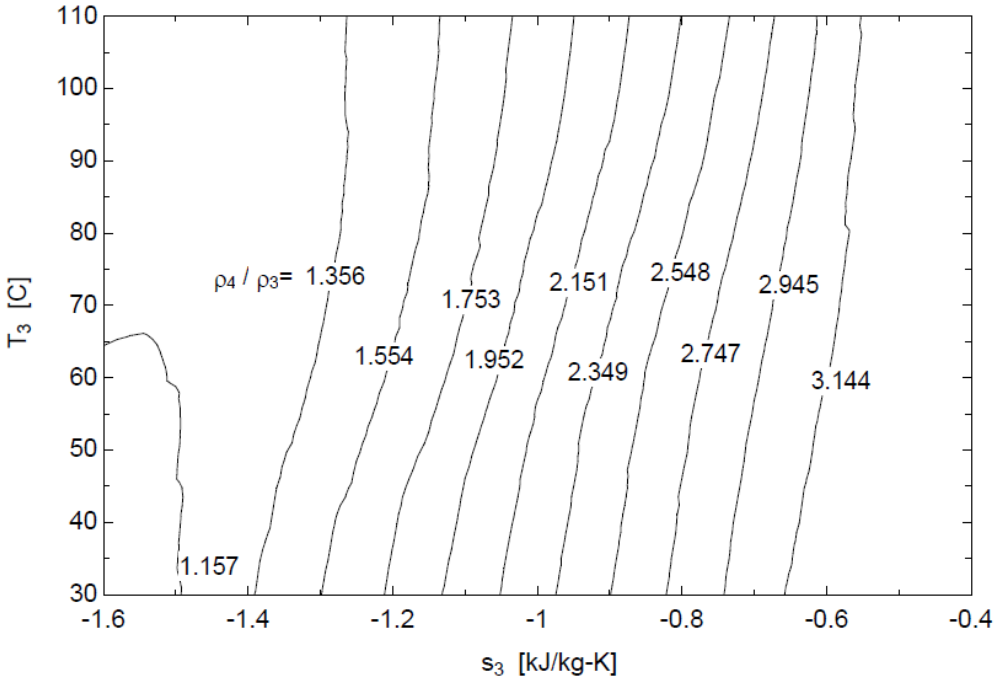

Figure 5-20: Density after compression over original density contour plot.

The cooling solution will still be a cooling tower. Since no mixed-phase is allowed in the pump, the temperature at point 3 will be at least 0.5ºC lower than the condensation temperature.

In the code, for the cases in which there is condensation in the cycle, the lower pressure was found as the saturation pressure for a given condensation temperature. For those cases in which the cycle does not enter into the dome (no condensation), a condensation temperature was still specified, but the lower pressure was found by finding the pressure for which the "condensation" temperature is reached with the same entropy as the critical point. This way, a fictional "condensation" temperature is reached in the vertical line that crosses the critical point in the T-s diagram.

5.3.2.5. Power Block Outputs

The electrical and thermal outputs of the power block are computed taking into account losses and efficiencies. Some assumptions taken are the following:

- Cooling tower power is stated to be 16 kW/MWth [21]. Given that the cooling tower has been designed for a higher mass flow rate of water, it is expected that the energy consumption is as well higher. However, this high mass flow rate also occurs at part load. A value of 25 kW/MWth was deemed reasonable.
- HTF pumping power: The ideal HTF pumping power required to go through the solar field is calculated with Eq. (5.19). The pressure loss through the PCHE is estimated in less than 8% of the HTF pressure. This estimation is discussed in the detail design section. Ideal pumping power is divided by 0.6 to obtain the actual power required, considering a 60% pump efficiency and other losses.

- Other parasitics: the gas burner, solar field drives, balance of plant… Since the highest parasitic losses are HTF pumping and cooling tower, the balance of plant energy consumption is represented with an efficiency of 95%.
- The generator efficiency is estimated at 95% (98% minus 3% due to frequency conversion) [21]. Power electronics' losses are an additional 2 or 5% [58]. They are required to convert to grid frequency and their efficiency is included in the generator efficiency.
- If the compressor is not turbine driven it requires a drive motor efficiency of 95%, but this was assumed to be represented in the balance of plant losses.

With these assumptions, the final efficiency values are calculated:

$$\eta_{sol,electric} = \frac{\dot{W}_{elec}}{\dot{Q}_{solar}} \tag{5.37}$$

$$\eta_{sol,cogen} = \frac{\dot{W}_{elec} + \dot{Q}_{cog}}{\dot{Q}_{solar}} \tag{5.38}$$

5.3.3. Economics

5.3.3.1. Simulation Results Used

As explained, the design code and the simulation code were assembled in parallel, meaning that to complete some part of the design code, specifically, the economics part, some results had to be retrieved from the simulation code, as explained in a later section in this chapter.

The simulation program shows the performance of the plant when responding to median/average days for each month in the year, assuming the plant is powered only by

solar energy. Extrapolating these results, global-year plant performance can be approximated as follows:

- Equivalent full-load hours in the year. This comes from assuming that the plant is operating for 8 hours every day in the year: 8*x*365=2920 hours.
- Equivalent solar full-load hours in the year. The energy generated in one year coming only from solar energy is used to compute this number.

$$t_{eq,FL,solar} = \frac{kWh_{yr,solar}}{\dot{W}_D} = 1190.9 \text{ h} \tag{5.39}$$

- Equivalent fossil full-load hours in the year. Obtained as the difference between the solar and the total full-load hours.

$$t_{eq,FL,fossil} = t_{eq,FL,total} - t_{eq,FL,solar} \tag{5.40}$$

5.3.3.2. First Approximation Calculations

This section was developed in parallel with the following section: Simulation with Median Days for Each Month, from which the output electricity and natural gas from the plant are known. Therefore, an income estimation can be made. Before anything it should be noted that the maximum income that can be obtained from this plant would come from operating for 8 hours every day (operation time assumption) at full load: 1 MW of electric generation based on producing 8000 MWh every day and billing the kWh at $0.08/kWh, the yearly income is $233,600/year. The simulation at College Station, TX reveals an income of $105,540/year (only solar energy), which aligns with the 53% load factor (over total operation time 8h/day) appreciated in the graphs of median days simulation for each month.

As to natural gas savings due to production of cogeneration heat, assuming $2.7/MMBtu of natural gas, the yearly income at College Station would be $14,329, which makes the total income equal to $119,870/year. If the required payback period of the project is 20 years, the capital investment should be less than 2.4 million dollars.

Following a reference, [59], the cost of the different components of the power block was estimated. The power devices have a cost associated to its nominal power in kW, and the heat exchangers' cost depends on their UA value. Since these values are already known, a first estimation of the cost can be made.

Table 5-7: First approximation power block components cost estimation

	UA (W/K)	$\dot{W}$ **(kW)**	**Cost Scaling Law,** [59]	**Cost ($)**
Primary HE	50000		$17.5(UA[W/K])^{0.8778}$	$233.235,11
Recuperator	14000		$5.2(UA[W/K])^{0.8933}$	$26.286,91
Condenser	25000		$76.25(UA[W/K])^{0.8919}$	$637.914,60
Compressor		600	$643.15(\dot{W}[kW])^{0.9142}$	$219.779,01
Turbine		1650	$9923.7(\dot{W}[kW])^{0.5886}$	$777.113,90
Total				**$1.894.329,52**

These cost scaling laws are obtained from commercial equipment with applicability to CO_2 power cycles data. Another source estimates the total cost of a 10 MWe s-CO_2 system at $35 million, [60]. The actual equipment is expected to be less expensive because the usual temperatures managed in CO_2 supercritical cycles are much higher (700^{o}C) than the temperatures considered for the solar plant, with the lower temperatures decreasing the cost of equipment.

These costs can be compared to the state-of-the-art power blocks in PTC plants. For example, a recently built plant is the Solana Power Plant, located in Arizona. This plant is much bigger (280 MW), but assuming scalable costs, the cost of a plant per MW can be estimated from Solana's total cost of $2 billion.

The cost breakdown for a solar PTC plant was found in a reference, [61], and is shown in Table 5-8. It is observed that the power block and balance of plant portion of the cost is cheaper (per MW) than the price of $1.8 million calculated in Table 5-7. This plant cost is not completely accurate because at a small scale, elements are usually more expensive per MW; however, this approximation helps to give an idea of the state-of-the-art costs.

Table 5-8: Solar PTC plant cost breakdown, [61]

	% cost	Normalized cost ($/MW)
Indirect costs	15%	$1.071.428,57
Power Block and BoP	15%	$1.071.428,57
Storage	20%	$1.428.571,43
HTF system	10%	$714.285,71
Solar field	35%	$2.500.000,00
Site improvements	5%	$357.142,86
	100%	$7.142.857,14

It should be noted that the payback period of the Solana power plant is about 16 years, which means that the capital investment is just about 16 times the yearly income. However, this payback period is not in the same line for the modeled CO_2 plant. Assuming that the considered plant could have the same cost per MW as Solana, but without Thermal Energy Storage (TES), the capital investment of the CO_2 plant should be about $6 million. With the calculated yearly income of the plant in College Station,

TX, the payback period would be close to 60 years, which is economically inadmissible. To improve this, the solution is either to increase yearly income or to reduce the capital cost. The first strategy seems more feasible than the second one since it is known that the plant's capital cost will be hard to decrease. Some ways of increasing the yearly income are:

- Incorporating TES: this would increase the load factor of the plant and it would allow it to operate during more hours in the day. However, this would also increase the capital investment.
- Incorporating a gas burner: this could contribute to increase both the hours of operation of the plant and the electric efficiency, and it would not be a dramatic increase in the investment. However, it would make the plant not completely renewable.
- Relocating the plant to an area with more sunshine. If it is deemed completely unfeasible for the initially chosen location

Solana incorporates 6 hours of TES at full load. Since the price of electricity at night is low, the plant operates at part load at night for a longer period of time (some 14 hours). This mode of operation and also the fact that the plant is able to operate at full load for 10 hours in the day (with the assistance of TES), is what makes the payback period low for this case study.

For the economics part, the next steps will be completing the design of the plant, finding ways of making it more viable and eventually calculating the LCOE.

5.3.3.3. Economic Analysis General Assumptions

Given the present state of development for sCO2 power cycles, the cost estimate developed is a Class 4 Feasibility Study, with an estimated accuracy range of -15/+50 percent [25]. The following assumptions were considered in the economic analysis:

- **Natural gas prices** [62]: According to reports from EIA, for industrial customers the price is about $4/MMBtu. For electricity generation it is $3/MMBtu and for commercial customers it goes up to $8/MMBtu.
- **Cost of electricity**: There are energy costs (per kWh) and demand costs (per kW_{max}). For US average industrial consumers, electrical energy cost is $0.067/kWh for industrial consumers, and $0.106 for commercial consumers [63]. In Texas, prices are lower: $0.056 and $0.0824, [63]. A design value of 7 cents per kWh was selected. As to the demand cost, with available data [64] it was estimated at some $70,000/MW-year.
- **Investment tax credit**: government aid for investments in solar power generation, 26%, [65].
- **Economic Analysis Period**: 25 years, typical value.
- **Discount rate**: 7.5%, typical value, also used in the reports to which this one was compared.

5.3.3.4. Equations Implemented in the Economic Analysis Code

5.3.3.4.1. Power Block Capital Expenditure

The fact that the supercritical CO_2 technologies are new makes it difficult to provide an estimation of their capital cost. Still, some references [59], [25], [22], [66] were found, providing cost estimations for the components of the cycle. For the design code, reasonably accurate estimates were sought, and as a result, the cost of the components was chosen as the largest of two approaches, namely (a) the output of the equations in Table 5-7 [59] and (b) the relationships in Table 5-9, found in reference [22].

Table 5-9: Cost estimation equations for sCO_2 components, [22]

Component	Specific cost
Recuperator	2500 $/(kW/K)
Primary Heater (Evaporator)	5000 $/(kW/K)
Shell and Tube Chiller (condenser and heat recovery)	1700 $/(kW/K)
Turbomachinery+Generator+Etc.	1000 $/kW

With these assumptions, the power block cost is approximately 2 million dollars for a 1-MW facility.

For individual component cost estimations, the following assumptions were made:

- Generator: In a reference [25] it was found that a generator of 230 MVA at a power factor of 90% (200 MW) would cost $110,000; making a specific cost of $0.53/kW. For a smaller size of 1 MW, a specific cost of $1/kW was assumed, having then a generator of $1000, which is 0.1% of the expected cost of the turbomachinery (pump and turbine).

- Pipes: the cost of pipes are due to the high pressures. It was assumed this cost would be 5% of the cost of the turbomachinery.
- Costs of other equipment: electronics and auxiliaries' cost could be lumped into a 10% of the turbomachinery cost.
- The UA-values of the heat recovery heat exchanger and the condenser were added together. This way, the shell and tube heat exchangers cost was lumped into one variable.
- Shell and tube heat exchangers cost was also roughly estimated looking at commercial samples and available information. For a gas at high pressure inside and liquid outside tubes (heat recovery HX), typical U-values range from 200 to 400 W/m^2K, while for organic vapors or ammonia outside and cooling water inside tubes it ranges from 300 to 1200 W/m^2K (condenser, assumed similar behavior to condensing CO_2), [67]. Therefore, with a design UA-value of 369 kW/K and a conservative U-value of 300 W/m^2K, the required area of shell and tube heat exchangers is 1230 m^2 or 13240 ft^2. Looking at Figure 5-21, for U-tube and Fixed-head heat exchangers, the cost can be estimated at less than $300,000. High pressure operation may increase the cost with a factor of 150%. $450,000 is therefore the chosen value to conservatively represent the shell and tube HX cost.

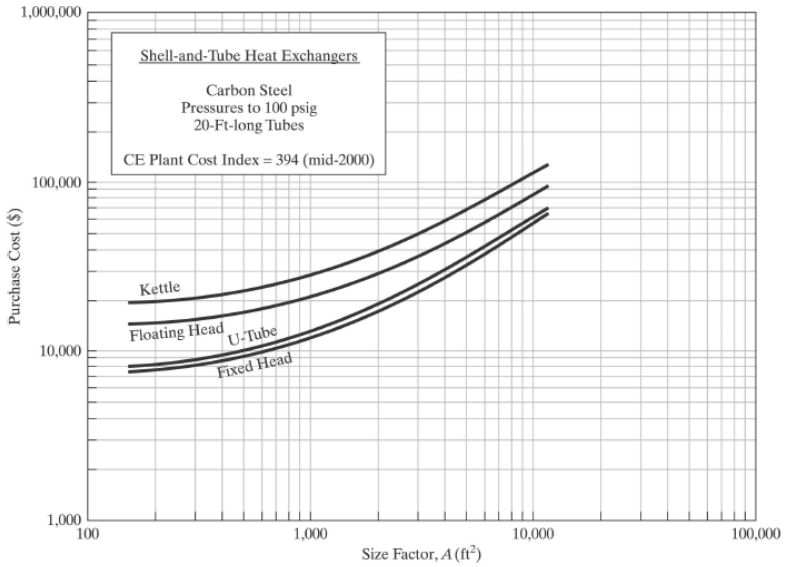

Figure 5-21: Shell and tube heat exchanger cost estimating diagram, reprinted from [68]

- Cooling tower costs: An inquiry was made to a commercial provider asking for the cost of a 600-ton cooling tower. It was learned that the cost of the tower was $33,500 plus $4,000 for shipping, for a total of 37,500; which makes approximately $63/ton. In another reference, [25], for 190 tons, the calculated cost is $29/ton. In a conservative approach, a cost of $100/ton was assumed.

These assumptions were used in addition to the equations provided in Table 5-7 [59], to reach a total cost of the power block of 2 million dollars. This is the same as the value of 2 million, calculated with the assumptions in Table 5-9.

5.3.3.4.2. Cost Scaling

For technologies whose cost is given in $/kW or $/MW, the assumption that the cost is linear is not always accurate. Economies of scale make larger components

cheaper in a specific cost basis; therefore, the cost is expected to be higher for smaller sizes.

One reference, [69], shows that for a plant 10 times smaller than first estimated, the cost would increase by a factor of 1.25; while for a plant 100 times smaller, the cost would increase by a factor of 1.5. Compared to the references ([22]), the designed plant is about 10 times smaller. Therefore, the estimated costs would need to be increased in 25% for those cases when linearity was assumed. Considering this, the cost of the power block would be estimated at 2.5 million dollars following Table 5-7 [59].

5.3.3.4.3. Solar Plant Capital Expenditure

The majority of these costs were estimated following SAM, NREL's advisor software for renewable energy projects, and they are contained in Table 5-10. Other assumptions are: no debt (the investment is out-of-pocket) and no incentives except for the ITC.

The boiler capacity was calculated as 85% of the full-load solar field thermal output, assuming that during operation there will always be at least 15% solar energy.

The cost of land is calculated with the total land area. A factor of 1.1 was used to convert the solar field area to the total plant area. Usually, a factor of 1.4 is used, but a CO_2 cycle is much more compact than a steam cycle.

Table 5-10: Solar plant costs estimated from SAM

Item	Cost	Reference and explanation
Direct Capital Cost (DCC)		
Site Improvements	30 $/m^2	[70] Over total aperture area.
Solar Field	170 $/m^2	[70] Over total aperture area.
HTF	70 $/m^2	[70] Over total aperture area.
BOP (Balance of Plant)	120 $/kW	[70]
Boiler	150$/kW	$35000/(MMBtu/h) = $120/kW [71] [72] [73] (4 kWth = 14 MMBtu/h): scaling and the fact that it is not for steam but therminol. Cost of auxiliary systems included (they can increase 50 to 100% the capital cost [71]).
Power Block	2500 $/kW	See above.
Bare Erected Cost (BEC) = DCC + Contingency		
Contingency	25%	Over DCC [25]
Total Plant Cost (TPC) = BEC + Indirect Costs (below)		
Land	$5/m^2	$12,000 to $20,000/acre + land is more expensive when it is close to main sites [74]
EPC and Owner Costs	10%	Over BEC [70] [21]
Sales tax rate	6.25%	Over indirect costs [75]. Up to 8%.

5.3.3.4.4. Operation and Maintenance Costs

According to a reference [76] for sCO_2 cycles, O&M costs should be smaller than for steam for a number of reasons. However, the high pressure in the cycle makes it easier for leaks to appear. Some leaking must be inevitable; therefore, a conservative approach must be taken when comparing O&M costs for sCO_2 cycles with steam cycles.

According to another reference [77], solar thermal CSP O&M costs can be estimated to be in the range of $0.02 to $0.04/kWh (including insurance). Table 5-11 shows the values used.

Table 5-11: O&M costs

Item	Cost	Reference and explanation
Fixed cost	72.6 $/kW	[70] + 10% contingency due to CO_2 cycle leaks and other issues… (grows closer to annual 0.04 $/kWh)
Variable cost	0.004 $/kWh	[70] Water, water treatment, consumables, maintenance materials, operating labor, maintenance labor, administration... kWh here are total, not just solar..
Fuel cost	4 $/MMBtu	Natural gas prices, see above. Calculated with non-solar operation hours (backup boiler). Boiler efficiency of 80%.

There are O&M fixed costs and variable costs. Variable costs increase with the production of energy. The fuel cost has been set aside, but it is also a variable cost. Fixed costs increase with the capacity of the plant. The fossil fuel cost is calculated from the MMBtu required by the cycle during the equivalent full-load hours of fossil fuel operation.

5.3.3.4.5. LCOE Calculation

The LCOE is a useful parameter that compares this technology to other technologies present in the market. Its calculation can be made simple or complex, depending on the different assumptions and parameters to made and used. In the developed code, the equations based on references [78] [79] used are shown below.

The levelized cost of energy is the sum of all the costs that the energy system is going to produce (or avoid) divided by the sum of all kWh that it is going to generate. To account for future cash flows or energy flows from/to the system it is necessary to make present value calculations using a discount rate, *r*, during a certain number of years, *n*. For this purpose, the following parameters are calculated. For example, SUM_{simpl} is the sum of all the discounts produced in the lifetime of the energy system, and should be

multiplied by a constant annual flow/amount. Another parameter, SUM_{degr}, is the same coefficient but taking degradation of the system into account. A degradation rate, δ, of 0.999 (0.1% degradation) was assumed for the first approximation.

$$SUM_{simpl} = \sum_{t=1}^{n} \frac{1}{(1+r)^t} = \frac{(1+r)^n - 1}{(r \cdot (1+r)^n)} \tag{5.41}$$

$$SUM_{degr} = \frac{1 - \frac{\delta^n}{(1+r)^n}}{1+r-\delta} \tag{5.42}$$

$$LCOE_{CAPEX} = \frac{C_{TPC}}{W_{e,yr} \cdot SUM_{\deg r}} \tag{5.43}$$

$$LCOE_{fixed} = \frac{C_{O\&M,\,fixed} \cdot SUM_{simpl}}{W_{e,yr} \cdot SUM_{\deg r}} \tag{5.44}$$

$$LCOE_{\text{var}} = \frac{(C_{O\&M,\text{var}} + C_{fuel} - I_{CO2,avoided} - I_{cogen,avoided}) \cdot SUM_{simpl}}{W_{e,yr} \cdot SUM_{\deg r}} \tag{5.45}$$

Equation (5.45) includes the income due to avoided fuel consumption associated with cogeneration, as well as the income due to avoided emissions of CO_2 associated with solar energy.

This last income value is not necessarily real in that it is just a parameter that helps to reward the avoidance of emissions. In this case, emissions are not penalized, and if they were, then there would definitely be a negative income due to emissions associated with a backup boiler. However, in the fictional case of emissions being penalized, compared to the case in which the system was fully fossil fired, this value would be a benefit.

The cost of avoided CO_2 is the cost of carbon capture that was avoided with the PTC solar field. For example, the cost of CO2 avoided is $89.4/tonne (metric), ($81.1/ton-american), for SC PC (Pulverized Coal) and $93.8/tonne ($85.1/ton) for NGCC (Natural Gas Combined Cycle) [25]. For this study, a value of $90/tm (metric ton) was assumed.

For natural gas, the emissions of CO_2 are 53.03 kg/MMBtu [80]. With the equivalent solar full-load hours, the avoided MMBtu of natural gas burned can be calculated. For both incomes, CO_2 avoided and natural gas avoided for cogeneration, an efficiency of 80% for the boiler was assumed.

A linear depreciation was considered over the total number of years. An additional equation must be inserted because the current tax code of the U.S. says that an investor claiming a 26% ITC (Investment Tax Credit) can only capitalize 87% (= 1- 0.26 * 0.5) of the system price for depreciation purposes. The depreciable basis is therefore the original minus 50% of the ITC. The corporate income tax rate is 21% [81]. The state corporate income tax rate in Texas for yearly incomes of less than 1 million dollars is 0.5%; and 1% for more than 1 million [82], which is added for a total income tax rate of 21.5 or 22%. The tax factor equation, which includes these parameters, is shown below, and it is used with the CAPEX (Capital Expenditure) component of the LCOE.

$$F_{tax} = \frac{1 - ITC - r_{tax} \cdot f_{cap} \cdot d \cdot SUM_{\deg r}}{1 - r_{tax}}$$

$$d = \frac{1}{n} \text{ (depreciation, linear)}$$

$$f_{cap} = 85\% = 1 - 0.3 \cdot 0.5 \quad (5.46)$$

$$r_{tax} = 21\% \text{ (corporate income tax rate)}$$

$$ITC = 30\% \text{ (Investment Tax Credit)}$$

$$LCOE = LCOE_{CAPEX} \cdot F_{tax} + LCOE_{fixed} + LCOE_{\text{var}} \quad (5.47)$$

5.3.4. Design Summary and Results

The stated assumptions and calculations yield a LCOE of \$0.258/kWh or \$258/MWh. Without the fictional income associated with CO_2 emissions avoided, the LCOE would rise to \$291.5/MWh. Figure 5-22 shows a basis to compare these results with actual market LCOEs, with a red line showing the calculated LCOE.

Figure 5-23 shows the global picture for renewable and fossil energy sources. The LCOE is expected to continue decreasing in 2020 for all sources. Solar photovoltaic is a technology that is undergoing an extraordinary cost reduction [5]. It should be noticed that the discount rate is also 7.5%, which makes the results comparable.

The LCOE associated with capital expenditure is the largest share of the total LCOE: \$0.2329. The LCOE associated with O&M (including fixed, variable and fuel costs) is \$0.053. The share of the fuel is almost the same size as the share of the fixed O&M costs, and they are both remarkably larger than the variable O&M costs.

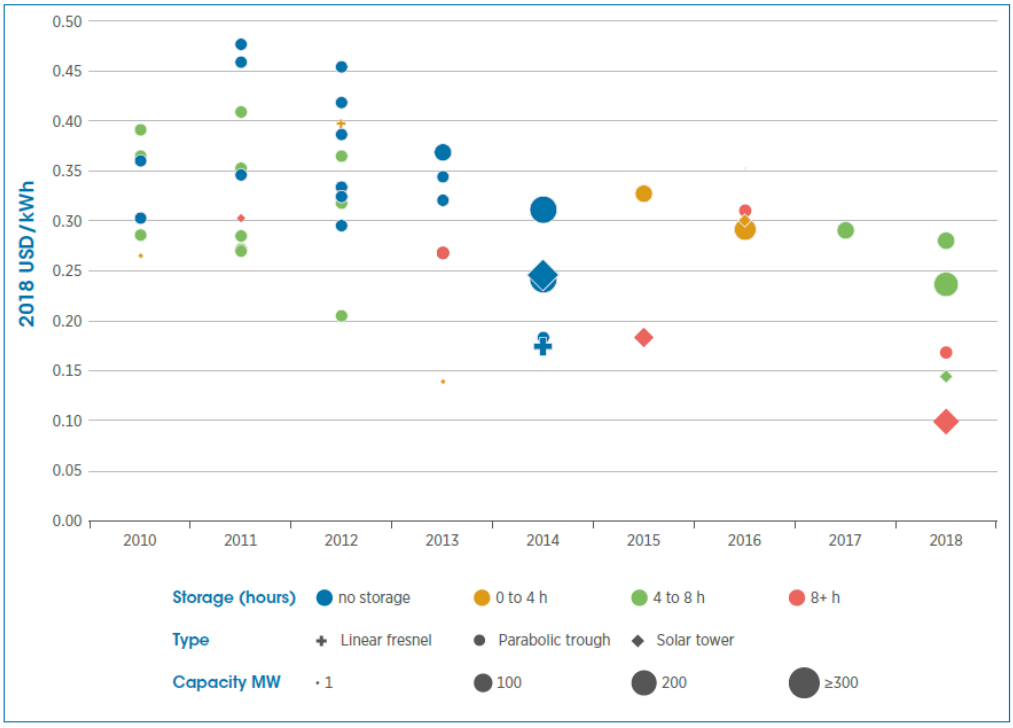

Figure 5-22: LCOE for CSP technologies up to 2018, reprinted from [77]

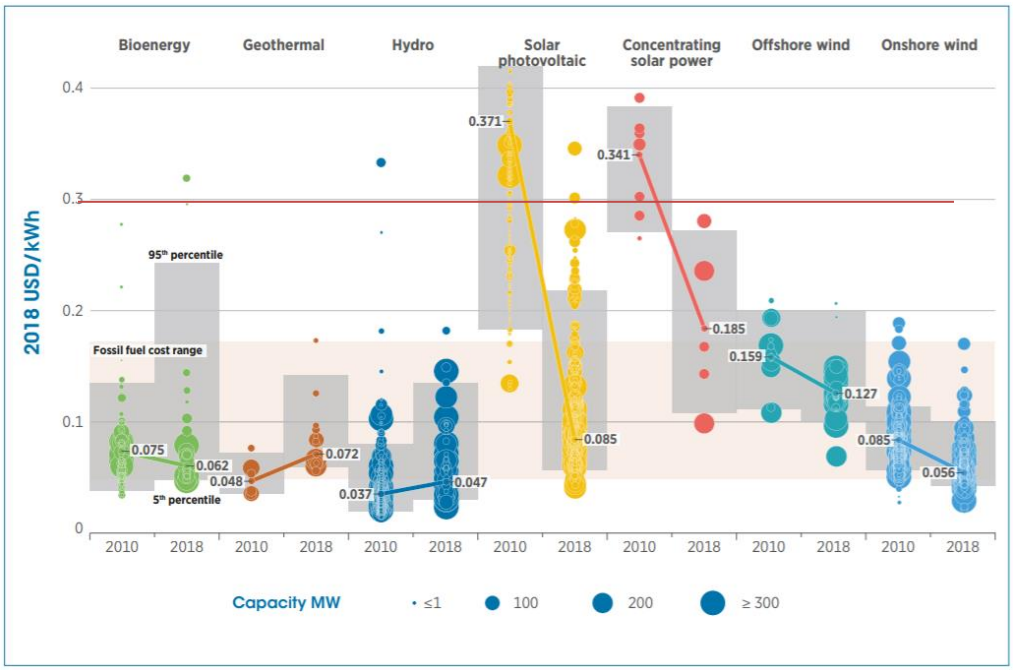

Figure 5-23: LCOE global renewable energy picture at utility-scale, reprinted from [77]

It can be observed that this technology is not too far away from penetrating the market. However, it is still far from the fossil fuel LCOE levels.

Other parameters to study are the capacity factor and the efficiencies. In this plant, the capacity factor is higher than in typical CSP plants (which usually operate for 2500 hours/year) because the backup boiler is used to extend the operation time. However, this results in a lot of energy coming from fossil fuels, and the calculated solar share of equivalent full-load hours is 45%. In a city like College Station, this is expected due to the abundant cloudiness, while in another location, this share is bound to increase.

The solar-to-electric efficiency of the plant is 13.1%, and the solar-to-cogeneration efficiency is 21.7%. These values are lower than expected because the cycle performance is not as high as it could be. However, improvements to this baseline cycle might make a difference. Annual solar-to-electric efficiencies for PTC plants are around 15% [14].

5.4. Simulation with Median Days for each Month

For a simplified evaluation of the performance of the plant under real conditions, an Analysis Simulation Code was prepared to simulate the designed plant on real meteorological days.

5.4.1. Assumptions and Code Development

A model of the solar plant was developed in EES, while MATLAB was used to pre-process weather data to obtain an input for the EES program. In the EES simulation, for each month, seven variables were inputted: day number in the year, solar time, DNI, ambient temperature, relative humidity, barometric pressure and wind speed. The

simulation uses these inputs to produce important outputs: plant power, efficiency, HTF temperature, mass flow, etc.

The optical load factor of the plant is defined as the radiation that reaches the receivers' surface divided by the radiation that reaches the receivers' surface at the design point (Equation (5.48)). This factor considers the optical efficiency in the load factor equation, with the reason that it is included being because what matters for the plant to function is the heat that is received. In the winter, although DNI might be high, the optical efficiency is low due to the solar angle effect, which makes the heat received low, as follows.

$$LF_{opt} = \frac{DNI\eta_{opt}}{(DNI\eta_{opt})_{Design}} \tag{5.48}$$

The plant does not work when the load factor is below 0.5 or above 1.25. For all conditions when the load factor is between these two values, the plant operates with the same performance. This is a modeling approximation that was taken due to lack of information about how the different devices of the plant behave at part load. More knowledge about this is presented after the component design phase.

The simulation program goes through the following steps:

1. A procedure calculates the solar angles (zenith, incidence, etc.) using the information of day number in the year, latitude and solar time.
2. A procedure receives the inputs of DNI, solar angles and PTC geometric parameters, and computes the optical performance.
3. The optical load factor is calculated.

4. A procedure calculates the overall performance of the solar field. The number of loops, number of collectors in each loop, collector length and aperture area, wind speed, incoming radiation, HTF inlet and outlet temperatures, ambient temperature and load factor must be inputted.
    a. First, the procedure verifies that the load factor is within the limits, and if not, it assigns all the outputs the value of zero.
    b. The mass flow rate of the HTF is estimated according to the load factor. In real life, the mass flow rate will be adjusted to obtain a certain maximum temperature in the CO_2. Simulating this is computationally expensive as it would require many iterations. The mass flow rate of the HTF is calculated using

$$\dot{m}_{HTF} = \frac{LF_{opt} \cdot \dot{Q}_{abs,D} \cdot N_{col,loop} \cdot A_a \cdot \eta_{th,T}}{\Delta h_{HTF}} \tag{5.49}$$

where L is the load factor, $\dot{Q}_{abs,D}$ is the heat absorbed (the radiation that reaches the absorber tube) per unit of aperture area, $N_{col,loop}$ is the number of PTCs in the loop, A_a is the aperture area, $\eta_{th,T}$ is an estimate of the total thermal efficiency of the loop, and Δh_{HTF} is the enthalpy increase in the HTF, which is the same for each loop. The total thermal efficiency is first estimated because its actual value is only known after calculating the thermal efficiency for each PTC in the loop, which is the next step. Another view is that this step should be iterated, but the approximation without iteration was deemed good

enough since the total thermal efficiency value is always around 85-90%.

c. Since each of the loops has a number of collectors in series, the temperature increments for each collector in the loop are calculated and added up. This is done using another procedure that computes the thermal losses in each collector. This procedure receives HTF properties and flow rate, and wind speed as inputs and computes the thermal efficiency for each collector. It also calculates the pressure drop.

d. The outputs of the solar field procedure are computed: total heat collected (adding up all the loops), total thermal efficiency, HTF maximum temperature, HTF fluid pressure loss, flow rate and finally pumping power.

5. A procedure then receives the outputs from the solar field and simulates the power cycle. Temperatures and pressures of all the points in the cycle are obtained independently from the solar field, just by knowing the cycle design parameters. For this step, component efficiencies such as turbine, pump and heat exchangers were assumed at a constant value. The only external input that changes the thermodynamic cycle is the ambient temperature. The CO_2 mass flow rate is calculated from the heat input from the solar field. Again, all the outputs will be set at zero if the load factor is out of bounds.

6. The global output procedure computes electrical generation power assuming a certain generator efficiency (95%), while considering an estimate of the power required to pump the non-working fluids of the plant: HTF, and cooling water as well as additional parasitic efficiency of 95%. It then computes the efficiencies of the plant: solar-to-electric and solar-to-cogeneration. It only yields positive values when the electrical load factor is between 0.5 and 1.25 of the design point.

$$\eta_{sol,electric} = \frac{\dot{W}_{elec}}{\dot{Q}_{solar}} \tag{5.50}$$

$$\eta_{sol,cogen} = \frac{\dot{W}_{elec} + \dot{Q}_{cog}}{\dot{Q}_{solar}} \tag{5.51}$$

5.4.2. PTC Optical Modeling

This section is based information published in [18] and [49]. Solar radiation (DNI) impinges on the collectors' aperture area, which is not the mirror area but the rectangular flat area calculated as the product of the collector's length times its width. PTCs are tracking collectors from E-W, and to calculate the component of radiation that is perpendicular to the aperture area, DNI needs to be projected on the E-W plane. The projection factor is the cosine of the incidence angle as shown in Figure 5-24.

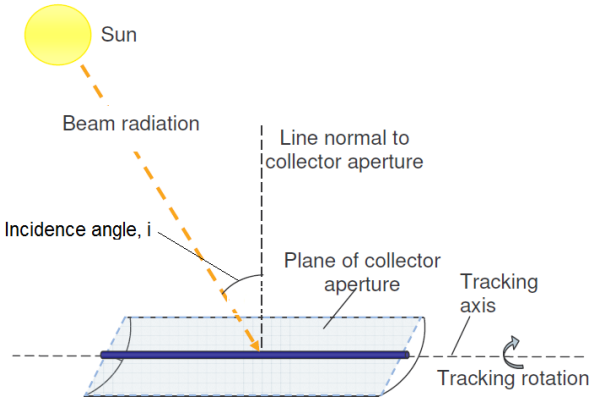

Figure 5-24: Projection of DNI on the aperture plane perpendicular direction, reprinted from [18]

In order to calculate the projection factor, it is necessary to look at the different solar angles and obtain them as a function of the time of the day and year. These angles are presented below:

- **Latitude angle, λ.** It depends on the location of the Earth, specifically on the parallel on which the location is.
- **Declination angle, δ**. It represents the tilt of the Earth's axis with respect to the plane of the Earth's orbit around the sun. It is a function of the day of the year, and it oscillates within ±23.5º. It is calculated with (5.52), [46].

$$\delta = 23.45 \cdot \sin\left((284 + n) \cdot \frac{360^{\circ}}{365} \right) \tag{5.52}$$

- **Hour angle, ω**. It is calculated from the solar time, presented in the MATLAB Equations section of this document. It is obtained through (5.53).

$$\omega = (t_{solar}[\text{h}] - 12\ \text{h}) \cdot 15^{\circ}/\text{h} \tag{5.53}$$

- **Zenith angle,** *z*. It is the angle between the solar beam and the vertical line perpendicular to the Earth's surface in a specific point of the Earth.
- **Incidence angle, *i***. It was introduced with Figure 5-24, and it is computed using Eq. (5.54), [18].

$$i = \arccos\left(\sqrt{(\cos(z))^2 + (\cos(\delta)\cdot\sin(\omega))^2}\right) \tag{5.54}$$

The optical efficiency of a PTC has its peak when the angle of incidence is zero, and it is given by Eq. (5.55), [49].

Some references also multiply by a soiling factor of 96% [49] to account for the periods in which the parabolic mirror is not clean.

$$\begin{aligned}
&\eta_{opt,peak} = \rho_m \tau_c \alpha_r \gamma_i \\
&\rho_m: \text{ clean mirror reflectance (0.93-0.94)} \\
&\tau_c: \text{glass envelope transmittance (0.93-0.96)} \\
&\alpha_r: \text{receiver absorptance (0.94-0.95)} \\
&\gamma_i: \text{intercept factor (0.92-0.94)}
\end{aligned} \tag{5.55}$$

When the angle of incidence is not zero, the peak efficiency needs to be multiplied by the so called Incidence Angle Modifier (IAM), whose governing equation is different for each collector type. A common commercially available PTC is the LS-2 type series, and its IAM equation is given by Eq. (5.56), [49], where the incidence angle is in degrees. The dimensions of the LS-2 collector are shown in Table 5-12: Characteristics of the LS-2 collector Table 5-12.

$$IAM = \frac{\cos(i) + 0.000884\cdot i - 0.00003077\cdot i^2}{\cos(i)} \tag{5.56}$$

Table 5-12: Characteristics of the LS-2 collector [83]

Parameter	Symbol	Value
Width	W_{PTC}	5 m
Length	L_{PTC}	7.8 m
Focal distance	*foc*	1.71 m
Aperture area	A_a	39 m^2
Concentration ratio	r_{conc}	22.74
Receiver inner diameter	D_{ri}	66 mm
Receiver outer diameter	D_{ro}	70 mm
Glass cover inner diameter	D_{ci}	109 mm
Glass cover outer diameter	D_{co}	115 mm
Inner receiver area	A_{ri}	1.617 m^2
Outer receiver area	A_{ro}	1.715 m^2
Inner cover area	A_{ci}	2.671 m^2
Outer cover area	A_{co}	2.818 m^2
Receiver emittance	ε_r	0.2
Receiver absorbance	α_r	0.96
Glass cover transmittance	τ_c	0.95
Glass cover emittance	ε_c	0.90
Concentrator reflectance	ρ_m	0.83
Intercept factor	γ_i	0.99
Optical peak efficiency	$\eta_{opt,peak}$	0.75

Three additional loss factors affect the optical performance of the PTC, as discussed below.

- **End losses**: they account for the portion of the receiver that is not illuminated by the solar rays due to their angle of incidence. An approximation to these losses is given by (5.57), [18]. Notice that the length used is not the one of a single collector but that of the SCA, because it is at the end of the SCA where a portion of the tube is not irradiated.

$$F_{EL} = 1 - \frac{foc}{L_{SCA}} \tan(i) \tag{5.57}$$

- **Row-shadow factor**. It accounts for the shading of one collector over another from a different row at certain times of the day (dawn and sunset). It is described by (5.58), [18]. This factor cannot be more than 1. After performing simulations it was learned that for an $L_{spacing}$ of 10 m, the row-shadow factor is kept at 1 between 8 am and 4 pm, solar time. This means a spacing of 10 m between rows is enough to allow 8 hours of operation for the plant without shading.

$$F_{RS} = \frac{L_{spacing}}{W_{PTC}} \frac{\cos(z)}{\cos(i)} \text{ , if } \frac{L_{spacing}}{W_{PTC}} \frac{\cos(z)}{\cos(i)} < 1$$
$$F_{RS} = 1 \text{ , if } \frac{L_{spacing}}{W_{PTC}} \frac{\cos(z)}{\cos(i)} \geq 1 \quad (5.58)$$

- **Solar field availability**: This factor is just the fraction of the solar field that is available, it is a value between 0 and 1, [18].

The optical peak efficiency, depending on the author, includes different parameters such as alignment errors, cleanliness and mirror surface properties. In a conservative approach, the optical peak efficiency was chosen following another reference, [18]; therefore, it is assumed to be equal to 0.7133 (for a collector type LS-2). This value includes all the possible losses, excluding those that are accounted in other loss factors.

Finally, the equation for the heat absorbed by the receiver is calculated per square meter of aperture area with Eq. (5.59).

$$\dot{Q}_{abs}\text{ " } [\text{kW/m}^2] = DNI \cos(i) \cdot IAM \cdot F_{RS} \cdot F_{EL} \cdot F_{available} \cdot \eta_{opt,peak} \quad (5.59)$$

This heat is to be inputted to the PTC thermal losses model to calculate the output heat of each collector and, finally, the output of the solar field.

The optical efficiency of the collector is defined as the factor that lumps in all the rest of the efficiency factors as shown in Eq. (5.60). The optical efficiency does not appear to depend as much of the solar irradiation, DNI, as of the solar time and day in the year (Figure 5-25 and Figure 5-26). In fact, at solar noon, in December and January, the solar efficiency is less than 50%, as shown in Figure 5-26.

$$\eta_{opt} = \frac{\dot{Q}_{abs}{}''}{DNI} = \cos(i) \cdot IAM \cdot F_{RS} \cdot F_{EL} \cdot F_{available} \cdot \eta_{opt,peak} \tag{5.60}$$

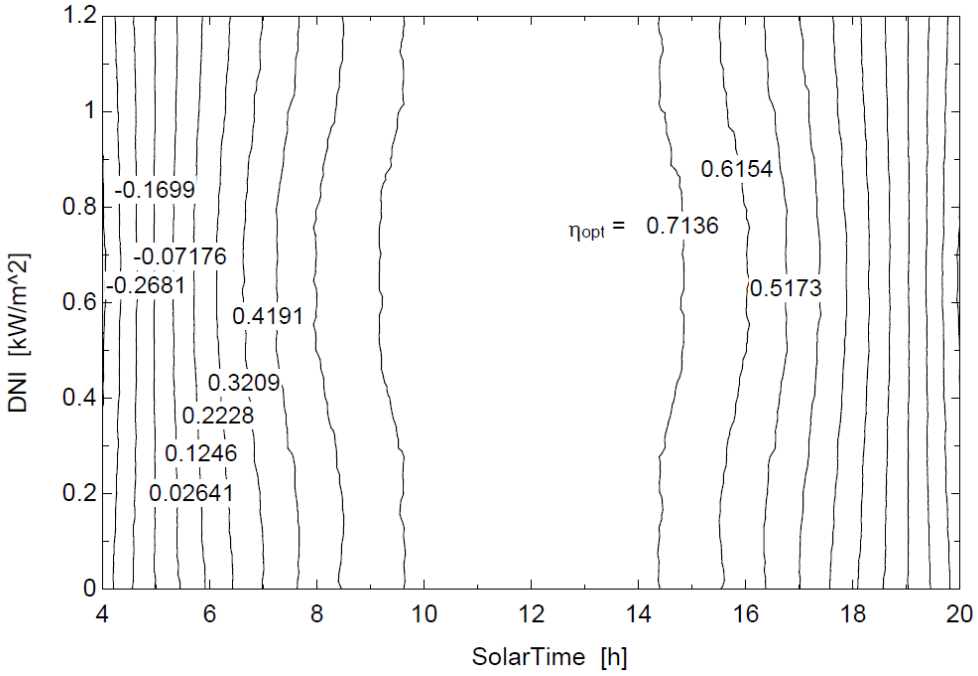

Figure 5-25: Evolution of optical efficiency with solar time and DNI

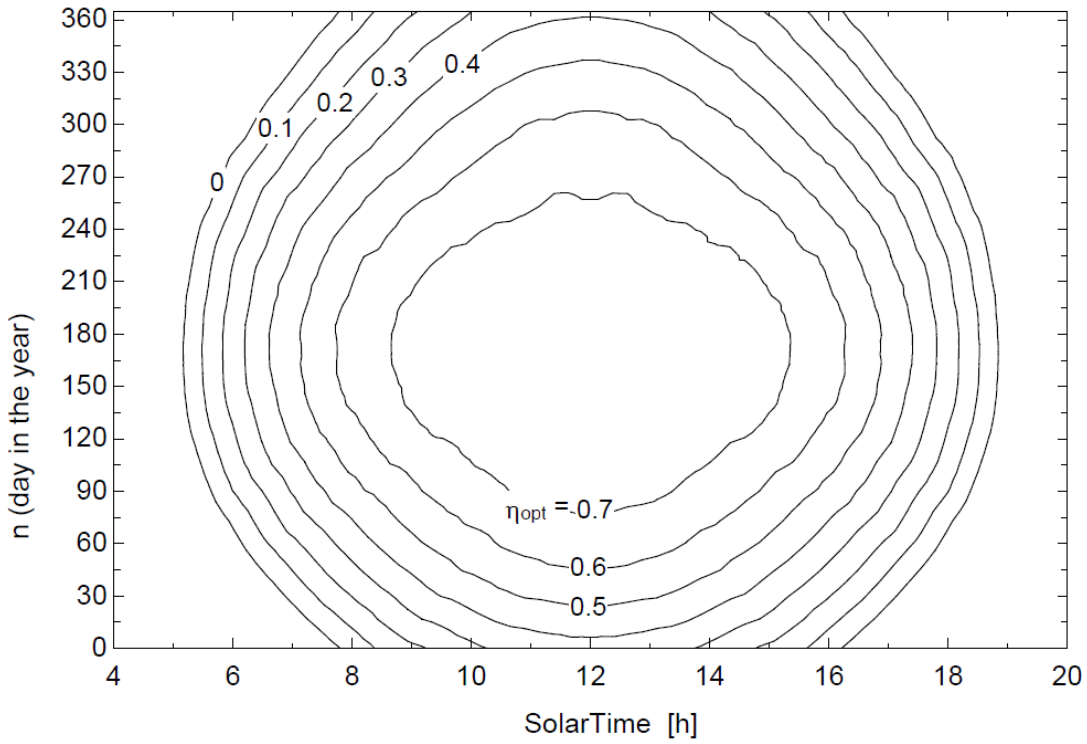

Figure 5-26: Optical efficiency contour plot as a function of the solar time and the day in the year

5.4.3. PTC Thermal Loss and Pressure Drop Modeling and Simulation

5.4.3.1. Thermal Loss

Of the heat that reaches the receiver tube, some is carried away by the HTF inside the receiver tube while another portion is lost through heat transfer to the environment. There are different approaches to model this heat loss. Some authors express this loss as a polynomic function of the HTF bulk temperature, [18]. Others have expressions using the overall heat transfer coefficient of the collector, U_{PTC}, which is typically less than 5 W/m^2K. In this project, a model that was validated against experimental data, and therefore proved to yield reliable results, is implemented [83]. The equations of this model are based in the following main assumptions.

- No thermal losses due to contact (conduction through the supporting metal structure)
- Convection between absorber and cover is neglected (vacuum in the glass cover)
- Uniform heat flux and small variation of temperature along one PTC, so that all properties can be estimated at PTC inlet temperature.
- Radiation losses are a function of ambient temperature (rather than sky temperature)
- Negligible temperature difference between cover and ambient temperature
- Negligible temperature difference between absorber and HTF temperature
- Fully developed flow and constant heat transfer coefficient along the collector

This model requires the calculation of different constants, whose derivation is not presented in this document but it is accessible in reference documents, [83]. Only the final equations and results are shown here, where $\dot{Q}_{col,PTC}$ is the heat output collected by one PTC, $\dot{Q}_{abs,PTC}$ is the absorbed heat calculated from the optical analysis and multiplied by the aperture area, σ is the Stefan-Boltzmann constant ($5.67 \cdot 10^{-11}$ kW/m^2-K^4), $T_{in,PTC}$ is the inlet temperature of the PTC and T_{am} is the ambient temperature (both temperatures in absolute scales).

$$\varepsilon_r' = \left(\frac{1}{\varepsilon_r} + \frac{(1-\varepsilon_c)}{\varepsilon_c} \cdot \frac{A_{ro}}{A_{ci}} \right)^{-1} \tag{5.61}$$

$$K_1 = A_{co}\varepsilon_c \sigma 4 T_{am}{}^3 + A_{co} h_{out} \tag{5.62}$$

$$K_2 = \frac{A_{ro}\varepsilon_r' \sigma}{1 + 4 T_{am}{}^3 A_{ro}\varepsilon_r' \sigma / K_1} \tag{5.63}$$

$$K_3 = \left(\frac{1}{A_{ri} h_{in}} + \frac{1}{2\dot{m}_{HTF} c_{p,HTF}} \right)^{-1} \tag{5.64}$$

$$\dot{Q}_{col,PTC} = \frac{\dot{Q}_{abs,PTC} - K_2 (T_{in,PTC}{}^4 - T_{am}{}^4)}{1 + 4 T_{in,PTC}{}^3 \frac{K_2}{K_3}} \tag{5.65}$$

Some of the nomenclature for these equations is included in Table 5-12. The rest of the considered properties are presented below.

- HTF properties. The properties for Therminol VP-2 are given by functions of its temperature, and these functions, for the liquid phase, are provided in reference [84].

$$\rho_{HTF}[\text{kg/m}^3] = -0.90797 \cdot T + 0.00078116 \cdot T^2 - 2.367 \cdot 10^{-6} \cdot T^3 + 1083.25 \tag{5.66}$$

$$\begin{aligned} c_{p,HTF}[\text{kJ/kg-K}] = {} & 0.002414 \cdot T + 5.9591 \cdot 10^{-6} \cdot T^2 \\ & -2.9879 \cdot 10^{-8} \cdot T^3 + 4.4172 \cdot 10^{-11} \cdot T^4 + 1.498 \end{aligned} \tag{5.67}$$

$$\begin{aligned} k_{HTF}[\text{kW/m-K}] = {} & (-8.19477 \cdot 10^{-5} \cdot T - 1.92257 \cdot 10^{-7} \cdot T^2 \\ & +2.5034 \cdot 10^{-11} \cdot T^3 - 7.2974 \cdot 10^{-15} \cdot T^4 + 0.137743) / 1000 \end{aligned} \tag{5.68}$$

$$\mu_{HTF}[\text{Pa}\times\text{s}] = \rho_{HTF} \cdot \left(1 \cdot 10^{-6} \cdot \exp\left(\frac{544.149}{T + 114.43} - 2.59578 \right) \right) \tag{5.69}$$

- Heat transfer coefficient to the ambient, h_{out}. It is obtained as a function of wind speed following a reference, [85].

$$h_{out} = 4 \cdot Wspd^{0.58} \cdot D_{co}{}^{-0.42} \tag{5.70}$$

- Heat transfer coefficient from the absorber to the HTF, h_{in}. It is obtained based on a heat transfer correlation of flow within a tube, the Gnielinski correlation, which is valid for the range $5 \cdot 10^6 > \text{Re} > 3000$, and smooth tubes, [53]. The friction factor, *f*, is

also obtained through a correlation, and it is presented in the following section since it is also useful to calculate the pressure drop.

$$Nu = \frac{(f/8)\cdot(\mathrm{Re}-1000)\cdot \mathrm{Pr}}{1+12.7\cdot(f/8)^{1/2}\cdot(\mathrm{Pr}^{2/3}-1)} \tag{5.71}$$

$$\mathrm{Pr} = \frac{\mu_{HTF}\cdot c_{p,HTF}}{k_{HTF}} \tag{5.72}$$

$$\mathrm{Re} = \frac{4\cdot \dot{m}_{HTF}}{\pi D_{ri}\mu_{HTF}} \tag{5.73}$$

$$h_{in} = \frac{Nu\cdot k_{HTF}}{D_{ri}} \tag{5.74}$$

The function of the heat loss with respect to HTF temperature was compared to other models, namely, a model that used a third-order polynomial regression, [18], shown in Figure 5-27.

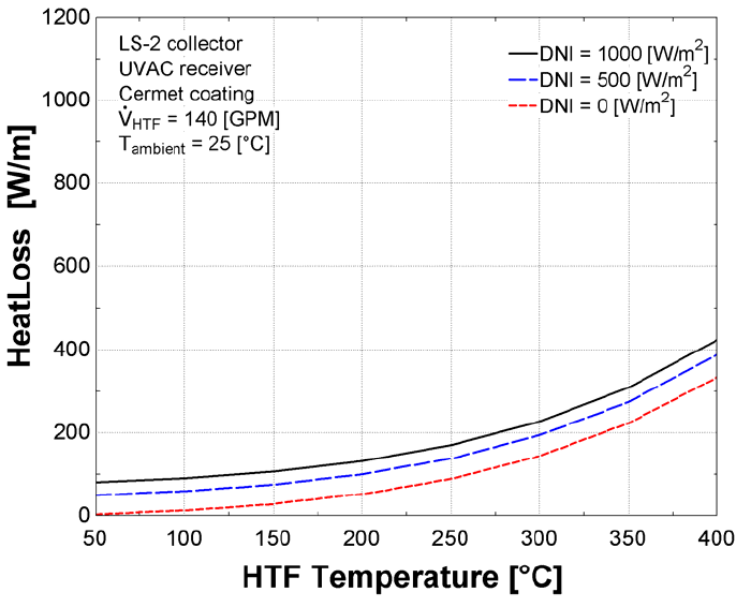

Figure 5-27: Results of the model of the heat loss using a third-order regression polynomial, reprinted from [18]

The regression was made for 140 gpm flow rate through the receiver and 25ºC of ambient temperature; therefore, these same values were inputted in the present model to compare. The results obtained with the present model when inputting the same conditions as in the reference model (Figure 5-27) are shown in Figure 5-28.

Comparing Figure 5-27 and Figure 5-28, it is observed that they yield very similar results and, since in the design phase there is no need for much accuracy, either of the two models is likely to yield reliable results, especially knowing that both have been experimentally validated.

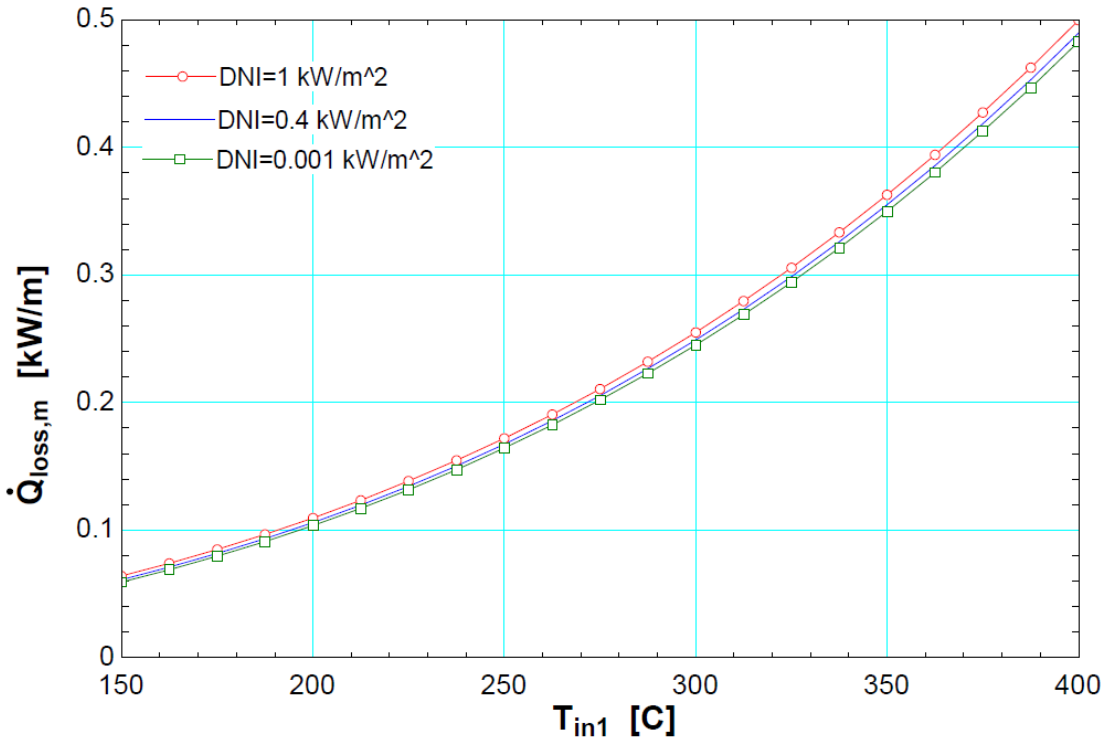

Figure 5-28: Results of simulating the presented model – Heat loss versus HTF inlet temperature at 25ºC ambient temperature and 140 gpm Therminol flow

The solar PTC model needed to be characterized as to HTF temperature and volumetric flow variations. The main findings were:

- Heat loss, and therefore heat collection, depends fundamentally on HTF temperature. Therefore, dependence on DNI and mass flow rate is negligible, and if assuming a certain HTF temperature, the heat collected is fairly bounded. This is shown by the thermal efficiency of the collector.
- The temperature difference between the inlet and the outlet of the collector is small (between 1 and 7°C, depending on the mass flow rate). This agrees with the assumption of small temperature variations. As a result, fluid mean temperature (the temperature at which fluid properties were calculated) is consistently assumed to be 2.5°C higher than the inlet temperature (Eq. (5.75)).

$$T_{fm} = T_{in} + 2.5^{\circ}\mathrm{C} \tag{5.75}$$

Thermal efficiency of the collector is defined as the collected heat over the absorbed heat, which is the heat that reaches the surface of the absorber tube. It is shown in Eq. (5.76).

$$\eta_{th,PTC} = \frac{\dot{Q}_{col,PTC}}{\dot{Q}_{abs,PTC}} \tag{5.76}$$

Figure 5-29 shows the dependence of the efficiency of the collector with inlet temperature and flow rate. This plot was obtained with the simulation program in EES.

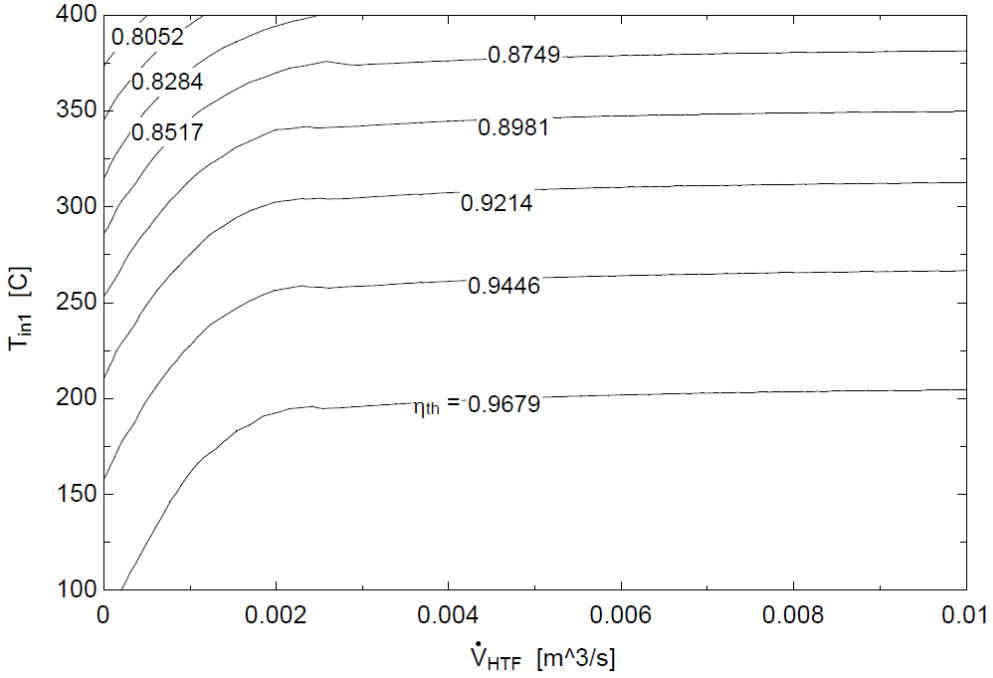

Figure 5-29: PTC thermal efficiency

5.4.3.2. Pressure Drop

The pressure drop in one PTC was modeled using the Darcy-Weisbach loss equation, (5.77), and equations for the friction factor, (5.78), following reference [53] and assuming smooth pipes where $\dot{W}_{pump1}$ is the power required to pump the HTF through one PTC, and D_{ri} is the internal diameter of the receiver. The behavior of the pressure loss and the pumping power is presented in Figure 5-30 and Figure 5-31.

$$\Delta P_{PTC}[kPa] = f \frac{L_{PTC}}{D_{ri}} \frac{1}{2} \rho_{HTF} v^2 \tag{5.77}$$

$$f = (0.790 \ln(\mathrm{Re}) - 1.64)^{-2} \quad ; \quad 3000 \le \mathrm{Re} \le 5 \times 10^6 \tag{5.78}$$

$$\dot{W}_{pump1}[kW] = \Delta P_{PTC} \cdot \dot{V}_{HTF} \tag{5.79}$$

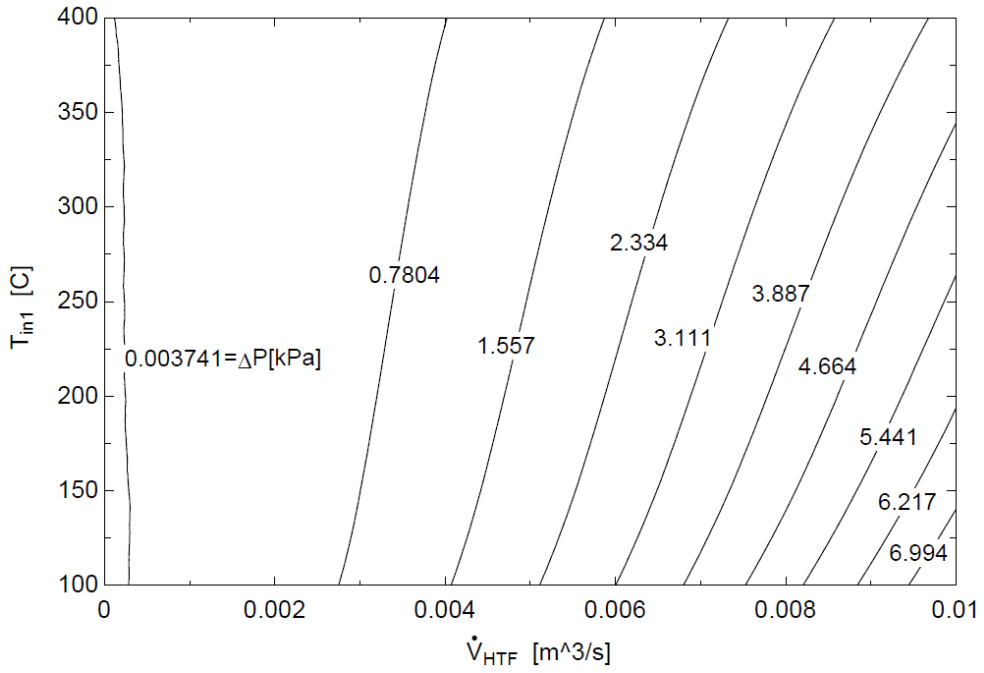

Figure 5-30: Contour plot of the pressure loss through one PTC as a function of HTF flow rate and inlet temperature

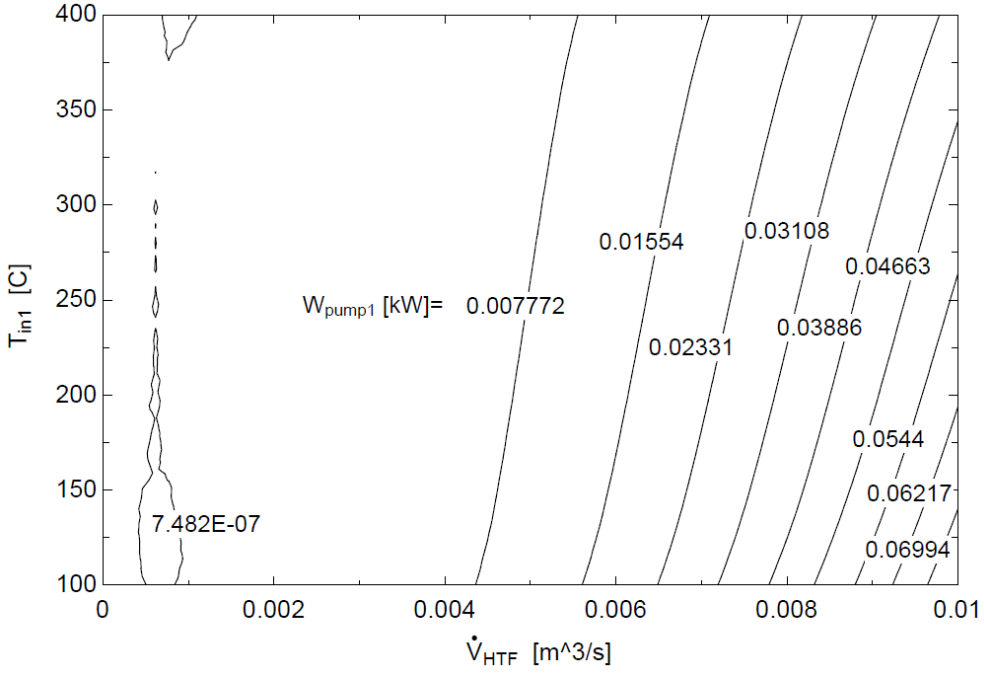

Figure 5-31: Contour plot of the pumping power through one PTC as a function of HTF flow rate and inlet temperature

5.4.4. Power Block and Other Systems

The simulation of the power block is performed with the same code as for cycle design and input/output calculations. Part-load performance is not implemented because it is assumed that the cycle will operate at full load for most of the time during the year because of the backup boiler, which will provide the additional heat needed to operate close to the design point.

The only variable that actually influences the cycle performance is the ambient temperature, as presented in the design section. Here, the assumption is taken that the condensation temperature is 7.5°C above the ambient temperature. When the ambient wet-bulb temperature is too high (namely 23°C or above), it is assumed that the plant still operates thanks to reduced temperature approach (about 5°C).

Above a 30°C condensation temperature, the plant does not operate, and a procedure was therefore implemented to make sure this condition was fulfilled. Another procedure was implemented in the code to facilitate the existence of the condensation temperature by narrowing the approach when the wet-bulb temperature increases. The schedule shown in Eq. (5.80). This schedule is not arbitrary, it has been assumed regarding the plots discussed in the cooling tower design schedule (Figure 5-14).

$$\begin{array}{lll} if & T_{WB} < 22 & T_{cond} - T_{WB} = 7.5^{o}C \\ if & 22 < T_{WB} < 25 & T_{cond} - T_{WB} = 5^{o}C \\ if & 25 < T_{WB} & T_{cond} - T_{WB} = 4^{o}C \end{array} \tag{5.80}$$

At the end of the day, this simulation is done with median days for each month. It is impossible to extrapolate all the different variables with just one sample for each

month, even if it is a representative sample. More accurate results will be obtained with SAM.

5.4.5. Simulation Results

Median days were simulated with just solar energy inputs and meteorological data; and the simulation data were processed in another MATLAB program. In this program, the total energy generated for each day (12 days, one for each month) was calculated by adding the energy of each hour. Then, an average energy generated was computed for all 12 days and, finally, this was multiplied by 365 days to get an annual value.

Figure 5-32 shows the simulation results of the median days for each month. The reason why the median day and not the average day is inputted is that the average day is not representative. In one month, radiation goes up and down and it rarely settles around the average. For example, when the average is too low, a month might yield load factor below the minimum, when the load factor might actually be more than the minimum for most days in the month.

These results show that the cloudiness makes the radiation input somewhat random. Plus, the load factor is usually not too high, which might make the location not appropriate for the solar plant to be placed there. The year-average load factor is 53% (counting just the 8 middle hours of the day, when the plant is supposed to be operative).

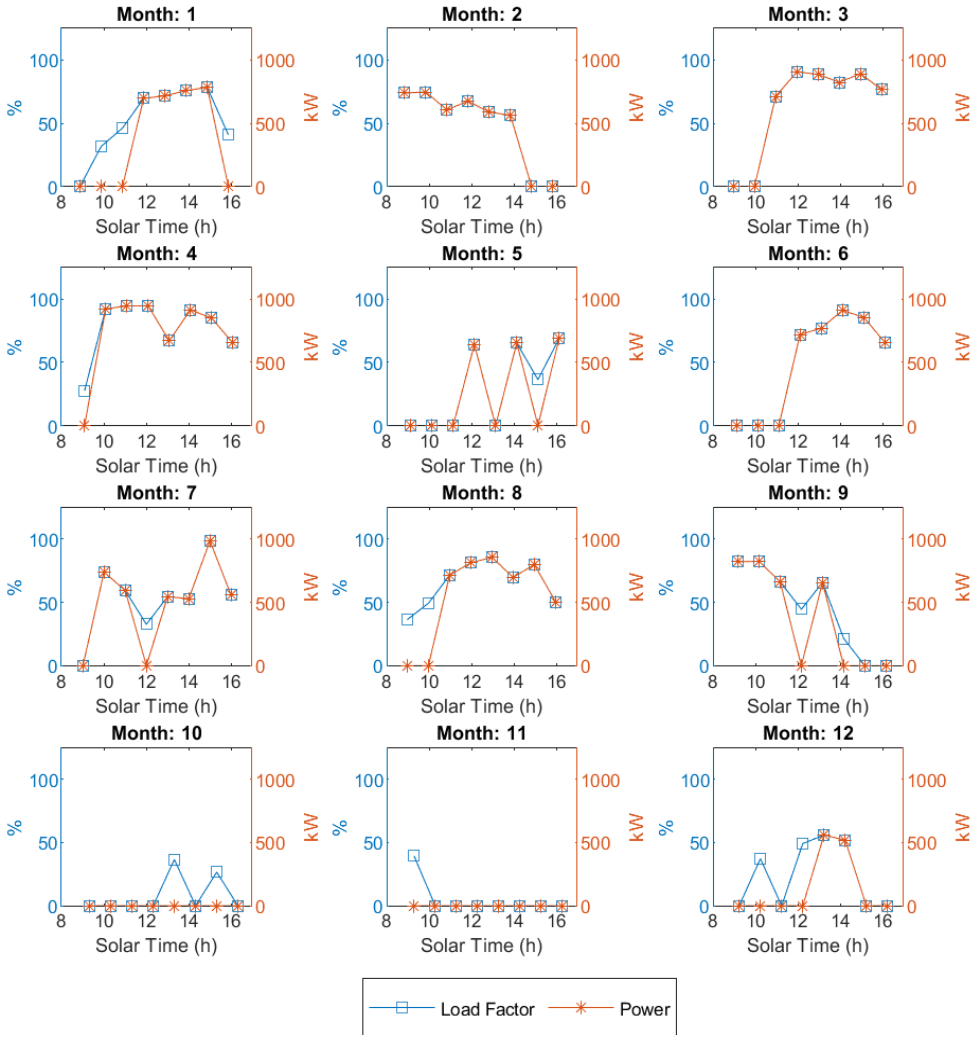

Figure 5-32: Results: solar plant load factor and power, College Station, TX

Figure 5-33 shows the energy generation plots. The upper plot shows the accumulation of energy generated (kWh) throughout the median day of each month. The final values (value of energy accumulated at 4 p.m. solar time) is shown in the lower plot for each month. Surprisingly, the highest value is not in the summer but in the spring (April). This is probably due to the randomness of the cloudiness.

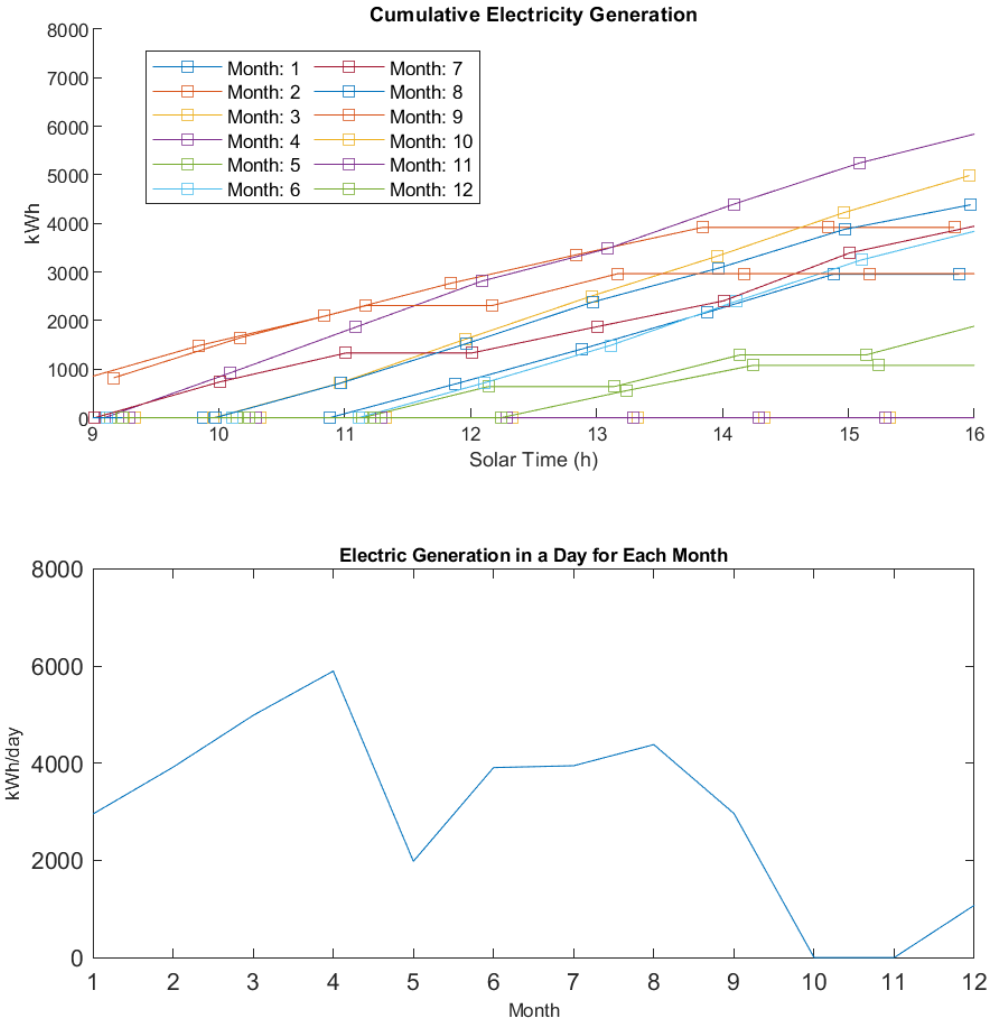

Figure 5-33: Results: solar plant energy generation, College Station, TX

It is seen that electric energy generation is zero in November, which is not completely true since in November, there might be days in which radiation is high enough so the plant can operate. However, since median days are being simulated, the 'randomness' of conditions is acceptable since this means there are the same number of

days with more radiation as with less radiation. The same information for heat cogenerated can be found in Figure 5-34.

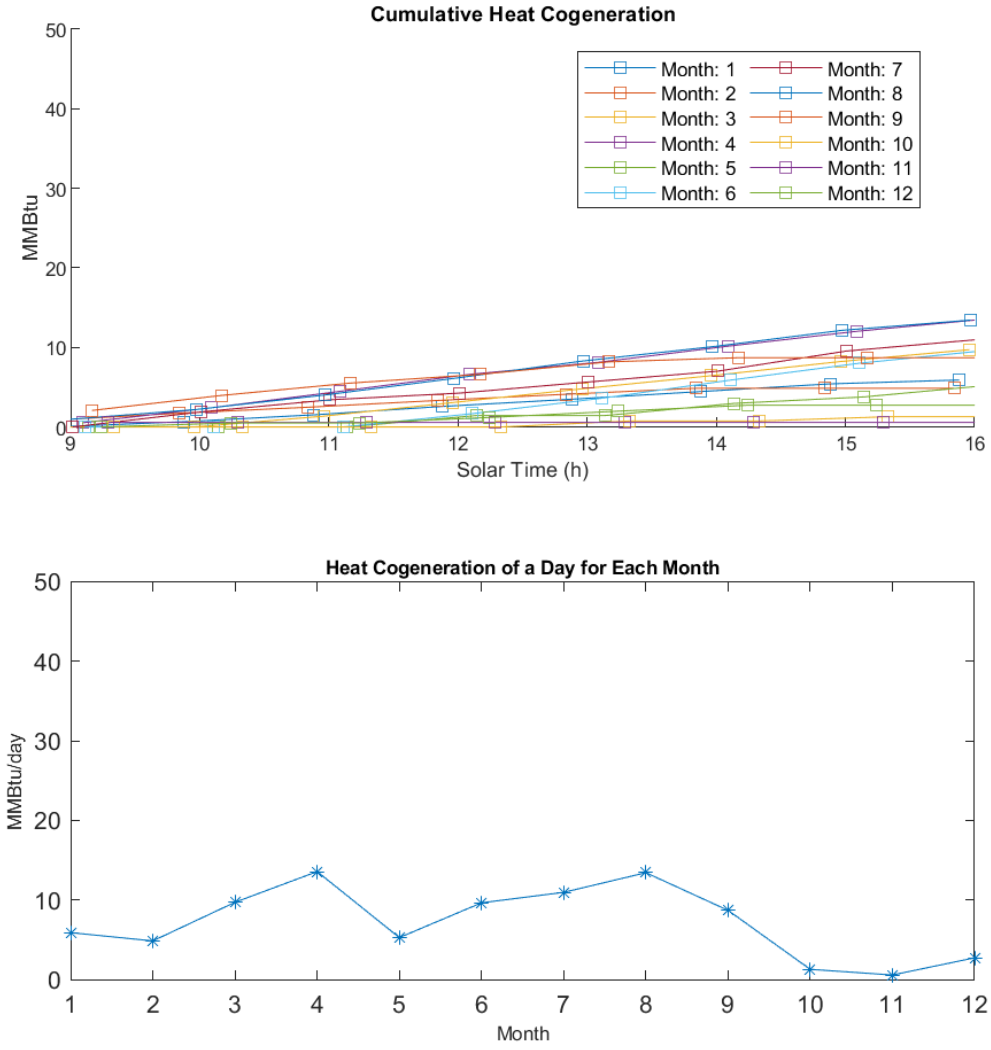

Figure 5-34: Results: solar plant heat cogeneration, College Station, TX

Figure 5-35 reveals the performance of the plant in terms of efficiencies. The efficiency is zero when the load factor is too low. When the load factor is within the operating bounds, the value of the efficiencies depends mostly on the cycle efficiency

and the optical efficiency. If the optical efficiency is high enough, values of 18% can be reached in solar to electric efficiency. The optical efficiency is usually a value between 0.6 and 0.7. The thermal efficiency of the field is usually 90%. Then the cycle has an efficiency of about 25%, which makes the overall plant solar-electric efficiency be around 15%.

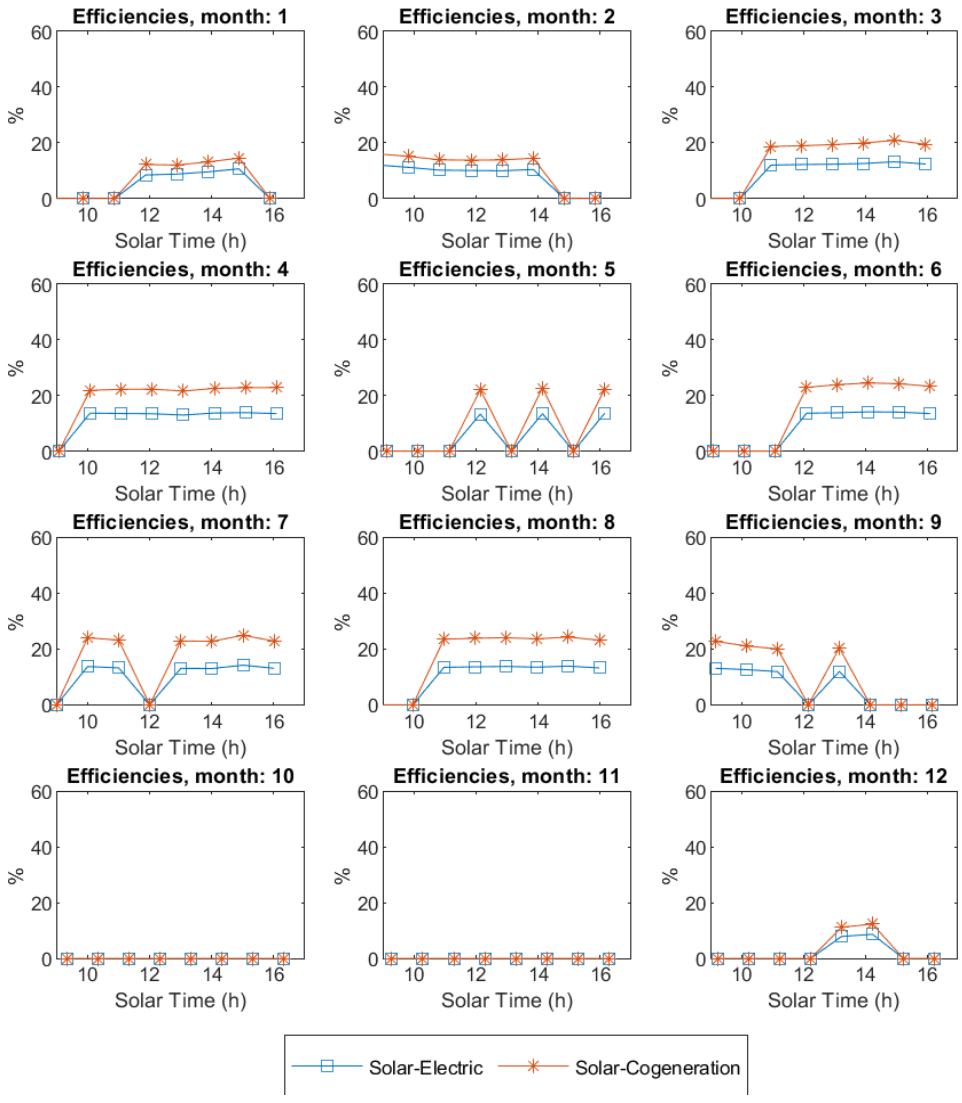

Figure 5-35: Results: solar plant efficiencies, College Station, TX

The same plots were obtained for another location: Phoenix, AZ (Figure 5-36); where the cloudiness is less frequent. It is observed that the year-average load factor increases to 85.7%. It should be noted that the plant should be redesigned for this location in that the design point from which the load factor is calculated has changed.

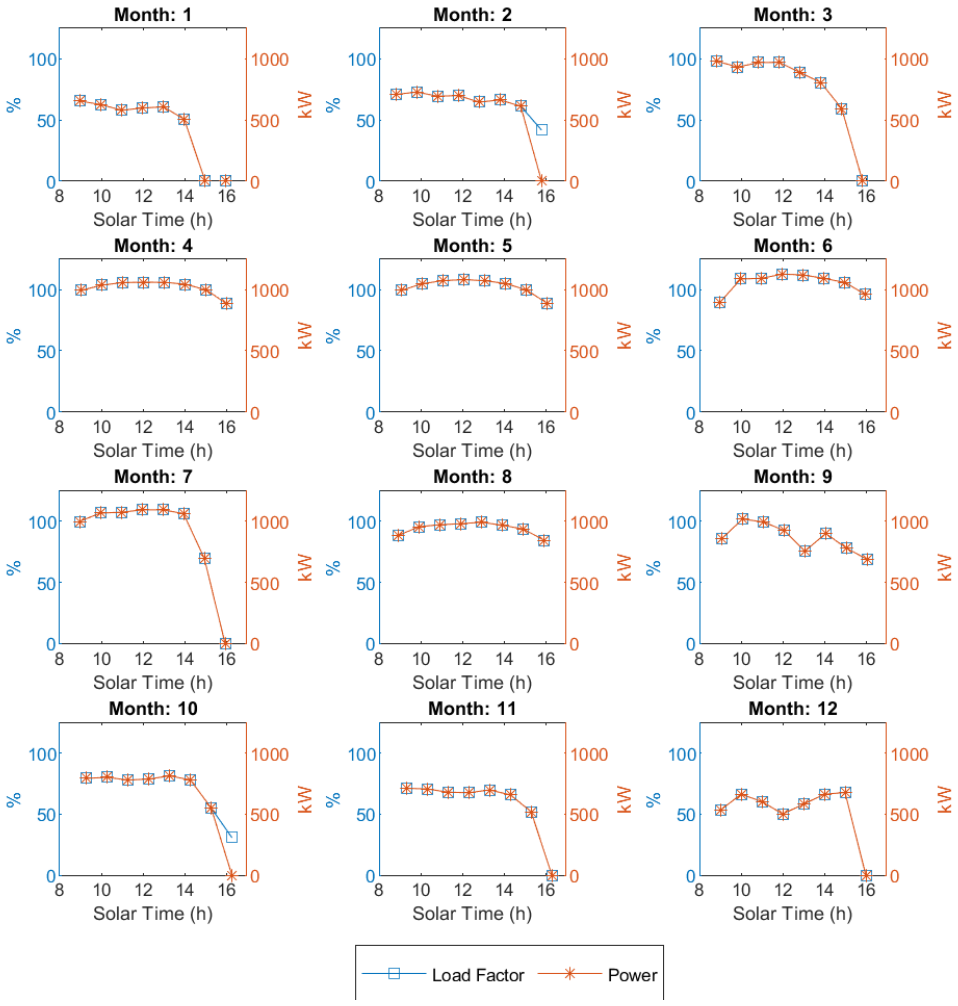

Figure 5-36: Results: solar plant load factor and power, Phoenix, AZ

The equivalent full-load hours are calculated dividing the total energy generated by the electrical power at design conditions, which is not 1000 kW but a little less (920

kW) due to generator and parasitic loses. The capacity factor is computed dividing the equivalent full-load hours by the number of hours in the year. For College Station, TX, the plant yields a total of 1,191 hours (capacity factor of 12.7%), while for Phoenix, AZ, we have 2,477 hours per year (28.3% capacity factor).

5.5. Detailed Design of Components

5.5.1. Turbomachinery

The main objectives of turbomachinery modeling were sizing and part-load operation (off-design) modeling. There are no definitive models that could be easily implemented in the EES code to simulate off-design turbomachinery behavior. However, some interesting and useful information about s-CO_2 turbomachines was found.

The turbomachinery is compact, which reduces material costs and weight [86]. The high pressures of the CO_2 result in high fluid density, and therefore, there is no clear distinction between pumps or compressors [86]. At most scales, the compressors are centrifugal, while turbines are typically radial below 10 MWe and axial above 50 MWe [86].

The rotating speeds are high, especially for low MWe, which requires power conversion devices to adapt to the grid frequency. In low MW scales, power electronics are used, gearboxes are used from 7 to 50 MWe, and above 50 MWe, synchronous generators are used [86].

Based on Figure 5-37, the size of the turbomachines designed for this application can be determined. The compressor should rotate in the region of 50,000 rpm, while the

turbine should operate at about 40,000 rpm. The diameter of the compressor should be 0.1 m, and the diameter of the turbine, 0.12 m.

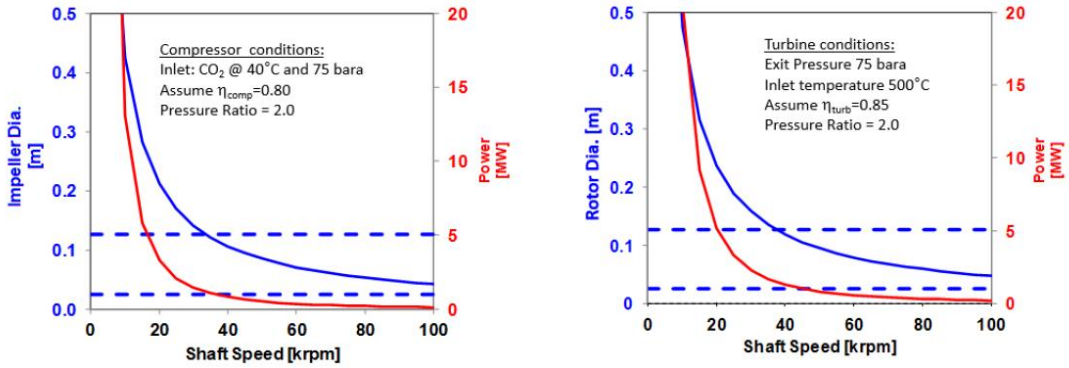

Figure 5-37: Example sizes and speeds for radial sCO_2 turbomachinery, reprinted from [24]

As to the bearings, their selection depends on many factors. In industrial scale sCO_2 applications, the fluid film oil bearing is expected to be the most prevalent [24].

For turbomachinery selection and performance prediction, two parameters are important: specific speed and specific diameter.

$$N_s = \frac{N \cdot \dot{V}^{1/2}}{H_{ad}^{3/4}} \tag{5.81}$$

$$D_s = \frac{D \cdot H_{ad}^{1/4}}{\dot{V}^{1/2}} \tag{5.82}$$

Balje's chart (Figure 5-38) is used in turbomachinery design to select the type of rotor. As introduced above, it is expected that both the compressor and the turbine are radial. These values will help in informing on efficiency and turbomachinery design.

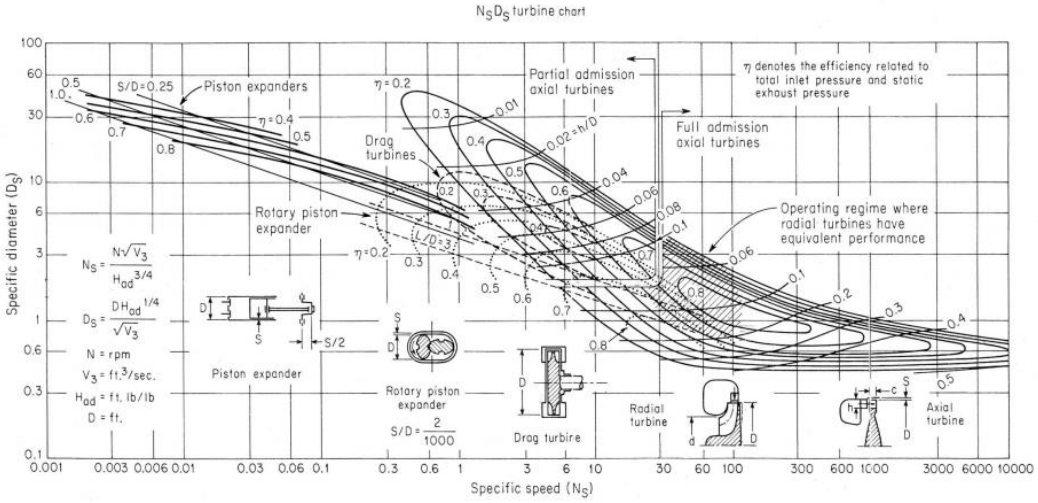

Figure 5-38: Balje's chart, reprinted from [87].

5.5.2. Printed Circuit Heat Exchangers

A code was developed to design PCHE (Printed Circuit Heat Exchangers), which are the type of heat exchangers more suitable for sCO_2 applications since they are able to withstand very high pressures and temperatures as shown in Figure 5-39. This is possible thanks to their manufacturing process, which includes diffusion bonding.

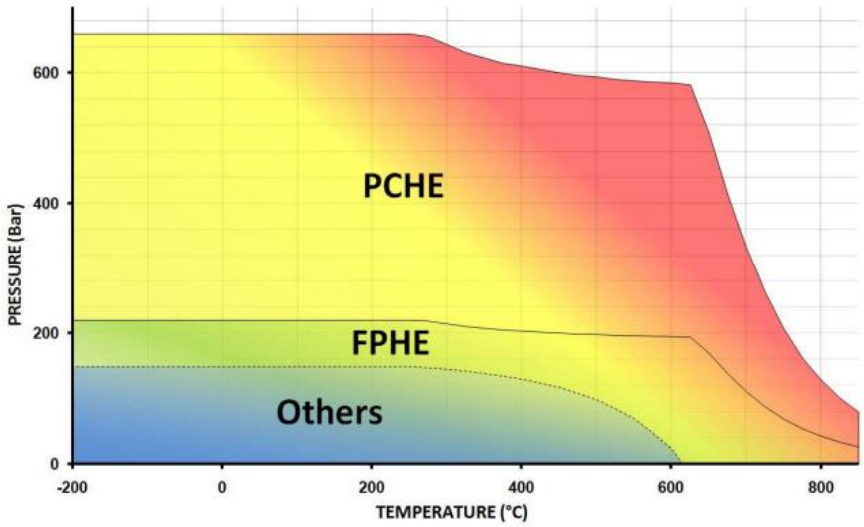

Figure 5-39: Operating conditions for heat exchanger types, reprinted from [50]

For the considered solar plant, due to the high CO_2 pressures, at least the evaporator (primary heat exchanger) is expected to be a PCHE. As it can be seen in Figure 5-40, the channels are arranged so that it can be treated as a counter flow type heat exchanger. There are also PCHEs arranged as a cross-flow type heat exchanger.

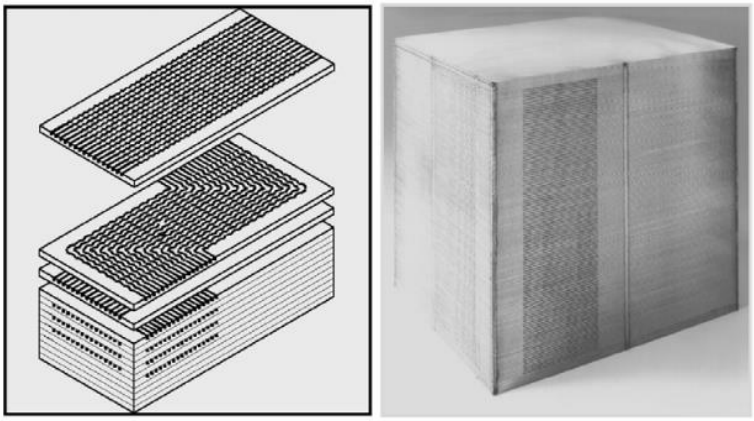

Figure 5-40: Chemically etched plates assembly, joined by diffusion bonding to form a PCHE, reprinted from [88]

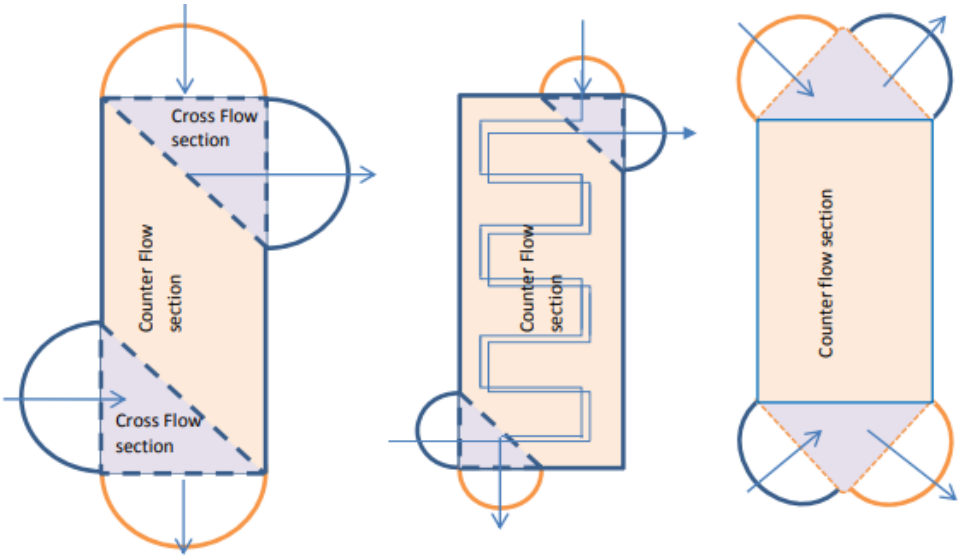

Figure 5-41: Header configurations for PCHE to maximize counter flow region, reprinted from [69].

The design of a PCHE can be approached using both the LMTD and ε-NTU methods if the fluid properties are not close to the critical point (31°C, 7.37 MPa). If the CO_2 is close to the critical point, rapid changes in the specific heat might create a heat exchange similar to an evaporation inside the dome, with fairly constant temperature. Figure 5-42 shows that the changes in the specific heat drastically decrease when the pressure increases further from the critical point. At 20 MPa, the specific heat changes are rather small, which makes the LMTD and ε-NTU methods more reliable for design in these conditions.

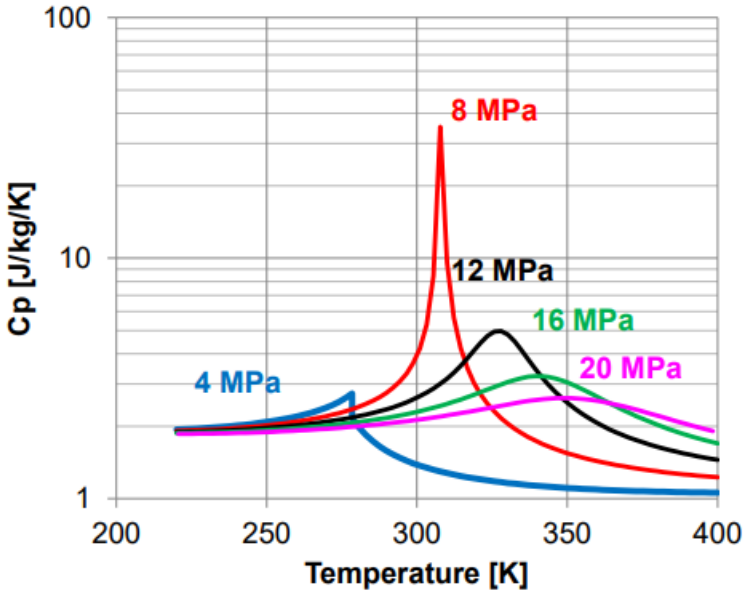

Figure 5-42: Specific heat changes near the critical point, reprinted from [51].

The ε-NTU method was used in the evaporator design needed for the solar field system. It helped to determine the temperatures of the heat exchanging fluids. The UA value obtained was refined with a code in EES that first used the LMTD method and then a heat exchanger discretization method. The LMTD method takes properties at an average temperature, while the discretization method divides the temperature increment

of one of the fluids into steps and calculates each step as if it was an individual heat exchanger, obtaining UA and heat exchange length for each of them. This approach assumes that the heat exchanger section is constant. This code was also used to translate this UA value into size and construction features of the heat exchanger.

The design code leaves the length of the heat exchanger as the dependent variable that will define the exchanger size, while the other parameters are either chosen or calculated for specifications. According to [19], the manufacturer of PCHE, Heatric, provides modules up to 1.5 m long, 0.6 m high and 0.6 m wide, meaning, the computed length will be divided by the module length to have a number of PCHE modules in series. Similarly, if the height is designed to be more than 0.6 m, it will mean that there will be more than one module connected in parallel. Table 5-13 contains the list of parameters used for or obtained from the design of the CO_2 primary heat exchanger (evaporator).

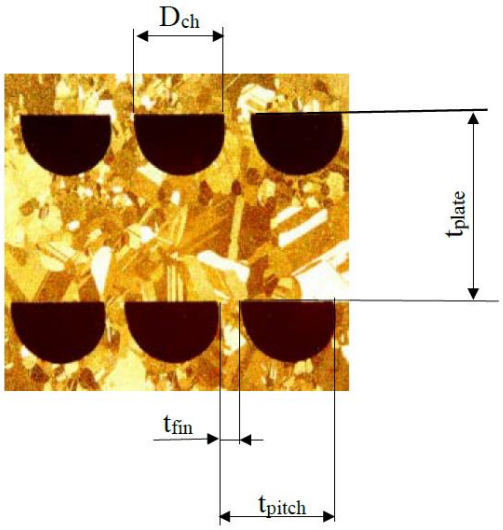

Figure 5-43: Geometric channel and plate parameters

Table 5-13: Evaporator (PCHE) design parameters summary

Parameter	Value	Range	Specification / Requirement
Material	Stainless steel AISI 304	Stainless steel AISI 304, 316 or Alloy 800	Materials commonly used in PCHEs, [89], [19].
Length (L_{length})	0.555 m	Up to 1.5 m	$L_{length} = \frac{A}{\left(1+\frac{\pi}{2}\right) D_{ch} \cdot \min(N_{ch,H}, N_{ch,C})}$ $A = \frac{\dot{Q}}{U \cdot LMTD}$ $U = \frac{1}{\left(\frac{1}{h_C X_{p,C}} + \frac{1}{h_H X_{p,H}}\right) \min(X_{p,C}, X_{p,H}) + \frac{\delta_w}{k_w}}$ where A is the heat transfer area corresponding to the fluid with less fraction of plates (the bottleneck area). The fluid film coefficients for hot and cold fluids, h_H and h_C, are multiplied by the plate ratio to the minimum plate fraction so that the area A is the bottleneck area. These equations are based on a reference, [90]. δ_w and k_w are the conduction wall thickness and conductivity that make up the conduction thermal resistance. According to [19], δ_w is 60% of t_{plate}. The calculation of the length assumes always counter flow, meaning, the actual length of the heat exchanger will be somewhere between the calculated length and the latter plus the width, as shown in Figure 5-41. This actual value should be less than 1.5 m.

Table 5-13: Evaporator (PCHE) design parameters summary (Continued)

Parameter	Value	Range	Specification / Requirement
Width (L_{width})	0.1 m	Up to 0.6 m	Design choice. The larger, the lesser fluid pressure loss. It is coupled with length because the PCHE always has some non-counter-flow length that is determined by the width as shown in Figure 5-41. Therefore, the smaller, the greater the counter flow section versus the cross flow section.
Height (L_{height})	0.6 m	Up to 0.6 m	Design choice. The larger, the lesser fluid pressure loss.
Channel diameter (D_{ch})	2 mm	0.5 mm to 5.0 mm	For most applications, HEATRIC found the economic thermal performance optimum channel diameter to be 2 mm [19].
Plate thickness (t_{plate})	2.38 mm (stainless steel, gauge 13)	0.5 mm to 5.0 mm	As low as possible to reduce fluid pressure drop, but it must be greater than fin thickness (t_{fin}) and channel radius (half diameter). It should be large enough so that PCHE length is not too low compared to its width. Commercially available plate thicknesses can be found at [91]. Minimum plate thickness is 1.5 mm at 500°C as recommended by HEATRIC, [19].
Fin thickness (t_{fin})	0.315 mm		$t_{fin} = \frac{t_{pitch}}{\frac{\sigma_y}{\Delta p} + 1}$ Where σ_y is the allowable stress in the material, 215 MPa for AISI 304, and Δp is the maximum pressure difference between fluids.
Channel pitch (t_{pitch})	2.315 mm		$t_{pitch} = D_{ch} + t_{fin}$ Since t_{fin} also is calculated from t_{pitch}, its calculation must be iterated.
Number of channels for the hot fluid ($N_{ch,H}$)	567		$N_{p,H} = N_{plates} \cdot N_{ch,plate} \cdot X_{p,H} = \frac{L_{height}}{t_{plate}} \cdot \frac{L_{width}}{t_{pitch}} \cdot X_{p,H}$ $X_{p,H}$: fraction of plates for hot fluid = 3/4
Number of channels for the cold fluid ($N_{ch,C}$)	189		$N_{p,C} = N_{plates} \cdot N_{ch,plate} \cdot X_{p,H} = \frac{L_{height}}{t_{plate}} \cdot \frac{L_{width}}{t_{pitch}} \cdot X_{p,C}$ $X_{p,C}$: fraction of plates for cold fluid =1/4

For the calculation of Nusselt numbers, the flow through the channels was calculated for both the hot and cold fluids. The fluid properties were calculated at an average temperature, in both the LMTD and discretization approaches, between two temperature ends, namely inlet and outlet, or discretization points. The following (5.83) correlation was used, [90].

$$Nu = \begin{cases} 3.657 & \mathrm{Re} \le 2300 \\ 0.023 \cdot \mathrm{Re}^{0.8}\,\mathrm{Pr}^{0.33} & \mathrm{Re} > 2300 \end{cases} \tag{5.83}$$

The fluid pressure drop was calculated using the friction factor estimation, [90].

$$f = \begin{cases} 15.78 / \mathrm{Re} & \mathrm{Re} \le 2300 \\ 0.478 \cdot \mathrm{Re}^{-0.26} & \mathrm{Re} > 2300 \end{cases} \tag{5.84}$$

The design constraints that drive the direction of the optimal design are listed below.

- PCHE length should be reasonably greater than the width
- Pressure drop in both fluids should be less than 8% in the HTF and 1% in the CO2.
- Plate thickness must be greater than the channel radius (D_ch/2)
- Channel diameter should be 2 mm (optimal according to reference [19]).

For the optimal design, the following parameters were varied in a trial and error method while adhering to the design constraints.

- **Plate fractions**: increasing the plate fraction for one of the fluids decreases its pressure drop and increases its heat transfer capabilities.
- **Increase height**: decreases pressure loss, it also decreases PCHE length

- **Increase diameter**: decreases pressure loss and increases length due to decreased heat transfer
- **Decrease plate thickness**: decreases pressure loss but also decreases length

In the discretized model, the computation is expected to be much more accurate. However, it was found that there was no great difference between the LMTD method and the discretized method.

Table 5-14: Evaporator final design values obtained with different methods

	LMTD method	Discretized PCHE method	ε-NTU method (solar field design)
UA	49.21 kW/K	49.27 kW/K	47.95 kW/K

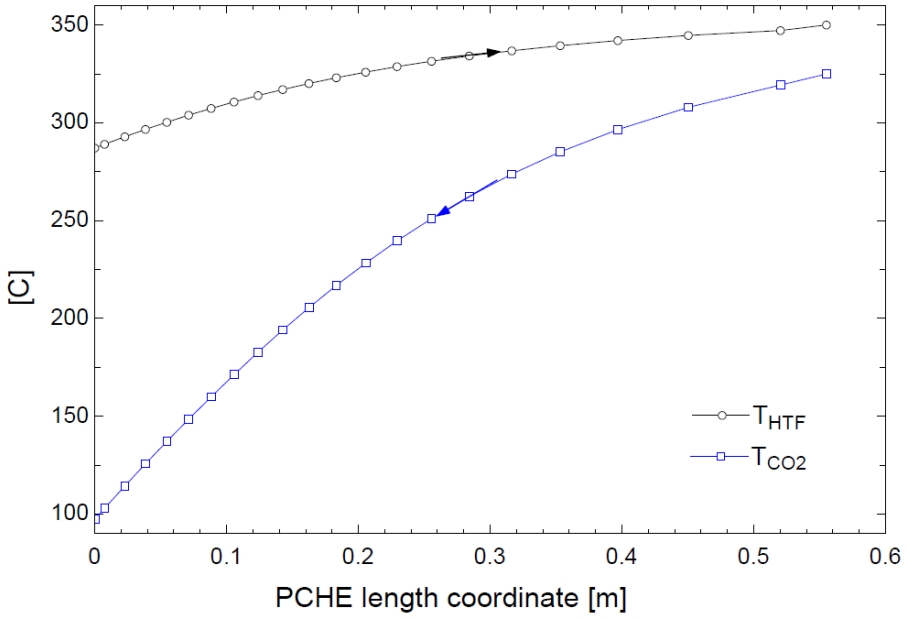

Figure 5-44: Discretized PCHE calculation output

This same design is also being performed for the regenerator. The third heat exchanger of the plant, the condenser, can be designed to hold smaller pressures (and

lower temperatures), which is the reason why the shell-and-tube type heat exchanger is considered. This is the same situation for the heat recovery heat exchanger.

5.5.3. Pipe sizing

A simple pipe sizing calculation was performed for the power block for different points of the baseline cycle (1 through 6). The calculation was made using a recommended fluid velocity through the pipes. The maximum velocity is obtained with an equation from a reference [92]. With that, the velocity is calculated considering a maximum of 1.25 load factor. Finally, the pipe diameter is estimated from the CO_2 flow rate.

$$v_{\max} = \frac{122[m/s]}{\sqrt{\rho_i / 1[kg/m^3]}} \; ; i = 1...6 \text{ (cycle points)}$$
$$v_i = \frac{v_{\max}}{1.25} \tag{5.85}$$

$$D_i = \sqrt{\frac{4 \cdot \dot{V}_i}{\pi \cdot v_i}} \tag{5.86}$$

The diameters that were calculated range from 0.07 to 0.14 meters (2.75 to 5.5 inches), with the maximum pipe diameter occurring right after the turbine expansion. At the 35 MPa pressure level, the maximum pipe size is 0.096m, which is also the point with maximum temperature.

These results are important for determining the pipe thickness. For the point of maximum pressure and maximum temperature, the pipe thickness is about less than 10% of the inner pipe diameter as shown in equation (5.87).

$$\sigma_{\max} = \frac{pD}{2t} \Rightarrow t_{\min} = \frac{pD}{2\sigma} = \frac{35MPa \cdot 0.096m}{2 \cdot 200MPa} = 8.4mm = 0.33in \tag{5.87}$$

6. SIMULATION AND ASSESSMENT

6.1. Simulation with System Advisor Model (SAM)

SAM is a software program developed by NREL to perform analysis of renewable energy projects from parametric design to economic analysis. The codes developed in EES in the Design and Modeling section of this document are limited, and the results they produce should be verified with a more advanced software such as SAM.

The Empirical Parabolic Trough Model is used because of its simplicity and accuracy, and unlike the physical model, it calculates the performance of the plant based on real data regressions.

6.1.1. Assumptions and Comments

The location chosen is again College Station, TX, with some values for the solar field being chosen based on the design that was made in a previous section. The rest of the parameters used by SAM (deploy and stow angle, piping heat loss coefficients, etc.) are default values. The piping heat loss coefficient (in W/m^2) was double checked with a reference [93].

For the simulation, it is assumed that 1% of the receivers have lost vacuums and 0.5% of the receivers have broken glass.

The power block requires that one inputs a cycle efficiency, namely26%, and nominal power, namely 1 MW, while limits of operation are 50% to 125% of the nominal power and the boiler LHV efficiency is 80%. Part load equation coefficients can also be inputted with SAM taking the part load efficiency as a 4^{th} order regression

polynomial that is a function of the turbine operation factor. These coefficients can be inputted or selected from default in SAM. In this case, default values were chosen from the SEGS 30 MWe Turbine. Although the behavior of this turbine may be different, it is known that the plant would rarely operate at part-load. There are other coefficients that define the power block behavior at off-design such like the electrical-thermal coefficients, which calculates the backup fossil energy required.

Table 6-1: Solar field main parameters

Input Parameters		
Parameter	**Value**	**Explanation**
Solar multiple	1	No TES
Row spacing	10 m	Operating hours
Ambient temperature	23.3^{o}C	TMY3 data analysis
DNI	780 W/m^2	TMY3 data analysis
Wind velocity	5 m/s	TMY3 data analysis
Non-solar field area multiplier	1.4	
HTF	Therminol VP-1	
SCA type	Luz LS-2	
Number of SCAs per row	4	6 PTCs per SCA.
Calculated Parameters		
Aperture area	8210.97 m^2	
Optical efficiency	0.724	
Solar field land area	4 acres	
Total land area	6 acres	
Number of SCAs	35	SCA: solar collector assembly, made up of a number of PTCs
Turbine thermal input	3.846MW	

No storage (TES) is present in this plant, and the dispatching periods are summarized in Table 6-2. The fossil fill fraction is the turbine output fraction up to which fossil backup is operated to fill in the remaining energy so that the system achieves desired output when solar energy is not enough. Figure 6-1 shows the different

dispatch schedules that make up the different plant operating conditions. More energy is produced during weekdays and summertime because more demand is expected.

Table 6-2: Dispatch control

Period	Turbine output fraction	Fossil fill fraction
1	1.25	1
2	1.15	1
3	1	1
4	1	0.75
5	0.75	0.75
6	0	0

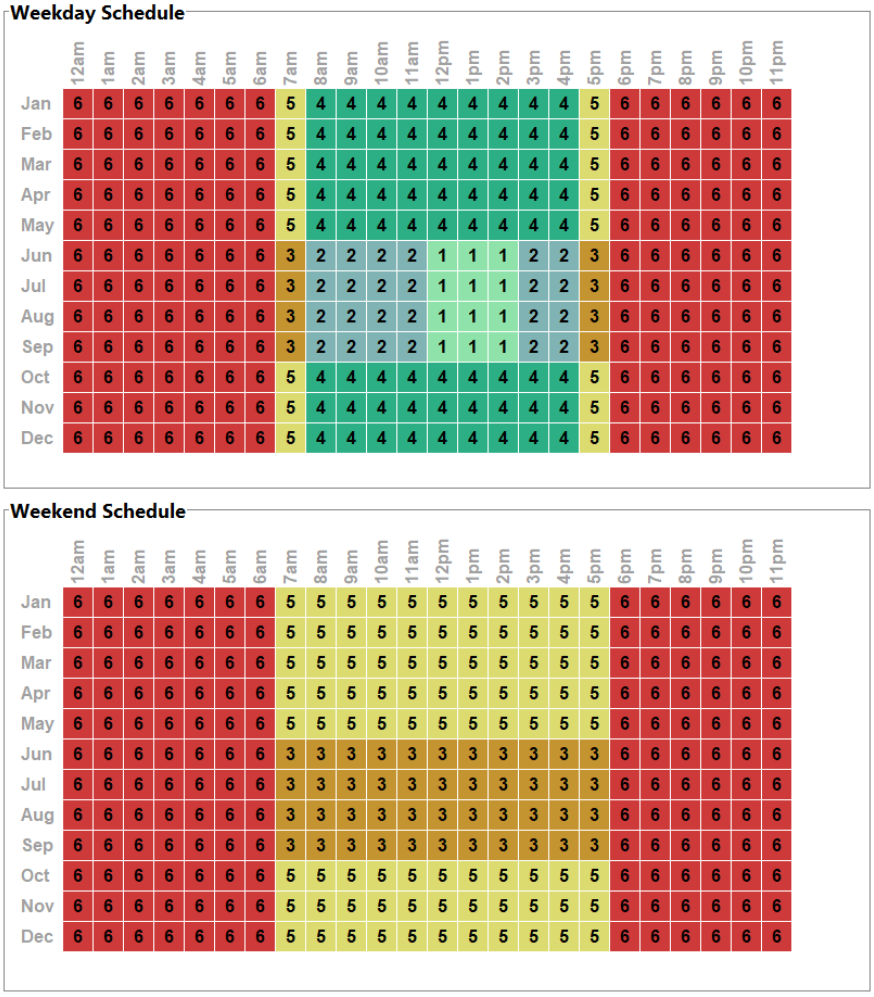

Figure 6-1: Dispatch schedules

Parasitic losses are implemented with default values from APS 1 MW ORC wet cooling in SAM. Compared to the EES results, they are larger and reduce the output power by almost by 20%.

The system costs are those described in Table 5-10. As to the O&M costs, Table 5-11 values are implemented, with SAM also applying inflation to these costs, which means the costs will be higher at the end of the life of the project. It should be noted that fuel prices are unpredictable and they were set to a constant value ($4/MMBtu), ignoring inflation for now, because a sensitivity analysis would be made later. A degradation of 0.999 each year was assumed, following the initial design. Again, zero debt was assumed, and the economic analysis parameters assumed were the same as described earlier in this document. Two additional economic assumptions are:

- **Inflation rate**: According to [94], inflation in 2019 was 1.76%, and this value is adopted as the inflation rate for the project. In this same reference, the inflation rate values for previous years are also accessible and they do not follow a specific trend.
- **WACC or discount rate**: According to [95], the WACC in the industrial goods and services sector in the U.S. is 8.09% while for utilities it is 5.74%. The value of 7.5% was selected as explained in design chapter of this thesis.

As to taxes: federal income, state income and sales; values have been discussed in a previous chapter. One additional value is incorporated, namely an annual insurance

rate of 0.5% (SAM default value). As to the depreciation, MACRS 7 years schedule was chosen.

6.1.2. Results

The obtained nominal LCOE with SAM is 30.50 ¢/kWh, and the real LCOE is 26.24 ¢/kWh (real levelized cost is a constant dollar, inflation-adjusted value; nominal LCOE is a current dollar value). These values are relatively close to the ones calculated with EES, and they show once again that although this technology is not yet marketable, it is not far from market penetration.

Other economical parameters such like NPV, IRR and payback period, are nonexistent because this project does not break even, which is expected for any underdeveloped technology.

Figure 6-2 shows the profiles of different solar field variables for every month. One surprising observation is that even during irradiation hours, the energy output from the field is not too high, especially in the winter. Compared to the EES model, the design aperture area computed in SAM is smaller (about 1000 m^2 smaller).

Another interesting result is the outcome of running the program without any fossil fuel backup (fossil fill fraction equal to zero). This procedure was also used in EES to calculate the solar-equivalent full-load hours of operation. The result with SAM is 830 hours per year (9.5% capacity factor), while with EES it was 1191 h/yr. In this case, the approximation with EES is more reliable because SAM includes part load performance simulation, which in this case is less realistic since the actual operation uses a backup boiler, which means the plant does not have to operate at part load.

Figure 6-2 shows the behavior of the solar field and heat input to the power block. It is observed that the HTF temperature is as high as it should be for most of the simulation time, meaning that the plant should be operating at the design point for most of the hours. It is also noted that fossil fuel consumption increases at the beginning and at the end of the day, which happens because solar energy is not enough to power the plant at dawn and sunset. It also makes sense that in the winter months, the conversion of energy from solar to field thermal power has a worse performance due to low optical efficiencies.

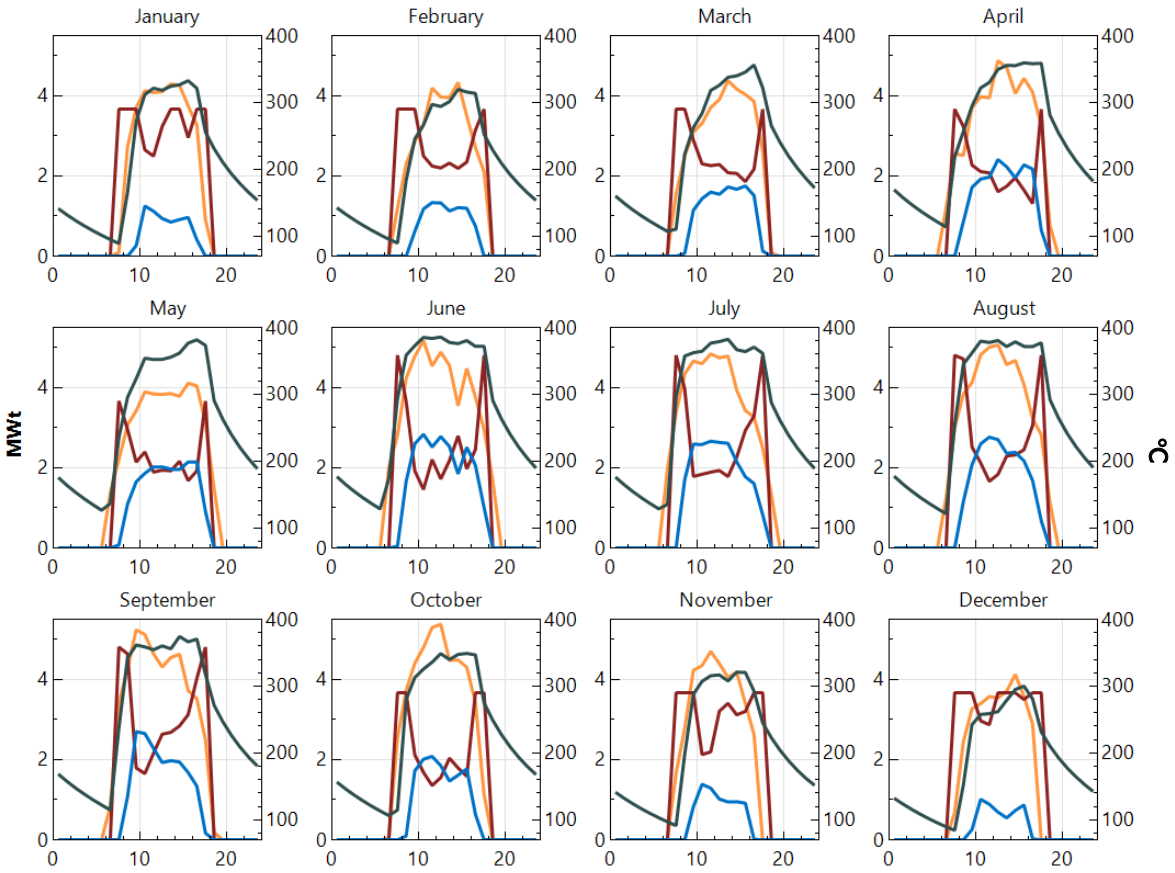

Figure 6-2: SAM results. Blue – field thermal total power produced; yellow – field thermal total power incident; brown – fossil thermal power produced; green – field HTF temperature hot header outlet.

Figure 6-3 shows the outputs from the power block and parasitic efficiencies. An observation is that, although the nominal power is 1 MW, the plant only operates at this capacity during the summer months.

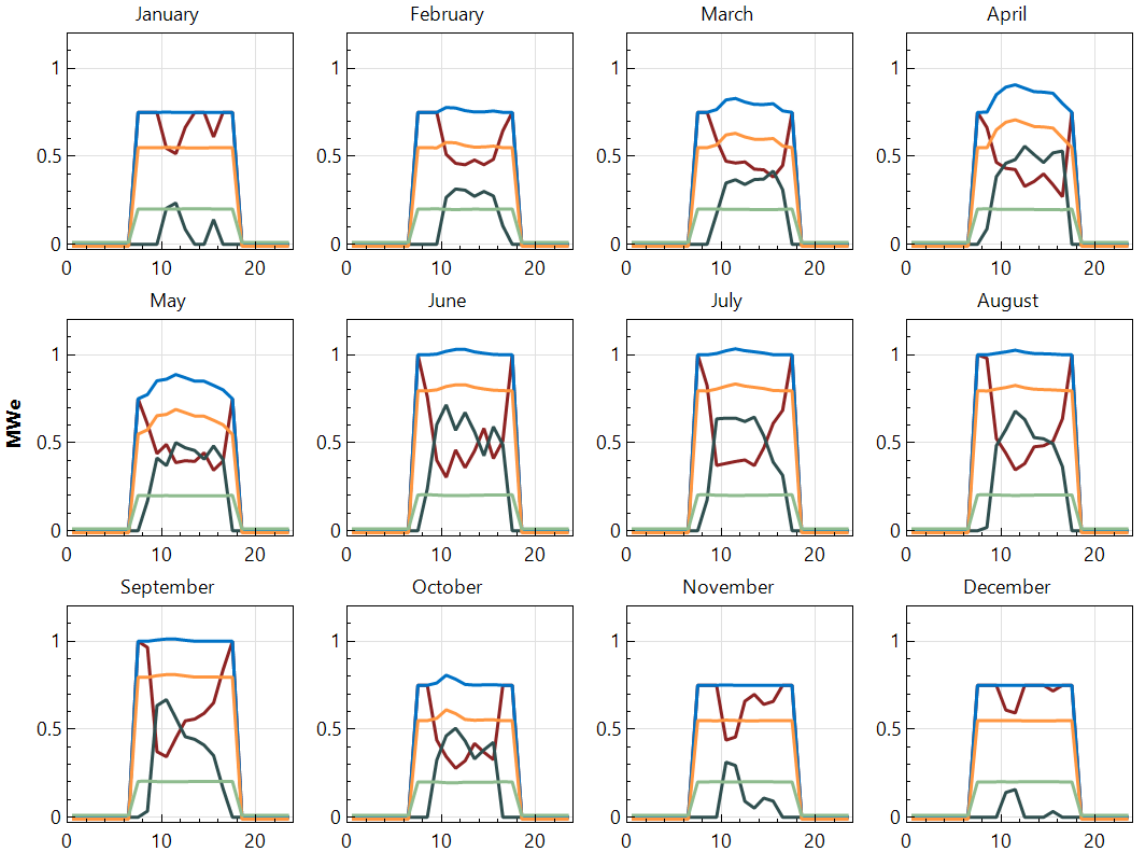

Figure 6-3: SAM results. Blue – cycle electrical power output (gross); yellow – cycle electrical power output (net); brown – cycle electrical power output (gross, fossil share); dark green – cycle electrical power output (gross, solar share); light green – parasitic power total consumption.

6.2. Sensitivity Analysis and Parametric Optimization

The sensitivity analysis is performed to evaluate the importance of the assumptions, as well as to identify parameters that have the highest impact on the plant performance. Even though it can also be used to optimize the plant, this analysis is mostly qualitative; in order to perform an actual optimization of the plant, more

advanced software and algorithms should be used because changing one parameter too much might result in having a completely different system that would need to be optimized in a completely different way. For example, in order to optimize the CO_2 power cycle if the maximum temperature is changed, the maximum pressure will no longer be the optimal for that temperature. In order to optimize the plant properly, all variables must be considered, as well as boundary conditions.

6.2.1. Parametric Analysis: Temperatures and Pressures

For the purpose of sensitivity analysis, it is better to fix boundary conditions for the cycle. Therefore, instead of having to choose variables such as C_r and effectiveness for the design of the PCHE that absorbs heat from the solar field, it was preferred to fix the inlet and outlet temperatures of the solar field at 293^{o}C and 393^{o}C. Then, the LMTD method is used to calculate the heat exchanger UA.

6.2.1.1. Maximum Temperature and Maximum Pressure

The maximum temperature of the power cycle should be as high as possible to improve cycle efficiency. The same happens for the maximum pressure; however, for a certain maximum temperature, there is a maximum pressure above which the efficiency no longer increases. For 325^{o}C, this pressure is 35 MPa. According to reference [21], cycle pressure should not go above 35 MPa (5000 psi), meaning that for temperatures higher than 325^{o}C, the allowable pressure that maximizes the efficiency is 35 MPa.

6.2.1.1.1. Maximum Pressure

Figure 6-4 shows the influence of the maximum pressure variation in the LCOE and cycle efficiency. As discussed above, 35 MPa yields the optimal maximum pressure

for the given cycle maximum temperature. However, in the LCOE calculation, the effect of more expensive components due to increased pressure was not considered. This is an approximation because in the manufacturing of the PCHE it is assumed that there will not be great difference associated with the operating pressure. However, for pressures above 25 MPa, there is not a great difference in the cycle efficiency. Therefore, it might be desirable to implement the cycle with a lower maximum pressure.

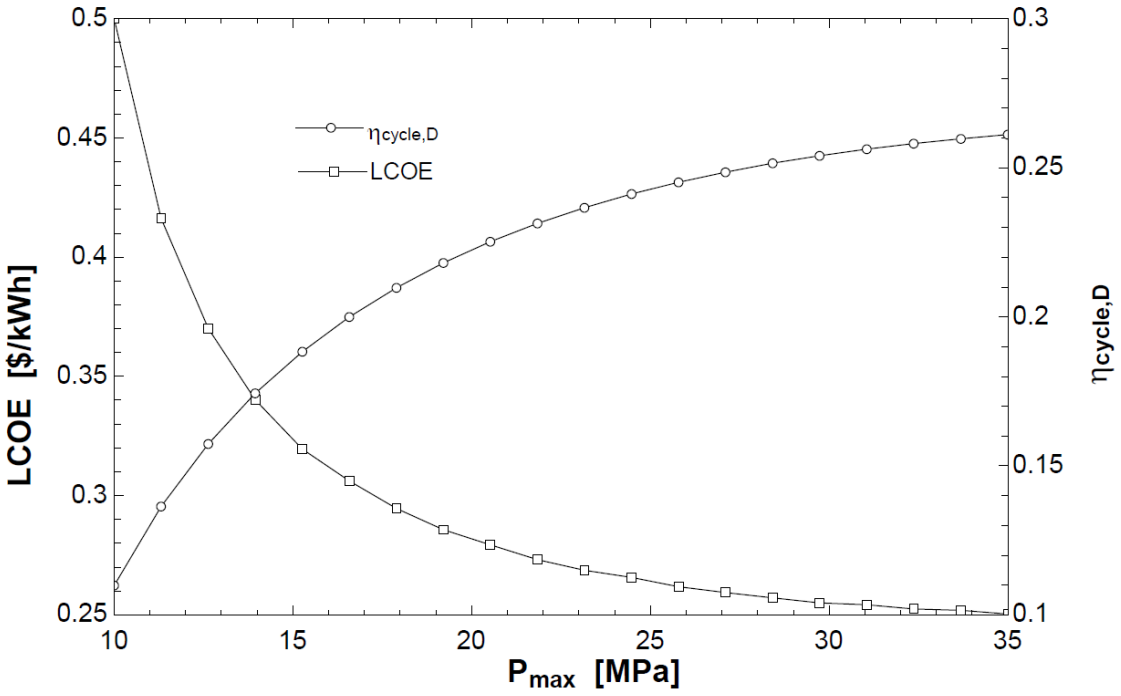

Figure 6-4: Maximum Pressure variation influence

6.2.1.1.2. Maximum Temperature

The maximum temperature of the cycle is bounded by the maximum temperature achieved in the solar field. However, as exposed in the boundary conditions at the beginning of this document, there is a possibility of using the exhaust heat of the Texas A&M campus gas turbine as a heater for the CO_2, which would require an additional

heat exchanger (PCHE) from the flue gas to the CO_2. Additional equations were implemented to account for this, with the box below showing the equations implemented in the EES cycle procedure while Figure 6-5 shows the modified cycle.

Additional burning optional

If $(T_{max} > 370 \ [C])$ Then

$T_{1b} := 370 \ [C]$

$P_{1b} := P_1$

$h_{1b} := \mathbf{h}(\text{CarbonDioxide}, T = T_{1b}, P = P_{1b})$

$s_{1b} := \mathbf{s}(\text{CarbonDioxide}, T = T_{1b}, P = P_{1b})$

$q_{add} := h_1 - h_{1b}$

$q_{col} := h_{1b} - h_6$

Else

$q_{add} := 0$

$q_{col} := h_1 - h_6$

EndIf

$T_{g,1} := 510 \ [C]$

$T_{g,2} := 400 \ [C]$

$$LMTD := \frac{T_{g,1} - T_{max} - (T_{g,2} - T_{1,sfD})}{\ln\left[\frac{T_{g,1} - T_{max}}{T_{g,2} - T_{1,sfD}}\right]}$$

$$UA_{add} := \frac{\dot{Q}_{add,D}}{LMTD}$$

$$UA_{h,D} = UA_{ev,D} + UA_{add,D}$$

$$C_{ev} := 17.5 \ [\$] \cdot \left[\frac{UA_{h,D}}{1 \ [kW/K]} \cdot 1000\right]^{0.8778}$$

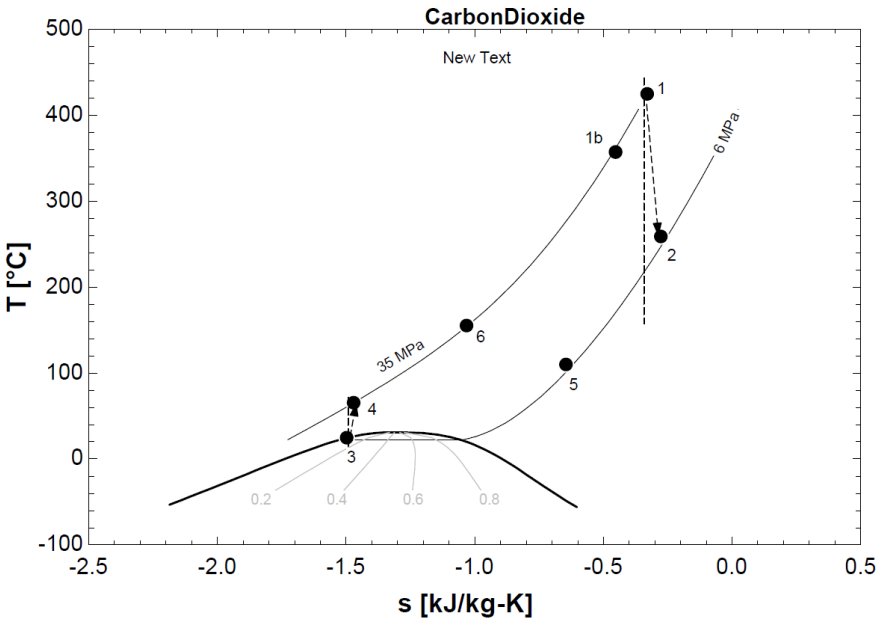

Figure 6-5: Cycle with additional heating up to 425°C

The UA-value for the additional heat exchanger is computed and lumped into the PCHE at high pressure / high temperature costs. Additional heat is needed only above 370^{o}C to raise the temperature to more than the solar field achievable limit. This additional heat was also lumped into the fossil fuel boiler capacity and the fuel costs. This is a conservative approach because although the heat could be assumed to be waste heat, it might also be used to produce steam. Therefore, the fuel and boiler capital costs associated with the additional heat account for the steam that could be generated with the waste heat for the gas turbine, which is instead used to heat the CO_2.

The flue gas from the turbine is known to be at 950^{o}F (510^{o}C) [13], and then, it is assumed that it transfers heat to the CO_2 until it cools down to 400^{o}C. The waste heat at 400^{o}C is assumed to be used for some other heat recovery process. For example, it can be used to heat steam because steam at 600 psi has an evaporation temperature of 254^{o}C.

It should be noted that the temperature should not be raised too much because we could arrive at a completely different system with a completely different optimization. This happens when T_1 is increased too much, meaning more regeneration is available and therefore T_6 increases as well, to the point where heat absorbed from the solar field is too low. T_6 should not go above the minimum temperature of the solar field (293^{o}C), a limit of 250^{o}C was put so that T_6 cannot go above it. When the waste heat cannot go into regeneration, more process heat is available at a higher temperature, which would change the design of the heat exchangers, etc. Fortunately, this does not happen before T_1 reaches 500^{o}C, which means within the parametric study range, the complications of redesign are avoided.

Figure 6-6 shows the impact of the maximum temperature variation, from 325 to 500ºC. The LCOE is seen to be reduced until T_{max} reaches 425ºC. At that point the cycle has an efficiency of 30%. If the temperature is to be increased even more, the capital cost of heat exchangers ($LCOE_{capex}$) makes the investment undesirable. Another trough is found close to 465ºC. For both optimums, the LCOE is \$0.282/kWh, which is not a huge change from the \$0.2915 value from the original model with the temperature at 370ºC, therefore, the complexities of implementation might make the improvement undesirable.

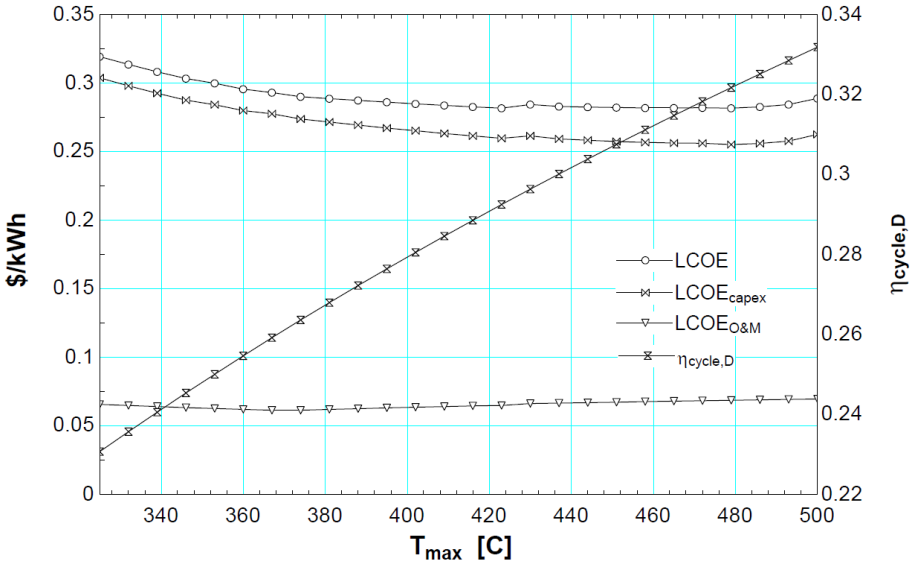

Figure 6-6: Maximum Temperature variation influence

6.2.1.2. Other Temperatures

6.2.1.2.1. Design Wet-Bulb Temperature

The design wet-bulb temperature would change if the geophysical location of the plant changed, or if the plant was designed for a specific season. Figure 6-7 shows that the change in LCOE is not much when lowering the temperature. Also, it is known that

the lower the temperature of the cycle, then the higher the efficiency. However, the impact in the LCOE does not seem to be significant, even more, the LCOE at some point increases when the wet-bulb temperature decreases.

The condensation temperature is shown in the right y-axis, which is illustrative as to why there are abrupt changes in the trend of the LCOE when increasing the wet-bulb temperature. Specifically, it is because the condensation temperature distance to the wet-bulb temperature is decreased in order to keep the CO_2 condensing below 30ºC, since its critical point occurs at 31ºC.

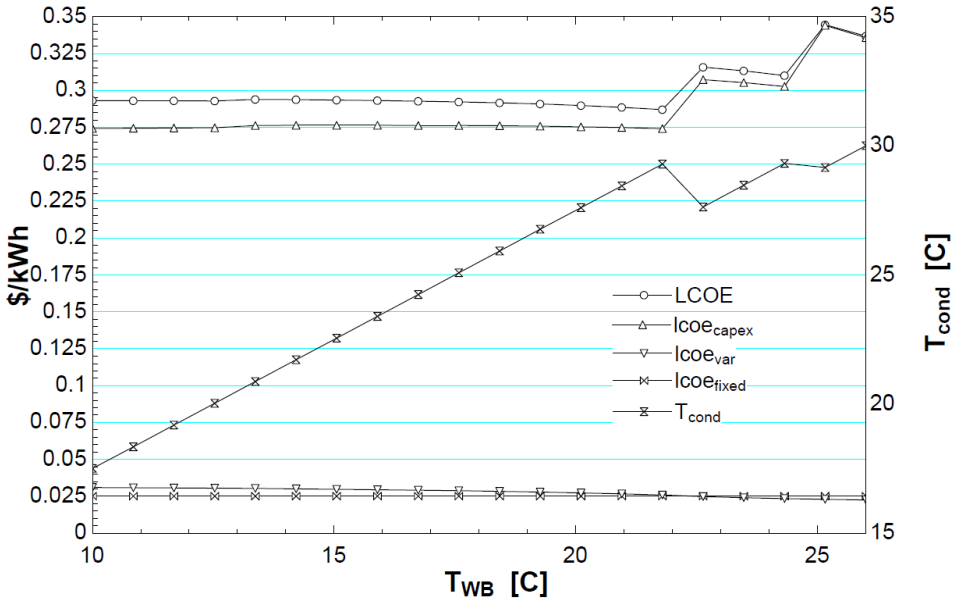

Figure 6-7: Wet-Bulb Temperature variation influence

6.2.1.2.2. HTF Field Inlet Temperature

In the design of the solar field, having a lower HTF field inlet temperature was desirable because this would mean less energy is consumed while warming up, making better use of the high temperatures. However, the results obtained show a different trend.

It is observed in Figure 6-8 that the increase of the HTF minimum temperature significantly benefits the LCOE, which is due to the exponential decrease in UA-value of the evaporator (heat exchanger HTF to CO_2), thus decreasing the capital expenditure. It is also true that the energy required to warm up the solar field was not accounted for; however, this is expected to have a smaller impact because typically, the HTF would be stored in a tank that will mostly keep its temperature overnight.

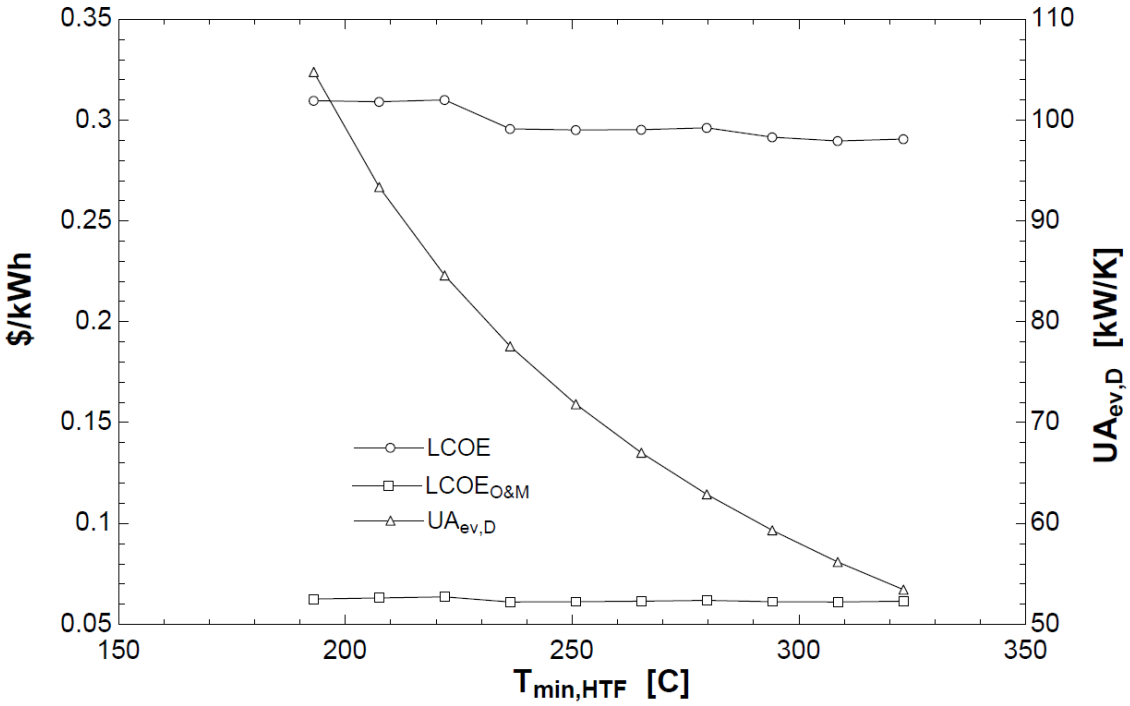

Figure 6-8: HTF Minimum Temperature variation influence

6.2.1.2.3. Cooling Tower Water Exit Temperature

As explained in the design chapter, the value of the cooling tower water exit temperature depends on the approach, which depends on the cooling tower water flow rate and temperature range. The temperature approach will be lower if the temperature range is smaller and if the flow goes below the design point flow.

The value of the cooling water minimum temperature has an impact on the required UA of the condenser, and this appears to affect the LCOE significantly as shown in Figure 6-9. As expected, to decrease the LCOE, this temperature must be decreased, not only to achieve better cycle efficiency, but also for a smaller condenser.

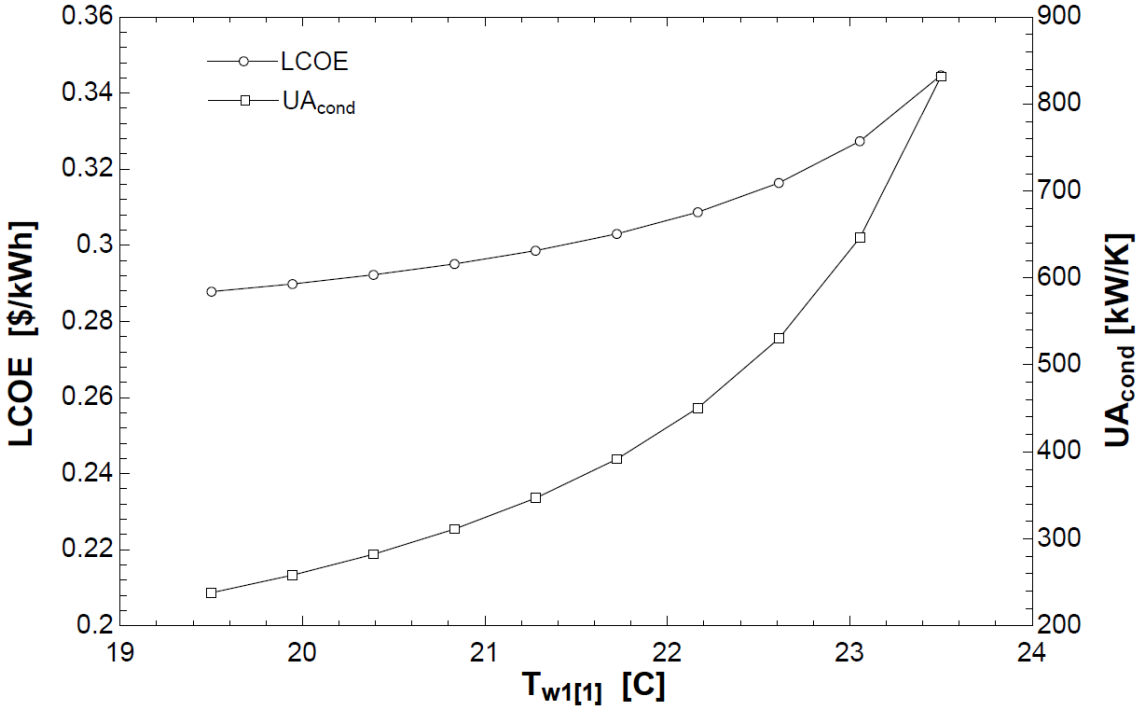

Figure 6-9: Cooling Water Minimum Temperature variation influence

6.2.1.2.4. Design Condensation Temperature

The condensation temperature is calculated by adding a certain increase to the wet-bulb temperature. This increase is 7.5°C at the design point, and it is lower at higher wet-bulb operating temperatures.

At first, it was believed that the decrease of the condensation temperature would benefit the cycle. However, the discovered trend shows that the increase in capital expenditure has a higher impact on the LCOE. It is therefore desirable to increase the

condensation temperature despite the decrease in efficiency, which is very low. Figure 6-10 shows the increase in UA of the condenser associated with the decrease in condensation temperature, which is responsible for the worse LCOE performance.

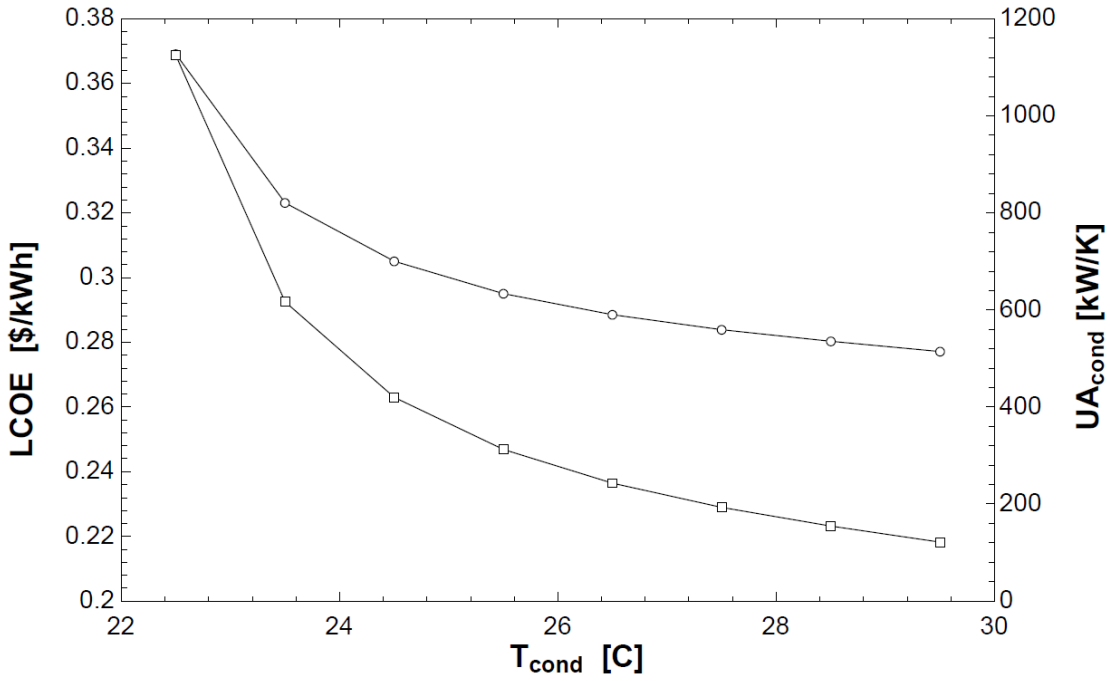

Figure 6-10: Condensation Temperature variation influence

6.2.1.2.5. Design Cogeneration Temperature

The design cogeneration temperature is the temperature at which recuperation is interrupted in the CO_2 cycle, directing the rest of the cooling to the process heat, producing hot water at 180°F (80°C).

As expected, lowering the temperature results in a higher cycle efficiency, which in turn provides a lower LCOE. Unlike previous analyses, this temperature has a higher impact on the cycle efficiency, which makes it desirable to have a larger heat exchanger to recover the heat produced. However, this might not be possible with a shell-and-tube

heat exchanger. Specifically, in the design chapter, it was discussed how the heat recovery heat exchanger is already pushed to the limits of what these kinds of heat exchangers can do.

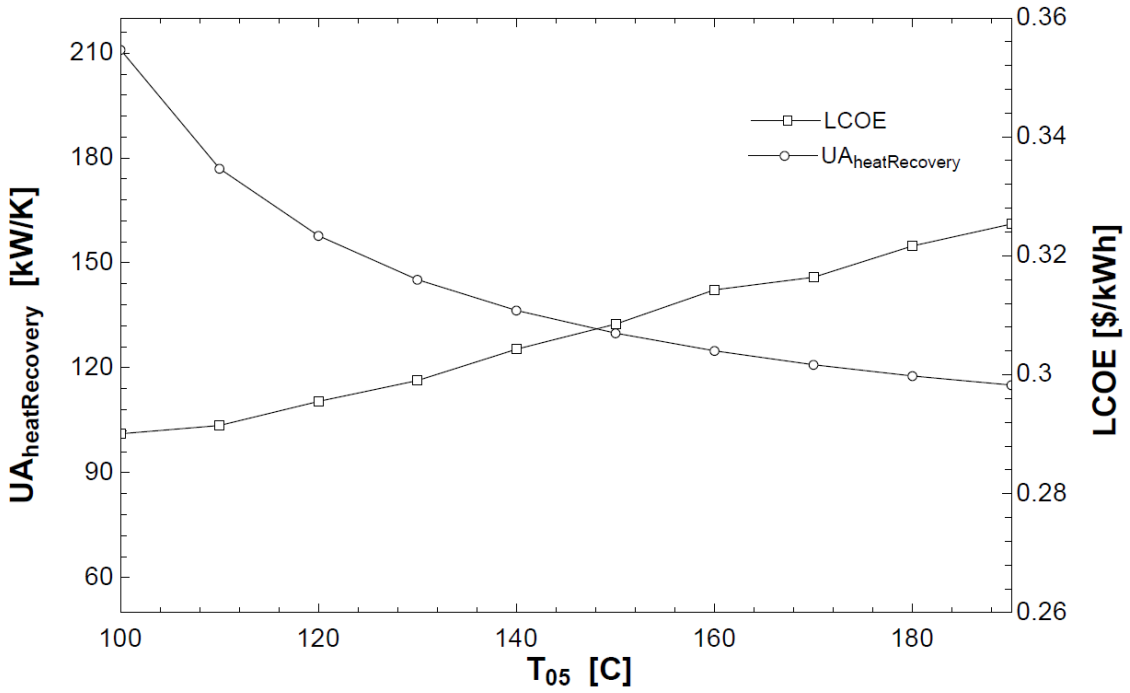

Figure 6-11: Cogeneration Temperature variation influence

6.2.2. Parametric Analysis: Efficiencies

The efficiencies of the different components of the plant were chosen based on assumptions and previous studies. The inaccuracy of these assumptions might be more significant than expected, which is the reason why this sensitivity analysis is crucial. Figure 6-12 shows that the efficiencies of the turbine and the parasitic losses are the ones that most define the LCOE. In contrast, the boiler efficiency is the one that would not have a great impact on the LCOE, even knowing that having lower boiler efficiency could increase fuel consumption. The pump isentropic efficiency affects the LCOE but

not as significantly as the turbine isentropic efficiency. A change of turbine efficiency from 85% to 80% would increase the LCOE approximately $2/kWh, which is due to the cycle efficiency being greatly dependent on these efficiencies as shown in Figure 6-13. As a side note, the generator efficiency has the same effect as the parasitic loss efficiency because they multiply in the same equation.

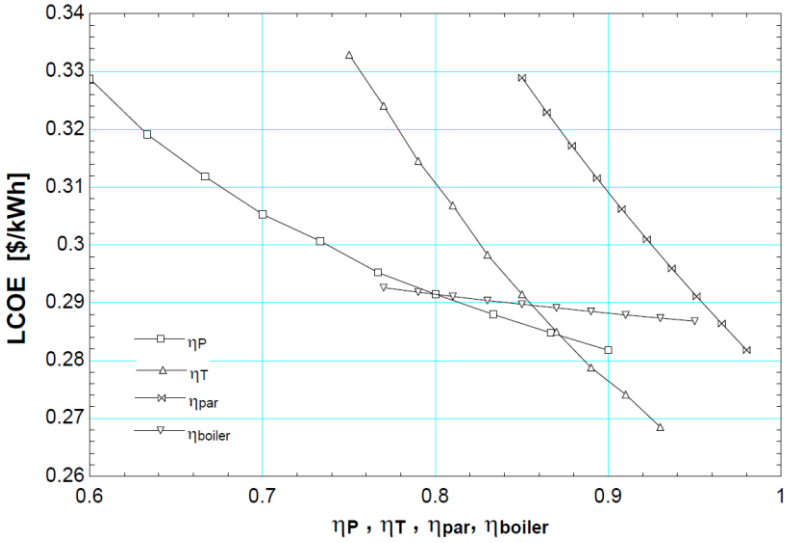

Figure 6-12: Impact of component efficiencies on LCOE

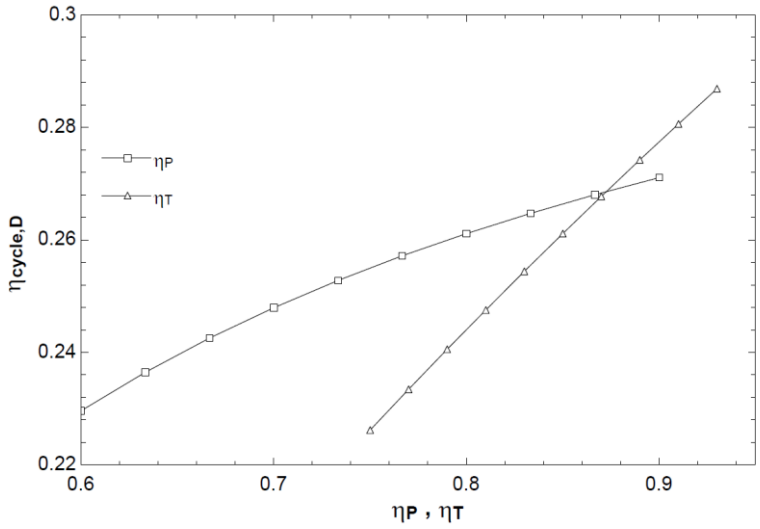

Figure 6-13: Impact of pump and turbine isentropic efficiencies on cycle efficiency

6.2.3. Parametric Analysis: Costs and Sizes

6.2.3.1. Main Capital Costs

The main capital costs considered in the design were chosen based on assumptions and previous studies. These costs have a great impact on the LCOE and their variation should be studied, with two main capital expenditures being the power block costs and solar field costs.

At design, the power block cost was around 2.5 million dollars ($2500/kW). Figure 6-14 shows the influence of the power block on the LCOE, as well as the solar field specific cost (upper horizontal axis).

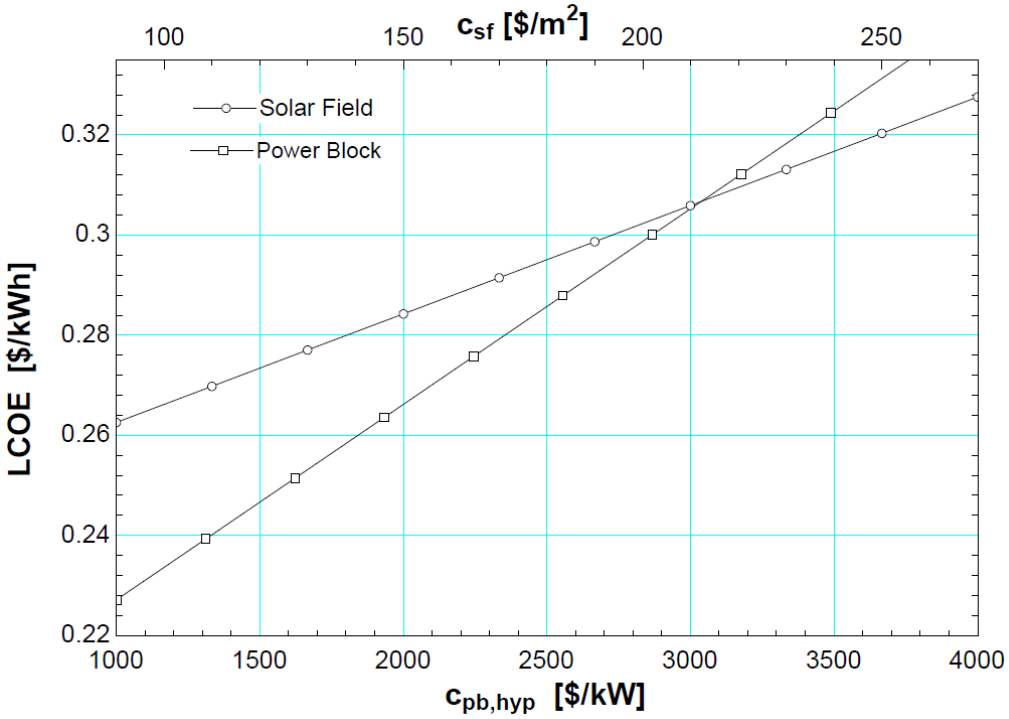

Figure 6-14: Power Block and Solar Field Costs variation influence

As it can be seen in Figure 6-15, both, solar field and power block have a significant influence in the LCOE. The power block has a little more weight on the total

capital expenditure; however, the solar field costs do not include the HTF system or the BOP systems, which could make the investment in solar energy harnessing expensive.

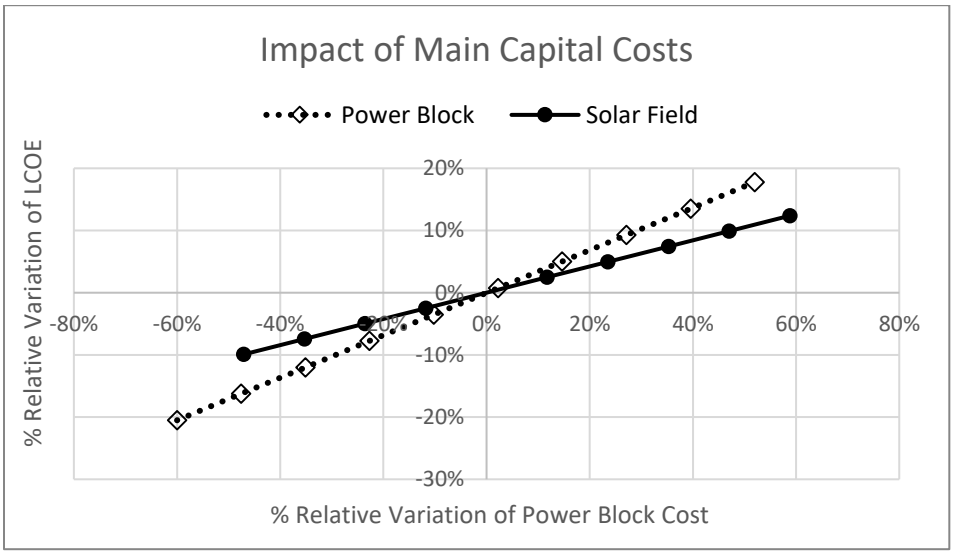

Figure 6-15: Impact of Main Capital Costs

6.2.3.2. Main O&M costs

Natural gas is the fuel used for powering the backup boiler auxiliary to the solar field. According to government agencies, natural gas prices have experienced great oscillation in the last years. Plus, they depend on the end-user. Figure 6-16 illustrates this.

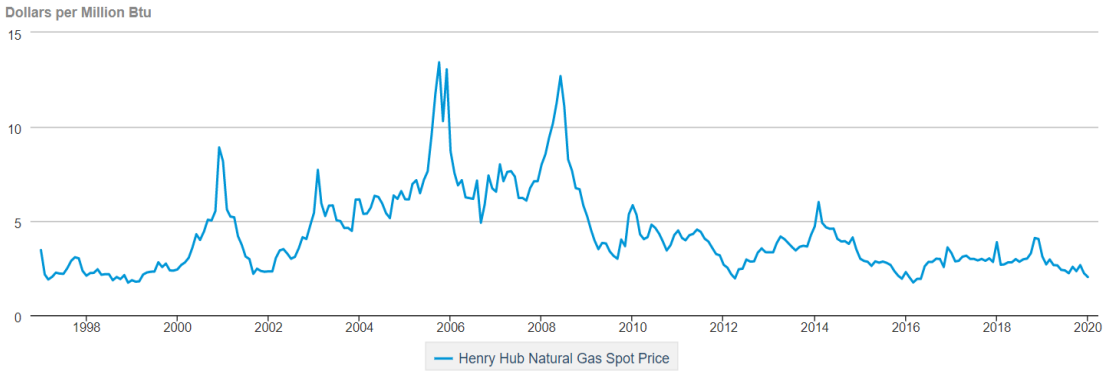

Figure 6-16: Natural Gas Prices in the last two decades, reprinted from [96]

Figure 6-17 shows the variation in LCOE for changes in the price of natural gas. As observed, if natural gas became more expensive, the LCOE would increase significantly.

O&M fixed costs also affect the LCOE in the same manner as the natural gas costs. For example, at design, these costs were set at $72.5/kW, which ended up being less than $0.04/kWh-yr. Figure 6-18 shows that the relative variation slope is similar for both costs, which means that both have approximately the same weight in the LCOE calculation.

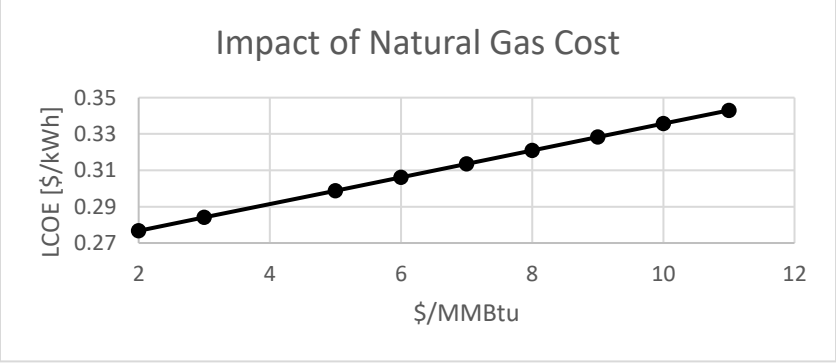

Figure 6-17: Natural Gas Cost variation influence

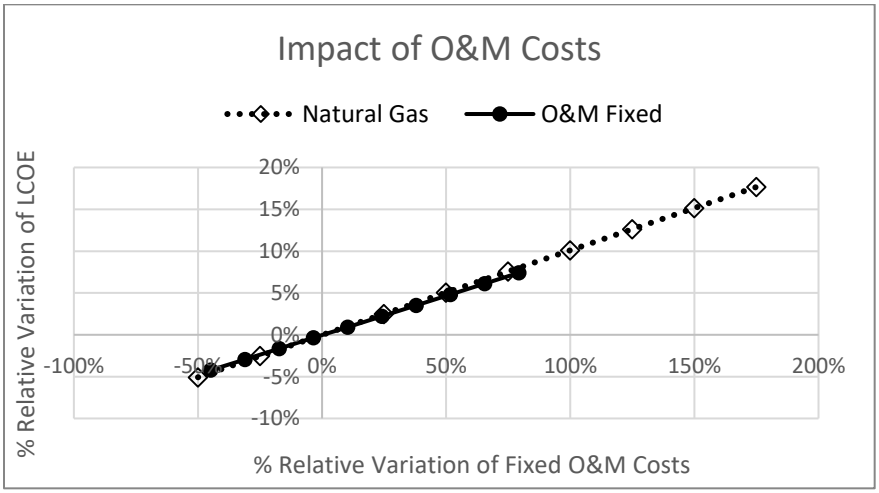

Figure 6-18: Influence of O&M costs

6.2.4. Parametric Analysis: Operation

The calculation of the LCOE was performed assuming a certain number of hours of operation every day, and a certain number of solar energy operation hours during the year, based on median days simulation. Figure 6-19 shows that the increase in daily operation hours makes the LCOE decrease rapidly. The increase in equivalent full-load solar hours also decreases the LCOE, but to a lesser degree. This also means that in a location with more radiation e.g., more than double equivalent full-load hours than College Station, such as Phoenix, AZ; the LCOE would not be much different.

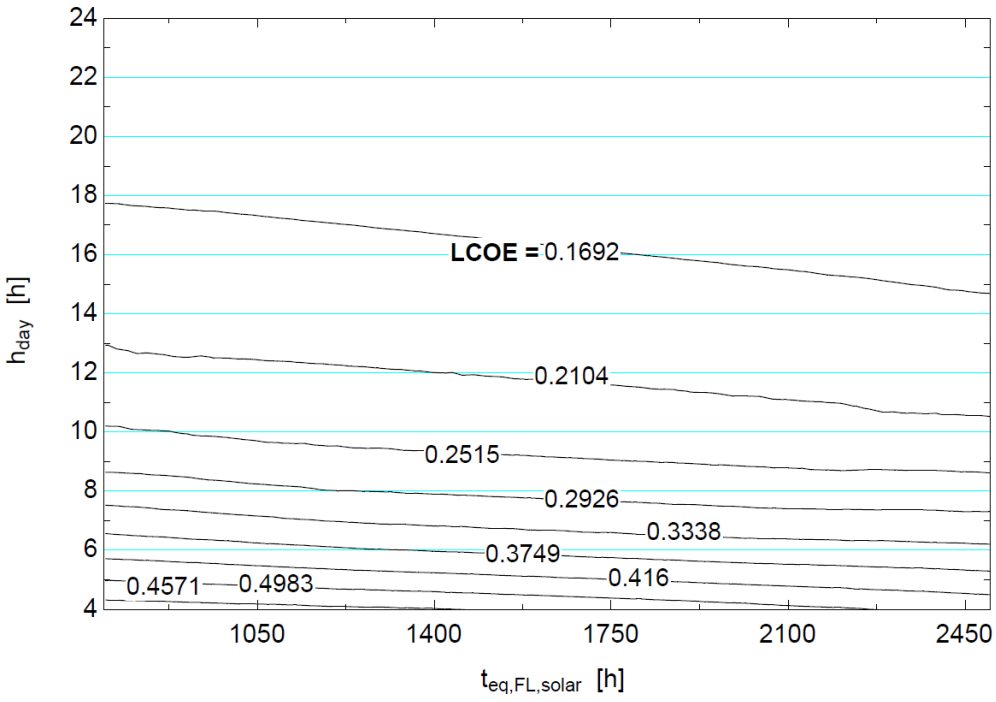

Figure 6-19: LCOE contour plot for equivalent full-load solar hours in the year and daily operation hours.

The effect of solar energy hours is more significant when the fictional income of avoiding CO_2 emissions is incorporated to the LCOE, as shown in Figure 6-20. However, the most effective way of making energy cheaper is by increasing the capacity

factor of the plant, which has a disadvantage in that the solar energy share of the energy generated will be lower because solar energy is only available in a restricted number of hours during the day (Figure 6-21). If the operation time is to be increased, this must be made up with fossil fuel energy. The higher the slope of the solar share curves, then the more solar hours will be required to keep the same solar share with increased operation time.

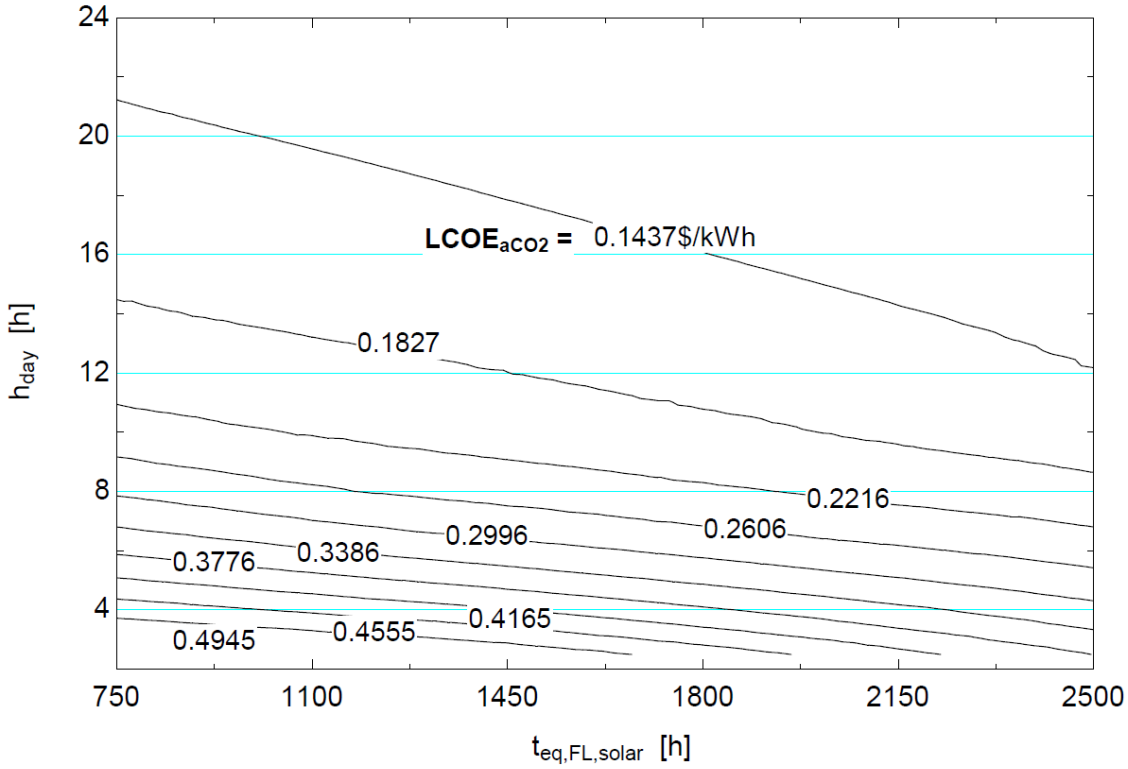

Figure 6-20: LCOE contour plot for equivalent full-load solar hours in the year and daily operation hours (including income of avoided CO_2 capture).

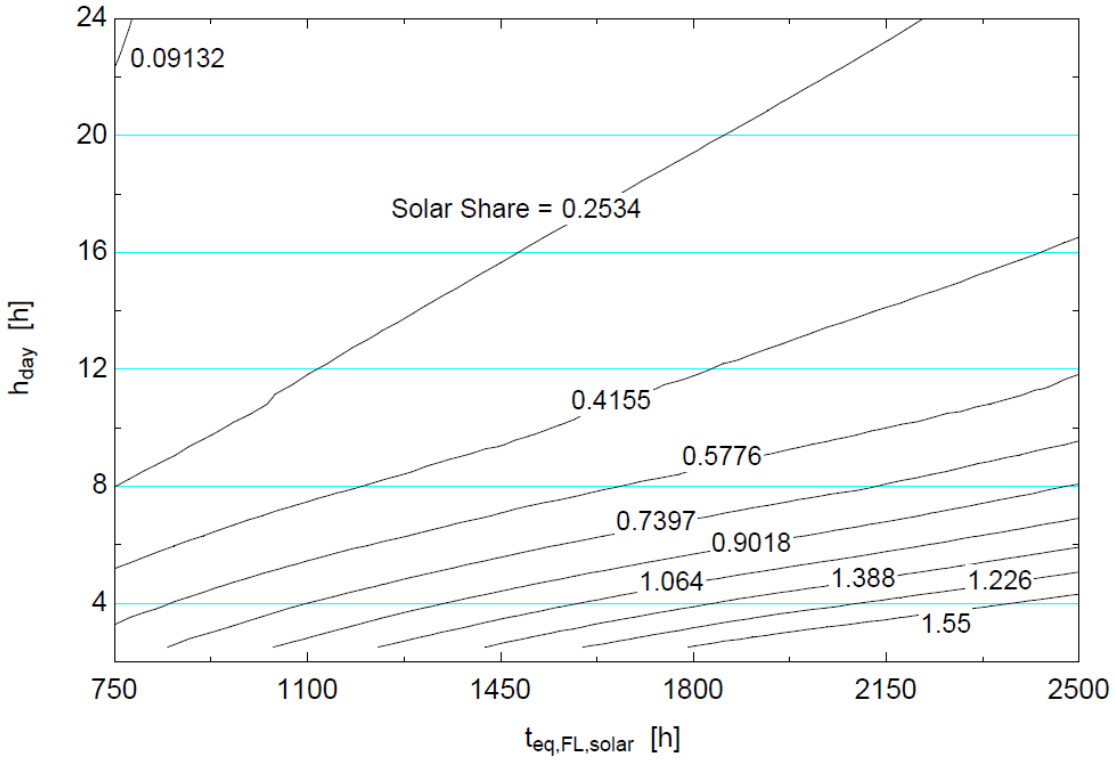

Figure 6-21: Solar share contour plot for equivalent full-load solar hours in the year and daily operation hours.

6.2.5. Parametric Analysis: Economic parameters

Economic parameters such like project analysis period, discount rate and degradation rate have a great impact on the LCOE. Figure 6-22 shows that an increase of the discount rate from 7.5% to 10% would increase the LCOE by 20% to $0.35/kWh, which is significant. As to the analysis period, increasing the number of years would not decrease the LCOE as steeply as decreasing them would increase it.

The LCOE is sensitive to the degradation rate. For example, with a degradation rate of 0.999, at the end of the project life, the capacity would have been reduced to 97.5%. However, with a 0.99 degradation rate, the plant would yield 77% of the capacity it was initially built for, which would increase the LCOE by 8% to $0.31/kWh.

Figure 6-22: Impact of Discount Rate

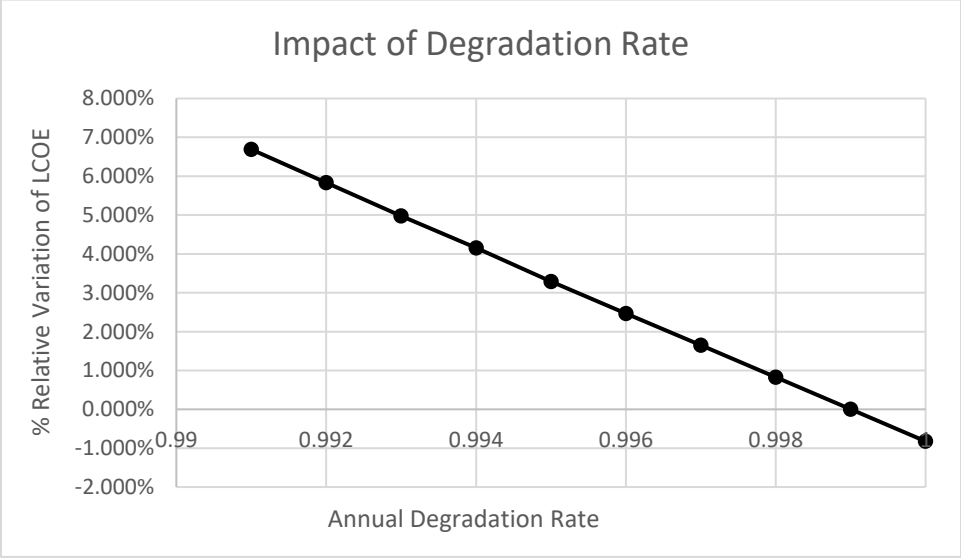

Figure 6-23: Impact of Degradation Rate

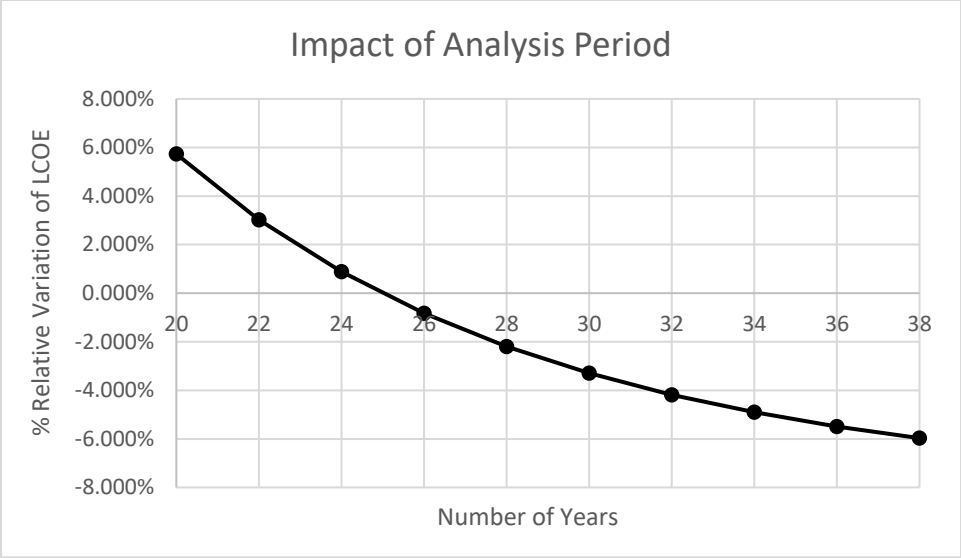

Figure 6-24: Impact of Analysis Period

6.2.6. Parametric Analysis: Design Specifications with SAM

A study of the chosen value of DNI for the design point is appropriate. Simulating this with EES would be lengthy because the equivalent solar full-load hours would vary, and SAM was therefore used for this purpose.

With the same location and conditions, the following variation of LCOE presented in Table 6-3 shows that there is not a big change. Even so, is not so surprising that the LCOE would increase when increasing the design DNI because a greater DNI would decrease the design size of the solar field, which is one of the heaviest capital expenditures.

Table 6-3: Influence of design DNI

DNI design (W/m^2)	LCOE with SAM ($/kWh)
680	30.62
780	30.58
880	30.28
980	29.74

6.2.7. Summary and Conclusions of Parametric Analysis

There is a benefit as well as a difficulty in making a complex model in that there are many variables on which results depend. Most of this sensitivity analysis has been performed with the design program in EES by changing design parameters and seeing how results were affected. The LCOE has been identified as the main parameter that summarizes the overall performance of the designed plant both energetically and economically. The elasticity has been defined as the relative increment of LCOE over the relative increment of a certain variable, close to the design point. Considering differential increments, the definition of the elasticity of the LCOE with respect to a variable *x* is defined in Eq. (5.88). Table 6-4 shows the elasticity of all the variables described in the above sections.

$$e_x = \frac{d(LCOE)/LCOE}{dx/x} = \frac{d(LCOE)}{dx}\frac{x}{LCOE} \approx \frac{\Delta LCOE/LCOE}{\Delta x/x} \tag{5.88}$$

Table 6-4: Summary of LCOE elasticity with respect to different variables

Variable	LCOE elasticity	Variable	LCOE elasticity
Temperatures and Pressures		**Efficiencies**	
T_{max}	-45%	η_T	-95%
P_{max}	-18%	η_P	-29%
$T_{min,HTF}$	-13%	$\eta_{parasitics}$	-110%
T_{WB}	-5%	η_{boiler}	-10%
T_{05} (cogeneration)	10%	**Economic Parameters**	
T_{cond}	-57%	Discount rate	57%
Specific Costs		Degradation	-822.5%
Natural Gas	10%	Analysis Period	-19%
Power Block	34%	**Operation**	
Solar Field	20%	Hours per day	-74%
O&M fixed	9.5%	Solar full load hours	-9.5%
Boiler	7.5%		

If the elasticity is negative, a positive change in that variable reduces the LCOE. The elasticity is similar to a non-dimensional derivative that helps identify which parameters have a greater impact on the LCOE. It also reads as the change in LCOE when the *x* variable has a change of 100%, which is why some values are remarkably high, such as the degradation rate. A change of 100% in the degradation rate is hypothetical. The reader must also understand that some variables would only tolerate small increments. The plots presented above show the behavior outside the design point.

6.3. Exploration of Alternatives

6.3.1. Plant Scale: 10 MW Texas A&M University Utility Plant

In the extrapolation of the plant from 1 MW to 10 MW various parameters and conditions change. Nonetheless, the requirements of electricity and heat or boundary conditions are the same. In the EES design code, it is not just enough to change the design power from 1 to 10 MW. Other considerations are described below:

a) The maximum temperature changes from 370 to 470^{o}C because of the assumption that the heat from the gas turbine in the Texas A&M utility plant can be recovered to heat the CO_2 as described previously in this chapter, which changes the LCOE from $0.2915/kWh to $0.2818/kWh.

b) The design output power changes from 1 to 10 MW, which affects the capital expenditure cost scaling factor, turns from 1.25 to 1. In other words, the specific cost of the cycle components no longer needs to be increased by 25% due to scaling (smaller devices are more expensive on a per kW basis). It

should be noted that this scaling factor is only applied to the power block costs while the rest of the costs are assumed linear for simplicity following [70]. This changes the LCOE from $0.2818/kWh to $0.268/kWh because the power block cost changes from $2500/kW to $2000/kW.

c) Efficiencies of the turbine and compressor/pump are considered the same as well as parasitic loss efficiencies. It is known that they should increase, but no quantitative results were found to base these assumptions on and as a result they were left equal. However, the generator efficiency, which includes the frequency conversion losses, must change because for plants bigger than 3 MW, electronics are no longer preferred but rather a gearbox to convert rotating speed. The gearbox has an efficiency of 99% [21], and when multiplied by 97% then the generator efficiency results in a 96% efficiency, and the LCOE changes from $0.268/kWh to $0.2648/kWh.

d) The ratio of the total land area to the solar field area must also decrease because the power block is still compact, and its size does not increase as much as the solar field size with the design power. The area ratio was changed from 1.1 to 1.05, decreasing the LCOE from $0.2648/kWh to $0.2647/kWh.

e) The boiler efficiency is expected to be higher for a larger boiler. It was changed from 80% to 88%, decreasing the LCOE from $0.2647/kWh to $0.2613/kWh.

As a result, the final LCOE achieved with the plant size increase for the Texas A&M Utility plant is $0.2613/kWh, which is a 10.36% decrease from $0.2915/kWh for the original size of 1 MW for the small industry case.

Using SAM, the following assumptions were changed:

- Area ratio (total land to solar field area) from 1.1 to 1.05
- Cycle efficiency due to increased maximum temperature: from 26% to 31.73%.
- Design power: from 1 to 10 MW.
- Power block cost: from $2500 to $2000/kW.
- Load data: the required electrical load for savings calculation is scaled with a factor of 10 – from 2 MW demand during 8 hours per day to 20 MW.

The resulting nominal LCOE in SAM is 25.45 ¢/kWh, which from the baseline 30.50 ¢/kWh represents a 16.56% decrease. As to the real LCOE in SAM, its value is 21.0 ¢/kWh.

6.3.2. Layout Alternatives

6.3.2.1. Recompression Cycle

The Recompression cycle was introduced in the Preliminary Studies chapter as a potential alternative because of its high electrical efficiency. The question was whether that boost in efficiency is worth the increase in cost. To find an answer for this, the EES design code was remodeled into a new version, with the same solar and fossil equivalent full load hours, but with a Recompression Cycle. The same design steps as with the

simple transcritical cycle were followed here. Remarkable design aspects are presented below.

a) The maximum pressure for which the cycle has optimized efficiency is 20 MPa for a maximum temperature of 370°C. The lower maximum pressure was not considered in cost estimations because it is expected to have a rather small effect. PCHEs usual materials are strong enough to withstand this and superior levels of pressure.

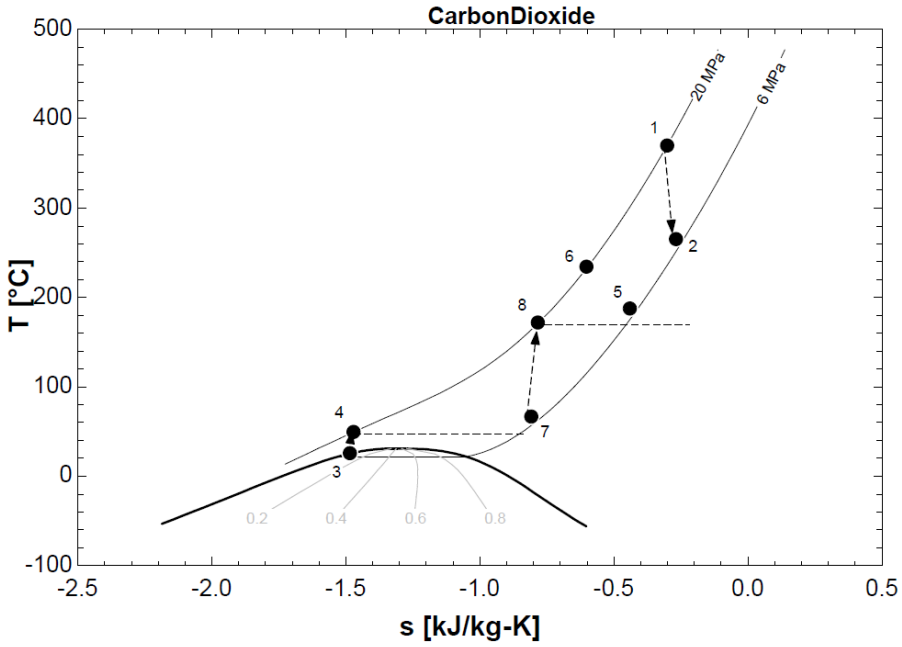

Figure 6-25: Recompression Cycle T-s diagram

b) This cycle contains two regenerators. Its efficiency is slightly higher than 30%. Figure 6-25 shows the different states of the cycle. The lower temperatures of regeneration processes can be identified with dashed lines.

There is a split at point 7: part of the flow is recompressed to 8 and the other part is cooled down to 3.

c) The fraction of the flow that goes to the condenser is called x_L. It is specifically used to multiply the main mass flow rate when designing the cooling part of the cycle. It also helps to decrease the total heat rejected.

d) No cogeneration energy is available because T_7 is 60°C, which is the lower temperature limit of useful cogeneration. This condition might mean an improvement because according to the sensitivity analysis, the LCOE increased when T_5 decreased (in this cycle, T_7). The design of the cooling heat exchangers followed the same scheme as above, namely two water circuits (WC1 and WC2). Once the water has passed through the condenser (WC1), a small fraction of the flow is directed to the heat recovery exchanger to cool down the CO_2 at a temperature higher than T_{cond}. Finally, both flows are directed to the cooling tower. The UA values for the condenser and the heat recovery exchanger are lower than for the baseline cycle but of the same order, which is probably due to the smaller heat rejection that is taking place.

e) The maximum water temperature reached was set at 50°C. The heat recovery exchanger has an F design factor (LMTD method) of 0.75 with 4 shells. The cooling water temperature range is 3°C, which means the design of the cooling tower is similar to the baseline one. Temperature increments were set at the values shown in Table 6-5.

Table 6-5: Summary of design temperature increments

$\Delta T_{w11} = T_{w1,in} - T_{WB} = \Delta T_{approach}$	1.75°C
$\Delta T_{w12} = T_{w1,out} - T_{w1,in}$	1.75°C
ΔT_{cond}	8.5°C

f) An additional parameter in the design is the regenerators effectiveness. A high value increases too much the cost but boosts the efficiency. An optimum for this value was found at 0.833. With this effectiveness, the UA of both regenerators were lumped into one UA to compute a total cost of regenerators. The cost associated with 264 kW/K is much higher than the 21 kW/K in the baseline cycle. This is because the temperatures considered are much closer in range, which results in a low LMTD. The power block cost is increased from 2.5 to more than 3 million (cost obtained with Table 5-9, which is the maximum and therefore preferred cost) due to the investment in regeneration PCHEs.

g) The turbomachinery will be designed for different specific work and flow rates, compared to the baseline plant. For the cost estimation of turbomachinery, an increase in cost is associated with having an additional compressor and more turbine power (2 MW versus 1.6 MW baseline). In the cost model described in Table 5-9, only the net power is important, which is the same as for the baseline plant. Therefore, no changes in turbomachinery costs were considered, although it is known there should be an increase. In

the cost model reference, the case considered also had more than one compression machines [22].

The LCOE for the Recompression Cycle is $0.3086/kWh, which is a 6% increase from the baseline cycle. Contrary to what was expected, the economic competitiveness of the Recompression Cycle is not as clear, and this is mainly due to increased estimated capital cost, which comes particularly from the regeneration PCHEs.

6.3.2.2. Supercritical Brayton Cycle

Making the cycle supercritical was considered as a potential improvement because it would facilitate heat transfer to the ambient temperatures. However, increasing the heat rejection temperature could produce a decrease in efficiency that is not worth the change.

To assess the suitability of the transcritical cycle, a redesign was accomplished with changes in the following aspects:

a) The supercritical cycle was first optimized thermodynamically. The new "condensation" temperature was still called T_{cond}, and it is the temperature for which the specific entropy of the CO_2 is the critical entropy. Although no condensation takes place at this temperature, it helps as a reference of the peak of the liquid-vapor dome in the T-s diagram. T_3 is the lowest temperature of the cycle and it was set to be 1°C below the fictional T_{cond}, as shown in Figure 6-26. The optimal allowable maximum pressure (maximizing efficiency) for a maximum temperature of 370°C is 35 MPa as in the transcritical cycle. All the rest of the cycle parameters such as

turbomachines efficiencies and other temperatures remained the same, making it comparable to the original design.

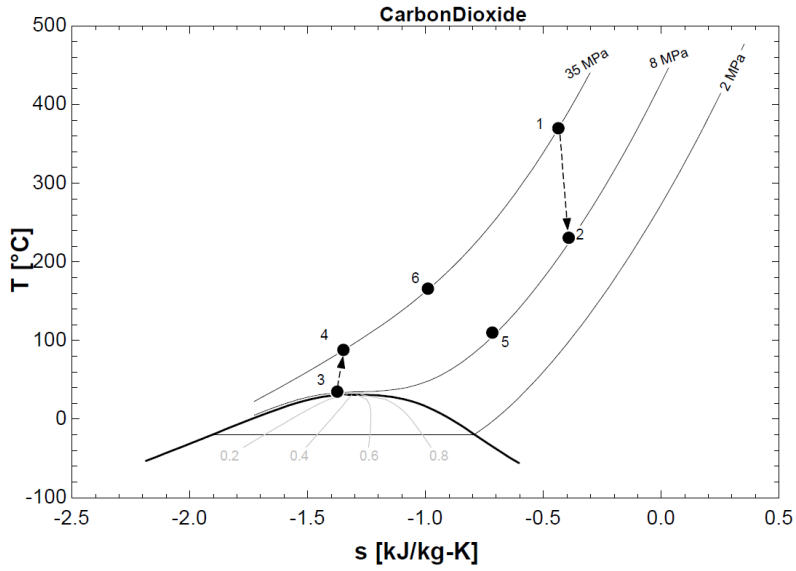

Figure 6-26: Supercritical CO_2 cycle T-s diagram

b) For the heat exchangers design, shell-and-tube type was considered to be suitable although the pressure of the CO_2 was now higher at low temperature. Some references [23] state that 6 MPa is the limit for this type of heat exchangers. However, since in this case there is no condensation, the CO_2 can be on the tube side, which withstands high pressures better. Plus, some references also state that shell and tube heat exchangers can operate above 6 MPa [22].

c) To keep as close as possible to the original design, the new 'condenser' would be a heat exchanger that brings the CO_2 from a temperature $T_{h1,in}$ to $T_3=T_{h1,out}$. The difference between this two temperatures is a design choice, and it is called $\Delta T_{cond\,2} = T_{h2,in} - T_{h2,out} = T_{h2,in} - T_3 = T_{h2,in} - (T_{cond} - 1)$.

d) Using the LMTD method, the UA value was computed for the 'condenser' (WC1) and the heat recovery exchanger (WC2). Since the temperatures in the CO_2 were higher, the cogeneration water temperature was raised from 80°C to 90°C, which was the original desired value. The final design results are shown in Table 6-6, including the F factors (obtained online, [57]) for the LMTD design of U-tube and shell heat exchangers. It is observed that the cooling tower is less demanded, with a lower gpm and a higher temperature range and approach. The number of shells in the heat recovery exchanger was chosen following the transcritical cycle design, in order to make it as comparable as possible. More shells would result in a lower UA value while less shells increase the F factor so drastically that the design might not be possible.

Table 6-6: Cooling water loops design values

Design choices (inputs)		**Design results (outputs)**	
Variable	**Value**	**Variable**	**Value**
T_{cond}	36°C	ΔT_{range}	5°C
$T_{w2,out}$	90°C	$T_{w2,in}=T_{w1,out}$	24.5°C
$T_3=T_{h1,out}= T_{cond}$ -1°C	35°C	$\dot{V}_{w1}$	1613 gpm
$\Delta T_{cond\,2}$	5°C	$\dot{V}_{w2}$	122.4 gpm
$\Delta T_{w11} = T_{w1,in} - T_{WB} = \Delta T_{approach}$	3.5°C	F-heat recovery	0.81
$\Delta T_{w12} = T_{w1,out} - T_{w1,in}$	2.5°C	F-condenser	0.98
N° shells (heat recovery)	4	$UA_{heatRecovery}$	147.9 kW/K
N° shells (condenser)	1	UA_{cond}	76.34 kW/K

e) T_{cond} was evaluated in the range from 36 to 46°C, finding that the LCOE increases as T_{cond} is increased above the critical point. Similarly, $\Delta T_{cond\,2}$ was

also found to increase with the LCOE. However, a value of 5ºC was deemed reasonable. Further lowering of $T_{h2,in}$ would result in a new F value for the heat recovery exchanger that is not acceptable, but this can only be known by iterative optimization, which is not in the scope of this analysis.

f) In the pump, the density change in the compression from points 3 to 4 is 28%, which means the fluid behavior is still close to a liquid. In the transcritical cycle it was 17%.

g) The total UA in the shell and tube heat exchangers is UA_{cool}=224.2 kW/K, which is a reduction from the transcritical cycle value of 369 kW/K. The new heat exchanging estimated area is 7,000 ft^2, and the cost estimated following Figure 5-21 is $60,000 plus 50% due to high pressure operation: $90,000. Since the cooling tower no longer needs oversizing, its cost will be reduced to $70/ton. This is a significant cost reduction from the transcritical cycle, resulting in 1.8 million dollars for the whole power block. However, in a conservative approach, between the two procedures of cost estimation, the highest cost obtained was chosen. This was still the cost obtained with Table 5-9, which resulted in some 2.2 million dollars of power block cost.

The LCOE obtained for the supercritical CO_2 plant was $0.2743/kWh, which is a reduction of 6% from the baseline transcritical plant ($0.2915/kWh). The cycle efficiency is still high: 25.7%, and the capital cost reduction seems to appear justified. This is not what was first thought in that condensation would result in lower temperatures that would increase the efficiency and LCOE.

7. CONCLUSIONS

7.1. Summary of Results

The computational analysis was performed in this project for the purposes of exploring different alternatives and possibilities for the integration of the supercritical CO_2 power plant with a solar Parabolic Trough Collectors (PTC) plant for heat input. Accomplishing this goal required developing a design and simulation code that was able to estimate the LCOE and the overall performance of this technology. Table 7-1 shows the main results obtained.

The capacity factor was estimated using a simulation code in EES for College Station, TX with the result being 33.3% (operation hours per total hours in the year). For approximately 40% of the operation time the plant is operated solely with solar energy.

A more advanced simulation software, SAM, was used as well so as to provide additional results, revealing an LCOE that is close to the results obtained with EES, namely, a nominal LCOE of about 30 cents per kWh.

Although all the plant alternatives were designed for the same design power (except the 10 MW one), the annual electrical energy produced changes because of parasitic losses associated with the solar field size, which changes for each alternative.

Table 7-1: Summary of technologies explored and their results

Parameter	Baseline - Small Industry - 1 MW	Campus Utility - 10 MW	Recompression - 1 MW	Supercritical - 1 MW
LCOE ($/kWh)	0.2915	0.2613	0.3086	0.2743
Annual energy (kWh)	$2.68x10^6$	$2.67x10^7$	$2.67x10^6$	$2.697x10^6$
Solar field area (m^2)	18,542	152,596	15,485	18,842
Solar-to-electric efficiency (%)	12.72%	15.35%	15.18%	12.49%
Cooling heat exchangers UA (kW/K)	451.2	3431	374.7	224.2
Heating heat exchangers UA (kW/K)	59.56	962.4	95.22	72.44
Recuperator exchangers UA (kW/K)	21.02	249	263.8	53.01
Turbine power (kW)	1615	14914	2004	1798
Cogeneration heat (kW_{th})	600	4566	0	968.4
Cogeneration temperature (^oC)	80	80	n/a	90
Cycle Maximum Point	370^{o}C, 35 MPa	470^{o}C, 35 MPa	370^{o}C, 20 MPa	370^{o}C, 35 MPa
Power Block Cost (M$)	2.647	21.27	3.466	2.345
Total Capital Cost (M$)	8.165	69.22	8.586	7.848

7.2. Discussion

None of the alternatives shown in Table 7-1 is close to the break even point of providing electricity at a cost lower than 7 cents per kWh, which is the typical cost of electricity for industrial consumers in Texas, and specifically in College Station.

The main reasons why the technology studied and evaluated herein is still far from being in a position for market penetration are as follows:

- Low capacity factors: As seen in the sensitivity analysis, increasing the hours of operation per year dramatically decreases the LCOE, but this is difficult to do with solar energy, unless implementing storage or fossil fuel backup. In this project, the backup strategy was chosen for analysis, and the main disadvantage is the decrease of the share of renewable energy. Another option was to make sure the facility is located in a a place with an abundance of solar resource.
- Solar to electric efficiencies are lower than with the conventional steam cycle. This is mainly because the sCO_2 cycle outperforms the steam cycles at temperatures higher than those provided by a PTC solar field. Still, the possibilities of hybridization (additional heat from fossil) and usage of waste heat could produce a boost in efficiency.
- Solar field costs are high. Even with the most established solar technology (PTC collectors), the solar field costs are still somewhat higher than the power block costs, even knowing that the power block type is not in the

market yet. A key advancement for solar energy technology is reduction of solar energy collecting and storage equipment costs.

- Power block costs are higher than for steam, although not much higher. Reduction in heat exchanger costs is necessary. An example of this is the analysis made for the Recompression cycle, where the regenerators' cost made the capital cost increase drastically.
- Scale: The LCOE is known to be reduced for larger scales of energy generation. Although this study was made for small scale generation applications, a key for market penetration is to develop this technology in a larger utility-scale generation project.

There are still technologies to which this plant could be compared for small scale cogeneration such as ORC, fuel cells and steam turbines. Some of the references studied during the literature search state that the Rankine sCO_2 cycles can be up to 10% more efficient than ORCs [23]. Even so, the LCOE shows that even compared to these technologies, the sCO_2 PTC plant would have a long payback period and small return on investment.

The procedures used for plant design and cost estimation were conservative, which might also be part of the reason why the LCOEs obtained are high. Even so, they are not much higher than the LCOEs of other technologies in the market, and they are actually very close to the LCOEs of the CSP technologies in the past years (refer to Figure 5-22 and Figure 5-23).

Another finding is that the Rankine transcritical cycle evaluated herein seemed at the beginning to be more competitive due to increased efficiency, but then it was found to be not better than the Brayton supercritical cycle. In fact, a lower LCOE was found for the supercritical cycle, which also sheds light as to the benefit of small increases in efficiency: they are usually not worth the increase in cost.

7.3. Future Steps

From the findings herein, several new paths have been opened for future work, with these are described here:

- Improvement of the cost models: this requires more detailed design of components. Some of this design was started in this project, but there is still a lot to do.
- Combination of improvements: The sensitivity analysis, along with the evaluation of alternatives, provided important clues as to how to reduce the LCOE, with the parameters being varied individually in the sensitivity analysis. Further optimization would require variation of more than one parameters at a time, in order to obtain a better thermo- economic performance.
- Exploration of new alternatives: In the preliminary studies, a number cycles were assessed as to their potential for improved performance. In addition, during the project, new alternatives were found in the literature, and evaluation of these can now be more easily accomplished with the codes developed.

It is the hope of the author that this project helps to shed light in the investigation about sCO_2 technologies and solar energy. Research is sometimes a work of many iterations, and satisfying results are not always reached before extensive work. The significance of the findings made in this thesis will not be major without further investigation and usage of the knowledge acquired.

REFERENCES

[1] US EIA, "U.S. Energy Facts Explained," U.S. Energy Information Administration, August 2019. [Online]. Available: https://www.eia.gov/energyexplained/us-energy-facts/. [Accessed January 2020].

[2] D. F. R. M. M. W. a. K. A. Ran Fu, "U.S. Solar Photovoltaic System Cost Benchmark: Q1 2017," NREL, 2017.

[3] N. H. A. A. R. S. Md Tasbirul Islam, "A comprehensive review of state-of-the-art concentrating solar power (CSP)," *Renewable and sustainable energy reviews,* no. 91, pp. 987-1018, 2018.

[4] Fraunhofer Institute for Solar Energy Systems, ISE, "www.ise.fraunhofer.de," 19 March 2019. [Online]. Available: https://www.ise.fraunhofer.de/content/dam/ise/de/documents/publications/studies/Photovoltaics-Report.pdf. [Accessed 8 4 2019].

[5] A. Boretti, "Cost and production of solar thermal and solar photovoltaics power plants in the United States," *Renewable Energy Focus,* vol. 26, 2018.

[6] M. J. Joseph Gosselar, "Solar Thermal Energy for Industrial Uses," Environmental and Energy Study Institute, Washington, DC, 2011.

[7] N. H. M. P. M. R. S. Shahjadi Hisan Farjana, "Solar process heat in industrial systems – A global review," *Renewable and Sustainable Energy Reviews*, no. 82, pp. 2270-2286, 2018.

[8] IDAE, "Nota resumen explicativa del Plan Nacional Integrado de Energía y Clima 2021-2030," [Online]. Available: https://www.miteco.gob.es/es/cambio-climatico/participacion-publica/notaexplicativadelborradordelpniec2021-2030_tcm30-487346.pdf. [Accessed 26 04 2019].

[9] IEA-ETSAP, "Solar Heat for Industrial Processes - Technology Brief," January 2015. [Online]. Available: https://www.irena.org/publications/2015/Jan/Solar-Heat-for-Industrial-Processes. [Accessed 05 2019].

[10] R. Druzin, "Big growth on tap for Shiner beer," Victoria Advocate, 2015. [Online]. Available: https://www.victoriaadvocate.com/news/business/big-growth-on-tap-for-shiner-beer/article_3d8c27c1-decc-519e-b0de-a96fa0b2eb24.html. [Accessed 2019].

[11] Brewers Association, "Energy Usage, GHG Reduction, Efficiency and Load Management Manual," 2012. [Online]. Available: https://www.brewersassociation.org/attachments/0001/1530/Sustainability_Energy_Manual.pdf. [Accessed 2019].

[12] Google, "Google Maps," [Online]. Available: https://www.google.com/maps/place/Spoetzl+Brewery/@29.4344396,-97.1683556,634m/data=!3m1!1e3!4m5!3m4!1s0x864308b80e30d853:0x464addc0cdbb9334!8m2!3d29.433337!4d-97.16739.

[13] TAMU Utilities and Energy Services, "Combined Heat and Power," [Online]. Available: https://utilities.tamu.edu/combined-heat-power/. [Accessed January 2020].

[14] M. Tasbirul Islam, N. Huda, A. Abdullah and R. Saidur, "A comprehensive review of state-of-the-art concentrating solar power (CSP) technologies: Current status and research trends," *Renewable and Sustainable Energy Reviews,* no. 91, pp. 987-1018, 2018.

[15] N. S. T. S. B. M. B. R. J. G. W. W. S. ,. F. B. Ming Liu, "Review on concentrating solar power plants and new developments in high temperature thermal energy storage technologies," *Renewable and Sustainable Energy Reviews,* no. 53, pp. 1411-1432, 2016.

[16] W. Seidel, "Model Development and Annual Simulation of the Supercritical Carbon Dioxide Brayton Cycle for Concentrating Solar Power Applications," University of Wisconsin, Madison, 2010.

[17] A. AlZahrani, "Development and Analysis of a Solar-Based Integrated System with a CO2 Rankine Power Cycle," University of Ontario Institute of Technology, Toronto, 2013.

[18] A. M. Patnode, "Simulation and Performance Evaluation of Parabolic Trough Solar Power Plants," University of Wisconsin, Madison, 2006.

[19] V. Dostal, A supercritical carbon dioxide cycle for next generation nuclear reactors., Massachussets Insitute of Technology, 2004.

[20] Supercritical CO2 Power Cycles Symposium, [Online]. Available: http://sco2symposium.com/.

[21] N. Weiland and D. Thimsen, "A Practical Look at Assumptions and Constraints for Steady State Modeling of sCO2 Brayton Power Cycles," in *5th International Symposium - Supercritical CO2 Power Cycles*, San Antonio, TX, 2016.

[22] S. A. Wright, C. S. Davidson and W. O. Scammel, "Thermo-Economic Analysis of Four sCO2 Waste Heat Recovery Power Systems," in *5th Supercritical CO2 Symposium*, San Antonio, TX, 2016.

[23] G. O. Musgrove, R. Le Pierres and J. Nash, "Heat Exchangers for Supercritical CO2 Power Cycle Applications," in *2014 sCO2 symposium*, 2014.

[24] T. C. Allison, J. C. Wilkes, J. J. Moore and K. Brun, "Turbomachinery Overview for Supercritical CO2 Power Cycles," in *46th Turbomachinery and 33rd Pump Symposia*, Houston, TX, 2017.

[25] N. Weiland, W. Shelton, T. Shultz, C. White and D. Gray, "Performance and Cost Assessment of a Coal Gasification Power Plant Integrated with a Direct-Fired sCO2 Brayton Cycle," NETL, 2017.

[26] X.-R. Zhang, H. Yamaguchi and D. Uneno, "Experimental study on the performance of solar Rankine System using supercritical CO2," *Elsevier*, 2006.

[27] Y. Song, J. Wang, Y. Dai and E. Zhou, "Thermodynamic analysis of a transcritical CO2 power cycle driven by solar energy with liquified natural gas as its heat sink," *Elsevier, Applied Energy*, 2011.

[28] L. Pan, B. Li, X. Wei and T. Li, "Experimental investigation on the CO2 transcritical power cycle," *Elsevier*, p. 8, 2015.

[29] E. Limer, "Popular Mechanics," [Online]. Available: https://www.popularmechanics.com/technology/infrastructure/a20359/ge-minirotor-co2-powered-turbine/. [Accessed 2018].

[30] P. Huck, S. Freund, M. Lehar and P. Maxwell, "Performance comparison of supercritical CO2 versus steam bottoming cycles for gas turbine combined cycle

applications," *GE Global Research,* no. The 5th International Symposium - Supercritical CO2 Power Cycles, 2016.

[31] S. Matasci. [Online]. Available: https://news.energysage.com/how-much-does-the-average-solar-panel-installation-cost-in-the-u-s/.

[32] K. Emery, "Rating PV Power and Energy: Cell, Module, and System Measurements," June 2011. [Online]. Available: https://www.nrel.gov/docs/fy16osti/65976.pdf. [Accessed 28 04 2019].

[33] J. Kinnear, Solar Power Authority, 2008. [Online]. Available: https://www.solarpowerauthority.com/whats-better-solar-thermal-or-solar-pv/. [Accessed 2019].

[34] J. Gosselar and M. Johnson, "Solar Thermal Energy for Industrial Uses," Environmental and Energy Study Institute, Washington, DC, 2011.

[35] Free Hot Water Solar Thermal Solutions, 2012. [Online]. Available: http://www.freehotwater.com/wp-content/uploads/2013/07/Woodys-Laundromat-Case-Study-PDF.pdf. [Accessed 2019].

[36] NREL, "nrel.gov," [Online]. Available: https://www.nrel.gov/gis/solar.html. [Accessed 2019].

[37] California Solar Initiative Thermal Program, "energycenter.org," [Online]. Available: https://energycenter.org/csi-thermal/lakehouse-hotel-resort-case-study. [Accessed 2019].

[38] Engineering ToolBox, "Pipes - Typical Fluid Velocities," 2014. [Online]. Available: https://www.engineeringtoolbox.com/fluid-velocities-pipes-d_1885.html. [Accessed 01 05 2019].

[39] Engineering ToolBox, "Pressure and Temperature Ratings of A-53 B, A-106 B, A333, A334 and API 5L Carbon Steel Pipes - Imperial Units.," 2003. [Online]. Available: https://www.engineeringtoolbox.com/a106-carbon-steel-pipes-d_370.html. [Accessed 01 05 2019].

[40] "Thread: Pressure drop on evaporators," [Online]. Available: https://hvac-talk.com/vbb/showthread.php?90362-Pressure-drop-on-evaporators. [Accessed 05 2019].

[41] J. Munoz-Anton, C. Rubbia, A. Rovira and J. M. Martinez-Val, "Performance study of solar power plants with CO2 as working fluid. A promising design window," *Energy conversion and management,* vol. 92, pp. 36-46, 2015.

[42] M. Montes, A. Abanades, J. Martinez-Val and M. Valdes, "Solar múltiple optimization for a solar-only thermal power plant, using oil as heat transfer fluid

in the parabolic trough collectors," *Solar Energy,* vol. 83, no. 12, pp. 2165-2176, 2009.

[43] C. G. .. D. F. Y. M. Kim, "Transcritical or supercritical CO2 cycles using both low- and high-temperature heat sources," *Energy,* vol. 43, no. 1, pp. 402-415, 2012.

[44] G. D. Perez-Pichel, J. I. Linares, L. E. Herranz and B. Y. Moratilla, "Thermal analysis of supercritical CO2 power cycles: Assessment of their suitability to the forthcoming sodium fast reactors," *Nuclear Engineering and Design,* vol. 250, pp. 23-34, 2012.

[45] I. D. Abdullah A. AlZahrani, "Thermodynamic analysis of an integrated transcritical carbon dioxide power cycle for concentrated solar power systems," *Solar Energy,* no. 170, pp. 557-567, 2018.

[46] J. A. Duffie and W. A. Beckman, Solar engineering of thermal processes, New Jersey: Hoboken: John Wiley and Sons, 2013.

[47] R. Stull, "Wet-Bulb Temperature from Relative Humidity and Air Temperature," *Journal of Applied Meteorology and Climatology,* vol. 50, no. November 2011, pp. 2267-2269, 2011.

[48] Heatric, "What is a Heatric Printed Circuit Heat Exchanger?," [Online]. Available: https://www.heatric.com/heat-exchangers/. [Accessed 10 2019].

[49] Y. Goswami, Principles of Solar Engineering, Boca Raton, FL: CRC Press, 2015.

[50] R. Le Pierres, "Compact Heat Exchangers from offshore to onshore: from heat exchangers to reactors," in *PINNL AUTUMN SESSION*, 2012.

[51] G. O. Musgrove, M. Portnoff and S. Sullivan, "Heat Exchangers for Supercritical CO2 Power Cycle Applications," in *6th International Symposium for Supercritical CO2 Power Cycles*, Pittsburgh, PA, 2018.

[52] R. Le Pierres, "Challenges and Development of sCO2 Heat Exchangers," in *DOE sCO2 Workshop*, 2019.

[53] F. P. Incropera, D. P. Dewitt, T. L. Bergman and A. S. Lavine, Fundamentals of Heat and Mass Transfer, John Wiley & Sons.

[54] J. J. Moore and R. Fuller, "Tutorial: Turbo Machinery Design for Supercritical CO2 Applications," in *4th International Symposium on Supercritical CO2 Power Cycles*, Pittsburg, Pennsylvania, 2014.

[55] ASHRAE, 2016 ASHRAE Handbook - Heating, Ventilating, and Air-Conditioning Systems and Equipment, ASHRAE, 2016.

[56] Carrier Rental Systems, "1000-Ton Cooling Tower," [Online]. Available: https://www.shareddocs.com/hvac/docs/1003/Public/04/RENTAL-SPEC-1000T-CT.pdf. [Accessed 12 02 2020].

[57] CHECALC, "LMTD CORRECTION FACTOR CHARTS," [Online]. Available: https://checalc.com/solved/LMTD_Chart.html. [Accessed 02 2020].

[58] A. McClung, N. Smith, T. Allison and B. Tom, "Practical Considerations for the Conceptual Design of an sCO2 Cycle," in *The 6th International Supercritical CO2 Power Cycles Symposium*, Pittsburgh, Pennsylvania, 2018.

[59] C. K. Ho, M. Carlson, P. Garg and P. Kumar, "Cost and Performance Tradeoffs of alternative solar-driver s-CO2 Brayton Cycle Configurations," in *ASME Power and Energy Conversion Conference*, San Diego, California, 2015.

[60] D. Fleming, T. Holschuh, T. Conboy, J. Pasch, S. Wright and G. Rochau, "Scaling Considerations for a Multi-Megawatt Class Supercritical CO2 Brayton Cycle and Path Forward for Commercialization," in *ASME Turbo Expo*, Copenhagen, Denmark, 2012.

[61] IRENA, "Renewable Energy Technologies: Cost Analysis Series. Concentrating Solar Power.," IRENA, 2012.

[62] EIA, "Selected national average natural gas prices, 2014-2019," January 2020. [Online]. Available: https://www.eia.gov/naturalgas/monthly/pdf/table_03.pdf. [Accessed 02 2020].

[63] EIA, "Average Price of Electricity to Ultimate Customers by End-Use Sector," December 2019. [Online]. Available:

https://www.eia.gov/electricity/monthly/epm_table_grapher.php?t=epmt_5_6_a. [Accessed 02 2020].

[64] NREL, "Maximum demand charge rates for commercial and industrial electricity tariffs in the United States," 2017. [Online]. Available: https://data.nrel.gov/submissions/74.

[65] EnergySage, "Investment tax credit for solar power," 01 2020. [Online]. Available: https://www.energysage.com/solar/cost-benefit/solar-investment-tax-credit/. [Accessed 02 2020].

[66] M. D. Carlson, B. M. Middleton and C. K. Ho, "Techno-Economic Comparison of Solar-Driven sCO2 Brayton Cycles Using Component Cost Models Baselined with Vendor Data and Estimates," in *ASME 2017 11th International Conference on Energy Sustainability*, Charlotte, NC, 2017.

[67] J. Primo, "Shell and Tube Heat Exchangers Basic Calculations," [Online]. Available: https://www.pdhonline.com/courses/m371/m371content.pdf. [Accessed 02 2020].

[68] W. D. Seider, "Equipment Sizing and Capital Cost Estimation," [Online]. Available: https://www.seas.upenn.edu/~dlewin/FOCAPD_2004/LECTURE_06_Equipment_Sizing_and_Capital_Cost_Estimation.pdf. [Accessed 02 2020].

[69] D. Shiferaw, J. Montero and R. Le Pierres, "Economic analysis of SCO2 cycles with PCHE Recuperator design optimisation," in *The 5th International Symposium - Supercritical CO2 Power Cycles*, San Antonio, TX, 2016.

[70] P. Kurup and C. S. Turchi, "Parabolic Trough Collector Cost Update for the System Advisor Model (SAM)," 2015. [Online]. Available: https://sam.nrel.gov/concentrating-solar-power/csp-cost-data. [Accessed 02 2020].

[71] IEA, Energy Technology Network, "ETSAP - Industrial Combustion Boilers," 05 2010. [Online]. Available: https://iea-etsap.org/E-TechDS/PDF/I01-ind_boilers-GS-AD-gct.pdf. [Accessed 02 2020].

[72] US EPA, "Fact Sheet: CHP as a Boiler Replacement Opportunity," U.S. Environmental Protection Agency, 2013.

[73] The UK 2050 Calculator, "Gas Boiler Cost Data," [Online]. Available: http://2050-calculator-tool-wiki.decc.gov.uk/cost_categories/82. [Accessed 02 2020].

[74] Lands of Texas TM, "Land for sale in College Station, Texas," [Online]. Available: https://www.landsoftexas.com/College-Station-TX/all-land/. [Accessed 02 2020].

[75] comptroller.texas.gov, "Local Sales and Use Tax Frequently Asked Questions," [Online]. Available: https://comptroller.texas.gov/taxes/sales/faq/local.php. [Accessed 02 2020].

[76] T. J. Held, "Supercritical CO2 Plants for Gas Turbine Combined Cycle Power Plants," in *Power Gen International*, Las Vegas.

[77] IRENA, "Renewable Power Generation Costs in 2018," International Renewable Energy Agency, Abu Dhabi, 2019.

[78] S. D. Comello, G. Glenk and S. Reichelstein, "Levelized Cost of Electricity Calculator: A User Guide," Stanford School of Business, 2017.

[79] DOE Office of Indian Energy, "Levelized Cost of Energy (LCOE)," U.S. Department of Energy.

[80] Energy Information Administration , "Carbon Dioxide Emissions Coefficients," EIA, 02 2016. [Online]. Available: https://www.eia.gov/environment/emissions/co2_vol_mass.php. [Accessed 02 2020].

[81] The Tax Policy Center, "The Tax Policy Center's Briefing Book," The Tax Policy Center, 2017. [Online]. Available: https://www.taxpolicycenter.org/briefing-book/how-does-corporate-income-tax-work. [Accessed 02 2020].

[82] Northwest Registered Agent, "Texas Department Of Revenue, Texas Tax," Texas State Comptroller, [Online]. Available: https://www.northwestregisteredagent.com/texas-comptroller-franchise-tax.html. [Accessed 02 2020].

[83] E. Bellos and C. Tzivanidis, "Analytical Expression of Parabolic Trough Solar Collector Performance," *Designs*, vol. 2, no. 9, 2008.

[84] SOLUTIA, "Therminol VP-1," [Online]. Available: http://twt.mpei.ac.ru/tthb/hedh/htf-vp1.pdf. [Accessed 10 2019].

[85] N. Naeeni and M. Yaghoubi, "Analysis of wind flow around a parabolic collector (2) heat transfer from receiver tube," *Renewable Energy*, no. 32, pp. 1259-1272, 2007.

[86] TMI Staff and Contributors, "SCO2 turbomachinery systems," Turbomachinery International Magazine, 27 October 2018. [Online]. Available: https://www.turbomachinerymag.com/sco2-turbomachinery-systems/. [Accessed 11 2019].

[87] K. E. Nichols, "How to Select Turbomachinery for your Application. Barber Nichols.," [Online]. Available: https://www.barber-nichols.com/sites/default/files/wysiwyg/images/how_to_select_turbomachinery_for_your_application.pdf. [Accessed 11 2019].

[88] A. M. Johnston, W. Levy and S. O. Rumbold, "Application of Printed Circuit Heat Exchanger Technology within Heterogeneous Catalytic Reactors," Meggitt (UK), 2001.

[89] W. Kim, Y.-J. Baik, S. Jeon, D. Jeon and C. Byon, "A mathematical correlation for predicting the thermal performance of cross, parallel, and counterflow PCHEs," *International Journal of Heat and Mass Transfer,* vol. 106, pp. 1294-1302, 2017.

[90] S.-J. Yoon, P. Sabharwall and E.-S. Kim, "Analytical Study on Thermal and Mechanical Design of Printed Circuit Heat Exchanger," Idaho National Laboratory, 2013.

[91] Engineering ToolBox, "Gauge and Weight Chart.," 2005. [Online]. Available: https://www.engineeringtoolbox.com/gauge-sheet-d_915.html. [Accessed 11 2019].

[92] S. P. Peletiri, N. Rahmanian and I. M. Mujtaba, "CO2 Pipeline Design: A Review," *Energies,* vol. 11, 2018.

[93] T. A. Moss and D. A. Brosseau, "Final Test Results for the Schott HCE on a LS-2 collector," Sandia National Laboratories, Albuquerque, NM, 2005.

[94] I. Webster, "Inflation Calculator," [Online]. Available: https://www.in2013dollars.com/inflation-rate-in-2019. [Accessed 02 2020].

[95] WACC Expert, [Online]. Available: http://www.waccexpert.com/. [Accessed 02 2020].

[96] EIA, "Natural Gas Prices," Energy Information Administration, 02 2020. [Online]. Available: https://www.eia.gov/dnav/ng/hist/rngwhhdM.htm. [Accessed 02 2020].

APPENDIX A

MAIN CODES DEVELOPED IN EES

Design Code Equations

```
"**********************************CYCLE PROCEDURE*****************************************************"

Procedure cyclebase(T_max,P_max,T_cond,T_0,P_0,eta_P,eta_T,T_05:w_net,q_col,q_out,q_cog,q_add,eta_cycle,w_T
q_reg,T[1..6],P[1..6],h[1..6],s[1..6],T_cog[1..2],h_cog[1..2])

"Cycle"
P_1:=P_max
T_1:=T_max
h_1:=enthalpy(CarbonDioxide,T=T_1,P=P_1)
s_1:=entropy(CarbonDioxide,T=T_1,P=P_1)

Call Pump_Inlet(T_cond:T_3,P_3)
h_3:=enthalpy(CarbonDioxide,T=T_3,P=P_3)
s_3:=entropy(CarbonDioxide,T=T_3,P=P_3)

Dp_cond:=0.02 "% Pressure loss in the condenser+regenerator"
P_2:=P_3*(1+Dp_cond)
h_2s:=enthalpy(CarbonDioxide,s=s_1,P=P_2)
w_T:=eta_T*(h_1-h_2s)
h_2:=h_1-w_T
T_2:=temperature(CarbonDioxide,P=P_2,h=h_2)
s_2:=entropy(CarbonDioxide,T=T_2,h=h_2)

Dp_evap:=0.01 "% Pressure loss in the evaporator+regenerator"
P_4:=P_1*(1+Dp_evap)
h_4s:=enthalpy(CarbonDioxide,s=s_3,P=P_4)
w_P:=(h_4s-h_3)/eta_P
h_4:=h_3+w_P
T_4:=temperature(CarbonDioxide,P=P_4,h=h_4)
s_4:=entropy(CarbonDioxide,T=T_4,h=h_4)

"Regeneration"
P_5:=P_2*(1-Dp_cond/2)
T_5=T_05{T_5 is input}
h_5:=enthalpy(CarbonDioxide,P=P_5,T=T_5)
"Other way of getting T_5 and h_5:"
{epsilon_reg:=0.9
h_5opt=enthalpy(CarbonDioxide,P=P_5,T=T_4)
h_5=h_2-epsilon_reg*(h_2-h_5opt)
T_5=temperature(CarbonDioxide,P=P_5,h=h_5)}

h_6:=h_2-h_5+h_4

s_5:=entropy(CarbonDioxide,P=P_5,T=T_5)
P_6=P_4*(1+Dp_evap/2)
T_6:=temperature(CarbonDioxide,P=P_6,h=h_6)
s_6:=entropy(CarbonDioxide,P=P_6,h=h_6)

"Regeneration knowing temperature boundaries"
if (T_6>=250[C]) Then
T_6=250[C]
P_6=P_4*(1+Dp_evap/2)
h_6=enthalpy(CarbonDioxide,P=P_6,T=T_6)
s_6:=entropy(CarbonDioxide,P=P_6,h=h_6)

P_5:=P_2*(1-Dp_cond/2)
h_5:=h_2-h_6+h_4
T_5=temperature(CarbonDioxide,P=P_5,h=h_5)
s_5:=entropy(CarbonDioxide,P=P_5,h=h_5)

Endif

"Additional burning optional"
if (T_max>370[C]) Then
    T_1b=370[C]
    P_1b=P_1
    h_1b=enthalpy(CarbonDioxide,T=T_1b,P=P_1b)
    s_1b=entropy(CarbonDioxide,T=T_1b,P=P_1b)
```

```
    q_add=h_1-h_1b
    q_col=h_1b-h_6
Else
    q_add=0
    q_col=h_1-h_6
Endif

"Heat exchanging devices"
q_col:=h_1-h_6
q_out:=h_5-h_3
q_reg:=h_2-h_5

"Power devices"
w_net=w_T-w_P

"Note: once you know m_dot, you can insert a goto and recalculate eta_T and eta_P as well as the heat exchangers
performance"

"Electrical - power block efficiency"


"Cogeneration heat"
T_cog_max:=T_5
{T_cog_min:=T_cond+35[C]}
T_cog_min=62[C]
P_cog1:=P_3
P_cog2:=P_3
h_cog1:=h_5
h_cog2:=enthalpy(CarbonDioxide,T=T_cog_min,P=P_cog2)
s_cog1:=entropy(CarbonDioxide,T=T_cog_max,P=P_cog1)
s_cog2:=entropy(CarbonDioxide,T=T_cog_min,P=P_cog2)

q_cog:=h_cog1-h_cog2
q_cond:=q_out-q_cog
q_ratio:=q_cond/q_cog
q_ratio2:=q_cond/(q_cog+q_reg)


"Efficiencies"

eta_cycle:=w_net/q_col
eta_cycle2:=1-q_out/q_col

"Exergy"
{J_standard= 0.9515 [kW/m2]
X_dot_irr=J_standard*Aperture*total*0.5
psi_max=h_1-h_0-T_0K*(s_1-s_0)
h_0=enthalpy(CarbonDioxide,T=T_0,P=P_0)
s_0=entropy(CarbonDioxide,T=T_0,P=P_0)
X_dot_max=psi_max*m_dot}

"Second law efficiency"

{eta_IIa=W_dot_net/X_dot_irr
eta_IIb=W_dot_net/X_dot_max}
T_standard:=5273[K]
T_0K:=converttemp(C,K,T_0)
T_condK:=converttemp(C,K,T_cond)
T_maxK:=converttemp(C,K,T_max)
eta_Carnot1:=1-T_condK/T_standard
eta_Carnot2:=1-T_condK/T_maxK
eta_IIc1:=eta_cycle/eta_Carnot1
eta_IIc2:=eta_cycle/eta_Carnot2


"Vectors for graphic output"
T[1]=T_1
T[2]=T_2
```

```
T[3]=T_3
T[4]=T_4
T[5]=T_5
T[6]=T_6
T_cog[1]=T_cog_max
T_cog[2]=T_cog_min
s[1]=s_1
s[2]=s_2
s[3]=s_3
s[4]=s_4
s[5]=s_5
s[6]=s_6
s_cog[1]=s_cog1
s_cog[2]=s_cog2
h[1]=h_1
h[2]=h_2
h[3]=h_3
h[4]=h_4
h[5]=h_5
h[6]=h_6
h_cog[1]=h_cog1
h_cog[2]=h_cog2
P[1]=P_1
P[2]=P_2
P[3]=P_3
P[4]=P_4
P[5]=P_5
P[6]=P_6
P_cog[1]=P_cog1
P_cog[2]=P_cog2


3:End

 "********************************** PUMP INLET  PROCEDURE ************************************************"

Procedure Pump_Inlet(T_cond:T_3,P_3)
T_crit:=T_crit(CarbonDioxide)
P_crit:=P_crit(CarbonDioxide)
s_crit:=Entropy(CarbonDioxide,T=T_crit,P=P_crit)
If(T_cond<T_crit) Then
    P_3=p_sat(CarbonDioxide,T=T_cond)
    T_3=T_cond-1[C]
Else
    P_3=pressure(CarbonDioxide,T=T_cond,s=s_crit)
    "That the lower T heat transfer region is low enough but high enough at the specified T_cond"
    T_3=T_cond-1[C]
EndIf
End

"************************************************ PROPERTIES PROCEDURES ************************************************"
Procedure htfproperties(T,P:rho_HTF,c_p_HTF,h_HTF,mu_HTF,k_HTF)
"T in C"

{rho_HTF:=-0.90797*T + 0.00078116*T^2 - 2.367e-6*T^3+1083.25 "kg/m3"
c_pHTF:=(0.002414*T + 5.9591e-6*T^2- 2.9879e-8*T^3 + 4.4172e-11*T^4+ 1.498)  "kJ/kgK"
k_HTF:=(-8.19477e-5*T - 1.92257e-7*T^2 + 2.5034e-11*T^3 - 7.2974e-15*T^4+ 0.137743)/1000 "kW/mK"
mu_HTF:=rho_HTF*(1e-6*exp(544.149/(T+114.43)-2.59578)) "Pa s"}

rho_HTF:=density(Therminol_VP1, T=T)
c_p_HTF:=specheat(Therminol_VP1, T=T)
k_HTF:=conductivity(Therminol_VP1, T=T)*convert(W,kW)
mu_HTF:=viscosity(Therminol_VP1, T=T)
h_HTF:=enthalpy(Therminol_VP1, T=T,P=P)

End

Procedure co2properties(T,P:rho_CO2,c_p_CO2,h_CO2,mu_CO2,k_CO2)
```

```
rho_CO2:=density(CarbonDioxide, T=T,P=P)
c_p_CO2:=specheat(CarbonDioxide, T=T,P=P)
k_CO2:=conductivity(CarbonDioxide, T=T,P=P)*convert(W,kW)
mu_CO2:=viscosity(CarbonDioxide, T=T,P=P)
h_CO2:=enthalpy(CarbonDioxide, T=T,P=P)

End

Procedure waterproperties(T,P:rho_W,c_p_W,h_W,mu_W,k_W)

rho_W:=density(Water, T=T,P=P)
c_p_W:=specheat(Water, T=T,P=P)
k_W:=conductivity(Water, T=T,P=P)*convert(W,kW)
mu_W:=viscosity(Water, T=T,P=P)
h_W:=enthalpy(Water, T=T,P=P)

End

"**********Max temperature in solar field**********"

procedure tmaxsf(T_max:T_1_sfD)

if(T_max>370[C]) Then T_1_sfD=370[C]
if(T_max<=370[C]) Then T_1_sfD=T_max

End

"**********SOLAR FIELD DESIGN PROCEDURE**********"
procedure SolarFieldDesign(DNI_D,Q_dot_col_D,eta_PTC_D,L_PTC,A_a,D_ri,L_spacing,C_r0,N_loops0,epsilon_ev_0,
T_6_D,T_1_D,m_dot_D,q_col_D,P_HTF,T_min_HTF:N_col_D,A_field,N_col_loop,T_M_D,m_dot_HTF_D,
V_dot_HTF_DT,vel_HTF,UA_ev_D,W_dot_HTF_ideal,C_r,N_loops,epsilon_ev_D)

"First approach"
epsilon_ev_D=epsilon_ev_0
N_loops=N_loops0
C_r=C_r0

"Evaporator predesign"
C_CO2:=Q_dot_col_D/(T_1_D-T_6_D)
Q_max:=Q_dot_col_D/epsilon_ev_D

"CO2 as minimum heat capacity"
C_HTF:=C_CO2/C_r
C_min:=C_CO2

{"HTF as minimum heat capacity"
C_HTF:=C_CO2*C_r
C_min:=C_HTF}

"Same for both options:"
{T_M_D:=T_6_D+Q_max/C_min
T_min_HTF:=T_M_D-Q_dot_col_D/C_HTF}

"Now: fixing HTF temperatures and assuming it is going to have the minimum temperature difference"
T_M_D:=393[C]

C_HTF=Q_dot_col_D/(T_M_D-T_min_HTF)
C_r=C_CO2/C_HTF
epsilon_ev_D=Q_dot_col_D/(C_min*(T_M_D-T_6_D))
NTU:=1/(C_r-1)*ln((epsilon_ev_D-1)/(epsilon_ev_D*C_r-1))
UA_ev_D:=NTU*C_min

"Mass flow of HTF and number of loops"

T_HTF_avg:=(T_min_HTF+T_M_D)/2
call htfproperties(T_HTF_avg,P_HTF:rho_HTF,c_p_HTF,h_HTF,mu_HTF,k_HTF)
m_dot_HTF_DT:=C_HTF/c_p_HTF
```

```
11:m_dot_HTF_D:=m_dot_HTF_DT/N_loops
V_dot_HTF_DT:=m_dot_HTF_DT/rho_HTF
V_dot_HTF_D:=V_dot_HTF_DT/N_loops
vel_HTF:=V_dot_HTF_D/(pi/4*D_ri^2)

if (vel_HTF<2[m/s]) Then
N_loops=N_loops-1
Goto 11
Endif

if (vel_HTF>4[m/s]) Then
N_loops=N_loops+1
Goto 11
Endif

"Solar Field design"
Q_dot_1:=DNI_D*A_a*eta_PTC_D
N_col_D:=Q_dot_col_D/Q_dot_1
A_field:=L_PTC*L_spacing*N_col_D
N_col_loop:=round(N_col_D/N_loops)


"Pressure drop"

Re:=4*m_dot_HTF_D/(pi*D_ri*mu_HTF)
f:=(0.79*ln(Re)-1.64)^(-2)
DP_PTC:=f*L_PTC/D_ri*0.5*rho_HTF*vel_HTF^2*convert(Pa,kPa)
DP_field:=N_col_loop*DP_PTC
DP_evap:=0.08*P_HTF*convert(MPa,kPa)
W_dot_HTF_ideal:=(DP_field+DP_evap)*V_dot_HTF_DT


End

"**********ADDITIONAL HEATING**********"
"We have to consider the cost of the PCHE"
procedure qadditional(T_max,T_1_sfD,Q_dot_add_D,epsilon_ev_D:UA_add,epsilon_add_D)

if (Q_dot_add_D=0) Then
UA_add=0
epsilon_add_D=0
Else
{Assume gas temperatures and spec heat close to air}
c_p_g=1.1[kJ/kg-K]
T_g_1=510[C]
T_g_2=400[C]

C_dot_g=Q_dot_add_D/(T_g_1-T_g_2)
C_dot_CO2=Q_dot_add_D/(T_max-T_1_sfD)
C_r=C_dot_g/C_dot_CO2
C_min=C_dot_g
epsilon_add_D=(T_g_1-T_g_2)/(T_g_1-T_1_sfD)


LMTD=((T_g_1-T_max)-(T_g_2-T_1_sfD))/ln((T_g_1-T_max)/(T_g_2-T_1_sfD))
UA_add=Q_dot_add_D/LMTD

Endif

End


"**********REGENERATOR**********"
procedure regenerator_design(T_H_in,T_H_out,T_C_in,T_C_out,Q_dot:UA_reg)

LMTD_reg=((T_H_in-T_C_out)-(T_H_out-T_C_in))/ln((T_H_in-T_C_out)/(T_H_out-T_C_in))
UA_reg=Q_dot/LMTD_reg
```

```
End

"**************************************HEAT REJECTION TEMPERATURES*******************"

procedure Dtemp(T_WB:DELTAT_cond,DELTAT_w11,DELTAT_w12)

if(T_WB<=22) Then
DELTAT_cond=7.5[C]
DELTAT_w11=1.75[C]
DELTAT_w12=1.5[C]
Endif

if(T_WB>22) AND (T_WB<=25) Then
DELTAT_cond=5[C]
DELTAT_w11=1.75[C]
DELTAT_w12=1.5[C]
Endif

if(T_WB>=25) Then
DELTAT_cond=4[C]
DELTAT_w11=1.75[C]
DELTAT_w12=1.5[C]
Endif

End

"**************************************HEAT RECOVERY AND REJECTION***************"

procedure heat_out(T_WB,DELTAT_w11,DELTAT_w12,T[1..6],P[1..6],h[1..6],T_cog[1..2],h_cog[1..2],m_dot:Q_dot_cog,
Q_dot_am,Q_dot_cool,Q_dot_hR,V_dot_w1,C_w1,eta_heatRecovery,DELTAT_range,T_w1[1..2],T_w2[1..3],h_g,
T_h2_out)

q_cog=h_cog[1]-h_cog[2]
q_cool=h_cog[1]-h[3]
Q_dot_cool=m_dot*q_cool

"Critical point protection"
T_crit:=T_crit(CarbonDioxide)
P_crit:=P_crit(CarbonDioxide)
s_crit:=Entropy(CarbonDioxide,T=T_crit,P=P_crit)
If(P[3]<P_crit) Then
    h_g=enthalpy(CarbonDioxide,P=P[3],x=1)
    T_h2_out:=temperature(CarbonDioxide,P=P[3],x=1)
Else
    h_g=enthalpy(CarbonDioxide,s=s_crit,P=P[3])
    T_h2_out:=temperature(CarbonDioxide,P=P[3],s=s_crit)
EndIf

"Water temperatures"
T_w1[1]=T_WB+DELTAT_w11 {in=1, out =2, cog=3}
T_w1[2]=T_w1[1]+DELTAT_w12

T_w2[1]=T_w1[2]
T_w2[3]=60[C]
T_w2[2]=80[C]

c_pw=4.18[kJ/kg-C]
rho_w=1000[kg/m3]

"WC1"
m_dot_w1=m_dot*(h_g-h[3])/(c_pw*(T_w1[2]-T_w1[1]))
C_w1=m_dot_w1*c_pw
V_dot_w1=m_dot_w1/rho_w
"WC2"
m_dot_w2a=m_dot*(h_cog[1]-h_g)/(c_pw*(T_w2[2]-T_w2[1]))
m_dot_w2b=m_dot*(h_cog[1]-h_cog[2])/(c_pw*(T_w2[2]-T_w2[3]))
m_dot_w2=min(m_dot_w2a,m_dot_w2b)
V_dot_w2=m_dot_w2/rho_w
```

```
Q_dot_cog:=m_dot_w2*c_pw*(T_w2[2]-T_w2[3])
Q_dot_hR:=m_dot_w2*c_pw*(T_w2[2]-T_w2[1])
Q_dot_am:=Q_dot_cool-Q_dot_cog

eta_heatRecovery=Q_dot_cog/m_dot/q_cog

x_w2=m_dot_w2/m_dot_w1
T_tower_in=(x_w2*T_w2[3]+(1-x_w2)*T_w1[2])
DELTAT_range=T_tower_in-T_w1[1]

End


"***********************************CONDENSER and PIPE SIZING************************"

Procedure condenser&pipes(T[1..6],P[1..6],h[1..6],T_cog[1..2],h_cog[1..2],m_dot_D,T_WB,DELTAT_w11,DELTAT_w12:
D_m[1..6],DensityChange,V_dot_w1,UA_heatRecovery,UA_cond,Q_dot_cool,Q_dot_cog_D,Q_dot_am_D,T_w1[1..2],
T_w2[1..3])
"Pipe sizing"
i:=1
Repeat
call co2properties(T[i],P[i]:rho[i],c_p[i],h[i],mu[i],k[i])
V_dot[i]=m_dot_D/rho[i]
{D=1.5[in] "1,1/2 in pipe schedule 80"}
v_max[i]=122[m/s]/sqrt(rho[i]/1[kg/m^3]) {API, see energies CO2 pipes document}
v[i]=v_max[i]/1.25 {Reasonable assumption given maximum load factor, etc.}
D_m[i]=(4*V_dot[i]/PI/v[i])^0.5

{"OR: Zhang et Al, see document"
D_m[i]=0.363*V_dot[i]^0.45*rho[i]^0.13*mu[i]^0.025
}
D_in[i]=D_m[i]*convert(m,in)
Re[i]=rho[i]*v[i]*D_m[i]/mu[i]

i:=i+1
Until (i>6)

"Pump sizing"
DensityChange=(rho[4]-rho[3])/rho[3]
rho[6]=density(CarbonDioxide,T=T[6],P=P[6])
DensityChange2=(rho[6]-rho[3])/rho[3]

"Condenser+cogenerator sizing"
call heat_out(T_WB,DELTAT_w11,DELTAT_w12,T[1..6],P[1..6],h[1..6],T_cog[1..2],h_cog[1..2],m_dot_D:Q_dot_cog_D,
Q_dot_am_D,Q_dot_cool,Q_dot_hR,V_dot_w1,C_w1,eta_heatRecovery,DELTAT_range,T_w1[1..2],T_w2[1..3],h_g,
T_h2_out)

"Heat recovery"
T_h2_in:=T_cog[1]
LMTD_hR=((T_h2_in-T_w2[2])-(T_h2_out-T_w2[1]))/ln((T_h2_in-T_w2[2])/(T_h2_out-T_w2[1]))
{"PCHE"
UA_cond=Q_dot_fg_cond/(LMTD_cond)}

"Assume shell and tube: CO2 tubeside for this one, not in the condenser"
P:=(T_w1[2]-T_w1[1])/(T_h2_in-T_w1[1])
R:=(T_h2_in-T_h2_out)/(T_w1[2]-T_w1[1])
F:=0.75 {https://checalc.com/solved/LMTD_Chart.html} {the closer the fluid temperatures, the higher the F}
UA_heatRecovery=Q_dot_hR/(LMTD_hR*F)
{in=1, out =2, cog=3}
{T_w1_out=21; T_w2_out=80; we have F=0.75 for 4 shells and DTrange is 3; gpm is 3300gpm}
{T_w1_out=24.8; T_w2_out=75; we have F=0.8 for 5 shells and DTrange is 5; gpm is 1895gpm}
{T_w1_out=24.8; T_w2_out=80; we have F=0.7 for 5 shells and DTrange is 4.8; gpm is 1883gpm}
{T_w1_out=23.8; T_w2_out=85; we have F=0.65 for 5 shells and DTrange is 2.8; gpm is 3043gpm; too much}
{What is better, to have lower F or to have less shells? UA_cond is drastically decreased with T_w1_out}

"Condenser"
Q_dot_cond=C_w1*(T_w1[2]-T_w1[1])
```

```
T_h1_in=T_h2_out
C_r=0
epsilon_cond=(T_w1[2]-T_w1[1])/(T_h1_in-T_w1[1])
NTU_cond=-ln(1-epsilon_cond) {Incropera}
UA_cond=C_w1*NTU_cond

End


"******************* OUTPUTS and efficiencies procedure *********************"
Procedure outputs(W_dot_D,Q_dot_solar,W_dot_net,Q_dot_cog,Q_dot_am,W_dot_HTF,pwr_cool,eta_par0,eta_gen,
T_WB,T_cond:LF_ele,W_dot_elec,eta_sol_electric,eta_sol_cogen)

W_dot_cool=pwr_cool*Q_dot_am*convert(kW,MW)
eta_parasitics_other=eta_par0 {If compressor is not turbine driven it requires as well drive motor efficiency of 95%}
W_dot_elec=W_dot_net*eta_gen*eta_parasitics_other-W_dot_cool-W_dot_HTF

LF_ele:=W_dot_elec/W_dot_D

"Minimum and maximum load factors: if electrical energy is too low, the plant is switched off"
if(LF_ele<0.5) OR (LF_ele>1.25) OR (T_cond>30.1) {OR (T_WB>=25) }Then
W_dot_elec:=0; eta_sol_electric:=0; eta_sol_cogen:=0; LF_ele:=0; m_dot:=0
Goto 5
Endif

eta_sol_electric=W_dot_elec/Q_dot_solar
eta_sol_cogen=(W_dot_elec+Q_dot_cog)/Q_dot_solar

5:End

"*********************************CAPEX*********************************"

procedure capex1_powerblock(W_dot_D,m_dot_D,w_T_D,w_net_D,UA_h_D,UA_reg_D,UA_cool,Q_dot_am_D:
C_powerblock1)

"Assumptions from Ho"
W_dot_T=w_T_D*m_dot_D
W_dot_P=(w_T_D-w_net_D)*m_dot_D
C_T=9923.7[$]*(W_dot_T/1[kW])^0.5886
C_P=643.15[$]*(W_dot_P/1[kW])^0.9124
C_G=1[$/kW]*W_dot_D {see Assumptions_comments}
C_pipes=0.05*(C_T+C_P)
C_other=0.1*(C_T+C_P) {gearbox/power electronics, auxiliary equipment}
C_ev=17.5[$]*(UA_h_D/1[kW/K]*1000)^0.8778
C_reg=5.2[$]*(UA_reg_D/1[kW/K]*1000)^0.8933
C_cool=450000[$] {review assumptions & comments}

"Using assumptions in: http://sco2symposium.com/papers2016/SystemModeling/059pres.pdf"

C_ev_b=5000[$/(kW/K)]*UA_h_D
C_reg_b=2500[$/(kW/K)]*UA_reg_D
C_cool_b=1700[$/(kW/K)]*UA_cool
C_T_P_G_rest=1000[$/kW]*W_dot_D
if(round(W_dot_D/1000[kW])=1) Then f_scale=1.25
if(round(W_dot_D/1000[kW])=10) Then f_scale=1

"Cooling tower"
tons=Q_dot_am_D*convert(kW,ton)
{C_tower=125000[$] {review assumptions & comments}}
C_tower=100[$/ton]*tons {after making inquiry to manufacturer: https://www.wearelel.com/critical/buy/cooling-towers/600-
ton-marley-cooling-towers-all-stainless-steel; conservative}
{manufacturer said 33500 for 600 tons + 4000 of shipping to Texas: $37500/600ton=$62.5/ton}
{looking at Cost and Performance article we have 5550$/190 tons = 29$/ton}

C_powerblock1a=C_T+C_P+C_G+C_ev+C_reg+C_cool+C_tower+C_pipes+C_other
C_powerblock1b=f_scale*(C_ev_b+C_reg_b+C_cool_b+C_T_P_G_rest)

C_powerblock1=max(C_powerblock1a,C_powerblock1b)
```

```
End


"********************CAPEX SOLAR PLANT*********************************"

procedure capex1_solarfield&plant(A_aT,A_total,W_dot_D,Q_dot_D_fossil,eta_cycle_D,c_sf,c_shtf,c_boiler,c_sbop,
c_scont,C_powerblock1:C_BEC,C_TPC)

C_siteImprovements=30[$/m^2]*A_aT {SAM cost update article}
C_solarField=c_sf*A_aT {SAM cost update article}
C_HTF=c_shtf*A_aT {SAM cost update article}
C_fossil=c_boiler*Q_dot_D_fossil {see Assumptions_comments, https://iea-etsap.org/E-TechDS/PDF/I01-ind_boilers-GS-AD-gct.pdf and the fact that the boiler will not be for water but for therminol}
C_bop= c_sbop*W_dot_D {SAM cost update article}
C_DCC=C_siteImprovements+C_solarField+C_HTF+C_fossil+C_bop+C_powerblock1

C_contingency=c_scont*C_DCC
C_BEC=C_contingency+C_DCC

{Indirect costs}
C_land=5[$/m^2]*A_total {land cost discussed in Assumptions_Comments; conservative approach since field will be located near important facilities such like campus}
C_epc&owner=0.10*C_BEC {from SAM default value}
C_indirect=(C_land+C_epc&owner)*1.08 {sales tax rate: https://comptroller.texas.gov/taxes/sales/faq/local.php}
C_TPC=C_BEC+C_indirect

{Assume no debt}

{Assume no incentives}

{compared with SAM: close enough}

End

"*****************************O&M*****************************"

procedure o&m_costs(W_dot_D,Q_dot_D_fossil,eta_boiler,t_eq_FL_solar,t_eq_FL_fossil,t_eq_FL_total,c_ng,c_sfix:
C_o&m_yr,C_o&m_fixed,C_o&m_var,C_fuel)

C_o&m_fixed=c_sfix*W_dot_D {SAM cost update article}

C_o&m_var=0.004[$/kWh]*W_dot_D*t_eq_FL_total

MMBtu_FL=Q_dot_D_fossil*t_eq_FL_fossil*convert(kWh,MMBtu)/eta_boiler
C_fuel=c_ng*MMBtu_FL

C_o&m_yr=C_o&m_fixed+C_o&m_var+C_fuel

End

"*****************************LCOE**********************"

procedure lcoe1(r,degr,n_yr,ITC,C_TPC,C_o&m_fixed,C_o&m_var,C_fuel,I_CO2_avoided,I_cogen_avoided,W_e_yr:
LCOE,LCOE_aCO2,lcoe_capex,lcoe_O&M)

SUM_simpl=((1+r)^n_yr-1)/(r*(1+r)^n_yr)
SUM_degr=(1-degr^n_yr/(1+r)^n_yr)/(1+r-degr)

lcoe_capex=C_TPC/(W_e_yr*SUM_degr)
lcoe_fixed=C_o&m_fixed*SUM_simpl/(W_e_yr*SUM_degr)
lcoe_var=(C_o&m_var+C_fuel{-I_CO2_avoided}-I_cogen_avoided)/W_e_yr
lcoe_var_aCO2=(C_o&m_var+C_fuel-I_CO2_avoided-I_cogen_avoided)/W_e_yr
lcoe_O&M=lcoe_fixed+lcoe_var

tax_i=0.21 {corporate income tax rate}
d_i=1/n_yr {depreciation, linear}
```

```
{The current tax code of the U.S. states that an investor claiming a 30% ITC can only capitalize 85% (= 1- 0.3 * 0.5) of the system price for depreciation purposes. See info at the bottom of the SAM window for more detail: The depreciable basis is the original minus 50% of the ITC}
f_cap=1-0.5*ITC

tax_factor=(1-ITC-tax_i*f_cap*d_i*SUM_degr)/(1-tax_i)

LCOE=lcoe_capex*tax_factor+lcoe_fixed+lcoe_var
LCOE_aCO2=lcoe_capex*tax_factor+lcoe_fixed+lcoe_var_aCO2

End

"*******************************INCOME***********************************"

Procedure income(W_dot_elec,Q_dot_cog,t_eq_FL:I_ele,I_ng,I_tot_gross,O&M)

I_ele=W_dot_elec*t_eq_FL*0.07[$/kWh] {it is 7 cents because it is approx the average price for the US}
I_ng=Q_dot_cog*convert(kW,MMBtu/h)*t_eq_FL*4[$/MMBtu]
"Demand assumed 6 $/kW-mo"
I_ele_d=W_dot_elec*6[$/kW]*12

"Missing here: more detail O&M costs, etc."

O&M=0.02[$/kWh]*W_dot_elec*t_eq_FL {See Assumptions and comments to understand why}

I_tot_gross=I_ele+I_ng+I_ele_d-O&M

End




"**********************MAIN PROGRAM*****************************************"
"Variables coming from Matlab:"
nd=124 {day in the year}
SolarTime=12[h]
DNI=0.78[kW/m^2]
T_0=23.3[C]
RH=0.77
BarP=0.101325[MPa]
Wspd=4.5[m/s]


"*********Main parameters: Cycle**************************"
T_max=370[C]
P_max=35[MPa]
P_0=BarP
{T_0 defined above}
{T_WB=wetbulb(AirH2O,T=T_0,R=RH,P=BarP)}
T_WB=18.5[C]

{call Dtemp(T_WB:DELTAT_cond,DELTAT_w11,DELTAT_w12)}
"OR"
DELTAT_cond=7.5[C]
DELTAT_w11=1.75[C]
DELTAT_w12=1.5[C]

T_cond=T_WB+DELTAT_cond "Assuming cooling tower, remember that there is a cooling tower fan..."

"Design CYCLE"
{T_cond_D=27[C]}
T_cond_D=T_cond
```

```
"Isentropic efficiencies"
eta_T=0.85
eta_P=0.8
T_05=110[C] {Because we are cogenerating and we want to stop T_5 from decreasing more}
call cyclebase(T_max,P_max,T_cond_D,T_0,P_0,eta_P,eta_T,T_05:w_net_D,q_col_D,q_out_D,q_cog_D,q_add_D,
eta_cycle_D,w_T_D,q_reg_D,T[1..6],P[1..6],h[1..6],s[1..6],T_cog[1..2],h_cog[1..2]) {For each 6-element vector you have to
insert 6 spaces to represent the 6 output elements of the procedure ( , , , , , , , , , , , , , , , , , , , , , , , , , , ) }

"Mass flow rate and sizing"
W_dot_D=1000[kW]
eta_T_D=eta_cycle_D
eta_ev_D=0.97 "You need to insert the evaporator dynamics here... for now let it be 0.97; parasitics and electrical
conversion would be 0.91"
eta_parasitics_D=0.91  {estimate for design purposes}

m_dot_D=W_dot_D/w_net_D/eta_parasitics_D

Q_dot_col_D=q_col_D*m_dot_D/eta_ev_D
Q_dot_add_D=q_add_D*m_dot_D
W_dot_net_D=m_dot_D*w_net_D
Q_dot_reg_D=m_dot_D*q_reg_D

"Solar Field Design input"
DNI_D=0.78[kW/m^2]
N_loops0=4
eta_PTC_D=0.6
L_PTC=7.8[m]
A_a=39[m^2] "Aperture area"
D_ri=66e-3[m]
wdth_PTC=5[m] {*(D_ri/66e-3[m])} {In case you also want to reduce the solar field size, decrease L_spacing too (it should
go with PTC size)}
L_spacing=10[m]
C_r0=0.25
epsilon_ev_0=0.9

"Solar field parameters"
P_HTF=11[bar]*convert(bar,MPa)
{T_am=27[C]}
T_am=T_0
{T_6_D=97.22[C]}
T_6_sfD=T[6]
call tmaxsf(T_max:T_1_sfD)

"SOLAR FIELD DESIGN AND ADDITIONAL BURNER"
T_min_HTF=293[C]

Call SolarFieldDesign(DNI_D,Q_dot_col_D,eta_PTC_D,L_PTC,A_a,D_ri,L_spacing,C_r0,N_loops0,epsilon_ev_0,
T_6_sfD,T_1_sfD,m_dot_D,q_col_D,P_HTF,T_min_HTF:N_col_D,A_field,N_col_loop,T_M_D,m_dot_HTF_D,
V_dot_HTF_DT,vel_HTF,UA_ev_D,W_dot_HTF_ideal,C_r,N_loops,epsilon_ev_D)

Call qadditional(T_max,T_1_sfD,Q_dot_add_D,epsilon_ev_D:UA_add_D,epsilon_add_D)

UA_h_D=UA_ev_D+UA_add_D

"Other IMPORTANT variables:"
Alat=30[deg] {not needed but for the hours}
SF_Avail=1
N_SCA_loop=2 {see configuration of the field}
N_PTC_SCA=N_col_loop/N_SCA_loop
A_aT=N_col_loop*N_loops*A_a {N_col_loop is an integer, unlike N_col_D}

"CONDENSER AND PIPES"
Call condenser&pipes(T[1..6],P[1..6],h[1..6],T_cog[1..2],h_cog[1..2],m_dot_D,T_WB,DELTAT_w11,DELTAT_w12:
D_m[1..6],DensityChange,V_dot_w1,UA_heatRecovery,UA_cond,Q_dot_cool,Q_dot_cog_D,Q_dot_am_D,T_w1[1..2],
T_w2[1..3])
{s_w1[1..2]=[s[3], entropy(CarbonDioxide,T=T_cond,x=1)]
s_w2[1..3]=[entropy(CarbonDioxide,T=T_cond,x=1),s[5],entropy(CarbonDioxide,T=T_cog[2],h=h_cog[2])]}
```

```
"REGENERATOR"
Call regenerator_design(T[2],T[5],T[4],T[6],Q_dot_reg_D:UA_reg_D)

"Cycle outputs and efficiencies"
eta_ev=eta_ev_D
Q_dot_in=(Q_dot_col_D+Q_dot_add_D)/eta_ev
Q_dot_solar=DNI_D*A_aT
W_dot_HTF=W_dot_HTF_ideal/0.6
pwr_cool=25[kW/MW]
eta_par0=0.95
eta_gen=0.95 {generator + frequency conversion}

Call outputs(W_dot_D,Q_dot_solar,W_dot_net_D,Q_dot_cog_D,Q_dot_am_D,W_dot_HTF,pwr_cool,eta_par0,eta_gen,
T_WB,T_cond:LF_ele,W_dot_elec,eta_sol_electric,eta_sol_cogen)

W_dot_T=m_dot_D*w_T_D


"ECONOMICS"

"From Matlab after post-processing"
h_day=8[h]
t_eq_FL_solar=1.190938e+03[h]
t_eq_FL_total=h_day*365
t_eq_FL_fossil=t_eq_FL_total-t_eq_FL_solar {equivalent fossil energy at full load is also multiplied by 1MW regardless of
the boiler capacity because it is full electric load}
solar_share=t_eq_FL_solar/t_eq_FL_total

"Power Block"
UA_cool=UA_heatRecovery+UA_cond {for rough calculations this should be permitted: UAs are additive}
call capex1_powerblock(W_dot_D,m_dot_D,w_T_D,w_net_D,UA_h_D,UA_reg_D,UA_cool,Q_dot_am_D:C_powerblock1)

"Rest of Plant"
A_ratio=1.1
A_total=A_field*A_ratio {spare some area for the plant; however, most of the costs are calculated with the total aperture
area}
Q_dot_D_fossil=Q_dot_col_D*0.85+Q_dot_add_D  {Assuming that there will always be at least 15% of solar...}
{This is Q_dot fossil, not fuel, meaning we still have to use the boiler efficiency to calculate the fuel energy}

c_pb_hyp=2500[$/kW]
C_powerblock2=c_pb_hyp*W_dot_D

c_sf=170[$/m^2] {SAM cost update article}
c_shtf=70[$/m^2] {SAM cost update article}
c_boiler=150[$/kW] {see Assumptions_comments, https://iea-etsap.org/E-TechDS/PDF/I01-ind_boilers-GS-AD-gct.pdf
and the fact that the boiler will not be for water but for therminol}
c_sbop= 120[$/kW] {SAM cost update article}
c_scont=0.25

call capex1_solarfield&plant(A_aT,A_total,W_dot_D,Q_dot_D_fossil,eta_cycle_D,c_sf,c_shtf,c_boiler,c_sbop,c_scont,
C_powerblock1:C_BEC,C_TPC)

"O&M"
c_sfix=72.6[$/kW]
c_ng=4[$/MMBtu]
eta_boiler=0.8

call o&m_costs(W_dot_D,Q_dot_D_fossil,eta_boiler,t_eq_FL_solar,t_eq_FL_fossil,t_eq_FL_total,c_ng,c_sfix:C_o&m_yr,
C_o&m_fixed,C_o&m_var,C_fuel)

"LCOE"
W_e_yr=W_dot_elec*t_eq_FL_total
r=0.075
degr=0.999
n_yr=25
ITC=0.26
CO2_avoided_yr=t_eq_FL_solar*Q_dot_D_fossil/eta_boiler*convert(kWh,MMBtu)*53.07[kg/MMBtu]*convert(kg,tonne)
I_CO2_avoided=CO2_avoided_yr*90[$/tonne]



I_cogen_avoided=t_eq_FL_total*Q_dot_cog_D/eta_boiler*convert(kWh,MMBtu)*c_ng

call  lcoe1(r,degr,n_yr,ITC,C_TPC,C_o&m_fixed,C_o&m_var,C_fuel,I_CO2_avoided,I_cogen_avoided,W_e_yr:LCOE,
LCOE_aCO2,lcoe_capex,lcoe_O&M)
```

Simulation Code Equations

```
"************************************SOLAR ANGLES PROCEDURE*****************************************************************"
Procedure solarangles(n,Alat,SolarTime:Ad,Ah,Az,cos_i,Ai)
B:=(360[deg]*(284+n)/365)
Ad:=23.45[deg]*sin(B) {work in degrees}
Ah:=(SolarTime-12[h])*15[deg/h]
Az:=arccos(cos(Ad)*cos(Alat)*cos(Ah)+sin(Ad)*sin(Alat))
{Reality: collectors start tracking at 10 degrees above the horizon till 10 degrees above the horizon}
{Assumption: collectors track all day long}
{Plane rotated about a horizontal north-south axis with east-west tracking}
cos_i:=sqrt((cos(Az))^2+(cos(Ad)*sin(Ah))^2)
Ai:=arccos(cos_i)

Ad2=Ad
Aalpha=arcsin(sin(Ad2)*sin(Alat)+cos(Ad2)*cos(Alat)*cos(Ah))
Aas=arcsin(cos(Ad2)*sin(Ah)/cos(Aalpha))
cos_i2=sqrt(1-(cos(Aalpha)*cos(Aas))^2)


End

"************************************PTC Optical Performance PROCEDURE*****************************************************"
Procedure qabs(DNI,cos_i,Ai,Az,N_PTC_SCA,L_PTC,SF_Avail,L_spacing,wdth_PTC:Q_dot_abs_i,eta_opt)
 "Incidence angle modifier: reflection and absorption losses"
"Depends on the collector, in this case LS-2 tested by Sandia"
K:=cos_i+0.000884[deg^-1]*Ai-0.00003077[deg^-2]*Ai^2 {Ai in degrees}
{Reviewed; IAM is was implemented following SAM}
IAM:=K/cos_i

"W_ap=5m for LS-2, L_spacing=15m for SEGS-VI"
F_RS:=L_spacing/wdth_PTC*cos(Az)/cos_i
If(F_RS>1) Then F_RS:=1
"foc: focal length, 5m; L_SCA=50m"
foc:=1.71[m]
{L_SCA:=49[m]}
L_SCA:=N_PTC_SCA*L_PTC
F_EL:=1-foc*tan(Ai)/L_SCA

"Shortcut for SEGS-VI as to field and HCE efficiencies"
eta_opt_peak=0.7133

Q_dot_abs_i:=DNI*cos_i*IAM*F_RS*F_EL*SF_Avail*eta_opt_peak
if(DNI<>0) Then
eta_opt:=Q_dot_abs_i/DNI
Else
eta_opt:=0
Endif

End

"****************************************** PROPERTIES PROCEDURES ******************************************"
Procedure htfproperties(T,P:rho_HTF,c_p_HTF,h_HTF,mu_HTF,k_HTF)
"T in C"

{rho_HTF:=-0.90797*T + 0.00078116*T^2 - 2.367e-6*T^3+1083.25 "kg/m3"
c_pHTF:=(0.002414*T + 5.9591e-6*T^2- 2.9879e-8*T^3 + 4.4172e-11*T^4+ 1.498)  "kJ/kgK"
k_HTF:=(-8.19477e-5*T - 1.92257e-7*T^2 + 2.5034e-11*T^3 - 7.2974e-15*T^4+ 0.137743)/1000 "kW/mK"
mu_HTF:=rho_HTF*(1e-6*exp(544.149/(T+114.43)-2.59578)) "Pa s"}

rho_HTF:=density(Therminol_VP1, T=T)
c_p_HTF:=specheat(Therminol_VP1, T=T)
k_HTF:=conductivity(Therminol_VP1, T=T)*convert(W,kW)
mu_HTF:=viscosity(Therminol_VP1, T=T)
h_HTF:=enthalpy(Therminol_VP1, T=T,P=P)
```

```
End

Procedure co2properties(T,P:rho_CO2,c_p_CO2,h_CO2,mu_CO2,k_CO2)

rho_CO2:=density(CarbonDioxide, T=T,P=P)
c_p_CO2:=specheat(CarbonDioxide, T=T,P=P)
k_CO2:=conductivity(CarbonDioxide, T=T,P=P)*convert(W,kW)
mu_CO2:=viscosity(CarbonDioxide, T=T,P=P)
h_CO2:=enthalpy(CarbonDioxide, T=T,P=P)

End

Procedure waterproperties(T,P:rho_W,c_p_W,h_W,mu_W,k_W)

rho_W:=density(Water, T=T,P=P)
c_p_W:=specheat(Water, T=T,P=P)
k_W:=conductivity(Water, T=T,P=P)*convert(W,kW)
mu_W:=viscosity(Water, T=T,P=P)
h_W:=enthalpy(Water, T=T,P=P)

End

"****************************************PTC Thermal Loss PROCEDURE*****************************************************"
Procedure qcol(DNI,L_PTC,A_a,D_ri,Wspd,Q_dot_abs_i,T_in1,T_am,m_dot_HTF,c_pHTF,mu_HTF,k_HTF,rho_HTF:
Q_dot_col1,Q_dot_col_i,Q_dot_col_m,T_out1,T_fm1,Q_dot_loss1,Q_dot_loss_i, Q_dot_loss_m,eta_th,DELTAP_1,
DELTAP_m,Q_dot_sol1)
"Converting T to K"
T_in1K:=converttemp('C','K',T_in1)
T_amK:=converttemp('C','K',T_am)
"Notice that this procedure calculates losses for one PTC, therefore, Q_dot_abs needs not to be per m2"
Q_dot_abs1:=Q_dot_abs_i*A_a


"Assuming dimensions are proportional:"
D_ro:=70/66*D_ri
D_ci:=109/66*D_ri
D_co:=115/66*D_ri
A_ro:=PI*D_ro*L_PTC
A_ri:=PI*D_ri*L_PTC
A_co:=PI*D_co*L_PTC
A_ci:=PI*D_ci*L_PTC

sigma:=5.67e-11[kW/m^2 K^4]
epsilon_c:=0.9
epsilon_r:=0.2
epsilon_r_p:=(1/epsilon_r+(1-epsilon_c)/epsilon_c*A_ro/A_ci)^(-1)

Re:=4*m_dot_HTF/(PI*D_ri*mu_HTF)
Pr:=mu_HTF*c_pHTF/k_HTF
"Gnielinski correlation- Assuming 5e6>Re>3000 and smooth pipe; see Incropera"
f:=(0.790*ln(Re)-1.64)^(-2)
vel:=m_dot_HTF/rho_HTF/(pi/4*D_ri^2)
DELTAP_1:=1/2*rho_HTF*vel^2*(f*L_PTC/D_ri)*convert(Pa,kPa)
DELTAP_m:=DELTAP_1/L_PTC
Nu:=(f/8)*(Re-1000)*Pr/(1+12.7*(f/8)^0.5*(Pr^(2/3)-1))
"Dittus-Boelter correlation, Re>1e4"
{Nu:=0.023*Re^0.8*Pr^0.4}
h_in:=Nu*k_HTF/D_ri

"Article by Naeeni and Yaghoubu (and then by Mullick and Nanda)"
{h_out:=0.01[kW/m^2 K]}
h_out:=4[kW/m^2-K]*(Wspd/1[m/s])^0.58*(D_co/1[m])^(-0.42)

K1:=A_co*epsilon_c*sigma*4*T_amK^3 + A_co*h_out
```

```
K2:=A_ro*epsilon_r_p*sigma/(1+4*T_amK^3*A_ro*epsilon_r_p*sigma/K1)
K3:=1/(1/(A_ri*h_in)+1/(2*m_dot_HTF*c_pHTF))

Q_dot_col1:=(Q_dot_abs1-K2*(T_in1K^4-T_amK^4))/(1+4*T_in1K^3*K2/K3)
Q_dot_col_i:=Q_dot_col1/A_a

T_out1K:=T_in1K+Q_dot_col1/(m_dot_HTF*c_pHTF)
T_out1:=converttemp('K','C',T_out1K)

T_fm1:=(T_in1+T_out1)/2

Q_dot_loss1:=Q_dot_abs1-Q_dot_col1
Q_dot_loss_i:=Q_dot_abs_i-Q_dot_col_i

Q_dot_col_m:=Q_dot_col1/L_PTC
Q_dot_loss_m:=Q_dot_loss1/L_PTC
eta_th:=Q_dot_col1/Q_dot_abs1
Q_dot_sol1:=DNI*A_a

End

"**************************************SOLAR FIELD PROCEDURE**************************************************"
{Old design: 285 PTCs, 15 loops of 19 PTCs, estimated DT per loop is 172: going from 178 to 350 C}
Procedure solarfield(DNI,DNI_D,N_col_loop,N_loops,L_PTC,A_a,D_ri,Wspd,Q_dot_abs_i,T_min_HTF,T_M_D,P_HTF,T_am,
LF_opt:T_M,Q_dot_col_field,DELTAP_loop,Q_dot_solar,eta_th_T,m_dot_HTF_T,V_dot_HTF,V_dot_HTF_T,W_dot_HTF)

"Minimum and maximum load factors - optical LF is usually higher than electrical because of PLR..."
"0.3 is taken as the optical LF limit so that below that it is not worth calculating anything"
if(LF_opt<0.3) Then
T_M:=0; Q_dot_col_field:=0; DELTAP_loop:=0; Q_dot_solar:=0; eta_th_T:=0; m_dot_HTF_T:=0; V_dot_HTF:=0;
V_dot_HTF_T:=0; W_dot_HTF:=0; Goto 4
Endif
if(LF_opt>1.25) Then
T_M:=0; Q_dot_col_field:=0; DELTAP_loop:=0; Q_dot_solar:=0; eta_th_T:=0; m_dot_HTF_T:=0; V_dot_HTF:=0;
V_dot_HTF_T:=0; W_dot_HTF:=0;
Goto 4
Endif

i:=0
Q_dot_col_loop:=0[kW]
DELTAP_loop:=0[kPa]
T_in1:=T_min_HTF

Q_dot_sol_loop:=0[kW]

"HTF mass flow rate estimation (iterate with thermal efficiencies of collectors until reaching  T_M_D)"
"Approximately P_HTF remains constant"
h_min_HTF:=enthalpy(Therminol_VP1, T=T_min_HTF,P=P_HTF)
h_M_D:=enthalpy(Therminol_VP1, T=T_M_D,P=P_HTF)
DELTAh_HTF:=h_M_D-h_min_HTF
Q_dot_abs_iD:=0.68*DNI_D {Assuming eta_opt_D is 0.7}
eta_th_T:=0.88 {Assumed too}
2:m_dot_HTF:=1/DELTAh_HTF*LF_opt*Q_dot_abs_iD*N_col_loop*A_a*eta_th_T {m_dot_HTF is proportional to Qabs to
achieve always the same temperature}
"We would iterate with the actual eta_th"

Repeat

i:=i+1
T_fm_avg:=T_in1+2.5[C] "Assuming this 5 C T increase per collector: half is 2.5"
Call htfproperties(T_fm_avg,P_HTF : rho_HTF,c_pHTF,h_HTF,mu_HTF,k_HTF)
Call qcol(DNI,L_PTC,A_a,D_ri,Wspd,Q_dot_abs_i,T_in1,T_am,m_dot_HTF,c_pHTF,mu_HTF,k_HTF,rho_HTF:Q_dot_col1,
Q_dot_col_i,Q_dot_col_m,T_out1,T_fm1,Q_dot_loss1,Q_dot_loss_i, Q_dot_loss_m,eta_th,DELTAP_1,DELTAP_m,
Q_dot_sol1)
```

```
Q_dot_col_loop:=Q_dot_col_loop+Q_dot_col1
DELTAP_loop:=DELTAP_loop+DELTAP_1
T_in1:=T_out1
Q_dot_sol_loop:=Q_dot_sol_loop+Q_dot_sol1

Until (i>=N_col_loop-1)

T_M:=T_out1
Q_dot_col_field:=N_loops*Q_dot_col_loop
Q_dot_solar:=N_loops*Q_dot_sol_loop

eta_th_T:=Q_dot_col_field/(Q_dot_abs_i*N_col_loop*A_a*N_loops)
eta_PTC:=Q_dot_col_field/Q_dot_solar

{if(abs(T_M-T_M_D)>=1) Then Goto 2} "It takes too much calculation time"

T_fm_avgD:=(T_min_HTF+T_M_D)/2
Call htfproperties(T_fm_avgD,P_HTF:rho_HTF,c_pHTF,h_HTF,mu_HTF,k_HTF)
V_dot_HTF:=m_dot_HTF/rho_HTF
V_dot_HTF_T:=N_loops*V_dot_HTF
m_dot_HTF_T:=N_loops*m_dot_HTF
"HTF pressure drop in evaporator included through the 1.08 multiplier"
4:W_dot_HTF:=DELTAP_loop*V_dot_HTF_T*1.08/0.8 {overestimating because the V_dot will be lower in the pump, since it is
at T_min_HTF}


End


"********************************* PUMP INLET  PROCEDURE ************************************************"

Procedure Pump_Inlet(T_cond:T_3,P_3)
T_crit:=T_crit(CarbonDioxide)
P_crit:=P_crit(CarbonDioxide)
s_crit:=Entropy(CarbonDioxide,T=T_crit,P=P_crit)
If(T_cond<T_crit) Then
    P_3=p_sat(CarbonDioxide,T=T_cond)
    T_3=T_cond-1[C]
Else
    P_3=pressure(CarbonDioxide,T=T_cond,s=s_crit)
    "We just want that the lower T heat transfer region is low enough but high enough at the specified T_cond"
    T_3=T_cond-1[C]
EndIf
End

"*********************************SOLAR FIELD DESIGN PROCEDURE*******************************"
procedure SolarFieldDesign(DNI_D,Q_dot_col_D,eta_PTC_D,L_PTC,A_a,D_ri,L_spacing,C_r0,N_loops0,epsilon_ev_0,
T_6_D,T_1_D,m_dot_D,q_col_D,P_HTF:N_col_D,A_field,N_col_loop,T_M_D,T_min_HTF,m_dot_HTF_D,V_dot_HTF_DT,
vel_HTF,UA_ev_D,W_dot_HTF_ideal,C_r,N_loops,epsilon_ev_D)

"First approach"
epsilon_ev_D=epsilon_ev_0
N_loops=N_loops0
C_r=C_r0

"Evaporator predesign"
C_CO2:=Q_dot_col_D/(T_1_D-T_6_D)
Q_max:=Q_dot_col_D/epsilon_ev_D

"CO2 as minimum heat capacity"
C_HTF:=C_CO2/C_r
C_min:=C_CO2
```

```
{"HTF as minimum heat capacity"
C_HTF:=C_CO2*C_r
C_min:=C_HTF}

"Same for both options:"
{T_M_D:=T_6_D+Q_max/C_min
T_min_HTF:=T_M_D-Q_dot_col_D/C_HTF}

"Now: fixing HTF temperatures and assuming it is going to have the minimum temperature difference"
T_M_D:=393[C]
T_min_HTF:=293[C]
C_HTF=Q_dot_col_D/(T_M_D-T_min_HTF)
C_r=C_CO2/C_HTF
epsilon_ev_D=Q_dot_col_D/(C_min*(T_M_D-T_6_D))
NTU:=1/(C_r-1)*ln((epsilon_ev_D-1)/(epsilon_ev_D*C_r-1))
UA_ev_D:=NTU*C_min

"Mass flow of HTF and number of loops"

T_HTF_avg:=(T_min_HTF+T_M_D)/2
call htfproperties(T_HTF_avg,P_HTF:rho_HTF,c_p_HTF,h_HTF,mu_HTF,k_HTF)
m_dot_HTF_DT:=C_HTF/c_p_HTF
11:m_dot_HTF_D:=m_dot_HTF_DT/N_loops
V_dot_HTF_DT:=m_dot_HTF_DT/rho_HTF
V_dot_HTF_D:=V_dot_HTF_DT/N_loops
vel_HTF:=V_dot_HTF_D/(pi/4*D_ri^2)

if (vel_HTF<2[m/s]) Then
N_loops=N_loops-1
Goto 11
Endif

if (vel_HTF>4[m/s]) Then
N_loops=N_loops+1
Goto 11
Endif

"Solar Field design"
Q_dot_1:=DNI_D*A_a*eta_PTC_D
N_col_D:=Q_dot_col_D/Q_dot_1
A_field:=L_PTC*L_spacing*N_col_D
N_col_loop:=round(N_col_D/N_loops)


"Pressure drop"

Re:=4*m_dot_HTF_D/(pi*D_ri*mu_HTF)
f:=(0.79*ln(Re)-1.64)^(-2)
DP_PTC:=f*L_PTC/D_ri*0.5*rho_HTF*vel_HTF^2*convert(Pa,kPa)
DP_field:=N_col_loop*DP_PTC
DP_evap:=0.08*P_HTF*convert(MPa,kPa)
W_dot_HTF_ideal:=(DP_field+DP_evap)*V_dot_HTF_DT


End


"****************************************HEAT RECOVERY AND REJECTION***************"

procedure heat_out(T_WB,DELTAT_w11,DELTAT_w12,T[1..6],P[1..6],h[1..6],T_cog[1..2],h_cog[1..2],m_dot:Q_dot_cog,
Q_dot_am,Q_dot_cool,Q_dot_hR,V_dot_w1,C_w1,eta_heatRecovery,DELTAT_range,T_w1[1..2],T_w2[1..3],h_g,T_h2_out)

if(m_dot=0) Then
```

```
Q_dot_cog=0;Q_dot_am=0;Q_dot_cool=0;Q_dot_hR=0;V_dot_w1=0;C_w1=0;eta_heatRecovery=0;DELTAT_range=0;
T_w1[1..2]=[0,0];T_w2[1..3]=[0,0,0];h_g=0;T_h2_out=0
Goto 12

Endif

q_cog=h_cog[1]-h_cog[2]
q_cool=h_cog[1]-h[3]
Q_dot_cool=m_dot*q_cool

"Critical point protection"
T_crit:=T_crit(CarbonDioxide)
P_crit:=P_crit(CarbonDioxide)
s_crit:=Entropy(CarbonDioxide,T=T_crit,P=P_crit)
If(P[3]<P_crit) Then
    h_g=enthalpy(CarbonDioxide,P=P[3],x=1)
    T_h2_out:=temperature(CarbonDioxide,P=P[3],x=1)
Else
    h_g=enthalpy(CarbonDioxide,s=s_crit,P=P[3])
    T_h2_out:=temperature(CarbonDioxide,P=P[3],s=s_crit)
EndIf

T_w1[1]=T_WB+DELTAT_w11 {in=1, out =2, cog=3}
T_w1[2]=T_w1[1]+DELTAT_w12

T_w2[1]=T_w1[2]
T_w2[3]=60[C]
T_w2[2]=80[C]

c_pw=4.18[kJ/kg-C]
rho_w=1000[kg/m3]

m_dot_w1=m_dot*(h_g-h[3])/(c_pw*(T_w1[2]-T_w1[1]))
C_w1=m_dot_w1*c_pw
V_dot_w1=m_dot_w1/rho_w
m_dot_w2a=m_dot*(h_cog[1]-h_g)/(c_pw*(T_w2[2]-T_w2[1]))
m_dot_w2b=m_dot*(h_cog[1]-h_cog[2])/(c_pw*(T_w2[2]-T_w2[3]))
m_dot_w2=min(m_dot_w2a,m_dot_w2b)
V_dot_w2=m_dot_w2/rho_w

Q_dot_cog:=m_dot_w2*c_pw*(T_w2[2]-T_w2[3])
Q_dot_hR:=m_dot_w2*c_pw*(T_w2[2]-T_w2[1])
Q_dot_am:=Q_dot_cool-Q_dot_cog

eta_heatRecovery=Q_dot_cog/m_dot/q_cog

x_w2=m_dot_w2/m_dot_w1
T_tower_in=(x_w2*T_w2[3]+(1-x_w2)*T_w1[2])
DELTAT_range=T_tower_in-T_w1[1]

12:End


"*******************************CYCLE PROCEDURE*************************************************"
Procedure cyclebase(T_max,P_max,T_cond,T_0,P_0:w_net,q_col,q_out,q_cog,eta_cycle,w_T,q_reg,T[1..6],P[1..6],h[1..6],
s[1..6],T_cog[1..2],h_cog[1..2])

"Isentropic efficiencies"
eta_T:=0.9
eta_P:=0.8

"Cycle"
P_1:=P_max
T_1:=T_max
```

```
h_1:=enthalpy(CarbonDioxide,T=T_1,P=P_1)
s_1:=entropy(CarbonDioxide,T=T_1,P=P_1)

Call Pump_Inlet(T_cond:T_3,P_3)
h_3:=enthalpy(CarbonDioxide,T=T_3,P=P_3)
s_3:=entropy(CarbonDioxide,T=T_3,P=P_3)

Dp_cond:=0.02 "% Pressure loss in the condenser+regenerator"
P_2:=P_3*(1+Dp_cond)
h_2s:=enthalpy(CarbonDioxide,s=s_1,P=P_2)
w_T:=eta_T*(h_1-h_2s)
h_2:=h_1-w_T
T_2:=temperature(CarbonDioxide,P=P_2,h=h_2)
s_2:=entropy(CarbonDioxide,T=T_2,h=h_2)

Dp_evap:=0.01 "% Pressure loss in the evaporator+regenerator"
P_4:=P_1*(1+Dp_evap)
h_4s:=enthalpy(CarbonDioxide,s=s_3,P=P_4)
w_P:=(h_4s-h_3)/eta_P
h_4:=h_3+w_P
T_4:=temperature(CarbonDioxide,P=P_4,h=h_4)
s_4:=entropy(CarbonDioxide,T=T_4,h=h_4)

"Regeneration"
P_5:=P_2*(1-Dp_cond/2)
T_5:=110[C] {Because we are cogenerating and we want to stop T_5 from decreasing more}
h_5:=enthalpy(CarbonDioxide,P=P_5,T=T_5)
"Other way of getting T_5 and h_5:"
{epsilon_reg:=0.9
h_5opt=enthalpy(CarbonDioxide,P=P_5,T=T_4)
h_5=h_2-epsilon_reg*(h_2-h_5opt)
T_5=temperature(CarbonDioxide,P=P_5,h=h_5)}

h_6:=h_2-h_5+h_4

s_5:=entropy(CarbonDioxide,P=P_5,T=T_5)
P_6=P_4*(1+Dp_evap/2)
T_6:=temperature(CarbonDioxide,P=P_6,h=h_6)
s_6:=entropy(CarbonDioxide,P=P_6,h=h_6)

"Heat exchanging devices"
q_col:=h_1-h_6
q_out:=h_5-h_3
q_reg:=h_2-h_5

"Power devices"
w_net=w_T-w_P

"Note: once you know m_dot, you can insert a goto and recalculate eta_T and eta_P as well as the heat exchangers
performance"

"Electrical - power block efficiency"


"Cogeneration heat"
T_cog_max:=T_5
T_cog_min:=T_cond+35[C]
P_cog1:=P_3
P_cog2:=P_3
h_cog1:=h_5
h_cog2:=enthalpy(CarbonDioxide,T=T_cog_min,P=P_cog2)
s_cog1:=entropy(CarbonDioxide,T=T_cog_max,P=P_cog1)
s_cog2:=entropy(CarbonDioxide,T=T_cog_min,P=P_cog2)
```

```
q_cog:=h_cog1-h_cog2
q_cond:=q_out-q_cog
q_ratio:=q_cond/q_cog
q_ratio2:=q_cond/(q_cog+q_reg)

"Efficiencies"

eta_cycle:=w_net/q_col
eta_cycle2:=1-q_out/q_col

"Exergy"
{J_standard= 0.9515 [kW/m2]
X_dot_irr=J_standard*Aperture*total*0.5
psi_max=h_1-h_0-T_0K*(s_1-s_0)
h_0=enthalpy(CarbonDioxide,T=T_0,P=P_0)
s_0=entropy(CarbonDioxide,T=T_0,P=P_0)
X_dot_max=psi_max*m_dot}

"Second law efficiency"

{eta_IIa=W_dot_net/X_dot_irr
eta_IIb=W_dot_net/X_dot_max}
T_standard:=5273[K]
T_0K:=converttemp(C,K,T_0)
T_condK:=converttemp(C,K,T_cond)
T_maxK:=converttemp(C,K,T_max)
eta_Carnot1:=1-T_condK/T_standard
eta_Carnot2:=1-T_condK/T_maxK
eta_IIc1:=eta_cycle/eta_Carnot1
eta_IIc2:=eta_cycle/eta_Carnot2
T_sun:=5778[K]
{eta_Petela=1-4/3*T_0K/T_sun+1/3*(T_0K/T_sun)^4
eta_IId=eta_plant/eta_Petela
eta_ChambadalNovikov=1-(T_0K/T_sun)^0.5
eta_IIe=eta_plant/eta_ChambadalNovikov}

"Vectors for graphic output"
T[1]=T_1
T[2]=T_2
T[3]=T_3
T[4]=T_4
T[5]=T_5
T[6]=T_6
T_cog[1]=T_cog_max
T_cog[2]=T_cog_min
s[1]=s_1
s[2]=s_2
s[3]=s_3
s[4]=s_4
s[5]=s_5
s[6]=s_6
s_cog[1]=s_cog1
s_cog[2]=s_cog2
h[1]=h_1
h[2]=h_2
h[3]=h_3
h[4]=h_4
h[5]=h_5
h[6]=h_6
h_cog[1]=h_cog1
h_cog[2]=h_cog2
P[1]=P_1
P[2]=P_2
P[3]=P_3
```

```
P[4]=P_4
P[5]=P_5
P[6]=P_6
P_cog[1]=P_cog1
P_cog[2]=P_cog2


{T_sun:=5778[K]
eta_Petela=1-4/3*T_0K/T_sun+1/3*(T_0K/T_sun)^4
eta_IId=eta_plant/eta_Petela
eta_ChambadalNovikov=1-(T_0K/T_sun)^0.5
eta_IIe=eta_plant/eta_ChambadalNovikov}

3:End

"******************* OUTPUTS and efficiencies procedure *********************"
Procedure outputs(W_dot_D,Q_dot_solar,W_dot_net,Q_dot_cog,Q_dot_am,W_dot_HTF,pwr_cool,eta_par0,eta_gen,T_WB,
T_cond:LF_ele,W_dot_elec,eta_sol_electric,eta_sol_cogen)

W_dot_cool=pwr_cool*Q_dot_am*convert(kW,MW)
eta_parasitics_other=eta_par0 {If compressor is not turbine driven it requires as well drive motor efficiency of 95%}
W_dot_elec=W_dot_net*eta_gen*eta_parasitics_other-W_dot_cool-W_dot_HTF

LF_ele:=W_dot_elec/W_dot_D

"Minimum and maximum load factors: if electrical energy is too low, the plant is switched off"
if(LF_ele<0.5) OR (LF_ele>1.25) OR (T_cond>=30) {OR (T_WB>=25)} Then
W_dot_elec:=0; eta_sol_electric:=0; eta_sol_cogen:=0; m_dot:=0
Goto 5
Endif

eta_sol_electric=W_dot_elec/Q_dot_solar
eta_sol_cogen=(W_dot_elec+Q_dot_cog)/Q_dot_solar

5:End

"************************************HEAT REJECTION TEMPERATURES******************"

procedure Dtemp(T_WB:DELTAT_cond,DELTAT_w11,DELTAT_w12)

if(T_WB<=22) Then
DELTAT_cond=7.5[C]
DELTAT_w11=1.75[C]
DELTAT_w12=1.5[C]
Endif

if(T_WB>22) AND (T_WB<=25) Then
DELTAT_cond=5[C]
DELTAT_w11=1.75[C]
DELTAT_w12=1.5[C]
Endif

if(T_WB>=25) Then
DELTAT_cond=4[C]
DELTAT_w11=1.75[C]
DELTAT_w12=1.5[C]
Endif

End


"*****************************COND*********************************************"

{procedure tcond(T_WB:T_cond)
```

```
if (T_WB<23) Then T_cond=T_WB+7.5[C]
if (T_WB>=23) AND (T_WB<25) Then T_cond=T_WB+5[C]
if (T_WB>=25) Then T_cond=T_WB+7.5[C]

End}
```

```
"*********************MAIN PROGRAM**********************************************"
"Variables coming from Matlab:"
nd=124
SolarTime=12[h]
DNI=0.78[kW/m^2]
T_0=23.3[C]
RH=0.59
BarP=0.101325[MPa]
Wspd=4.5[m/s]

"*********Main parameters: Cycle**************************"
T_max=370[C]
P_max=35[MPa]
P_0=BarP
{T_0 defined above}
{T_WB=wetbulb(AirH2O,T=T_0,R=RH,P=BarP)}
T_WB=1[C]*(T_0/1[C]*pi/180*arctan(0.151977*(RH*100+8.313659)^0.5)+pi/180*arctan(T_0/1[C]+RH*100)-pi/180*arctan(RH*
100+1.676331)+0.00391838*(RH*100)^(3/2)*pi/180*arctan(0.023101*RH*100)-4.686035)

call Dtemp(T_WB:DELTAT_cond,DELTAT_w11,DELTAT_w12)
{T_cond=T_WB+7.5[C] "Assuming cooling tower, remember that there is a cooling tower fan..."}
{call tcond(T_WB:T_cond)}
T_cond=T_WB+DELTAT_cond



"Design CYCLE"
T_0_D=23.3[C]
T_cond_D=27[C]
call cyclebase(T_max,P_max,T_cond_D,T_0_D,P_0:w_net_D,q_col_D,q_out_D,q_cog_D,eta_cycle_D,w_T_D,q_reg_D, , , , ,
,T_6_D, , , , , , , , , , , , , , , , , , , , , , ) {For each 6-element vector you have to insert 6 spaces to represent the 6 output
elements of the procedure}

"Mass flow rate and sizing"
W_dot_D=1000[kW]
eta_ev_D=0.97 "You need to insert the evaporator dynamics here... for now let it be 0.97; parasitics and electrical conversion
would be 0.91"
eta_parasitics_D=0.91 {estimate for design purposes}
Q_dot_col_D=W_dot_D/eta_cycle_D/eta_ev_D/eta_parasitics_D
m_dot_D=Q_dot_col_D/q_col_D
W_dot_net_D=m_dot_D*w_net_D
Q_dot_reg_D=m_dot_D*q_reg_D


"Solar Field Design input"
DNI_D=0.78[kW/m^2]
```

```
N_loops0=4
eta_PTC_D=0.6
L_PTC=7.8[m]
A_a=39[m^2] "Aperture area"
D_ri=66e-3[m]
wdth_PTC=5[m] {*(D_ri/66e-3[m])} {In case you also want to reduce the solar field size, decrease L_spacing too (it should go
with PTC size)}
L_spacing=10[m]
C_r0=0.25
epsilon_ev_0=0.9

"Solar field parameters"
P_HTF=11[bar]*convert(bar,MPa)
{T_6_D=97.22[C]}
{T_6_D=T[6]} {It comes from running the cycle design code}
T_1_D=T_max

call SolarFieldDesign(DNI_D,Q_dot_col_D,eta_PTC_D,L_PTC,A_a,D_ri,L_spacing,C_r0,N_loops0,epsilon_ev_0,T_6_D,
T_1_D,m_dot_D,q_col_D,P_HTF:N_col_D,A_field,N_col_loop,T_M_D,T_min_HTF,m_dot_HTF_D,V_dot_HTF_DT,vel_HTF,
UA_ev_D,W_dot_HTF_idealD,C_r,N_loops,epsilon_ev_D)


"Other IMPORTANT variables:"
Alat=30[deg] {not needed but for the hours}
SF_Avail=1
N_SCA_loop=2 {see configuration of the field}
N_PTC_SCA=N_col_loop/N_SCA_loop
A_aT=N_col_loop*N_loops*A_a {N_col_loop is an integer, unlike N_col_D}

"SOLAR FIELD SIMULATION"
{T_am=27[C]}
T_am=T_0

Call solarangles(nd,Alat,SolarTime:Ad,Ah,Az,cos_i,Ai)
Call qabs(DNI,cos_i,Ai,Az,N_PTC_SCA,L_PTC,SF_Avail,L_spacing,wdth_PTC:Q_dot_abs_i,eta_opt)

LF_opt=DNI*eta_opt/(DNI_D*0.6915)

Call solarfield(DNI,DNI_D,N_col_loop,N_loops,L_PTC,A_a,D_ri,Wspd,Q_dot_abs_i,T_min_HTF,T_M_D,P_HTF,T_am,
LF_opt:T_M,Q_dot_col_field,DELTAP_loop,Q_dot_solar,eta_th_T,m_dot_HTF_T,V_dot_HTF,V_dot_HTF_T,
W_dot_HTF_ideal)
Q_dot_solar2=DNI_D*A_aT

"CYCLE SIMULATION"
call cyclebase(T_max,P_max,T_cond,T_0,P_0:w_net,q_col,q_out,q_cog,eta_cycle,w_T,q_reg,T[1..6],P[1..6],h[1..6],s[1..6],
T_cog[1..2],h_cog[1..2])

"OUTPUTS AND EFFICIENCIES"
eta_ev=eta_ev_D "Insert evaporator dynamics"
Q_dot_in=Q_dot_col_field*eta_ev

m_dot=Q_dot_in/q_col
W_dot_net=m_dot*w_net
Q_dot_reg=m_dot*q_reg

"Cycle cooling"
call heat_out(T_WB,DELTAT_w11,DELTAT_w12,T[1..6],P[1..6],h[1..6],T_cog[1..2],h_cog[1..2],m_dot:Q_dot_cog,Q_dot_am,
Q_dot_cool,Q_dot_hR,V_dot_w1,C_w1,eta_heatRecovery,DELTAT_range,T_w1[1..2],T_w2[1..3],h_g,T_h2_out)


W_dot_HTF=W_dot_HTF_ideal/0.6
pwr_cool=25[kW/MW]
eta_par0=0.95
eta_gen=0.95 {generator + frequency conversion}


call outputs(W_dot_D,Q_dot_solar,W_dot_net,Q_dot_cog,Q_dot_am,W_dot_HTF,pwr_cool,eta_par0,eta_gen,T_WB,T_cond:
LF_ele,W_dot_elec,eta_sol_electric,eta_sol_cogen)

"ECONOMICS"

{Call income(W_dot_elec,Q_dot_cog,t_eq_FL:I_ele,I_ng,I_tot_gross,O&M)}
```

APPENDIX B

MAIN CODES DEVELOPED IN MATLAB

TMY3 Data Processing Code

```
% TMY3 data processing
clear
clc
close all

locations=readtable('Locations.xlsx');
loc=1;
filepath=char(locations.filepath(loc));
CZ=char(locations.ClimateZone(loc));
city=char(locations.City(loc));

TYA=readtable(filepath,'FileType','text');
latitude=locations.latitude(loc); % degrees
La=latitude*pi/180;
longitude=-(locations.longitude(loc)); % degrees
Lo=longitude*pi/180;
HourDifference=locations.TimeDifference(loc); % number of hours from GMT or UTC
(out of DST season)
StMeridian=-HourDifference*15; % 15 degrees/hour; angle from Greenwich
n=12;  % number of variables to study
% Last index columns: day of the year, solar time, GHI, DNI, DHI,  cosine of
angle of
% incidence (zenith angle when horizontal surface), DNIp (projected),
% dry-bulb T, wet-bulb T, relative hum., barometric pressure and wind speed
Beta=0*pi/180; % surface tilt angle
Gamma=0*pi/180; % surface azimuth angle

% Solar radiation data array
% Indexes: month (1-12), day of the month (1-31), hour (1:24)
SRD=cell(12,1);
SRD_s=cell(12,1);

mm=month(TYA.Date_MM_DD_YYYY_);
dd=day(TYA.Date_MM_DD_YYYY_);
% hh=hour(TYA.Time_HH_MM_);
nh=height(TYA);
hh=rem(1:1:nh,24)';


SolarT=zeros(nh,1);
w=zeros(nh,1);
d=zeros(nh,1);
mo_days=zeros(12,1);
WetBulb=zeros(nh,1);
cos_in=zeros(nh,1);
cos_in2=zeros(nh,1);
```

```
% Year variables initializing:
check=zeros(24,365);
STime=zeros(24,365);
GHI=zeros(24,365);
DNI=zeros(24,365);
DNIp=zeros(24,365);
DNIp2=zeros(24,365);
DHI=zeros(24,365);
n_check=0;
sumcheck=0;

T_DB=zeros(24,365);
T_WB=zeros(24,365);
RH=zeros(24,365);
BarP=zeros(24,365);
Wspd=zeros(24,365);


for i=[1 3 5 7 8 10 12]
    SRD{i}=zeros(31,24,n);
    SRD_s{i}=zeros(31*24,n);
    mo_days(i)=31;
end
for i=[4 6 9 11]
    SRD{i}=zeros(30,24,n);
    SRD_s{i}=zeros(30*24,n);
    mo_days(i)=30;
end
SRD{2}=zeros(28,24,n);
SRD_s{2}=zeros(28*24,n);
mo_days(2)=28;

avg_mo_days=mean(mo_days);

SRD{1}(1,[1 2],1)=1;
E=zeros(365,1);

for i=1:1:nh
    % Better use 24 than 0 for midnight
    if hh(i)==0
        hh(i)=24;
    end
    % Counting the days of the year:
    if i~=1
        if dd(i)==dd(i-1)
            SRD{mm(i)}(dd(i),hh(i),1)=SRD{mm(i-1)}(dd(i-1),hh(i-1),1);
            % If we didn't use 24 for midnight we would
            % add 1 to the hour index because indexes cannot be zero
        else
            SRD{mm(i)}(dd(i),hh(i),1)=SRD{mm(i-1)}(dd(i-1),hh(i-1),1)+1;
        end
    end
    SRD_s{mm(i)}((dd(i)-1)*24+hh(i),1)=SRD{mm(i)}(dd(i),hh(i),1);
    % Equation of time:
    dayofyear=SRD{mm(i)}(dd(i),hh(i),1);
```

```
    B=2*pi/365*(dayofyear-1);
    E(dayofyear)=229.18*(0.000075+0.001868*cos(B)-0.032077*sin(B)-
0.014615*cos(2*B)-0.04089*sin(2*B));
    SolarT(i)=hh(i)-0.5+(StMeridian-longitude)/15+E(dayofyear)/60;
    STime(i)=SolarT(i);
    % Variables to study
    SRD{mm(i)}(dd(i),hh(i),2)=SolarT(i);
    SRD_s{mm(i)}((dd(i)-1)*24+hh(i),2)=SolarT(i);
    % -0.5 because  the definition says: amount of solar radiation received
    % during the 60-minute period ending at the timestamp
    SRD{mm(i)}(dd(i),hh(i),3)=TYA.GHI_W_m_2_(i);
    SRD{mm(i)}(dd(i),hh(i),4)=TYA.DNI_W_m_2_(i);
    SRD{mm(i)}(dd(i),hh(i),5)=TYA.DHI_W_m_2_(i);
    SRD_s{mm(i)}((dd(i)-1)*24+hh(i),3)=TYA.GHI_W_m_2_(i);
    SRD_s{mm(i)}((dd(i)-1)*24+hh(i),4)=TYA.DNI_W_m_2_(i);
    SRD_s{mm(i)}((dd(i)-1)*24+hh(i),5)=TYA.DHI_W_m_2_(i);
    % hour angle
    w(i)=15*(SolarT(i)-12)*pi/180;
    % declination angle
    d(i)=23.45*sin(2*pi/365*(dayofyear+284))*pi/180;
%     d(i)=0.006918-0.399912*cos(B)+0.070257*sin(B)-
0.006758*cos(2*B)+0.000907*sin(2*B)-0.002697*cos(3*B)+0.00148*sin(2*B);
    % rest of the variables
    cos_in(i)=sin(d(i))*(sin(La)*cos(Beta)-
cos(La)*sin(Beta)*cos(Gamma))+cos(d(i))*cos(w(i))*(cos(La)*cos(Beta)+sin(La)*si
n(Beta))+cos(d(i))*sin(Beta)*sin(Gamma)*sin(w(i));
    zenith=acos(cos(d(i))*cos(La)*cos(w(i))+sin(d(i))*sin(La));
    cos_in2(i)=sqrt((cos(zenith))^2+(cos(d(i))*sin(w(i)))^2); % Tracking
surface angle cosine
    if cos_in(i)<=0
        cos_in(i)=0;
    end
    if cos_in2(i)<=0
        cos_in2(i)=0;
    end
    SRD{mm(i)}(dd(i),hh(i),6)=cos_in(i)*SRD{mm(i)}(dd(i),hh(i),4);
    SRD{mm(i)}(dd(i),hh(i),7)=cos_in(i);
    SRD_s{mm(i)}((dd(i)-1)*24+hh(i),6)=cos_in2(i)*SRD{mm(i)}(dd(i),hh(i),4);
    SRD_s{mm(i)}((dd(i)-1)*24+hh(i),7)=cos_in2(i);
    % Assume: TMY3 data comes without DST
    % Rest of meteorological variables:
    SRD{mm(i)}(dd(i),hh(i),8)=TYA.Dry_bulb_C_(i);
    SRD_s{mm(i)}((dd(i)-1)*24+hh(i),8)=TYA.Dry_bulb_C_(i);
%     SRD{mm(i)}(dd(i),hh(i)+1,9)=TYA.Dew_point_C_(i); % Instead of dew point:
wet bulb
    SRD{mm(i)}(dd(i),hh(i),10)=TYA.RHum___(i);
    SRD{mm(i)}(dd(i),hh(i),11)=TYA.Pressure_mbar_(i);
    SRD{mm(i)}(dd(i),hh(i),12)=TYA.Wspd_m_s_(i);
    SRD_s{mm(i)}((dd(i)-1)*24+hh(i),10)=TYA.RHum___(i);
    SRD_s{mm(i)}((dd(i)-1)*24+hh(i),11)=TYA.Pressure_mbar_(i);
    SRD_s{mm(i)}((dd(i)-1)*24+hh(i),12)=TYA.Wspd_m_s_(i);
    % Wet bulb temperature correlation for sea level pressure (University
    % of British Columbia):
    rh=TYA.RHum___(i);
```

```
    T=TYA.Dry_bulb_C_(i);
    SRD{mm(i)}(dd(i),hh(i),9)=T*atan(0.151977*(rh+8.313659)^(1/2))+atan(T+rh)-
atan(rh-1.676331)+0.00391838*(rh)^(3/2)*atan(0.023101*rh)-4.686035;
    SRD_s{mm(i)}((dd(i)-1)*24+hh(i),9)=SRD{mm(i)}(dd(i),hh(i),9);
    WetBulb(i)=SRD{mm(i)}(dd(i),hh(i),9);

    if TYA.GHI_W_m_2_(i) ~= 0 % you don't want to consider the values at night
for averaging each time step
        GHI(i)=SRD{mm(i)}(dd(i),hh(i),3);
        DNI(i)=SRD{mm(i)}(dd(i),hh(i),4);
        DNIp(i)=SRD{mm(i)}(dd(i),hh(i),6);
        DNIp2(i)=cos_in2(i)*SRD{mm(i)}(dd(i),hh(i),4);
        DHI(i)=SRD{mm(i)}(dd(i),hh(i),5);
%         % Checking the equation GHI=DHI+DNIcos(Z) (choose either absolute
%         error or relative error, not both, comment the unused one)
%         % Set Beta at zero
% %         check(i)=abs(SRD{mm(i)}(dd(i),hh(i)+1,3)-
(SRD{mm(i)}(dd(i),hh(i)+1,5)+SRD{mm(i)}(dd(i),hh(i)+1,7)))./SRD{mm(i)}(dd(i),hh
(i)+1,3)*100;
%         check(i)=abs(SRD{mm(i)}(dd(i),hh(i)+1,3)-
(SRD{mm(i)}(dd(i),hh(i)+1,5)+SRD{mm(i)}(dd(i),hh(i)+1,6)));
%         n_check=n_check+1;
%         sumcheck=sumcheck+check(i);
    end

    T_DB(i)=SRD{mm(i)}(dd(i),hh(i),8); % deg C
    T_WB(i)=SRD{mm(i)}(dd(i),hh(i),9); % deg C
    RH(i)=SRD{mm(i)}(dd(i),hh(i),10); % in %
    BarP(i)=SRD{mm(i)}(dd(i),hh(i),11)/1000; % Barometric pressure in Bar
    Wspd(i)=SRD{mm(i)}(dd(i),hh(i),12);  % m/s
end

% checkMax=max(check,[],'all');
% checkMean=sumcheck/n_check;
% checkMeanCol=mean(check,2);

% Averages
STime_yrAvg=mean(STime,2);
GHI_yrAvg=mean(GHI,2);
DNI_yrAvg=mean(DNI,2);
DNIp_yrAvg=mean(DNIp,2);
DNIp2_yrAvg=mean(DNIp2,2);
DHI_yrAvg=mean(DHI,2);

T_DB_yrAvg=mean(T_DB,2);
T_WB_yrAvg=mean(T_WB,2);
RH_yrAvg=mean(RH,2);
BarP_yrAvg=mean(BarP,2);
Wspd_yrAvg=mean(Wspd,2);

T_DB_totAvg=mean(T_DB_yrAvg);
T_DB_intAvg=mean(T_DB_yrAvg(9:17));
T_DB_noonAvg=T_DB_yrAvg(13);
T_WB_totAvg=mean(T_WB_yrAvg);
T_WB_intAvg=mean(T_WB_yrAvg(9:17));
```

```
T_WB_noonAvg=T_WB_yrAvg(13);
RH_totAvg=mean(RH_yrAvg);
RH_intAvg=mean(RH_yrAvg(9:17));
RH_noonAvg=RH_yrAvg(13);

% Medians
m=find(sum(DNIp2,1)==median(sum(DNIp2,1)));
if numel(m)>1
    m=m(1);
end
% OR with DNI peaks
% m=find(max(DNI,[],1)==median(max(DNI,[],1)));
% if numel(m)>1
%     m=m(1);
% end
% OR based on radiation at noon
% m=find(DNI(12,:)==median(DNI(12,:)));
% OR, with temperature at noon
% m=find(T_DB(12,:)==median(T_DB(12,:)));
% There are many days with the same temperature at noon
% And they are very different

day_n_yrm=m;
STime_yrm=STime(:,m);
GHI_yrm=GHI(:,m);
DNI_yrm=DNI(:,m);
DNIp_yrm=DNIp(:,m);
DNIp2_yrm=DNIp2(:,m);
DHI_yrm=DHI(:,m);

T_DB_yrm=T_DB(:,m);
T_WB_yrm=T_WB(:,m);
RH_yrm=RH(:,m);
BarP_yrm=BarP(:,m);
Wspd_yrm=Wspd(:,m);

T_WB_intm=median(T_WB(9:17,:),'all');
n_highT=sum(T_WB(9:17,:)>=25,'all');
T_DB_intm=median(T_DB(9:17,:),'all');
RH_intm=median(RH(9:17,:),'all');

% Average days for each month
SolarT_avg=zeros(12,24);
GHI_avg=zeros(12,24);
DNI_avg=zeros(12,24);
DHI_avg=zeros(12,24);
DNIp_avg=zeros(12,24);

T_DB_avg=zeros(12,24);
T_WB_avg=zeros(12,24);
RH_avg=zeros(12,24);
BarP_avg=zeros(12,24);
Wspd_avg=zeros(12,24);

% Median days for each month
% Based on peak radiation OR temperature
```

```
V=cell(12,1); % Contains scalars to determine the median day
for i=[1 3 5 7 8 10 12]
    V{i}=zeros(31,1);
end
for i=[4 6 9 11]
    V{i}=zeros(30,1);
end
V{2}=zeros(28,1);

% Median variables
SolarT_m=zeros(12,24);
GHI_m=zeros(12,24);
DNI_m=zeros(12,24);
DHI_m=zeros(12,24);
DNIp_m=zeros(12,24);

T_DB_m=zeros(12,24);
T_WB_m=zeros(12,24);
RH_m=zeros(12,24);
BarP_m=zeros(12,24);
Wspd_m=zeros(12,24);
day_n_m=zeros(12,1);


day_aux=0;
for  i=1:12
    for  j=1:24
        SolarT_avg(i,j)=mean(SRD{i}(:,j,2));
        GHI_avg(i,j)=mean(SRD{i}(:,j,3));
        DNI_avg(i,j)=mean(SRD{i}(:,j,4));
        DHI_avg(i,j)=mean(SRD{i}(:,j,5));
        DNIp_avg(i,j)=mean(SRD{i}(:,j,6));

        T_DB_avg(i,j)=mean(SRD{i}(:,j,8));
        T_WB_avg(i,j)=mean(SRD{i}(:,j,9));
        RH_avg(i,j)=mean(SRD{i}(:,j,10));
        BarP_avg(i,j)=mean(SRD{i}(:,j,11));
        Wspd_avg(i,j)=mean(SRD{i}(:,j,12));
    end
    for j=1:mo_days(i)
        V{i}(j)=sum(SRD{i}(j,:,4));
        % OR with DNI peak
%         V{i}(j)=max(SRD{i}(j,:,4));
        % OR with temperature:
%         V{i}(j)=max(SRD{i}(j,:,8));
    end
    m_aux=find(V{i} >= median(V{i}));
    V_aux=min(V{i}(m_aux));
    m=find(V{i} == V_aux);
    % m is the index of the minimum value greater than the median
    % this is also valid for those sets that don't contain their median
    if numel(m)>1
        m=m(1);
        % in case two days share the value of the median
```

```
    end
    if i~=1
       day_aux=day_aux+mo_days(i-1);
    end

    day_n_m(i)=day_aux+m;
    SolarT_m(i,:)=SRD{i}(m,:,2);
    GHI_m(i,:)=SRD{i}(m,:,3);
    DNI_m(i,:)=SRD{i}(m,:,4);
    DHI_m(i,:)=SRD{i}(m,:,5);
    DNIp_m(i,:)=SRD{i}(m,:,6);

    T_DB_m(i,:)=SRD{i}(m,:,8);
    T_WB_m(i,:)=SRD{i}(m,:,9);
    RH_m(i,:)=SRD{i}(m,:,10);
    BarP_m(i,:)=SRD{i}(m,:,11);
    Wspd_m(i,:)=SRD{i}(m,:,12);
end

% Graphics: (only the ones required for my research for now)

figure(3);
set(gcf, 'Position',  [100, 100, 650, 700])
for i=1:12
    subplot(4,3,i);
    plot(SolarT_avg(i,:),DNI_avg(i,:),'-s','DisplayName','DNI_{avg}');
    hold on
    plot(SolarT_m(i,:),DNI_m(i,:),'-*','DisplayName','DNI_{med}');
    scatter(SRD_s{i}(:,2),SRD_s{i}(:,4),1,'o','DisplayName','DNI_{scatt}');
    title(strcat('Month:  ',{' '},num2str(i)),'FontSize',8);
    xlabel('Solar Time (h)','FontSize',8);
    xticks(0:6:24);
    ylabel('W/m2','FontSize',8);
    axis([0 24 0  1000]);
    ax = gca;
    ax.FontSize = 8;
end
lgd=legend('Position',[0.5 0 0.05 0.05]);
lgd.NumColumns = 2; lgd.FontSize = 8;
saveas(3,'Monthly average and scatter DNI data.png')

%
% figure(5);
% for i=1:12
%     subplot(3,4,i);
%     plot(SolarT_avg(i,:),DNIp_avg(i,:),'DisplayName','DNI proj');
%     hold on
%     plot(SolarT_avg(i,:),DNIp_sin(i,:),'DisplayName','DNI proj sin');
%     xlabel('Solar time');
%     ylabel('W/m2');
%     lgd=legend;
%     lgd.Title.String=strcat('Month no:  ',num2str(i));
%     lgd.NumColumns = 1;
%     axis([0 23 0  1000]);
% end
```

```
figure(12);
% plot(STime_yrAvg,GHI_yrAvg,'DisplayName','GHI avg');
hold on
plot(STime_yrAvg,DNI_yrAvg,'-s','DisplayName','DNI avg');
plot(STime_yrm,DNI_yrm,'-*','DisplayName','DNI med');
% plot(STime_yrAvg,DNIp_yrAvg,'DisplayName','DNI proj avg');
% plot(STime_yrAvg,DNIp2_yrAvg,'DisplayName','DNI proj track avg');
% plot(STime_yrm,DNIp2_yrm,'DisplayName','DNI proj track med');
% plot(STime_yrAvg,DHI_yrAvg,'DisplayName','DHI avg');
% scatter(SolarT,TYA.GHI_W_m_2_,1,'DisplayName','GHI');
scatter(SolarT,TYA.DNI_W_m_2_,1,'o','DisplayName','DNI');
% scatter(SolarT,TYA.DHI_W_m_2_,1,'DisplayName','DHI');
% scatter(SolarT,TYA.DNI_W_m_2_.*cos_in,1,'DisplayName','DNIp');
% scatter(SolarT,TYA.DNI_W_m_2_,1.*cos_in2,'DisplayName','DNI proj track avg');
axis([0 24 0 1200]);
xlabel('Solar Time (h)');
xticks(0:3:24);
ylabel('kW/m^2');
lgd=legend;
lgd.Title.String=strcat(city,' CZ:',CZ);
title('Year average and scatter data');
saveas(12,'Year average and scatter data.png')

figure(15);
title('Year average and scatter data');
set(gcf, 'Position',  [100, 100, 1000, 900])

subplot(2,2,1);
hold on
% plot(STime_yrAvg,T_DB_yrAvg,'-^','DisplayName','T_{DB,avg}');
plot(STime_yrm,T_DB_yrm,'-*','DisplayName','T_{DB,med}');
% plot(STime_yrAvg,T_WB_yrAvg,'-d','DisplayName','T_{WB,avg}');
plot(STime_yrm,T_WB_yrm,'-s','DisplayName','T_{WB,med}');
scatter(SolarT,TYA.Dry_bulb_C_,1,'o','DisplayName','T_{DB}');
scatter(SolarT,WetBulb,1,'x','DisplayName','T_{WB}');
axis([0 24 -10  50]);
xlabel('Solar Time (h)');
xticks(0:6:24);
ylabel('C');
lgd=legend('location','best'); lgd.NumColumns = 2;
lgd.Title.String=strcat(city,' CZ:',CZ);

subplot(2,2,2);
hold on
plot(STime_yrAvg,RH_yrAvg,'-s','DisplayName','Rel. Hum. avg');
plot(STime_yrm,RH_yrm,'-*','DisplayName','Rel. Hum. med');
scatter(SolarT,TYA.RHum___,1,'o','DisplayName','Rel. Hum.');
axis([0 24 0  100]);
xlabel('Solar Time (h)');
xticks(0:6:24);
ylabel('RH%');
lgd=legend('location','best');
lgd.Title.String=strcat(city,' CZ:',CZ);
```

```
subplot(2,2,3);
hold on
plot(STime_yrAvg,BarP_yrAvg,'DisplayName','Barometric pressure avg');
scatter(SolarT,TYA.Pressure_mbar_./1000,1,'DisplayName','Barometric pressure');
axis([0 24 0.95  1.05]);
xlabel('Solar Time (h)');
xticks(0:6:24);
ylabel('Bar');
lgd=legend('location','best');
lgd.Title.String=strcat(city,' CZ:',CZ);

subplot(2,2,4);
hold on
plot(STime_yrAvg,Wspd_yrAvg,'-s','DisplayName','Wind speed avg');
plot(STime_yrm,Wspd_yrm,'-*','DisplayName','Wind speed med');
scatter(SolarT,TYA.Wspd_m_s_,1,'o','DisplayName','Wind speed');
axis([0 24 0  14]);
xlabel('Solar Time (h)');
xticks(0:6:24);
ylabel('m/s');
lgd=legend('location','best');
lgd.Title.String=strcat(city,' CZ:',CZ);

saveas(15,'Year average and scatter data rest.png')

figure(16);
set(gcf, 'Position',  [100, 100, 650, 700])
for i=1:12
    subplot(4,3,i);
%     plot(SolarT_avg(i,:),T_DB_avg(i,:),'DisplayName','T_{DB,avg}');
    hold on
    plot(SolarT_m(i,:),T_DB_m(i,:),'-s','DisplayName','T_{DB,med}');
%     plot(SolarT_avg(i,:),T_WB_avg(i,:),'DisplayName','T_{WB,avg}');
    plot(SolarT_m(i,:),T_WB_m(i,:),'-*','DisplayName','T_{WB,med}');
    scatter(SRD_s{i}(:,2),SRD_s{i}(:,8),1,'o','DisplayName','T_{DB,scatt}');
    scatter(SRD_s{i}(:,2),SRD_s{i}(:,9),1,'x','DisplayName','T_{WB,scatt}');
    title(strcat('Month:  ',{' '},num2str(i)),'FontSize',6);
    xlabel('Solar Time (h)','FontSize',8);
    xticks(0:6:24);
    ylabel('C','FontSize',8);
    axis([0 24 -10  50]);
    ax = gca;
    ax.FontSize = 8;
end
lgd=legend('Position',[0.5 0 0.05 0.05]); lgd.NumColumns = 2; lgd.FontSize = 8;
saveas(16,'Monthly average and scatter temperature data.png')


InputEES_yrMed=[STime_yrm DNI_yrm*1e-3 T_DB_yrm RH_yrm/100 BarP_yrm*0.1
Wspd_yrm];
InputEES_yrAvg=[STime_yrAvg DNI_yrAvg*1e-3 T_DB_yrAvg RH_yrAvg/100
BarP_yrAvg*0.1 Wspd_yrAvg];

nh=8; % Assuming 8 hours of operation, rows 10:17
niv=7;
```

```
InputEES_moMed=zeros(nh,niv,12);
InputEES_moAvg=zeros(nh,niv,12);
InputEES_AllMo=zeros(nh*12,niv);
aux=zeros(nh,1);
for i=1:12
    for j=1:nh
        aux(j)=day_n_m(i);
        if DNI_m(i,10+j-1)<=5
            DNI_m(i,10+j-1)=5;
        end
    end
    InputEES_moMed(:,:,i)=[aux SolarT_m(i,10:17)' DNI_m(i,10:17)'*1e-3
T_DB_m(i,10:17)' RH_m(i,10:17)'/100 BarP_m(i,10:17)'*0.1 Wspd_m(i,10:17)'];
    InputEES_moAvg(:,:,i)=[aux SolarT_avg(i,10:17)' DNI_avg(i,10:17)'*1e-3
T_DB_avg(i,10:17)' RH_avg(i,10:17)'/100 BarP_avg(i,10:17)'*0.1
Wspd_avg(i,10:17)'];
    InputEES_AllMo((i-1)*nh+1:i*nh,:)=InputEES_moMed(:,:,i);
end

% Bin data analysis
inc=1; % W/m2
Bin=round((0:inc:1250)');
BinH=zeros(size(Bin));

for i=1:numel(DNI)
    for j=1:numel(Bin)
        if  DNI(i)<=(Bin(j)+inc/2) && DNI(i)>(Bin(j)-inc/2)
            BinH(j)=BinH(j)+1;
        end
    end
end
Htot=sum(BinH);

figure(17);
plot(Bin,BinH);
title('Radiation Level Hours');
xlabel('W/m^2','FontSize',8);
ylabel('Number of hours in the year','FontSize',8);
axis([0 1000 0  30]);
ax = gca;
ax.FontSize = 8;
saveas(17,'Radiation Level Hours.png');

% % figure(18);
% % plot(Bin,BinH/Htot*100);
% % title('Radiation Level Hours Fraction (%)');
% % xlabel('W/m^2','FontSize',8);
% % ylabel(strcat('Fraction (%) over total',' ',num2str(Htot), ' sunlight
hours'),'FontSize',8);
% % axis([0 1000 0  10]);
% % ax = gca;
% % ax.FontSize = 8;
% % saveas(18,'Radiation Level Hour Fraction.png');

% Assuming a constant solar-electric efficiency of the plant, the optimal
```

```
% design radiation is calculated:
% Sum from 0.5*DNI_design to 1.25*DNI_design

y_min=0.5;
y_max=1.25;

DNI_design=((0.05/y_min):0.01:(1.25/y_max))*1e3;
Energy=zeros(numel(DNI_design),1);
for i=1:numel(DNI_design)
    i1=find(Bin==round(y_min*DNI_design(i)));
    i2=find(Bin==round(y_max*DNI_design(i)));
    Energy(i)=Bin(i1:i2)'*BinH(i1:i2)/1000;
end

figure(19);
plot(DNI_design,Energy);
title('Energy received for different design radiation choices');
xlabel('W/m^2','FontSize',8);
ylabel('kWh/m^2','FontSize',8);
ax = gca;
ax.FontSize = 8;
saveas(19,'Energy received for different design radiations.png');
DNI_D=DNI_design(Energy==max(Energy));
YearEnergyDesign=max(Energy);
% Check: sum(BinH) should be 8760
```

EES Results Post-Processing Code

```
% EES table post-processing file
clc
clear
close all
Table=readtable('ALL MONTHS new.txt');% Insert a first row with column numbers
DataCell=cell(12,1);
nv=21;
nh=8;
for i=1:12
    DataCell{i}=zeros(nh,nv);
end

for i=1:12
    for j=1:nh
        DataCell{i}(j,:)=table2array(Table((i-1)*nh+j,:));
    end
end
figure(1);
% Load Factor
YrLF=0; % Year average
set(gcf, 'Position',  [100, 100, 700, 700])
for i=1:12
    subplot(4,3,i);
    yyaxis left;
    plot(DataCell{i}(:,2),DataCell{i}(:,11)*100,'-s','DisplayName','Load
Factor');
```

```
    YrLF=(YrLF+mean(DataCell{i}(:,11)*100)/12);
    axis([8 17 0 125]);
    xlabel('Solar Time (h)','FontSize',8);
    ylabel('%','FontSize',8);
    hold on
    yyaxis right;
    plot(DataCell{i}(:,2),DataCell{i}(:,12),'-*','DisplayName','Power');
    axis([8 17 0 1250]);
    title(strcat('Month:  ',{' '},num2str(i)),'FontSize',8);
    ylabel('kW','FontSize',8);
    ax = gca;
    ax.FontSize = 8;
end
lgd=legend('Position',[0.5 0 0.05 0.05]);
lgd.NumColumns = 2; lgd.FontSize = 8;
saveas(1,'Results load factor and power.png')
figure(2);
set(gcf, 'Position',  [100, 100, 650, 900])
% Generation
E_gen=zeros(12,nh);
subplot(2,1,1);
hold on
for i=1:12
    for j=1:nh
        E_gen(i,j)=sum(DataCell{i}(1:j,12));
    end
    plot(DataCell{i}(:,2),E_gen(i,:)','-s','DisplayName',char(strcat('Month:
',{' '},num2str(i))));
    axis([9 16 0 8000]);
    xlabel('Solar Time (h)','FontSize',8);
    ylabel('kWh','FontSize',8);
    title('Cumulative Electricity Generation','FontSize',8);
    ax = gca;
    ax.FontSize = 8;
end
lgd=legend('Location','Best');
lgd.NumColumns = 2; lgd.FontSize = 8;
subplot(2,1,2);
E_genT=E_gen(:,nh)';
plot(1:12,E_genT);
axis([1 12 0 8000]);
xlabel('Month','FontSize',8);
ylabel('kWh/day','FontSize',8);
title('Electric Generation in a Day for Each Month','FontSize',8);
yrGenAvg=mean(E_genT);
saveas(2,'Results energy generation.png');
E_gen_yr=yrGenAvg*365;

figure(3);
set(gcf, 'Position',  [100, 100, 650, 900])
% Cogeneration heat
Q_cog=zeros(12,nh);
subplot(2,1,1);
hold on
```

```
for i=1:12
    for j=1:nh
        Q_cog(i,j)=sum(DataCell{i}(1:j,13))*3412/1e6; % convert to MMBtu
    end
    plot(DataCell{i}(:,2),Q_cog(i,:)','-s','DisplayName',char(strcat('Month:
',{' '},num2str(i))));
    axis([9 16 0 50]);
    xlabel('Solar Time (h)','FontSize',8);
    ylabel('MMBtu','FontSize',8);
    title('Cumulative Heat Cogeneration','FontSize',8);
    ax = gca;
    ax.FontSize = 8;
end
lgd=legend('Location','Best');
lgd.NumColumns = 2; lgd.FontSize = 8;
subplot(2,1,2);
Q_cogT=Q_cog(:,nh)';
plot(1:12,Q_cogT,'-*');
axis([1 12 0 50]);
xlabel('Month','FontSize',8);
ylabel('MMBtu/day','FontSize',8);
title('Heat Cogeneration of a Day for Each Month','FontSize',8);
yrCogAvg=mean(Q_cogT);
saveas(3,'Results heat cogen.png');
Q_cog_yr=yrCogAvg*365;

YrIncomeElec=E_gen_yr*0.08;
YrIncomeNG=Q_cog_yr*4;
YrIncome=YrIncomeElec+YrIncomeNG; % We don't need to assume a duty factor
because it is already avg
Eq_FL_hours=E_gen_yr/920;

figure(4);
% Efficiencies
set(gcf, 'Position',  [100, 100, 650, 700])
for i=1:12
    subplot(4,3,i);
    plot(DataCell{i}(:,2),DataCell{i}(:,15)*100,'-s','DisplayName','Solar-
Electric');
    axis([9 17 0 60]);
    xlabel('Solar Time (h)','FontSize',8);
    ylabel('%','FontSize',8);
    hold on
    plot(DataCell{i}(:,2),DataCell{i}(:,14)*100,'-*','DisplayName','Solar-
Cogeneration');
    title(strcat('Efficiencies, month:  ',{' '},num2str(i)),'FontSize',8);
    ax = gca;
    ax.FontSize = 8;
end
lgd=legend('Position',[0.5 0 0.05 0.05]);
lgd.NumColumns = 2; lgd.FontSize = 8;
saveas(4,'Results Efficiencies.png')
```